Daiane Laise da Silva

Identificação e caracterização bioquímica de inibidores de serinopeptidases isolados a partir da peçonha das anêmonas-do-mar *Anthopleura cascaia* e *Aulactinia veratra*

Tese apresentada ao Programa de Pós-Graduação em Ciências - Toxinologia do Instituto Butantan para obtenção do título de Doutora em Ciências

Versão corrigida.

São Paulo
2022

Daiane Laise da Silva

Identificação e caracterização bioquímica de inibidores de serinopeptidases isolados a partir da peçonha das anêmonas-do-mar *Anthopleura cascaia* e *Aulactinia veratra*

Tese apresentada ao Programa de Pós-Graduação em Ciências - Toxinologia do Instituto Butantan para obtenção do título de Doutora em Ciências

Orientador: Daniel Carvalho Pimenta

Coorientadora: Juliana Mozer Sciani

Versão corrigida.

São Paulo

2022

Versão corrigida

Este exemplar foi revisado e alterado em relação à versão original, sob responsabilidade única do autor e com a anuência de seu orientador.

São Paulo, 27 de outubro de 2022.

Daiane Laise da Silva

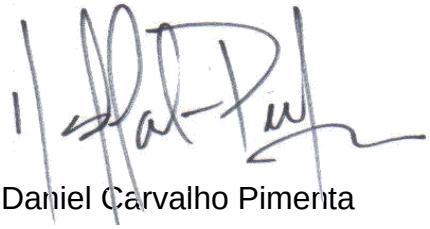

Daniel Carvalho Pimenta

Catalogação na Publicação
Instituto Butantan
Dados inseridos pelo(a) aluno(a)

da Silva, Daiane Laise
Identificação e caracterização bioquímica de inibidores de serinopeptidases isolados a partir da peçonha das anêmonas-do-mar Anthopleura cascaia e Aulactinia veratra / Daiane Laise da Silva ; orientador(a) Daniel Carvalho Pimenta, coorientador(a): Juliana Mozer Sciani - São Paulo, 2022.
219 p. : il.

Tese (Doutorado) - Escola Superior do Instituto Butantan, Programa de Pós-Graduação em Ciências - Toxinologia. Linha de pesquisa: Biopropecção e desenvolvimento.
Versão corrigida final

1. Anêmonas-do-mar 2. Peçonha. 3. Inibidores de Serinopeptidases. 4. Proteômica I. Pimenta, Daniel Carvalho. II. Escola Superior do Instituto Butantan. III. Programa de Pós-Graduação em Ciências - Toxinologia. IV. Título.

Ficha catalográfica elaborada pela equipe da Biblioteca do Instituto Butantan

Esta monografia foi elaborada com base no **Guia prático para elaboração de trabalho acadêmico** desenvolvido pela Biblioteca do Instituto Butantan, de acordo com as normas da ABNT (Associação Brasileira de Normas Técnicas).

AUTORIZAÇÃO PARA REPRODUÇÃO DE TRABALHO

Eu, Daiane Laise da Silva, aluna de doutorado do Programa de Pós-graduação em Ciências-Toxinologia do Instituto Butantan, autorizo a divulgação de minha tese por mídia impressa eletrônica ou qualquer outra, assim como a reprodução total desta dissertação/tese após publicação, para fins acadêmicos desde que citada a fonte.

Prazo de liberação da divulgação da tese após a data da defesa:

( ) Imediato

( ) 06 meses

(X) 12 meses

( ) Não autorizo a divulgação

Justifique:

São Paulo, 08 de maio de 2022.

Daiane Laise da Silva

De acordo,

Daniel Carvalho Pimenta

PÓS - GRADUAÇÃO
TOXINOLOGIA
INSTITUTO BUTANTAN

PÓS-GRADUAÇÃO EM CIÊNCIAS-TOXINOLOGIA
INSTITUTO BUTANTAN

RESULTADO DA DEFESA DE TESE

DOUTORADO

NOME DA ALUNA: Daiane Laise da Silva

DATA DO EXAME: 04/08/2022

BANCA EXAMINADORA: Profs. Drs.

NOME	Assinatura	Aprovada	Reprovada
Daniel Carvalho Pimenta (Presidente)		(X)	( )
Adriana Rios Lopes Rocha		(X)	( )
Álvaro Rossan de Brandão Prieto		(X)	( )
José Roberto Machado Cunha da Silva		(X)	( )
Juliana Mozer Sciani		(X)	( )

DECISÃO FINAL: APROVADA (X) **REPROVADA ( )**

Comentários da Banca (opcional):

Av. Vital Brasil, 1500
São Paulo,05503-900
Tel/Fax: (11) 2627-9767
cpgibu@butantan.gov.br
http://posgraduacao.butantan.gov.br

Ministério do Meio Ambiente - MMA

Instituto Chico Mendes de Conservação da Biodiversidade - ICMBio

Sistema de Autorização e Informação em Biodiversidade - SISBIO

Autorização para atividades com finalidade científica

Número: 72666-1	Data da Emissão: 11/12/2019 17:01:07	Data da Revalidação*: 11/12/2020
De acordo com o art. 28 da IN 03/2014, esta autorização tem prazo de validade equivalente ao previsto no cronograma de atividades do projeto, mas deverá ser revalidada anualmente mediante a apresentação do relatório de atividades a ser enviado por meio do Sisbio no prazo de até 30 dias a contar da data do aniversário de sua emissão.		

Dados do titular

Nome: Daniel Carvalho Pimenta	CPF: 176.276.378-80
Título do Projeto: Caracterização bioquímica de moléculas com atividade biológica relevante a partir de venenos e secreções animais.	
Nome da Instituição: INSTITUTO BUTANTAN	CNPJ: 61.821.344/0001-56

Cronograma de atividades

#	Descrição da atividade	Início (mês/ano)	Fim (mês/ano)
1	Obtenção de secreção cutânea de anfíbios	01/2020	01/2025
2	coleta conus	01/2020	01/2025
3	processamento de venenos de serpentens	01/2020	01/2025
4	processamento de venenos de artrópodes	01/2020	01/2025
5	processamento de secreção cutânea de anfíbios	01/2020	01/2025
6	processamento de venenos de conus	01/2020	01/2025
7	coleta de anemonas	01/2020	01/2020

Equipe

#	Nome	Função	CPF	Nacionalidade
1	Emidio Beraldo Neto	Aluno de Doutorado	413.126.898-11	Brasileira
2	Juliana Mozer Sciani	Pesquisadora	346.487.618-71	Brasileira
3	Tiago Henrique Moretto Del Rei	Aluno de Doutorado	355.566.048-94	Brasileira
4	Hugo Vigerelli de Barros	Pesquisador	335.504.618-36	Brasileira
5	Daiane Laise da Silva	Aluna de Doutorado	065.598.714-28	Brasileira

Ministério do Meio Ambiente - MMA

Instituto Chico Mendes de Conservação da Biodiversidade - ICMBio

Sistema de Autorização e Informação em Biodiversidade - SISBIO

Autorização para atividades com finalidade científica

Número: 72666-1	Data da Emissão: 11/12/2019 17:01:07	Data da Revalidação*: 11/12/2020
De acordo com o art. 28 da IN 03/2014, esta autorização tem prazo de validade equivalente ao previsto no cronograma de atividades do projeto, mas deverá ser revalidada anualmente mediante a apresentação do relatório de atividades a ser enviado por meio do Sisbio no prazo de até 30 dias a contar da data do aniversário de sua emissão.		

Dados do titular

Nome: Daniel Carvalho Pimenta	CPF: 176.276.378-80
Título do Projeto: Caracterização bioquímica de moléculas com atividade biológica relevante a partir de venenos e secreções animais.	
Nome da Instituição: INSTITUTO BUTANTAN	CNPJ: 61.821.344/0001-56

Observações e ressalvas

1	A autorização não eximirá o pesquisador da necessidade de obter outras anuências, como: I) do proprietário, arrendatário, posseiro ou morador quando as atividades forem realizadas em área de domínio privado ou dentro dos limites de unidade de conservação federal cujo processo de regularização fundiária encontra-se em curso; II) da comunidade indígena envolvida, ouvido o órgão indigenista oficial, quando as atividades de pesquisa forem executadas em terra indígena; III) do Conselho de Defesa Nacional, quando as atividades de pesquisa forem executadas em área indispensável à segurança nacional; IV) da autoridade marítima, quando as atividades de pesquisa forem executadas em águas jurisdicionais brasileiras; V) do Departamento Nacional da Produção Mineral, quando a pesquisa visar a exploração de depósitos fossilíferos ou a extração de espécimes fósseis; VI) do órgão gestor da unidade de conservação estadual, distrital ou municipal, dentre outras.
2	Em caso de pesquisa em UNIDADE DE CONSERVAÇÃO, o pesquisador titular desta autorização deverá contactar a administração da unidade a fim de CONFIRMAR AS DATAS das expedições, as condições para realização das coletas e de uso da infraestrutura da unidade.
3	O titular de autorização ou de licença permanente, assim como os membros de sua equipe, quando da violação da legislação vigente, ou quando da inadequação, omissão ou falsa descrição de informações relevantes que subsidiaram a expedição do ato, poderá, mediante decisão motivada, ter a autorização ou licença suspensa ou revogada pelo ICMBio, nos termos da legislação brasileira em vigor.
4	Este documento somente poderá ser utilizado para os fins previstos na Instrução Normativa ICMBio nº 03/2014 ou na Instrução Normativa ICMBio nº 10/2010, no que especifica esta Autorização, não podendo ser utilizado para fins comerciais, industriais ou esportivos. O material biológico coletado deverá ser utilizado para atividades científicas ou didáticas no âmbito do ensino superior.
5	As atividades de campo exercidas por pessoa natural ou jurídica estrangeira, em todo o território nacional, que impliquem o deslocamento de recursos humanos e materiais, tendo por objeto coletar dados, materiais, espécimes biológicos e minerais, peças integrantes da cultura nativa e cultura popular, presente e passada, obtidos por meio de recursos e técnicas que se destinem ao estudo, à difusão ou à pesquisa, estão sujeitas a autorização do Ministério de Ciência e Tecnologia.
6	O titular de licença ou autorização e os membros da sua equipe deverão optar por métodos de coleta e instrumentos de captura direcionados, sempre que possível, ao grupo taxonômico de interesse, evitando a morte ou dano significativo a outros grupos; e empregar esforço de coleta ou captura que não comprometa a viabilidade de populações do grupo taxonômico de interesse em condição in situ.
7	Esta autorização NÃO exime o pesquisador titular e os membros de sua equipe da necessidade de obter as anuências previstas em outros instrumentos legais, bem como do consentimento do responsável pela área, pública ou privada, onde será realizada a atividade, inclusive do órgão gestor de terra indígena (FUNAI), da unidade de conservação estadual, distrital ou municipal, ou do proprietário, arrendatário, posseiro ou morador de área dentro dos limites de unidade de conservação federal cujo processo de regularização fundiária encontra-se em curso.
8	Este documento não dispensa o cumprimento da legislação que dispõe sobre acesso a componente do patrimônio genético existente no território nacional, na plataforma continental e na zona econômica exclusiva, ou ao conhecimento tradicional associado ao patrimônio genético, para fins de pesquisa científica, bioprospecção e desenvolvimento tecnológico. Veja maiores informações em www.mma.gov.br/cgen.

Locais onde as atividades de campo serão executadas

#	Descrição do local	Município-UF	Bioma	Caverna?	Tipo
1	Praia	São Sebastião-SP	Marinho	Não	Fora de UC Federal

Ministério do Meio Ambiente - MMA

Instituto Chico Mendes de Conservação da Biodiversidade - ICMBio

Sistema de Autorização e Informação em Biodiversidade - SISBIO

Autorização para atividades com finalidade científica

Número: 72666-1	Data da Emissão: 11/12/2019 17:01:07	Data da Revalidação*: 11/12/2020
De acordo com o art. 28 da IN 03/2014, esta autorização tem prazo de validade equivalente ao previsto no cronograma de atividades do projeto, mas deverá ser revalidada anualmente mediante a apresentação do relatório de atividades a ser enviado por meio do Sisbio no prazo de até 30 dias a contar da data do aniversário de sua emissão.		

Dados do titular

Nome: Daniel Carvalho Pimenta	CPF: 176.276.378-80
Título do Projeto: Caracterização bioquímica de moléculas com atividade biológica relevante a partir de venenos e secreções animais.	
Nome da Instituição: INSTITUTO BUTANTAN	CNPJ: 61.821.344/0001-56

Atividades

#	Atividade	Grupo de Atividade
1	Coleta/transporte de espécimes da fauna silvestre in situ	Fora de UC Federal
2	Coleta/transporte de amostras biológicas in situ	Fora de UC Federal
3	Coleta/transporte de amostras biológicas ex situ	Atividades ex-situ (fora da natureza)
4	Manutenção temporária (até 24 meses) de invertebrados silvestres em cativeiro	Atividades ex-situ (fora da natureza)

Atividades X Táxons

#	Atividade	Táxon	Qtde.
1	Coleta/transporte de espécimes da fauna silvestre in situ	Lachesis	5
2	Coleta/transporte de espécimes da fauna silvestre in situ	Rhaebo	5
3	Coleta/transporte de espécimes da fauna silvestre in situ	Apis	300
4	Coleta/transporte de espécimes da fauna silvestre in situ	Rhinella	10
5	Coleta/transporte de espécimes da fauna silvestre in situ	Aparasphenodon	5
6	Coleta/transporte de espécimes da fauna silvestre in situ	Itapotihyla	5
7	Coleta/transporte de espécimes da fauna silvestre in situ	Corythomantis	5
8	Coleta/transporte de espécimes da fauna silvestre in situ	Trachycephalus	5
9	Coleta/transporte de amostras biológicas ex situ	Pithecopus	-
10	Coleta/transporte de espécimes da fauna silvestre in situ	Pithecopus	5
11	Manutenção temporária (até 24 meses) de invertebrados silvestres em cativeiro	Anemonia	-
12	Coleta/transporte de amostras biológicas ex situ	Anemonia	-
13	Coleta/transporte de amostras biológicas in situ	Anemonia	-
14	Coleta/transporte de espécimes da fauna silvestre in situ	Anemonia	30
15	Coleta/transporte de amostras biológicas ex situ	Phyllomedusa	-
16	Coleta/transporte de espécimes da fauna silvestre in situ	Phyllomedusa	5
17	Coleta/transporte de amostras biológicas ex situ	Crotalus	-
18	Coleta/transporte de espécimes da fauna silvestre in situ	Crotalus	10
19	Manutenção temporária (até 24 meses) de invertebrados silvestres em cativeiro	Bunodosoma	-
20	Coleta/transporte de amostras biológicas ex situ	Bunodosoma	-
21	Coleta/transporte de espécimes da fauna silvestre in situ	Bunodosoma	10
22	Coleta/transporte de amostras biológicas ex situ	Zoanthus	-
23	Coleta/transporte de amostras biológicas in situ	Zoanthus	-
24	Coleta/transporte de espécimes da fauna silvestre in situ	Zoanthus	30

Autorização para atividades com finalidade científica

Número: 72666-1	Data da Emissão: 11/12/2019 17:01:07	Data da Revalidação*: 11/12/2020

De acordo com o art. 28 da IN 03/2014, esta autorização tem prazo de validade equivalente ao previsto no cronograma de atividades do projeto, mas deverá ser revalidada anualmente mediante a apresentação do relatório de atividades a ser enviado por meio do Sisbio no prazo de até 30 dias a contar da data do aniversário de sua emissão.

Dados do titular

Nome: Daniel Carvalho Pimenta	CPF: 176.276.378-80
Título do Projeto: Caracterização bioquímica de moléculas com atividade biológica relevante a partir de venenos e secreções animais.	
Nome da Instituição: INSTITUTO BUTANTAN	CNPJ: 61.821.344/0001-56

Atividades X Táxons

#	Atividade	Táxon	Qtde.
25	Manutenção temporária (até 24 meses) de invertebrados silvestres em cativeiro	Anthopleura	-
26	Coleta/transporte de amostras biológicas ex situ	Anthopleura	-
27	Coleta/transporte de amostras biológicas in situ	Anthopleura	-
28	Coleta/transporte de espécimes da fauna silvestre in situ	Anthopleura	30
29	Manutenção temporária (até 24 meses) de invertebrados silvestres em cativeiro	Conus	-
30	Coleta/transporte de amostras biológicas ex situ	Conus	-
31	Coleta/transporte de amostras biológicas in situ	Conus	-
32	Coleta/transporte de espécimes da fauna silvestre in situ	Conus	30
33	Coleta/transporte de amostras biológicas ex situ	Bothrops	-
34	Coleta/transporte de espécimes da fauna silvestre in situ	Bothrops	10
35	Coleta/transporte de amostras biológicas ex situ	Tityus	-

Materiais e Métodos

#	Tipo de Método (Grupo taxonômico)	Materiais
1	Amostras biológicas (Anfíbios)	Ovos, Secreção, Animal encontrado morto ou partes (carcaça)/osso/pele
2	Amostras biológicas (Invertebrados Aquáticos)	Outras amostras biológicas(secreções)
3	Amostras biológicas (Invertebrados Terrestres)	Secreção
4	Amostras biológicas (Répteis)	Secreção, Outras amostras biológicas(peçonha)
5	Método de captura/coleta (Anfíbios)	Captura manual
6	Método de captura/coleta (Insetos)	Coleta manual
7	Método de captura/coleta (Invertebrados Aquáticos)	Captura manual
8	Método de captura/coleta (Répteis)	Captura manual

Este trabalho é dedicado aos meus pais – Edson José da Silva (Pedreiro) e Mauricéa Lucas da Silva (Professora) – por todo o exemplo, esforço e trabalho de sol a sol, dedicados à nossa educação.

AGRADECIMENTOS

Há uma grande diferença entre aqueles que cumprem no papel a função de orientar alunos de pós-graduação, e aqueles que ajudam os alunos a se tornarem pesquisadores. Posso dizer que meu professor, Daniel Carvalho Pimenta, é um dos poucos profissionais que são destinados à pesquisa e à formação de cientistas. O meu orientador foi um exemplo de quem abre portas – do laboratório; de oportunidades; do conhecimento – e de quem acredita no potencial dos seus alunos. Vou levar sempre seu exemplo comigo. Muito obrigada por me acolher no seu grupo, Daniel Pimenta. Obrigada por me "empurrar pra fora do ninho". Obrigada por, pacientemente, me ensinar.

Gostaria de agradecer imensamente ao meu colega de trabalho e amigo, Guilherme Rabelo Coelho, por fazer questão de sentar na bancada comigo e me ensinar; por cobrar a escrita de artigos; por me ensinar a arriscar mais e principalmente por acreditar em mim. Sempre com um sorriso no rosto, ele tornou tudo mais leve e o recomeço mais fácil. O Gui é claramente "cria" do Daniel, e que sorte a minha ter ele ao meu lado durante os quatro anos que passei neste grupo.

Agradeço também aos meus amigos: Emidio Beraldo; Rodrigo Valladão, Oscar Bento; Rayssa Oliveira; Ana Caroline Freitas e Hugo Vigerelli. Sem eles, este doutorado não teria sido concluído. Eles estavam sempre dispostos a ajudar, seja ensinando; auxiliando na bancada do laboratório; com discussões científicas; em coletas e no providenciamento de documentações. Como se fala na minha terra: Vocês são 'pau pra toda obra'! Quem tem esta equipe de trabalho, não precisa de mais nada. Foi um prazer aprender com vocês. Obrigada por me acolherem no grupo e por fazer parecer que ir trabalhar era, na verdade, ir passear. Vocês simbolizam o Laboratório de Bioquímica para mim.

Ainda gostaria de agradecer à minha co-orientadora, Juliana Sciani, por toda a assistência dada na linha de pesquisa de marinhos no início do desenvolvimento deste trabalho. Muito obrigada por sempre estar disponível a ajudar nos experimentos enzimáticos; por disponibilizar extratos e peçonhas de origem marinha, e pelas análises de massas, Ju!

Gostaria também de agradecer aos demais pesquisadores do Laboratório de Bioquímica: Adriana Rios, em especial, por ser uma excelente docente de acompanhamento, e por me orientar nas experimentações com inibidores. Ao Ivo Lebrun e Marilene Demasi pela disponibilidade em ajudar, seja com reagentes ou equipamentos. Muito obrigada!

Aos funcionários Admilson Cunha; Adrian Hand; Silvana Lima e Carlos Silva, por sempre estarem de bom humor e disponíveis a ajudar no uso de equipamentos e reagentes. Muito obrigada pela companhia durante estes anos.

Aos colegas e amigos do laboratório de Imunoquímica, que me ensinaram muito durante o primeiro ano da minha formação no Instituto Butantan: Elaine Rodrigues; Lia Aguiar; Thyago Leonel; Fabinho; Joel Megale; Ângela Amadeu, Felipe França; Guilherme Yoshikawa; Cinthia Okamoto; Ana Tung; Denise Tambourgi; Prof. Wilmar; Gisele Pidde; Priscila Hess; Isadora Villas Boas; Ricardo, Marcinha, dona Ana, Ana Cláudia, Alécio e Sr Ramos.

Aos meus colegas de trabalho da University of Queensland (UQ), Theo Crawford e Vanessa Schendel, por me auxiliarem durante o uso de equipamentos no Center for Advanced Imaging; pela companhia de bancada e pelas discussões científicas. Aos pesquisadores que abriram as portas dos seus laboratórios na Austrália: Prof. Mehdi Mobli da UQ e Prof. Peter Prentis da Queensland University of Technology, por toda a assistência e disponibilidade de material e equipamentos. Em especial, gostaria de agradecer ao meu orientador Eivind A.B. Undheim e ao meu co-orientador Brett Hamilton, pelo tempo e ensino dedicados à minha formação; principalmente quanto aos treinamentos e experimentações de MALDI-imaging; e na associação de dados de proteoma e transcriptoma de cnidários. Eu nem sei o quanto agradecer por todo ensino e acolhimento durante o ano que passei neste grupo de pesquisa incrível. Muito obrigada!

Aos amigos que ganhei na University of Queensland: Salma Ahmed, Gayathri Endiriweera, Weijing Chu, Biswa Prasanna e Mayara de Oliveira, por tornarem a estadia na Austrália e no CAI-UQ mais leve e feliz. Muito obrigada pela companhia.

À comissão de pós-graduação do Instituto Butantan, pelo auxílio durante todo o período dos 5 anos necessários à conclusão deste doutorado. Muito obrigada, às secretárias Kimie, Débora e Rosana por toda a assistência prestada

durante este período. Aqui, gostaria de deixar um agradecimento especial à ex-coordenadora da pós, Roxane Maria Fontes Piazza, que em um momento difícil, me acolheu como sua aluna e me ajudou a encontrar um novo orientador. Você fez muita diferença. Muito obrigada, Roxane!

À minha família: Mauricéa Lucas da Silva (mainha); Edson José da Silva (Papai), Edson José da Silva Junior (irmão), Caroline Antunes (cunhada). Muito obrigada por acreditarem nos meus sonhos; por darem o suporte necessário nos bastidores do desenvolvimento deste trabalho; e principalmente por estarem ao lado nos momentos de perda. Vocês foram fundamentais!

Ao meu companheiro de vida e marido – Valdir Santos – por estar sempre ao meu lado, apoiando cada sonho e enfrentando cada uma das fases da carreira científica comigo. Eu jamais teria chegado até aqui sem você. Muito obrigada!

Eu agradeço muito a Deus pela oportunidade de aprender com todos vocês.

Este trabalho teve apoio financeiro da CAPES – Coordenação de Aperfeiçoamento de Pessoal de Nível Superior – através do Programa de Demanda Social (n° de projeto: 88882.442324/2019-01) e do Programa de Doutorado Sanduíche no Exterior - PDSE (n° de projeto: 88881.362036/2019-01).

Meus sinceros agradecimentos à CAPES pela concessão de bolsas no Instituto Butantan e University of Queensland (Austrália). Graças à CAPES tive auxílio financeiro durante todas as fases de estudos de graduação, mestrado e doutorado. Muito obrigada.

RESUMO

DA SILVA, Daiane Laise. **Identificação e caracterização bioquímica de inibidores de serinopeptidases isolados a partir da peçonha das anêmonas-do-mar *Anthopleura cascaia* e *Aulactinia veratra*.** 2022. 219 p. Tese (Doutorado em Ciências -Toxinologia) – Instituto Butantan, São Paulo, 2022.

O filo Cnidaria é composto por mais de 10.000 espécies e cerca de 10% destas são anêmonas-do-mar. Estes animais são considerados fontes subexploradas de moléculas, possuindo um diverso arsenal de toxinas que podem agir sobre diferentes alvos farmacológicos, incluindo enzimas. Toxinas de anêmonas-do-mar representam cerca de 96% das toxinas anotadas para o filo Cnidaria, embora apenas 5% de suas espécies tenham sido estudadas quanto à composição de toxinas até o momento. Neste trabalho elucidamos por espectrometria de massas a composição da peçonha das anêmonas *Anthopleura cascaia* e *Aulactinia veratra*, buscando a identificação de inibidores de serinopeptidases. O arsenal de toxinas para ambas anêmonas foi elucidado. Ainda, descrevemos as etapas de purificação envolvidas na busca de inibidores e a seleção destes candidatos por meio da inibição da atividade da tripsina, avaliada por duas técnicas distintas: Cinética enzimática e Espectrometria de massas. Adicionalmente, descrevemos a localização de candidatos a inibidores no tecido das anêmonas através do Imageamento por espectrometria de massas. Na análise sobre a composição de toxinas destas anêmonas, vimos que a peçonha da *A. cascaia* apresentou a existência três tipos de toxinas incluindo citolisinas, fosfolipases e naterinas. Para a espécie *A. veratra,* a classificação de toxinas baseadas no blastp hit e na arquitetura de domínios das toxinas foi realizada. Esta análise revelou a presença de 59 proteínas e peptídeos pertencentes a 14 famílias de toxinas de anêmonas-do-mar; além do reconhecimento de 20 peptídeos apresentando 18 novos scaffolds de cisteínas. A peçonha desta anêmona é principalmente composto por neurotoxinas do tipo ShK-like, β-defensinas, SCRiP, ICK, EGF-like e inibidores de serinopeptidases. Os dados obtidos mostram que ambas anêmonas são ricas fontes de inibidores de serinopeptidases, especialmente tipo Kunitz e Kazal. Tais inibidores apresentam distribuição na região dos tentáculos, mesentério e disco pedal das anêmonas, o que pode indicar o estoque preferencial destas toxinas. Em

conclusão, o conjunto de abordagens metodológicas empregadas neste trabalho foi capaz de atender os objetivos propostos: identificar a presença de inibidores de serinopeptidases na peçonha e tecido de anêmonas, tanto por fracionamento cromatográfico seguido de ensaio enzimático, quanto por MALDI-Imaging.

Palavras-chave: Anêmonas-do-mar. Peçonha. Inibidores de serinopeptidases. Proteômica. Imageamento por Espectrometria de Massas.

ABSTRACT

DA SILVA, Daiane Laise. **Identification and biochemical characterization of serine peptidase inhibitors isolated from the venom of *Anthopleura cascaia* and *Aulactinia veratra* sea anemones.** 2022. 219 p. Doctoral dissertation (Doctorate degree in Sciences - Toxinology) – Instituto Butantan, São Paulo, 2022.

Phylum Cnidaria comprises more than 10,000 species and around 10% of them are represented by sea anemones. These animals are underexplored sources of molecules, possessing structurally diverse toxins that can act over a diverse range of pharmacological targets, including enzymes. Sea anemones represent almost 96% of the manually annotated toxins from the phylum, but until now only 5% of its species have been studied about their toxin content. In the present work, the venoms of the sea anemones *Anthopleura cascaia* and *Aulactinia veratra* were studied and accessed through mass spectrometry analysis for searching serine peptidase inhibitors. The arsenal of toxins from both venoms was elucidated. Additionally, venom's fractions were screened for inhibitory activity over trypsin, using time-course fluorescence-based kinetic assays or Mass spectrometry-based analysis. Beyond that, the spatial distribution of serine peptidase inhibitors in both sea anemones' tissues were shown through Mass Spectrometry Imaging by MALDI-TOF. In the analysis of toxins composition, it was seen that *A. cascaia* venom presents at least three types of toxins: cytolysins, phospholipases and a toxin similar to natterin. For *A. veratra*, the classification based on blastp hit similarity and relying on domain architecture of the toxin's sequences (translated transcripts) was performed. The thorough examination over toxins sequences led to the identification of 59 proteins and peptides belonging to 14 known toxin's families of sea anemones and to the acknowledge of 20 peptides presenting 18 new cysteine scaffolds. The venom of this sea anemone mainly relies on neurotoxins from ShK-like, β-defensins, SCRiP, ICK, EGF-like types and on serine peptidase inhibitors from Kazal and Kunitz types. Furthermore, serine peptidase inhibitors from both venoms were isolated and present main distribution over tentacles, mesenterial filaments and pedal disc of these sea anemones, suggesting the preferential stock of these toxins. In conclusion, the methodological approaches applied in this study were able of identifying the presence of serine peptidase inhibitors on the venom and tissue of

sea anemones through chromatographic techniques followed by enzymatic assays, and MALDI-Imaging.

Keywords: Sea anemones. Venom. Serine peptidase inhibitors. Proteomics. Mass Spectrometry Imaging.

LISTA DE ILUSTRAÇÕES

SUMÁRIO

1. INTRODUÇÃO

1.1 Cnidaria – Biodiversidade e Importância médica

Composto por mais de 13.000 espécies distribuídas em ambientes aquáticos de regiões tropicais e temperadas ao redor do mundo, o filo Cnidaria está dividido em três linhagens principais: Anthozoa, Medusozoa e Endocnidozoa (ZHANG et al., 2011; KAYAL et al., 2018; ASHWOOD et al., 2020). Anthozoa, composto por cerca de 7.200 espécies pertencentes à classe Anthozoa e subclasses Octocorallia, Hexacorallia e Ceriantharia, é caracterizado por animais que na fase adulta apresentam-se em forma de pólipos sésseis (corais, zoantídeos, anêmonas-do-mar, anêmonas-de-tubo). O segundo clado – Medusozoa – é formado por quatro classes: Hydrozoa, Cubozoa, Scyphozoa e Staurozoa, totalizando quase 4000 espécies de animais que na fase reprodutiva apresentam formato de medusas de vida livre, com exceção da classe Staurozoa, cujos animais são bentônicos. São representantes destas classes os hidróides; hidromedusas; águas-vivas e medusas. O terceiro e último clado, Endocnidozoa, composto por cerca de 2.200 espécies pertencentes às classes Myxozoa e Polypodiozoa, são exclusivamente parasitas (Fig. 1) (ASHWOOD et al., 2020; KAYAL et al., 2018; REMINGANTE et al., 2018; COLLINS; 2009; FOOX & SIDDALL, 2015).

Na América do Sul, o estudo envolvendo o censo de espécies do clado Medusozoa, revelou que existem 780 espécies destes cnidários nas águas marinhas de 10 países banhados pelos oceanos Atlântico e Pacífico. A maioria das espécies descritas (748 spp) pertencem à classe Hydrozoa, seguida por representantes da classe Scyphozoa (24 spp); Cubozoa (5 spp); e Staurozoa (3 spp) (OLIVEIRA et al., 2016). Adicionalmente, um segundo estudo publicado em 2020, envolvendo apenas a distribuição de espécies de anêmonas-do mar de águas rasas – clado Anthozoa – nas províncias Brasileira, Argentina (incluindo Uruguai) e patagônica, banhadas pelo sudeste do Atlântico, revelou que existem cerca de 124 espécies de anêmonas-do mar nestas regiões (TARGINO & GOMES, 2020).

Figura 1. Relações entre as linhagens Anthozoa, Endocnidozoa e Medusozoa baseado na reconstrução filogenética de representantes do filo Cnidaria.

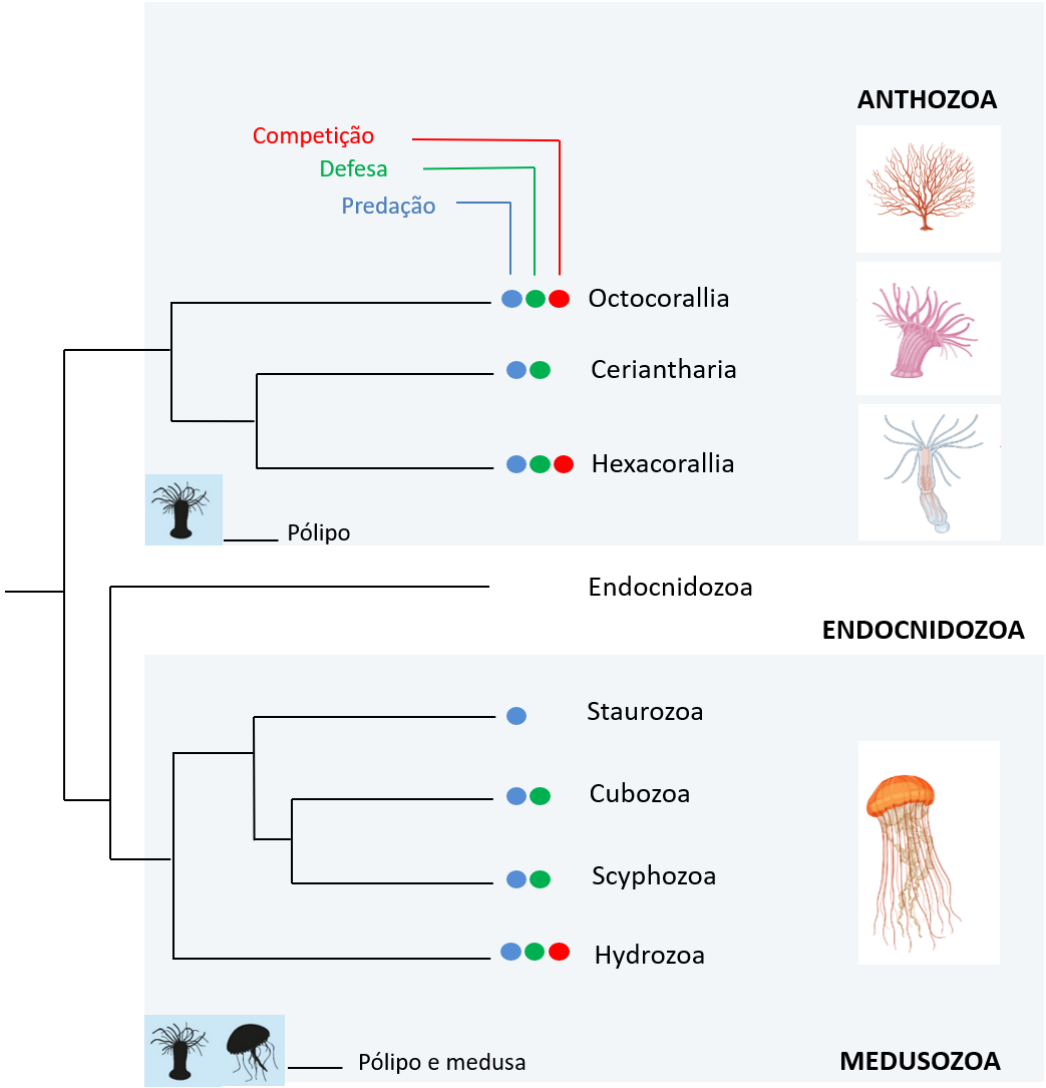

Fonte: Adaptado de Ashwood et al., 2020.

Ilustrações de cnidários foram obtidas no BioRender.com.

No Brasil, vários trabalhos têm demonstrado a ocorrência de cnidários. O país possui uma costa litorânea de mais de 8.500 km de extensão e entre os anos de 1999 e 2010, apenas no estado de São Paulo, foi relatada a ocorrência de 272 espécies de cnidários (SILVEIRA et al., 2011). Até o ano de 2011, de acordo com Silveira e colaboradores, o país abrigava cerca de 550 espécies do filo, havendo

representantes de todas as classes no país, exceto Staurozoa (SILVEIRA et al., 2011). Porém, a ocorrência rara de duas espécies de Staurozoa – *Kishinouyea corbini* e *Lucernariopsis capensis* – já foi demonstrada nos estados do Espírito Santo e São Paulo, respectivamente (MIRANDA & MARQUES, 2016; MIRANDA et al., 2012; GROHMANN et al, 1999).

Estudos mais recentes publicados entre 2019 e 2021 também enfatizam a presença de cnidários no Brasil: Mais de 300 pólipos da ordem Coronatae (Scyphozoa) e pertencentes aos gêneros *Nausithoe e Atorella* foram descritos em águas profundas da costa brasileira. Estudos anteriores revelam que dentre as espécies já descritas estão: *Atolla wyvillei*; *Nausithoe atlantica*; *N. aurea; N. punctata*; *Periphylla periphylla*; *Linuche unguiculata*; *Stephanoscyphistoma corniformis;* e *Stephanoscyphistoma simplex* (MOLINARI & MORANDIBI, 2019).

Recentemente, também foi descrita a presença da éfiras de *Lychnorhiza lucerna* (Scyphozoa) no estuário Lagoa dos Patos (RS) (NAGATA et al., 2021). Adicionalmente, 5 espécies de anêmonas da família Edwardsiide foram descritas entre os estados de Pernambuco, Rio de janeiro e São Paulo: *Isoscolanthus iemanjae, Isoscolanthus janainae, Scolanthus crypticus, Nemastotella vectensis e Edwardsia migottoi* (BRANDÃO et al., 2019). Além disso, um estudo mais recente demonstrou que dentre estas espécies, o Brasil detém ao todo 46 espécies de anêmonas em águas rasas (TARGINO & GOMES et al., 2020). Espécies de Ceriantharia também foram descritas nos estados do Rio de Janeiro; Rio Grande do Sul; Espírito Santo; São Paulo; Bahia e Atol das Rocas: *Ceriantheomorphe brasiliensis*, *Ceriantheopsis lineata*; *Pachycerianthus schlenzae*; *Isarachnanthus nocturnus*; *Isarachnanthus maderensis* (STAMPAR et al., 2020).

Devido à presença de cnidários em diferentes profundidades, tanto no mar aberto como em águas costeiras, com frequência são relatados contatos acidentais destes animais com humanos, resultando em impactos na saúde pública (REMINGANTE et al., 2018).

A incrível complexidade e diversificação das peçonhas encontrados neste filo representam um grande desafio terapêutico para o tratamento de acidentes causados por certas espécies (JOUIAEI et al., 2015). *Chironex fleckeri* e *Carukia barnesi*, por exemplo, possuem peçonhas letais que podem causar sérias complicações cardíacas. Outras espécies, pertencentes à classe Scyphozoa, são

consideradas menos perigosas, porém responsáveis pela maioria dos acidentes com cnidários ao redor do mundo (REMINGANTE et al., 2018).

Como consequência da marcada presença destes animais na costa brasileira, acidentes no país também vêm sendo relatados. Um estudo retrospectivo epidemiológico conduzido entre os anos de 2007 e 2013 por Reckziegel e colaboradores, mostrou que cerca de 13% dos acidentes com animais aquáticos no Brasil foram causados por águas vivas (RECKZIEGEL et al., 2015). Acidentes mais atuais causados entre os anos de 2017 e 2020 foram relatados com a cifomedusa *Chrysaora lactea* e hidromedusas *Olindias sambaquiensis* e *Physalia physalis* (HADDAD JUNIOR et al., 2018; HADDAD JUNIOR et al., 2019; BASTOS et al., 2017; CAVALCANTE et al., 2020). As manifestações clínicas em vítimas podem incluir reações locais como placas eritematosas, edema e dor intensa. Raramente estas manifestações são sistêmicas, mas podem incluir dispneia, hipotensão arterial e arritmia cardíaca (HADDAD JUNIOR, 2010).

1.2 Características únicas de Cnidaria e de sua peçonha

Diferentemente de outros animais peçonhentos, animais do filo Cnidaria não possuem um sistema centralizado de suas toxinas. Ao contrário disso, estes animais apresentam células especializadas produtoras de toxinas - cnidócitos - distribuídas por todo o corpo; sendo os únicos representantes animais a possuir este tipo celular em seus tecidos corporais (MADIO et al., 2019; FAUTIN et al., 2009). Estas células, exclusivas de cnidários, possuem cápsulas intracelulares especializadas chamadas de cnidocistos, que secretam misturas complexas de componentes bioativos e são reservatórios de toxinas (SHER et al., 2005; ORTS et al., 2013; LIAO et al., 2018; KILLI et al., 2020).

Cnidocistos são secretados especificamente pelo aparelho de Golgi e estão presentes em várias regiões do corpo dos cnidários, podendo ser classificados em três tipos principais – nematocistos, espirocistos e pticocistos (FAUTIN; 2009). Entre estes, apenas o nematocisto é encontrado em todos os cnidários e é caracterizado por ser uma cápsula penetrante, que ao ser estimulada mecanicamente ou quimicamente, sofre extrusão do túbulo interno, aderindo ao alvo e liberando assim seu conteúdo (Fig 2) (MARISCAL; 1974; FAUTIN; 2009;

KILLI et al., 2020; HAMLET et al., 2020). Estas organelas apresentam a maior diversidade morfológica e estrutural entre os cnidocistos. De acordo com Fautin (2009) mais de 30 tipos de nematocistos já foram descritos e comumente a morfologia destas organelas é utilizada na classificação taxonômica de cnidários (FAUTIN, 2009). Nematocistos são os grandes responsáveis pelo ataque e defesa destes animais, pois tais estruturas podem conter toxinas que são utilizadas para subjugar, aprisionar e digerir presas, além de defender os cnidários contra predadores (DAVID et al., 2008; JOUIAEI et al., 2015).

Figura 2. Estágios de descarga do nematocisto.

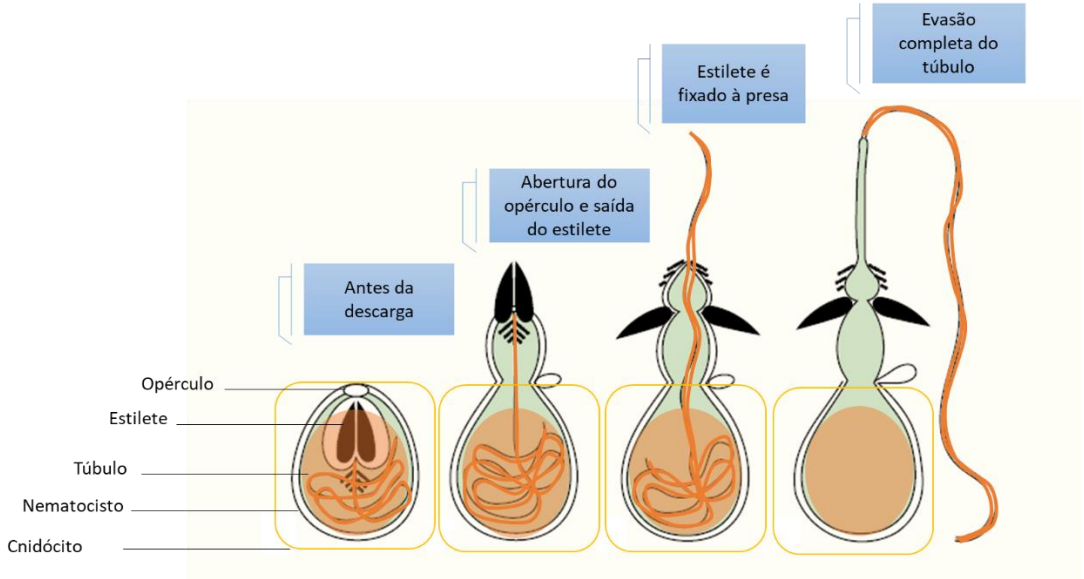

Fonte: Adaptado de Hamlet et al., 2020.

Estágios de descarga do nematocisto: A figura mostra que a partir da abertura do opérculo (círculo oval), há a saída do estilete que perfura a presa. A partir deste estágio há a entrada do túbulo na presa, havendo a injeção do conteúdo do nematocisto no alvo.

A peçonha encontrada no muco e no interior de cnidocistos apresenta um arsenal diverso de componentes, que vão desde purinas e aminas biogênicas até proteínas de alta massa molecular. Entre as toxinas encontradas em cnidários estão enzimas como fosfolipases A2 e metalopeptidases; citolisinas como

actinoporinas, toxinas relacionadas às hidralisinas, perforinas formadoras de complexo de ataque à membrana (MACPF); e neurotoxinas que atuam sobre canais iônicos dependentes de voltagem, como NaTxs (tipos I-III) e KTxs (tipos I, III e IV, V); entre outras (MORAN et al., 2012; JOUIAEI et al., 2015).

Um fato importante a ser destacado aqui é que várias das famílias de toxinas encontradas em animais de origem terrestre, como aranhas, serpentes e escorpiões também são encontradas em cnidários. Peptídeos do tipo Kunitz e toxinas bloqueadoras de canais de potássio Kv1 são exemplos de toxinas que ocorrem tanto em escorpiões como em anêmonas-do-mar (FRY et al., 2009, JOUIAEI et al., 2015). No entanto, apesar de serem da mesma família, as toxinas possuem sequências de aminoácidos diferentes, bem como atividades biológicas e potências farmacológicas diversas.

Para o estudo da peçonha de cnidários, ferramentas ômicas têm sido de crucial importância para a descrição do conteúdo destes. São exemplos genômica, transcriptômica e proteômica, que quando associadas à bioinformática prometem ser fortes aliados para a descoberta em larga escala de novas toxinas de anêmonas-do-mar, potencialmente terapêuticas. Tais ferramentas permitem uma caracterização robusta e possibilitam uma elucidação mais clara da complexidade do arsenal de toxinas (MADIO et al., 2017; RAMÍREZ-CARRETO et al., 2019).

1.3 Toxinas encontradas em anêmonas-do-mar

Anêmonas-do-mar são cnidários sésseis, bentônicos, com aspecto anatômico simples, que têm recebido especial atenção da comunidade científica devido à riqueza de biomoléculas encontradas em seus tecidos (MADIO et al., 2018; FAUTIN et al., 2009; FRAZÃO et al., 2012). Estes animais utilizam suas toxinas para competição intraespecífica, predação e defesa (ASHWOOD et al., 2020); e assim como outros cnidários, as mesmas possuem nematocistos distribuídos ao longo do seu corpo, incluindo coluna; filamentos mesentéricos; tentáculos e acrorhagi (FAUTIN et al., 2009; PRENTIS et al., 2018; RAMÍRES-CARRETO et al., 2019).

Detentores de toxinas com atividades fosfolipásica; citolítica e inibitória; além de toxinas que atuam sobre canais de sódio e potássio dependentes de voltagem,

estes animais ainda possuem muito a ser descoberto sobre suas moléculas (FRAZÃO et al., 2012; PRENTIS et al., 2018).

Atualmente as toxinas de anêmonas são classificadas dentro de quinze famílias, das quais quatro famílias de toxinas são comumente isoladas, são elas: 1. Família das Actinoporinas, subfamília anêmonas-do-mar; 2. Família de toxinas inibidoras de canais de sódio de anêmonas, subfamília tipo I; 3. Família das toxinas de canais de potássio tipo III de anêmonas-do-mar; 4. Família tipo kunitz da peçonha, subfamília de toxinas de canais de potássio II de anêmonas-do-mar (PRENTIS et al., 2018).

O trabalho mais recente envolvendo a diversidade de famílias de toxinas de anêmonas, revela que estas podem ser divididas de acordo com característica estrutural e função; sendo conhecidos pelo menos 17 '*scaffolds*' de toxinas de anêmonas. Estes scaffolds incluem toxinas enzimáticas como Fosfolipases tipo A2; serinopeptidases; Endonucleases D; peptídeos neurotóxicos como β-defensinas; ICK '*Inhibitor cystine-knot*'; BBK '*Boundless β-hairpin';* tipo Kunitz; SCRiP '*Small cysteine-rich peptides'* e toxinas não enzimáticas como actinoporinas. Além disso, estas toxinas podem agir em mais de 20 grupos farmacológicos incluindo canais TRPA1 (transient receptor potential channel type A1) e vários subtipos de canais Kv e Nav - canais de potássio e sódio dependentes de voltagem (MADIO et al., 2019).

1.4 Importância biológica das peptidases

A manutenção de seres vivos, desde suas formas mais simples às mais complexas, é dependente de eventos corriqueiros chamados de proteólise. As peptidases, enzimas capazes de hidrolisar seletivamente ligações peptídicas e aumentar a velocidade de reações, são ferramentas extraordinárias para concretização destes eventos e para a geração eficiente de produtos (ABBENANTE & FAIRLIE, 2005; XU & HUANG, 2020).

Peptidases podem desempenhar o papel de reguladores-chave positivos ou negativos de múltiplos processos biológicos. Como resultado direto de suas ações, estas enzimas influenciam a replicação e transcrição do DNA; proliferação e diferenciação celular; remodelamento, morfogênese e regeneração tecidual; necrose; apoptose; angiogênese; inflamação; digestão; fibrinólise; coagulação

sanguínea; imunidade; autofagia e fertilização, entre outros processos (PAGE & DI CERA, 2008; ARASTU-KAPUR et al., 2008; LÓPEZ-OTÍN; BOND, 2008; XU & HUANG, 2020).

Apesar de comum em sistemas vivos, a proteólise não pode ser chamada de um processo simples. A clivagem de um substrato por determinada enzima gerando um novo C-terminal e N-terminal envolve uma série de pré-requisitos para que este evento ocorra (XU & HUANG, 2020). Entre estes, talvez um dos principais seja o correto posicionamento de aminoácidos na estrutura da peptidase, a fim de formar o sítio catalítico. Serinopeptidases, por exemplo, possuem uma tríade catalítica formada por His, Asp e Ser, tais resíduos ocupam diferentes posições a depender do tipo da enzima.

As peptidases podem estar envolvidas em cascatas, vias e circuitos formados por componentes diversos. Entre estes estão cofatores, inibidores endógenos, substratos e produtos de clivagem que acabam por influenciar a atividade destas enzimas. Quando conectada, esta rede de peptidases e seus reguladores podem definir o potencial proteolítico de células e tecidos (AUF DEM KELLER et al., 2007).

Até o presente, segundo o MEROPS - The Peptidase Database do Instituto Europeu de Bioinformática, mais de um 1,1 milhão de sequências de peptidases já foram elucidadas. Este banco de dados, que leva em consideração a significância estatística nas similaridades entre as sequências de aminoácidos e estruturas de diferentes enzimas proteolíticas, contém informações sobre mais de 4000 peptidases, agrupando-as em famílias e clans (RAWLINGS et al., 2018).

Com base em seu mecanismo de catálise, estas enzimas são divididas em sete classes distintas: aspártica, glutâmica, asparagino-peptidase, cisteína-peptidase, treonina-peptidase, metalopeptidase e serinopeptidase (RAWLINGS et al., 2018; LÓPEZ-OTÍN & BOND, 2008).

Consideradas como o grupo de peptidases funcionalmente mais diverso e abundante, as serinopeptidases abrangem cerca de um terço das enzimas proteolíticas conhecidas. Devido a tal fato, os mecanismos moleculares que garantem a catálise e regulação destas enzimas têm ganhado bastante atenção ao longo dos anos (DI CERA, 2009).

As serinopeptidases são separadas em 13 clans e 40 famílias, podendo ser divididas principalmente em duas categorias com base em sua estrutura: tipo

tripsina (ou quimotripsina) ou tipo subtilisinas. Estas são caracterizadas pela presença de uma tríade catalítica encontrada entre a interface de dois barris β, no caso de serinopeptidases do tipo tripsina; e pela presença de uma dobra em três camadas αβα, em serinopeptidases do tipo subtilisinas. Apesar destas diferenças estruturais, as serinopeptidases apresentam características altamente conservadas como a existência de resíduos catalíticos de serina e histidina mantidos numa orientação geométrica idêntica (DI CERA, 2009, YUN, 2013).

Em humanos, as serinopeptidases desempenham funções fisiológicas importantes, que vão desde a coagulação sanguínea com a participação da trombina e dos fatores VII, IX, X e XII; até a apoptose celular, com a atuação das granzimas. Esta classe de peptidases contribui de tal forma para a saúde, que as mesmas correspondem a 178 das 699 peptidases encontradas em humanos (ABBENANTE & FAIRLIE, 2005; DI CERA, 2009). Devido à intricada relação de peptidases a processos fisiológicos fundamentais, como a angiogênese, digestão, formação de coágulos e remodelação óssea, a modulação da atividade proteolítica destas enzimas vem sendo alvo para o desenvolvimento de medicamentos (WANG, 2001). Até 2001, cerca de 14% das peptidases humanas conhecidas estavam sob investigação farmacêutica (SOUTHAN, 2001). Após 20 anos, a indústria farmacêutica tem apresentado um amplo leque de inibidores de peptidases com as mais diferentes aplicações.

Em bancos de dados públicos como o Drug Bank, mantido pelo Canadian Institutes of Health Research, Alberta Innovates - Health Solutions, e pelo The Metabolomics Innovation Centre, é possível identificar mais de 1800 drogas inibidoras de peptidases que estão sob investigação, experimentação ou que já foram aprovadas até o ano de 2018. São exemplos de inibidores comerciais o Indinavir e Saquinavir que se ligam ao sítio ativo de proteases responsáveis pela clivagem de precursores importantes para a infecção pelo HIV-1, o que resulta na formação de partículas virais imaturas e não infecciosas. O Alfa 1-antitripsina recombinante (rAAT), um inibidor de serinopeptidase sob investigação, capaz de inibir catepsina G, trombina e tripsina; atualmente indicado para o uso tópico em dermatites e psoríase. São ainda exemplos, os inibidores de peptidases disponíveis para o tratamento da Hepatite C (Grazoprevir), da Síndrome coronária aguda (Otamizaban); e da trombose (Proteína C), entre outros (WISHART et al., 2017).

Com a extensa variedade de peptidases existentes e o seu grande potencial em aplicações terapêuticas, a descoberta de agentes que tenham ótima seletividade para peptidases específicas e altos valores de potência são de crucial importância para o alcance de ferramentas farmacêuticas verdadeiramente úteis (LININGTON et al, 2007).

1.5 Inibidores de Serinopeptidases

Apesar de serem cruciais para a manutenção da homeostase em níveis celular e tecidual, as serinopeptidases podem causar sérios danos quando intensamente expressas ou quando presentes em altas concentrações. Tais fatores podem levar ao desencadeamento de patologias como a pancreatite, problemas na cascata de coagulação, desordens neurodegenerativas, doenças cardiovasculares, e até mesmo ao câncer (PESCOSOLIDO et al., 2014; JEDINÁK et al., 2006).

Devido a isto, a procura por inibidores desta classe de peptidases tem sido extensivamente realizada por pesquisadores ao longo do tempo. Como resultado de vários estudos, diversas famílias de inibidores foram descobertas, são exemplos as serpinas, os inibidores do tipo Kunitz e inibidores do tipo Kazal. Até o ano de 2011 estavam descritas cerca de 88 famílias de inibidores de serinopeptidases no MEROPS - The Peptidase Database (LESNER, et al., 2011).

As serpinas constituem uma superfamília de proteínas capazes de inibir serinopeptidases. Estes inibidores são encontrados em animais, bactérias, archaea e vírus, e compartilham uma estrutura terciária conservada composta por 3 folhas β, 8 a 9 α-hélices e um loop central reativo (RCL- do inglês *"Reactive Center Loop*") exposto (GETTINS, 2002; SILVERMAN et al., 2001). A inibição das serinopeptidases se dá pela formação de um complexo covalente entre o sítio ativo das mesmas e o RCL da serpina, que acaba sendo clivado no processo (YE et al., 2001). A serpina passa por uma mudança conformacional irreversível e o sítio catalítico da peptidase torna-se distorcido resultando em sua inativação (GETTINS & OLSON, 2016). Estes inibidores têm massa molecular de aproximadamente 45 kDa e participam da regulação de proteases envolvidas na coagulação sanguínea, ativação do complemento e inflamação (SILVERMAN et al., 2001; GETTINS, 2002).

Outros membros de superfamílias de inibidores de serinopeptidases não relacionados às serpinas são inibidores do tipo Kazal e os inibidores do tipo Kunitz (ENGHILD et al., 1993). Inibidores do tipo Kazal são encontrados em mamíferos, aves e invertebrados, e são caracterizados pela alta similaridade de sua estrutura primária, pela presença de três pontes dissulfeto e resíduos de cisteínas em posições homólogas (RIMPHANITCHAYAKIT & TASSANAKAJON, 2010; LASKOWSKI & KATO, 1980). São inibidores competitivos de serinopeptidases, com um mecanismo de inibição padrão e parecem estar envolvidos com o controle da atividade proteolítica da coagulação (LASKOWSKI & KATO, 1980; VEGA & ALBORES, 2005).

Inibidores do tipo Kunitz são classificados segundo as posições conservadas de seis resíduos de cisteínas formadores de três pontes dissulfeto responsáveis pela estabilidade destes. Estes inibidores podem conter um ou mais domínios capazes de inibir serinopeptidases diferentes, através da ligação destes à peptidase alvo como substratos. Os inibidores do tipo Kunitz de animais são proteínas de baixa massa molecular com aproximadamente 60 resíduos de aminoácidos (ROBERTS et al., 1995).

Particularmente, a inibição da tripsina tem sido utilizada como modelo para a procura por inibidores eficazes e com potencial farmacológico, devido ao fato desta ser o arquétipo para serinopeptidases que participam de importantes processos biológicos e patológicos (RENATUS, 1998). As plantas constituem uma rica fonte de tais inibidores. São exemplos os inibidores SBTI (do inglês *"soybean trypsin inhibitor"*) e SFTI (do inglês *"sunflower trypsin inhibitor"*). Os SBTI, inibidores de tripsina isolados da soja, são um grupo de pequenas moléculas capazes de interagir e inativar enzimas digestivas como tripsina e/ou quimotripsina e podem ser divididos em duas famílias principais: Inibidores do tipo Kunitz (KTi) de 20 kDa e inibidores Bowman-Birk (BBI) de 6 a 21 kDa (GILLMAN et al., 2015). Por outro lado, inibidores isolados da semente do girassol, como SFTI-1, têm sido utilizados como modelos para o desenho de novas drogas. Com 14 resíduos de aminoácidos, rigidez compacta, e estrutura bem definida, o SFTI-1 é considerado um dos inibidores de tripsina mais potentes dentro da família Bowman-Birk (LESNER et al., 2011).

1.6. Anêmonas-do-mar como fontes de inibidores de serinopeptidases

A habilidade de inibidores do tipo Kunitz em ligar eficientemente importantes serinopeptidases como tripsina, quimotripsina, calicreína e plasmina, levou ao amplo estudo da aplicação destas moléculas na medicina. Estes inibidores destacam-se devido à atividade antiproteolítica e antifibrinolítica desempenhadas, contribuindo de forma significativa para a homeostase, seja por inibir proteases liberadas por células inflamatórias ou neoplásicas, ou por atuar diretamente sobre a cascata da coagulação (WAXLER & RABITO, 2003).

Diferentemente de inibidores do tipo Kazal, inibidores do tipo Kunitz são amplamente descritos na literatura como parte do arsenal de toxinas de anêmonas-do-mar (MADIO et al., 2019; PRENTIS et al., 2018). O papel destas moléculas na peçonha de anêmonas não é completamente claro. Acredita-se que inibidores do tipo Kunitz protegem toxinas peptídicas contra a rápida degradação por proteases da presa ou predador; ou que estes podem agir como inibidores de proteases endógenas. Alguns desses inibidores têm sido classificados como toxinas do tipo Kv2, agindo tanto como bloqueadores de canais de potássio dependentes de voltagem, como inibidores de serinopeptidases. A função dupla desempenhada por estas moléculas pode indicar que estas não somente são utilizadas como instrumentos de defesa, mas como toxinas de agressão, responsáveis pela paralização de presas. São exemplos de toxinas Kunitz/Kv2 os AsKC1–AsKC3 da *Anemonia sulcata*, que bloqueiam canais do tipo Kv1.2 e ShPI-1 isolado da *Stichodactyla helianthus* e que liga canais Kv1.1, Kv1.2, e Kv1.6 (HONMA & SHIOMI, 2006; MACRANDER et al., 2015; SCHWEITZ et al., 1995; GARCÍA-FERNÁNDEZ et al., 2016).

Apesar de toxinas de anêmonas estarem agrupadas em famílias bem estabelecidas, incluindo os inibidores do tipo Kunitz, apenas 256 toxinas de anêmonas estão descritas na base de dados ToxProt (JUNGO et al., 2005, acesso em outubro de 2021). Tais toxinas, isoladas de apenas 5% de mais de 1.100 espécies de anêmonas conhecidas, representam apenas uma pequena parcela do que ainda pode ser explorado (PRENTIS et al., 2018; COELHO et al., 2021). Destas toxinas, cerca de 87% pertencem somente a espécies da superfamília Actinoidea, o que destaca a necessidade da investigação das peçonhas de outras

superfamílias de anêmonas, que podem conter peptídeos bioativos interessantes (JUNGO & BAIROCH, 2005; PRENTIS et al., 2018). Um bom exemplo a ser dado é peptídeo bloqueador de canais de potássio como o ShK isolado da anêmona *Stichodactyla helianthus*. Tal peptídeo levou ao desenvolvimento de um análogo (ShK-186) que apresentou ótimo desempenho nos ensaios clínicos de fase 1 e que está prestes a entrar em fase 2 para o tratamento de doenças auto-imunes (PRENTIS et al., 2018).

Como entre os cnidários, ainda é pequeno o número de espécies de anêmonas examinadas quanto ao potencial terapêutico de suas toxinas, aqui propomos a investigação do conteúdo das peçonhas de duas espécies de anêmonas – *Anthopleura cascaia* e *Aulactinia veratra* – ainda não caracterizadas quanto ao arsenal de suas toxinas; e propomos a busca pelo isolamento e caracterização de inibidores de serinopeptidases.

1.7 *Anthopleura cascaia*

O gênero *Anthopleura* possui mais de 50 espécies válidas, frequentemente encontradas no mediolitoral e amplamente distribuídas ao redor do mundo em regiões tropicais e temperadas (DALY & FAUTIN, 2022; DALY et al., 2017; CARLGREN, 1949, DA SILVA, 2009). As espécies deste gênero são diferenciadas morfologicamente pela abundância e distribuição de verrugas adesivas na coluna e pela estrutura e distribuição de seus nematocistos (SMITH & POTTS 1987; HAND, 1955).

No Brasil, existem três espécies registradas do gênero: *A. Krebsi*, *A. varioarmata* e *A. cascaia.* Sendo a última encontrada pelo litoral do país nas regiões Nordeste (PE, BA), Sudeste (RJ, SP, ES) e Sul (PR, SC) (GOMES, 2002).

Anêmonas da espécie *A. cascaia* são encontradas em fendas de recifes e permanecem contraídas durante a maré baixa, com a coluna coberta por cascalhos (Fig 3.B) (DA SILVA, 2009). Os estudos envolvendo esta espécie basicamente envolvem a pesquisa sobre a ecologia trófica e populacional destes animais (DA SILVA, 2009; DE CAPITANI, 2007). Porém, uma nova perspectiva sobre este animal veio a ser dada através do estudo realizado por MADIO (2012), que envolveu a caracterização bioquímica de sua fração neurotóxica. Em tal estudo foram isolados e caracterizados três peptídeos da peçonha da *A. cascaia*:

AcaIII1425 com 3337,4 Da, AcaIII2970 com 4881,7 Da e AcaIII3090 com 4880,5 Da. Tais peptídeos foram testados em diferentes canais Nav e Kv expressos em ovócitos de *Xenopus*, exibindo inibição seletiva para vários subtipos destes canais e consequentemente o potencial biotecnológico de suas moléculas (MADIO, 2012).

Figura 3. Distribuição da *Anthopleura* cascaia no Brasil.

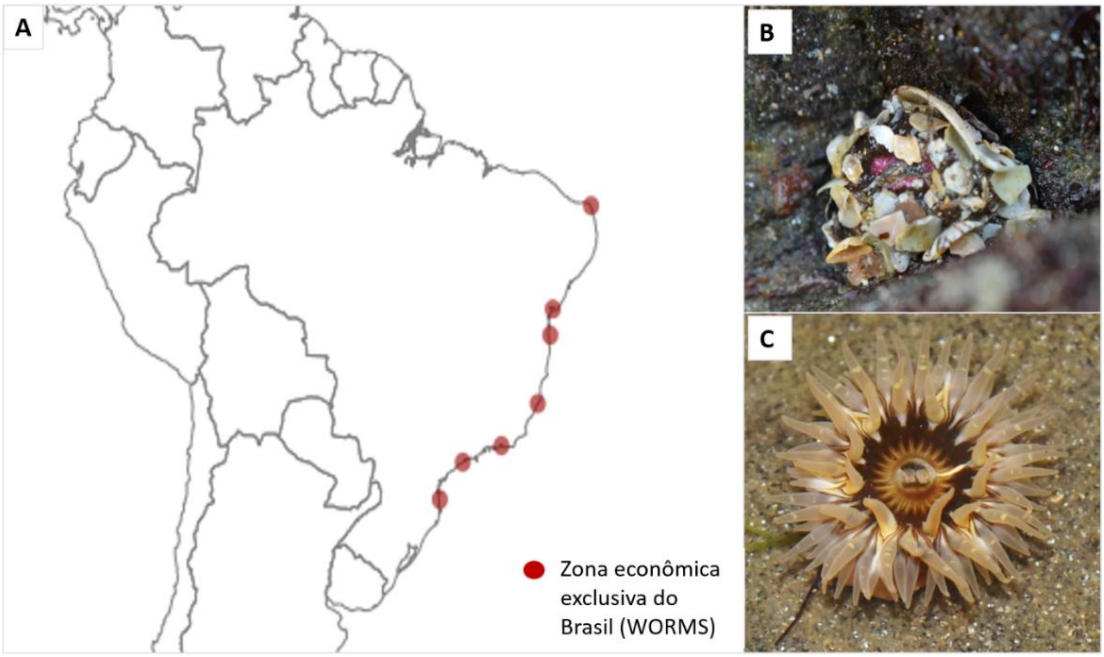

Fonte: A- World Register of Marine Species (WoRMS), 2022. **B e C-** Da Silva, D.L, 2022.

A- Distribuição da *Anthopleura cascaia* no Brasil, de acordo com a plataforma World Register of Marine Species (WoRMS). **B-** Imagem da espécie *A. cascaia* coberta por cascalhos, encontrada durante o período de maré baixa na praia das Cigarras em São Sebastião - SP. **C-** Imagem superior do disco oral e tentáculos da *A. cascaia* coletada e mantida em aquário no Laboratório de Bioquímica do Instituto Butantan.

1.8 Aulactinia veratra

A *Aulactinia veratra*, anêmona-do-mar formalmente registrada entre as espécies de anêmonas presentes na costa da Austrália e Nova Zelândia, está amplamente distribuída no litoral do estado de Queensland. Este cnidário, mesmo estando descrito desde 1846 (Drayton in Dana), está entre as espécies de anêmonas subexploradas quanto ao conteúdo e potencial de suas toxinas (WOLSTENHOLME & WALLACE, 2004; PRENTIS *et al,* 2018). Esta espécie pode

ser encontrada na zona entremarés, em costas rochosas, entre fendas e piscinas naturais. Geralmente apresenta coloração esverdeada ou marrom-avermelhada (menos comum), com disco pedal mais ou menos circular e bem desenvolvido; apresenta coluna com altura em torno de 20 mm, tendo ao longo da estrutura áreas com verrugas adesivas. Os tentáculos desta anêmona apresentam formato cônico com a mesma coloração do restante do corpo do animal (Fig.4) (EDMANDS & FAUTIN, 1991).

Figura 4. Distribuição da *Aulactinia veratra* na Austrália.

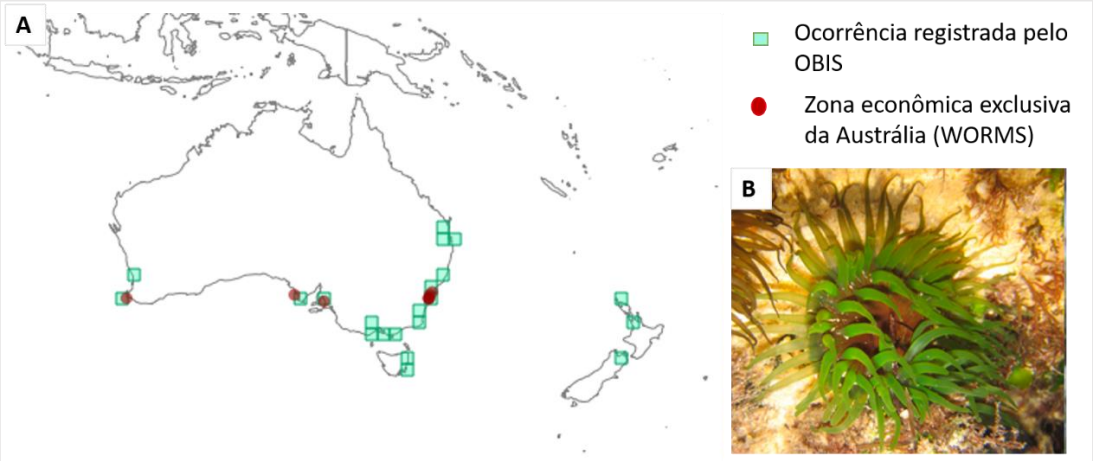

Fonte: A- World Register of Marine Species (WoRMS). **B-** Prentis et al., 2018.

A- Distribuição da *Aulactinia veratra* na Austrália, de acordo com a plataforma World Register of Marine Species (WoRMS) e Ocean Biodiversity Information System (OBIS). **B-** Imagem da espécie *A. veratra*, anêmona amplamente encontrada no litoral sul do estado de Queensland - Austrália.

A presente tese apresenterá a seguir dois principais conjuntos de resultados referentes às anêmonas *Anthopleura cascaia* e *Aulactinia veratra*. O primeiro conjunto – Manuscrito 1 – refere-se à *Anthopleura cascaia*, e pode ser encontrado no ***Apêndice A***. O manuscrito 1, intitulado ´Tracking serine peptidase inhibitors in the venom and tissue of the sea anemone *Anthopleura cascaia*´ compila a abordagem metodológica escolhida para o isolamento e seleção de inibidores de serinopeptidases a partir da peçonha da *A. cascaia* e a localização de tais

moléculas no tecido desta espécie. O segundo principal conjunto de resultados, refere-se à anêmona *Aulactinia veratra;* e pode ser encontrado no Manuscrito 2 do ***Apêndice B***. O segundo manuscrito, intitulado ´*Aulactinia veratra*‘s venom reveals a rich arsenal of toxins containing 18 new cysteine scaffolds: A multiomics analysis´, mostra como a associação de abordagens ômicas permitiu o estudo detalhado da peçonha desta anêmona e a elucidação de novos *scaffolds* de toxinas. Os demais resultados decorrentes da caraterização bioquímica da peçonha da *A. cascaia* e da purificação de inibidores da *A. veratra* estão dispostos na sessão de geral de ***Resultados*** desta tese.

2 OBJETIVOS

Caracterizar bioquimicamente as peçonhas das anêmonas-do-mar *Anthopleura cascaia* e *Aulactinia veratra,* e isolar compostos peptídicos e/ou de baixa massa molecular capazes de inibir a tripsina.

2.1 OBJETIVOS ESPECÍFICOS

- Avaliar o conteúdo molecular da peçonha da *A. cascaia* e da *A. veratra* por espectrometria de massas*;*

- Fracionar a peçonha da *A. cascaia* e a peçonha da *A. veratra* por RP-HPLC e selecionar frações contendo inibidores de serinopeptidases através do monitoramento da inibição da tripsina;

- Estabelecer um método de identificação da atividade da tripsina e inibição desta por MALDI-TOF;

- Identificar a localização tecidual de candidatos a inibidores de serinopeptidases no tecido da *A. veratra* e no tecido da *A. cascaia;*

- Estabelecer um ensaio de detecção da inibição da tripsina no tecido da *A. veratra* utilizando imageamento por espectrometria de massas (MALDI-IMS).

3 MATERIAL E MÉTODOS

3.1 Obtenção da peçonha da *Anthopleura cascaia*

Indivíduos adultos da espécie *A. cascaia* foram coletados manualmente em costões rochosos das praias do Cabelo Gordo e das Cigarras, em São Sebastião, litoral norte do estado de São Paulo. Os indivíduos foram coletados na zona entremarés durante os períodos de maré baixa. Após a coleta, os mesmos foram imediatamente acondicionados em tubos contendo água do mar. Os animais (n=10) foram coletados sob a autorização de n° 72666-1 do SISBIO (Sistema de Autorização e Informação em Biodiversidade). Os exemplares foram levados ao Centro de Biologia Marinha da USP (CEBIMar), onde foram lavados na água-do-mar artificial e logo em seguida imersos em água contendo 0,1% de ácido acético. A solução ácida (aproximadamente 50 mL) foi recuperada, sonicada e liofilizada. Após isso, o conteúdo foi suspenso em água ultrapura e armazenado a -20°C para os ensaios subsequentes.

3.2 Caracterização bioquímica da peçonha da *A. cascaia*

3.2.1 Análise eletroforética da peçonha da ***Anthopleura cascaia*** e proteômica baseada em gel

Amostras da peçonha da *A. cascaia* tiveram os perfis eletroforéticos analisados por SDS-PAGE, em condições redutoras, como descrito por Laemmli (1970). As proteínas foram reveladas pelo uso de Comassie Blue. Foram utilizados os marcadores de massa molecular 'Amersham Low Molecular Weight Calibration Kit for SDS Electrophoresis' (GE Healthcare).

As bandas obtidas no gel foram recortadas para identificação proteômica por espectrometria de massas. As bandas foram imersas em solução descorante contendo 75 mM/L de bicarbonato de amônio e etanol 40%, até completa descoloração. As proteínas foram reduzidas com 10 μL de solução de ditiotreitol (5 mM em 25 mM de bicarbonato de amônio), por 30 minutos a 60°C. E logo após foram alquiladas com 10 μL de iodoacetamida (55 mM em 25 mM de bicarbonato de amônio) por 30 minutos no escuro, e à temperatura ambiente. As bandas foram lavadas com bicarbonato de amônio 25 mM e acetonitrila (100%). O gel foi desidratado pelo uso de acetonitrila (100%) e seco em um sistema de *speed vac*. As proteínas foram digeridas empregando-se 10 μL de tripsina (40 ng/μL em tampão bicarbonato de amônio, 50 mM), e a incubação foi realizada "overnight" a

37°C. A extração dos peptídeos foi realizada pela adição de 20 μL de bicarbonato de amônio 50 mM às bandas, e banho ultra-som por 10 minutos. Logo após foi adicionado 20 μL de acetonitrila/5% TFA (1:1) e a amostra foi colocada novamente em banho ultra-som por mais 10 minutos. O sobrenadante contendo peptídeos foi recuperado, e todo o processo foi repetido por três vezes até completa extração de peptídeos.

3.2.2 Espectrometria de massas

Análises por espectrometria de massas foram realizadas em um espectrômetro ESI-IT-TOF (Ion Trap - Time of Flight - Shimadzu Co., Japão) e Axima Performance MALDI-TOF/TOF (Shimadzu) para determinação da massa molecular, e caracterização de moléculas, em função de cada tipo de análise realizada.

Para o ESI, as amostras foram inseridas no espectrômetro após uma cromatografia de fase reversa, em modo positivo. A voltagem utilizada da interface foi de 4,5 kV e a voltagem do detector, 1,85 kV, com temperatura de 200 °C. A fragmentação foi causada por gás de colisão argônio, com 50% de energia. Os espectros foram obtidos na faixa de 50 a 1600 m/z. No caso de análises MS^2, a seleção do íon precursor ocorreu em uma janela de ± 0,1 Da e a energia de colisão de 50% (unidades arbitrárias). Os espectros foram obtidos da faixa de 50 a 1800 m/z.

Os dados convertidos no formato MGF a partir dos dados brutos obtidos do ESI-IT-TOF MS/MS foram analisados no PEAKS 7.0, com a tolerância de erro de massa de 0.1 Da para o íon precursor e para o íon fragmentado. Foram incluídos na análise as modificações pós traducionais induzidas, a saber carbamidometilação e oxidação, e a enzima (tripsina) usada para gerar a clivagem. Os dados foram analisados em comparação à base de dados UniProt_SwissProt (todas as espécies) e ao bando de dados de Anêmonas. As proteínas identificadas no banco, ou os transcritos gerados foram consultados na base de dados NCBI usando como ferramenta de busca o BLASTx para a identificação de proteínas por similaridade.

As análises por MALDI-TOF foram realizadas de acordo com as condições usuais, empregando-se o modo de aquisição linear, e matrizes como

ácido α-ciano para análise de peptídeos (300 a 3000 m/z) e/ou ácido sinapínico para moléculas de maior massa.

3.3 Purificação de inibidores de serinopeptidases da *A. cascaia*

O fracionamento dos componentes do extrato aquoso de *A. cascaia* foi realizado em um sistema de cromatografia líquida de alta eficiência em fase reversa (RP-HPLC), (20A Prominence, Shimadzu Co. Kyoto, Japão). O perfil cromatográfico com distribuição de picos homogênea ao longo de um gradiente linear, foi obtido através do uso da coluna octadecil (C18). A eluição dos componentes a partir da fase estacionária da coluna foi monitorada através do detector Shimadzu SPD-M20A PDA, na faixa de 200 a 500 nm, e o comprimento de onda a 214 e 280 nm foram escolhidos como ideais para o monitoramento durante o fracionamento.

O fracionamento inicial do extrato foi conduzido em gradiente, onde inicialmente foi testada a condição 0 a 100% de B em 30 minutos, a um fluxo de 1mL/min. Foram utilizados os solventes A composto por ága ultrapura a 0,1% ácido acético e B composto por 90% acetonitrila e 0,1% ácido acético. Para fracionamentos posteriores, foram otimizadas as condições de separação de moléculas ao longo do gradiente. Para o fracionamento da F3 foi escolhida a condição de 5 a 40% de B em 40 min, e para o fracionamento da F4 foi escolhida a condição 0-45% de B em 40 min. As frações da *A. cascaia* que apresentaram inibição foram refracionadas usando o gradiente de 5 a 60% de B. Para o fracionamento da F3.7 e F3.8 foi usada a condição de 5 a 60% de B em 35 minutos.

3.4 Identificação da inibição da atividade enzimática da tripsina por frações da *A. cascaia*

A determinação da atividade da tripsina foi realizada com a utilização de Cloridrato de N-Alfa-CBZ-L-Arginina-7-Amido-4-Metilcumarina (Z-L-ARG-MCA) como substrato, dissolvido em DMSO e diluído em tampão Tris-HCl 0,1 M pH 8,5. Uma vez comprovada que a tripsina estava ativa, foram avaliados os efeitos de inibição da(s) molécula(s) presentes nas frações do extrato aquoso sobre a hidrólise de Z-L-ARG-MCA. Após a padronização das condições ótimas de ensaio (tempo de leitura e saturação da enzima com o substrato), 15 µL das frações candidatas foram incubados com a tripsina (40 ng/µL) (1:1) por 30 min. Após este período, 125µL da

solução de substrato a 0,1 mM foi adicionada às amostras. Os ensaios enzimáticos foram realizados a 30°C e a fluorescência do produto formado desta reação foi medida em Spectrofluorimetro Gemini (Molecular Devices), λex 330 nm, λem 430 nm. A quantificação da atividade inibitória presente nas frações foi realizada pela determinação da porcentagem de inibição em relação às atividades da amostra controle, composta de enzima e substrato. Todos os ensaios foram realizados com amostras em duplicata e foram avaliadas as médias de fluorescência. Os valores negativos de fluorescência foram igualados a 0.

3.5 Obtenção da peçonha da *Aulactinia veratra*

Exemplares da espécie *A. veratra* mantidos em água marinha artificial no aquário da School of Earth, Environmental and Biological Sciences, Queensland University of Technology (QUT), foram coletados e submetidos à eletroestimulação (1V) para a extração da peçonha. Os animais (n= 4) foram eletroestimulados individualmente a cada 7 dias por 4 semanas. A peçonha total obtida em água marinha artificial, foi mantida a -80°C até ser liofilizada. Após a liofilização, a peçonha foi suspensa em água ultrapura (70mL) e centrifugada a 7000 rcf por 30 minutos a fim de separar a fração solúvel da fração precipitada. Ambas as frações foram dialisadas usando tubos para diálise (Pur-A-lyzer Mega Dialysis- 1kDa cut-off) e água ultrapura sob agitação (250 rpm) e temperatura (5°C) constantes. A peçonha foi então recuperada, liofilizada e armazenada a -20°C para análises subsequentes.

3.6 Caracterização bioquímica da peçonha da *Aulactinia veratra*

3.6.1 Análise eletroforética da peçonha

As frações solúvel e precipitada da peçonha tiveram os perfis eletroforéticos elucidados por SDS-PAGE, em condições redutoras, como descrito por Laemmli (1970). As proteínas foram reveladas pelo uso de Comassie Blue (MORRISEY, 1980). Foram utilizados os marcadores de massa molecular ‘Novex Sharp Pre-Stained Protein Standard’ e géis Bolt™ 4- 12%, Bis-Tris, 1.0 mm da Invitrogen – Thermo Fisher Scientific.

3.6.2 Perfil da fração solúvel da peçonha da A. veratra em HPLC

O fracionamento da fração solúvel da peçonha foi realizado em um sistema de cromatografia líquida de alta eficiência (HPLC) Agilent 1100 Series, usando o software Chem Station. O perfil da peçonha foi obtido por cromatografia de fase reversa através do uso da coluna octadecil (Gemini 3µm NX-C18, 110 Å LC-Column 250 x 4.6 mm). A eluição dos componentes a partir da fase estacionária da coluna foi monitorada através do detector DAD (Diod Array Detector) G1316A da Agilent, sendo utilizados os comprimentos de onda 214 e 280 nm para o monitoramento dos picos durante o fracionamento.

O fracionamento foi conduzido em gradiente na condição de 5 a 95% de B em 40 minutos, sendo o solvente A composto de 0,05% TFA (ácido trifluoroacético) e solvente B composto de 90% acetonitrila e 0,05% TFA.

*3.6.3 Análise proteômica das frações solúvel e precipitada da peçonha da **A. Veratra***

3.6.3.1 Digestão em solução

Cerca de 10 µL (contendo entre 0,7 a 3,6 µg de proteínas) da fração precipitada e das subfrações F1 a F11 da fração solúvel foram colocadas em microtubos e a estas foram adicionados 8 µL de Bicarbonato de Amônio 100mM contendo 10% de Acetonitrila. As proteínas foram reduzidas pela adição de 1µL de ditiotreitol 50 mM, e aquecidas a 70°C por 10 minutos. Em seguida foram alquiladas pela adição de 1µL de iodoacetamida 100 mM e incubadas a 30°C por 30 minutos no escuro. As moléculas foram digeridas pela adição de 2uL (250 ng/µL) de tripsina (Trypsin from porcine pâncreas - Proteomics Grade, BioReagent, Dimethylated – SIGMA-ALDRICH), e as amostras foram incubadas “overnight” a 30°C. As amostras foram concentradas em sistema de *speed vac* por 10 min a 45 °C.

3.6.3.2 Espectrometria de massas e Identificação de proteínas

As frações digeridas foram analisadas por LC-MS/MS num sistema uHPLC (Japan) Shimadzu Nexera acoplado ao espectrômetro de massas Triple TOF 5600

(ABSCIEX, Canada) equipado com fonte de ionização com duplo eletrospray. Solventes A composto por 0.1% de ácido fórmico, e B contendo 90% acetonitrila e 0,1% de ácido fórmico, foram utilizados. 5µL de cada fração foi injetado em uma coluna Zorbax C18 1.8µm, 2.1mm x 100mm (Agilent) a 200µL/min. Para a eluição de peptídeos foi utilizado um gradiente linear de 1-40% de solvente B por 32 min a um fluxo de 200 µL/minuto, seguido por um gradiente de 40% a 98% do solvente B em 6 min. Cerca de 98% do solvente B foi utilizado por 3 min para lavar a coluna e a coluna foi reequilibrada com 1% do solvente B para a injeção da amostra subsequente.

Foi utilizada uma voltagem de 5.500 V no ionspray e potencial de decomposição (DP) de 100V, fluxo de gás 25, gás nebulizador 1 (GS1) 50, GS2 a 60, a interface aquecida a 150°C e o aquecedor turbo a 500°C. O espectrômetro de massas adquiriu um “scan” completo de dados TOF-MS por 200ms seguido por 10 a 200ms de completo “scan” dos íons-produto em modo IDA (Information Dependant Acquisition). O “scan” completo de dados TOF-MS foi adquirido na faixa de 300-2000 m/z e na faixa de 100-1800 m/z para o íon produto ms/ms. Os íons observados no TOF-MS excedendo o limite de 100 e com estado de carga de +2 to +5 foram considerados para a aquisição do íon produto e o espectro MS/MS resultou nos 10 íons mais intensos.

Os dados foram adquiridos e processados através do uso do Protein Pilot 5.0 software (ABSCIEX, Canada), onde foram utilizados os seguintes parâmetros na construção do método de análise ‘Paragon thorough’: 1. Modificações pós traducionais induzidas, a saber carbamidometilação e oxidação, 2. Enzima utilizada para gerar clivagem (Tripsina); 3. Substituição de aminoácidos; 4. Unused Proscore (Conf) > 0.05 (10%) e 5. Análise de taxa de falsas descobertas. Para realizar esta análise foi utilizado o banco de dados do Transcriptoma da espécie *Aulactinia veratra*, gentilmente cedido pelo pesquisador Peter Prentis da Queensland University of Technology. A sequência de nucleotídeos de cada transcrito foi traduzida para sequências de aminoácidos através do uso da plataforma GALAXY Australia e este foi utilizado como banco de dados. Após a obtenção da identidade dos transcritos, as sequências de peptídeos e proteínas foram submetidas à base de dados do NCBI usando como ferramenta de busca o BLASTp para a identificação de proteínas por similaridade, e as categorias de ‘non-reduntant

protein sequences' como banco de dados, e 'Sea Anemone Taxid 6103' como organismo.

As proteínas e peptídeos identificados foram classificados em superfamílias de acordo com os domínios conservados identificados nos 'hits' do 'Sea Anemone Taxid' do NCBI. As moléculas do proteoma classificadas como pertencentes à alguma classe de toxinas de anêmonas-do-mar, tiveram suas sequências submetidas à plataforma InterPro - Classificação de famílias de proteínas- do European Bioinformatics Institute (MITCHELL et al., 2019), para a confirmação da existência de domínios que caracterizam a devida classe de toxina.

Para o alinhamento de sequências de aminoácidos das toxinas identificadas e de transcritos semelhantes, foi utilizada a função MAFFT (Multiple alignment program for amino acid or nucleotide sequences) e método de acurácia L-INS-i do Galaxy Version 7.221.3 (AFGAN et al., 2018). O software JALVIEW (WATERHOUSE et al., 2009) também foi aplicado para a finalização do alinhamento de resíduos de aminoácidos que formam os domínios característicos destas toxinas.

3.7 Purificação de inibidores de serinopeptidases da *A. veratra*

O fracionamento da fração solúvel da peçonha foi realizado em um sistema de cromatografia líquida de alta eficiência (HPLC) Agilent 1100 Series, usando o software Chem Station. O perfil da peçonha foi obtido por cromatografia de fase reversa através do uso da coluna octadecil (Gemini 3µm NX-C18, 110 Å LC-Column 250 x 4.6 mm). A eluição dos componentes a partir da fase estacionária da coluna foi monitorada através do detector DAD (Diod Array Detector) G1316A da Agilent, sendo utilizados os comprimentos de onda 214 e 280 nm para o monitoramento dos picos durante o fracionamento.

O fracionamento foi conduzido em gradiente na condição de 5 a 50% de B em 40 minutos, sendo o solvente A composto de 0,05% TFA (ácido trifluoroacético) e solvente B composto de 90% acetonitrila e 0,05% TFA.

Para o estabelecimento da purificação de inibidores de serinopeptidases, a atividade inibitória das frações F1 a F11 foi testada. As frações que apresentaram inibição da tripsina foram refracionadas otimizando-se as condições de separação

de moléculas ao longo do gradiente. Foram utilizadas a coluna Onyx™ Monolithic C18, 100 x 3 mm; solvente A composto por 0,05% de TFA e solvente B composto por 90% acetonitrila, 0,05% TFA e um fluxo de 3 mL/min. Para o fracionamento da F4 foi escolhido o gradiente de 5-35% de B em 30 min. Para o fracionamento da F6 e F7 foi escolhida a condição 10-35% de B em 30 min, e para o fracionamento da F10 foi escolhida a condição 20-45% de B em 30 min.

Para o fracionamento seguinte, as frações contendo atividade inibitória foram submetidas à cromatografia de troca iônica usando a coluna PolyCATWAX™ 200 x 4,6 mm, 5µm, 1000 Å. Para a eluição de moléculas, foi utilizado um gradiente linear de 0-70% de solvente B por 35 min a um fluxo de 1mL/minuto, seguido por um gradiente de 70% a 80% de B em 5 min e 80 a 90% de B em 5 min. A concentração do solvente B foi mantida em 90% por 10 minutos e a coluna foi reequilibrada a 0% de B por 15 minutos entre as injeções de diferentes amostras. Os solventes A e B com pH 5,6 foram compostos por Acetato de Amônio 10 mM e 800 mM, respectivamente. O monitoramento da eluição de moléculas foi realizado a um comprimento de onda de 280 nm.

3.8 Identificação da inibição da atividade enzimática da tripsina por frações da peçonha da *A. veratra* utilizando MALDI-TOF

Para a identificação da inibição da atividade da tripsina foi necessário o estabelecimento de um ensaio onde a geração do produto a partir de um substrato clivado pela enzima pudesse ser avaliada pelo uso da espectrometria de massas. Para tanto, o Benzoyl-L-phenylalanyl-L-valyl-L-arginine-p-nitroanilide (Bz-FVR-pNA), cuja massa molecular corresponde a 644,7 g/mol, foi utilizado como substrato. Este substrato teve seu perfil de m/z (massa/carga) avaliado no espectrômetro de massas MALDI-TOF/TOF Ultraflex III (Bruker Daltonics). Uma vez estabelecido este perfil, foi testada a incubação da tripsina nas concentrações de 50 ng/µL, 25 ng/µL e 10 ng/µL em Bicarbonato de Amônio 25 mM com diferentes concentrações do substrato (50 µM/µL, 25 µM/µL e 10 µM/µL) e avaliada a geração de produtos Bz-FVR e pNA resultantes da clivagem no C-terminal da arginina do Bz-FVR-pNA. As massas dos produtos foram detectadas pela mudança de intensidade na m/z do íon gerado apenas no grupo teste contendo substrato (S) e tripsina (T) (1µL S + 1µL T + 8µL de água ultrapura). Como controle, amostras

contendo apenas substrato (1µL S + 9µL de água ultrapura) ou apenas tripsina (1µL T + 9µL de água ultrapura) foram comparadas aos grupos testados. As amostras foram incubadas por 40 minutos a 37 °C, e uma alíquota contendo 1uL desta incubação foi colocada em placas de MALDI-TOF nos tempos 0 e 40 min para a comparação da intensidade dos produtos no início da exposição do substrato a tripsina e após 40 min de reação. O software ChemDraw da PerkinElmer Informatics foi utilizado para a simulação da clivagem do substrato no C-terminal da arginina como forma de confirmar as massas detectadas pela espectrometria de massas.

Uma vez estabelecida a m/z do substrato e seu respectivo produto, foram realizados ensaios de inibição da tripsina pelas frações da peçonha da *A. veratra*. Para tanto, foi escolhida a concentração de 50ng/µL da enzima para a realização dos ensaios de inibição. 1 µL das frações candidatas foram adicionados a 1µL da tripsina em HCl 1mM diluída em 2µL de Bicarbonato de amônio, e 5µL de água ultrapura. A incubação se deu a 37°C por 30 min. Após este período, o substrato (1µL contendo 50µM/µL) foi adicionado à amostra, totalizando um volume de 10µL/tubo. A incubação foi realizada a 37°C em termobloco por 40 min. A intensidade do produto da reação foi avaliada ao 0 min e aos 40 min de reação por espectrometria de massas. Os ensaios iniciais de inibição correspondendo às fracões F1 a F11 foram realizados em unicata e por um período de 30 minutos. Os ensaios posteriores foram realizados com amostras em duplicata e foram avaliadas as médias de intensidade do produto e substrato.

As análises por MALDI-TOF foram realizadas de acordo com as condições usuais, empregando-se o modo de aquisição linear e a matriz ácido α-ciano para análise de peptídeos (180 a 5000 m/z).

3.9 Identificação da inibição da tripsina em tecido utilizando MALDI-IMS

Um espécime da *A. veratra* foi colocado em placa de petri e cortado longitudinalmente com o uso de um bisturi estéril. O tecido foi submerso em fixador RCL2 e etanol 100% (3:5) v/v, e fixado por 16 h a 8°C. Para a etapa de desidratação, o fixador foi removido e o tecido foi submetido à desidratação gradual

pelo uso de soluções de etanol a 60%, 70%, 80%, 90% e 100% com intervalos de 30 minutos entre cada concentração. O tecido foi embebido em parafina e estocado a -20°C até o momento do uso.

Para o preparo da amostra para MALDI-IMS, o tecido foi seccionado em micrótomo e foram obtidos cortes com 7µm de espessura. Os tecidos foram colocados em lâminas cobertas por Indium Tin Oxide (ITO glass slides- Bruker Daltonics), aquecidos a 58°C em termobloco, e tiveram a parafina removida pelo uso de xileno 100%.

O equipamento ImagePrep da Bruker Daltonics foi utilizado para a pulverização dos componentes do ensaio enzimático e da matriz sobre a amostra. Tecidos pertencentes aos grupos experimentais foram pulverizados com 1mL de Bicarbonato de Amônio (BA) 25 mM, até completa umidificação da amostra. Em seguida os tecidos foram pulverizados com 600 µL de substrato (0,5, 0,25 ou 0,1 µM/µL), e finalmente pulverizados com 1mL de tripsina 50 ng/µL. Para as pulverizações de BA e substrato, foi utilizado o método de 30 ciclos, intensidade de 30%, modulação de 15%, incubação de 30 seg e ‘drytime’ de 20 seg. Para a pulverização da tripsina, foram utilizados 40 ciclos, intensidade de 55%, modulação de 15%, incubação de 30 s e ‘drytime’ de 15s. Os grupos controles foram pulverizados apenas com BA; BA e substrato ou BA e tripsina. A fim de ser mantida a umidade do tecido durante a incubação, as lâminas foram colocadas em placas de petri vedadas com parafilme e os tecidos foram incubados por 2 h a 37°C em estufa. Após o período de incubação, os tecidos foram pulverizados com a matriz ácido alfa-ciano (105 mg de ácido alfa-ciano, 8 mL acetonitrila, 7 mL de água ultrapura e 30 µL de TFA). Imagens dos tecidos foram adquiridas em microscópio óptico antes e após a deposição dos componentes citados acima. As lâminas foram colocadas em placas adaptadoras para imageamento, a saber Bruker Daltonics MTP Slide Adapter II e inseridas no espectrômetro de massas MALDI-TOF/TOF Ultraflex III (Bruker Daltonics).

Os softwares Flex imaging e Flex Control foram utilizados para o demarcamento de pontos correspondentes no tecido e na imagem, para possibilitar a sobreposição da localização dos íons adquiridos na imagem. Foi utilizado o modo de aquisição linear (480 a 15000 m/z), 400 ‘shots’, Frequência de 200, intensidade

do laser a 71% e 100 µm de distância entre os pontos adquiridos. A aquisição do espectro de massas ocorreu dentro de regiões de interesse envolvendo os tentáculos, mesentério e disco basal da anêmona.

Para a identificação da distribuição dos inibidores do tipo Kunitz e Kazal no tecido da *A. veratra,* as sequências dos transcritos correspondentes às moléculas identificadas no proteoma foram utilizadas para a remoção do peptídeo sinal e propeptídeo. A previsão da massa molecular foi feita através do uso da plataforma ExPASy - Compute pI/Mw tool (GASTEIGER et al, 2003). As plataformas Signal P-5 e InterPro foram utilizadas para a identificação do peptídeo sinal. O sítio de clivagem do propeptídeo foram identificados com base no trabalho publicado por Kozlov e Grishin, 2007.

4 RESULTADOS

4.1 Caracterização bioquímica da peçonha da *A. cascaia*

Na primeira fase de estudos foi realizada a investigação da composição molecular da peçonha da *A. cascaia* (Fig 5.A), a partir do perfil de massas moleculares obtidas por SDS-PAGE, ESI-IT-TOF/MS-MS e MALDI-TOF. Em análise prévia por eletroforese foi revelado que estas anêmonas possuem em sua composição proteínas com massas moleculares que variam de 14 a 97 kDa, presentes tanto na fase sobrenadante quanto na fase precipitada da peçonha (Fig 5.B). A análise proteômica baseada em gel, em ESI-IT-TOF/MS-MS revelou que a fase sobrenadante da peçonha da *A. cascaia* possui uma ampla variedade de proteínas, relacionadas tanto a estrutura e metabolismo celular, quanto ao arsenal de toxinas destes animais. Foram identificadas um total de 20 proteínas, das quais apenas três apresentaram similaridade à toxinas: uma naterina exibindo 64% de identidade com natterin-4 de *Exaiptasia pallida*; uma PLA2 com 56% de identidade com a Fosfolipase A2 da *Exaiptasia pallida* e uma citolisina, com 100% de identidade com a *Delta-actitoxina AaS1a* da *Anthopleura asiatica* (Tabela 1).

Figura 5. Análise da peçonha de *Anthopleura cascaia* por cromatografia reversa (RP-HPLC) e SDS-PAGE.

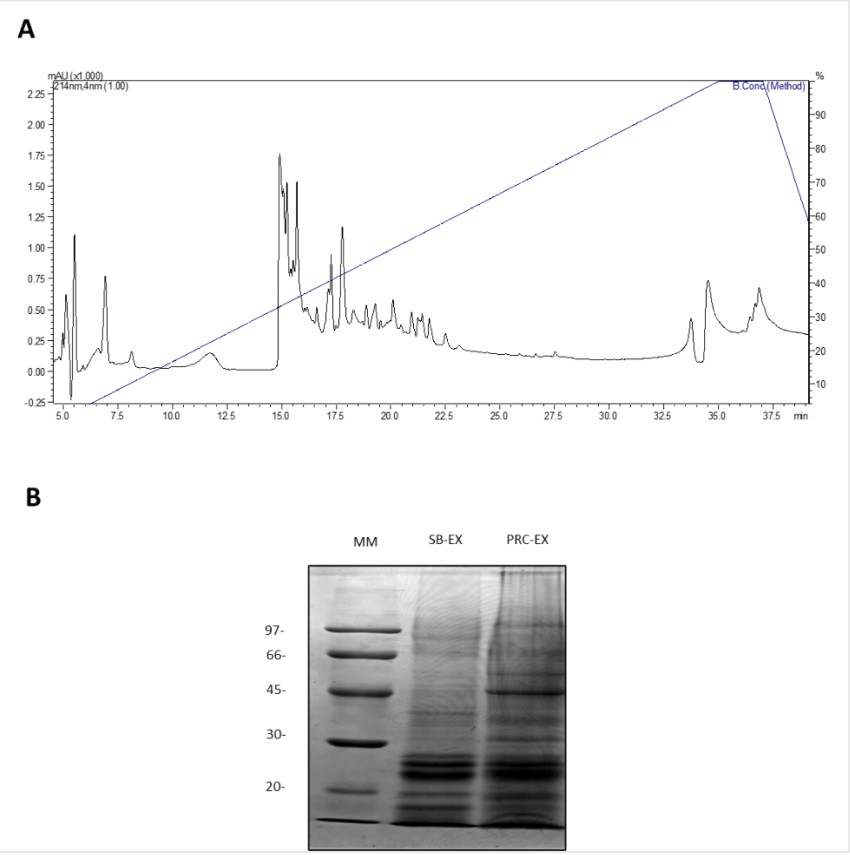

A- Perfil cromatográfico da peçonha de *A. cascaia*. A peçonha foi submetida à separação em RP-HPLC, usando coluna C18. O cromatograma mostra a absorbância de moléculas no comprimento de onda de 214 nm, ao longo do gradiente de 0 a 100% de B em 30 min. **B- Análise por SDS-PAGE da peçonha de *A. cascaia*.** Amostras (20 µL) do sobrenadante da peçonha (SB-EX) e precipitado (PRC-EX) foram submetidas à eletroforese por SDS-PAGE (12,5%), sob condições redutoras, e o gel corado com azul de Comassie. O gel mostra a distribuição de proteínas (bandas) encontradas.

Tabela 1. Proteoma da peçonha da *Anthopleura cascaia*. A tabela mostra os transcritos identificados no PEAKS 7 (banco *Anemona*) e as proteínas equivalentes identificadas no BLASTx. As proteínas C5NSL2/ACTP1 ANTAS e P62794/H4_URECA destacadas em azul foram diretamente identificadas pelo PEAKS 7 (banco *All species*) e confirmadas pelo BLASTp.

	PEAKS					BLASTx				
GEL	Código	-10 lgP	Cobertura (%)	Peptídeos identificados	Massa média (Da)	Proteína/ espécie	SuperFamília	E-value	Por identidade	Código de referência
	BCSc65355_g1_i2	50.41	4	3	143868	oncoprotein-induced transcript 3-like protein [*Anthopleura elegantissima*]	Zona pellucida	4E-62	85.19%	ABD04169.1
	BCGc23665_g1_i1	50.41	4	3	170240	oncoprotein-induced transcript 3-like protein [*Anthopleura elegantissima*]	Zona pellucida	4E-62	85.19%	ABD04169.1
BANDA 1	ABEcomp48292_c0_seq1	31.71	7	1	32069	ZP domain-containing protein [Exaiptasia pallida]	Zona pellucida	2E-41	61.26%	XP_020898845.1
BANDA 2	BCSc70892_g1_i3	92.56	5	5	186430	ZP domain-containing protein [*Exaiptasia pallida*]	Zona pellucida	3E-124	62.46%	XP_020898845.1
	ABEcomp48292_c0_seq1	50.63	19	3	32069	ZP domain-containing protein [*Exaiptasia pallida*]	Zona pellucida	2,00E-41	61,26%	XP_020898845.1
BANDA 3	BCSc70892_g1_i3	48.80	3	3	186430	ZP domain-containing protein [*Exaiptasia pallida*]	Zona pellucida	3E-124	62.46%	XP_020898845.1
BANDA 4	BCSc75725_g4_i5	30.25	1	2	313.655	lutropin-choriogonadotropic hormone receptor-like [*Exaiptasia pallida*]	7tm_GPCRs	2E-175	58,93%	XP_020892853.1
BANDA 5	ABEcomp1742_c0_seq2	55.69	8	2	81863	Zinc finger CCCH domain-containing protein 13 isoform X4 *Exaiptasia pallida*	COG1340	2,00E-74	84,57%	XP_028516639.1
BANDA 6	BCSc75705_g1_i6	29.71	3	1	64155	LOW QUALITY PROTEIN: stress response protein NST1-like (*Exaiptasia pallida*)		6,00E-04	53.17%	XP_020916604.1
	BCGc23186_g1_i1	61.06	8	3	65880	hypothetical protein [*Photorhabdus australis*]	Fascin-like	8.6E-13	32%	WP_036768483.1
	BCGc37493_g1_i2	37.48	0	2	507781	Basic phospholipase A2 myotoxin III [*Exaiptasia pallida*]	PTZ00121	5.2e-84	56.52%	KXJ24237.1
	BCSc79164_g1_i1	33.60	0	2	495209	FH1/FH2 domain-containing protein 1 isoform X1 [*Exaiptasia pallida*]		0	86.00%	XP_020894393.1
	BCGc68578_g1_i1	33.43	5	2	65491	Collagen alpha-1(XVII) chain [*Exaiptasia pallida*]		0.18	38.24%	KXJ20697.1
BANDA 7	C5NSL2|ACTP1_ANTAS	32.27	4	1	23315	DELTA-actitoxin-Aas1a OS=*Anthopleura asiatica*	Anemone_cytotox	2E-152	100.00%	C5NSL2.1
	ABEcomp2688_c0_seq1	57.47	7	2	59507	natterin-4 [*Exaiptasia pallida*]	DUF3421	2E-81	63.96%	XP_020902255.2
	BCGc31161_g1_i2	51.33	19	3	40873	copper/zinc superoxide dismutase-like protein [*Anthopleura elegantissima*]	Cu-Zn_superoxidoDismutase	1E-38	91.49%	ABD04189.1
BANDA 8	BCGc32404_g1_i1	41.63	4	2	85710	natterin-4 [*Exaiptasia pallida*]	DUF3421	3E-88	66.50%	XP_020902255.2
	BCGc39910_g2_i8	52.57	4	4	254701	hypothetical protein NEMVEDRAFT_v1g155159 [*Nematostella vectensis*]	H4	2E-44	100%	XP_001618258.1
	ABEcomp33947_c0_seq1	46.06	10	1	33707	Cysteine and glycine-rich protein 2 [*Exaiptasia pallida*]	LIM	2E-21	82.86%	KXJ07672.1
	BCGc20108_g1_i1	32.30	2	2	160422	predicted protein [*Nematostella vectensis*]	H2A	5E-61	100%	XP_001638352.1
	BCSc55374_g1_i1	31.26	6	1	35177	Cell surface glycoprotein 1 [*Exaiptasia pallida*]	Gal_lectin	0,0005	30.85%	KXJ29594.1
BANDA 9	P62794|H4_URECA	57.65	39%	4	11367	Histone H4 OS=*Urechis caupo*	H4			

4.2 Purificação de inibidores de serinopeptidases a partir da peçonha da *Aulactinia veratra*

No caso da *A. veratra,* a seleção de inibidores a partir das frações foi realizada com base na inibição da tripsina através de ensaios enzimáticos, onde a detecção da atividade enzimática foi realizada por MALDI-TOF.

Para o estabelecimento inicial deste ensaio enzimático, foi identificada a massa/carga do substrato Bz-FVR-pNA, sendo esta correspondente a 644 m/z (Fig6.B). Quando incubado com a tripsina, serinopeptidase que cliva substratos no C-terminal de resíduos de arginina ou lisina, foi detectado o claro aumento de intensidade do produto 523 m/z, em comparação aos grupos do tempo 0 e grupos controle com apenas tripsina (T) ou apenas substrato (S) em ambos os tempos de reação analisados, a saber T0 min e T40 min (Fig. 6A). Aqui é importante salientar que apesar da m/z do produto ser detectada no modo linear em amostras controle, o aumento de intensidade da m/z após 40 min de reação foi apenas identificado pela incubação do substrato com tripsina (S+T), indicando o consumo do substrato após os 40 min de reação (Fig. 6A). A figura 6.A mostra o resultado das incubações de 50 ng/µL da tripsina com 25µM/µL do substrato. Na otimização deste ensaio foi possível a identificação da atividade da tripsina em todas as condições testadas quando considerada a relação da concentração de substrato *versus* enzima (dados não mostrados).

A simulação de clivagem do substrato Bz-FVR-pNA é demostrada na figura 7. Esta simulação obtida a partir do software ChemDraw Professional mostra a geração de dois produtos possíveis, um de 523 m/z (produto 1), confirmado pelos resultados experimentais na figura 6A, e outro de 137 m/z (produto 2). A detecção do produto 2 não foi possível devido à supressão de sinal gerada pela matriz, que apresenta a ionização de componentes nesta faixa de m/z. Devido a isto, o produto correspondente à 523 m/z foi utilizado para o monitoramento da atividade enzimática da tripsina em ensaios posteriores.

A figura 6.C mostra a distribuição do íon 523 m/z quando avaliado em modo reflectron. Apesar deste modo de análise no MALDI-TOF possibilitar a diferenciação de massas/cargas semelhantes, geralmente agrupadas em um pico no modo linear, o mesmo apresenta forte ionização de componentes de menor massa, não sendo possível uma detecção clara do aumento do produto gerado pela

tripsina. Assim, para os nossos ensaios de detecção de inibição da tripsina, o modo de aquisição linear foi utilizado.

Figura 6. Análise por MALDI-TOF da atividade da tripsina.

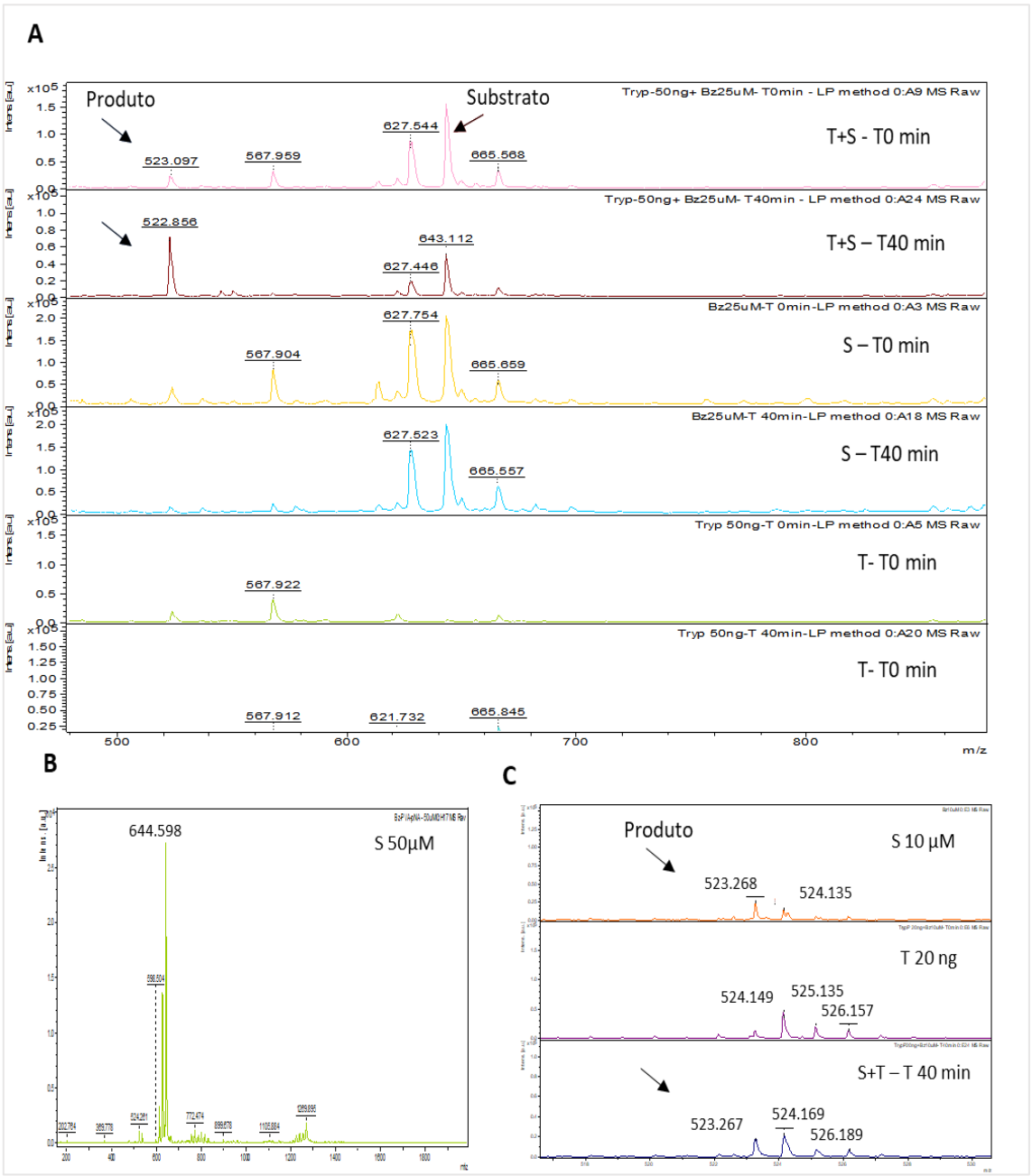

A- Tripsina na concentração de 50 ng/µl foi incubada com o substrato (50µM/µl) e a geração do produto (523 m/z) em relação ao substrato (644 m/z) foi acompanhada por modo de aquisição linear. O espectro de massas foi adquirido ao 0 min e aos 40 min de reação. É possível identificar o aumento da intensidade do 523 m/z após 40 min de reação. **B**- Perfil do substrato Bz-FVR-pNA na concentração de 50 µM/µL por MALDI-TOF**. C-** Perfil de m/z do produto por modo de aquisição reflectron. Em C é possível identificar a distribuição de m/z (vários picos) do produto, que no modo linear foi adquirido como único pico (em A). Grupos controle: Branco (S + tampão); e Controle positivo (T + S), onde S= Substrato e T= Tripsina.

Figura 7. Simulação de clivagem do substrato Bz-FVR-pNA pela tripsina.

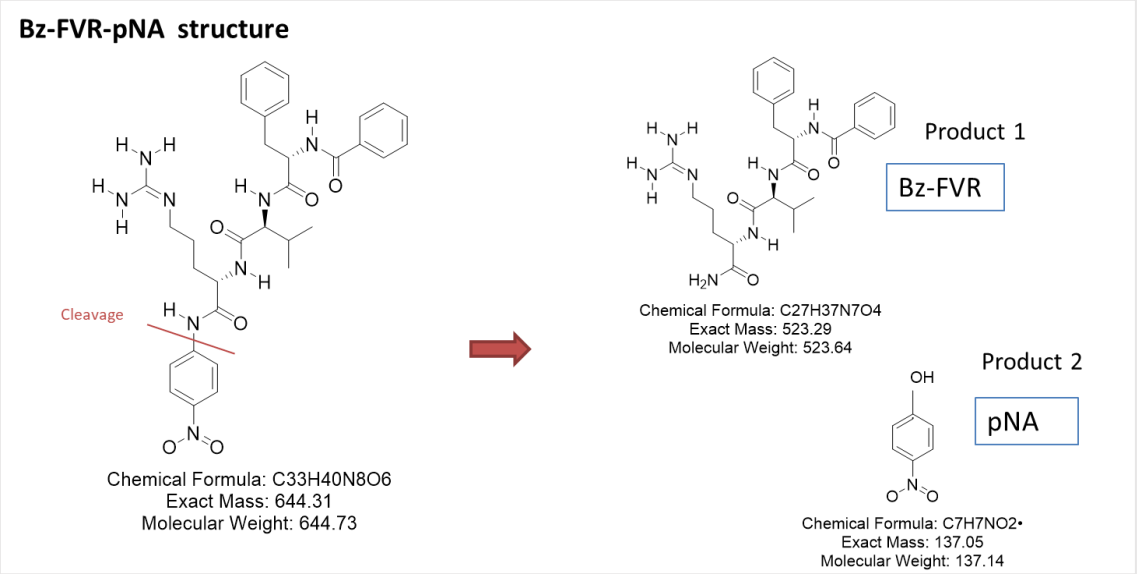

A figura 7 mostra o local de clivagem do Bz-FVR-pNA pela tripsina, enzima que cliva substratos no C-terminal de resíduos de arginina (R) ou lisina (K); e a consequente geração dos produtos 523 m/z e 137 m/z, através da simulação pelo software ChemDraw Professional.

Apesar da análise por MALDI-TOF aqui realizada não possibilitar a aquisição em tempo real da geração de produto a partir da clivagem do substrato, como nos ensaios de cinética enzimática realizados no isolamento de inibidores da *A. cascaia*, a mesma torna possível a utilização de pouquíssima amostra (1 a 2 µl) para a detecção de inibidores na fração. Esta é uma vantagem apresentada pela técnica sobre ensaios realizados em placas que demandam um volume bem maior de amostra. Outra vantagem é a não dependência de variações ou comprometimento do fluoróforo com relação a ensaios cuja detecção é realizada por fluorescência.

Uma vez estabelecido o método de avaliação da atividade da tripsina, frações da peçonha da *A. veratra* foram incubadas previamente com esta enzima e a posterior adição do substrato à amostra foi realizada. A leitura da ionização do produto da amostra em relação ao substrato foi feita aos 0 min e 40 min de reação. A inibição da tripsina foi identificada nas frações F4, F6, F7 e F10 (Fig 8).

As frações citadas acima foram selecionadas para um segundo fracionamento por RP-HPLC. Os fracionamentos são apresentados nas figuras 9.A (Fracionamento da F4), 11.A (fracionamento da F6), 13.A (Fracionamento da F7) e 15.A (Fracionamento da F10). Para detecção da inibição da tripsina, é possível ver a clara diferença entre a intensidade do substrato e seu produto em cada amostra. Amostras contendo apenas tripsina e substrato (controle positivo) apresentam alta intensidade do produto (523 m/z) em relação ao substrato (644 m/z). Amostras contendo tripsina, fração inibidora e substrato apresentam baixa intensidade da 523 m/z em relação ao seu substrato.

As figuras 10, 12, 14 e 16 mostram os espectros de massas adquiridos a partir da incubação da tripsina com subfrações da F4 (Fig. 10), F6 (Fig. 12), F7 (Fig. 14) e F10 (Fig. 16). As subfrações 4.2, 4.3 e 4.5 exibiram inibição da tripsina (Fig. 10). A fração 6.1 (Fig. 12) e frações 7.1, 7.3 e 7.4 (Fig. 14), assim como as frações 10.1 e 10.2 (Fig. 16), também apresentaram inibição da atividade desta serinopeptidase.

As subfrações da F4 com ação inibitória apresentaram a ionização de moléculas entre 2500 e 4000 m/z (Fig 9.C). A subfração F6.1 apresentou componentes com 1400 m/z (Fig 11.C). As subfrações inibitórias da F7 apresentaram moléculas entre 3500 a 6900 m/z (Fig 13.C). Enquanto as subfrações inibitórias da F10 exibiram componentes com m/z entre 1000 e 5500 (Fig 15.C). Os fracionamentos por troca iônica das frações 6.1, 7.1, 7.2 e 7.3 são apresentados da Fig17. Tais frações serão submetidas à análise quanto à inibição da tripsina.

Figura 8. Análise por MALDI-TOF da inibição da tripsina por frações da peçonha da *A. veratra*.

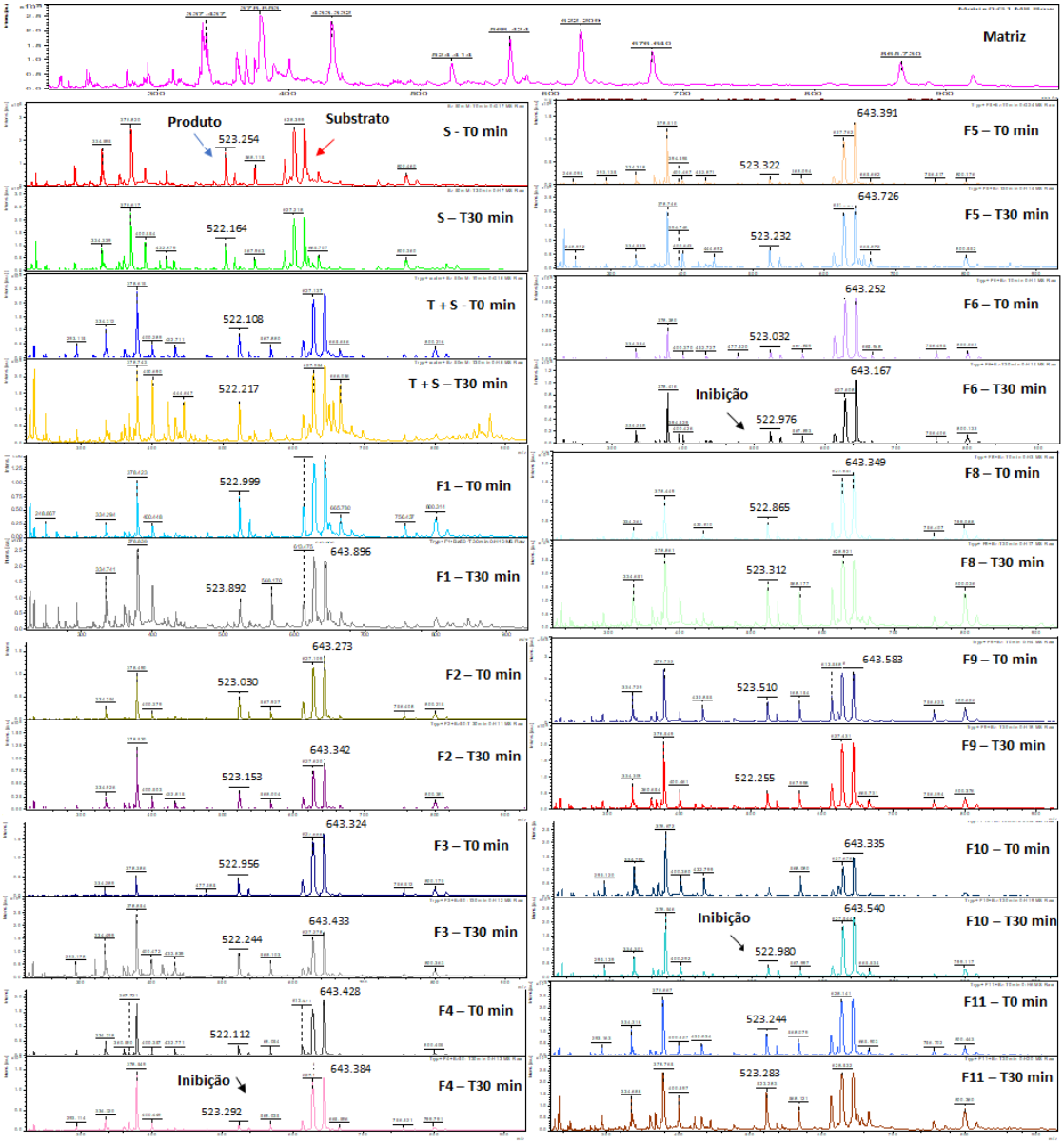

Frações da peçonha (1µl) foram incubadas com a tripsina (1:1) para a indução da inibição e logo após o substrato foi adicionado à amostra. A intensidade do produto (523 m/z) em relação ao substrato (644 m/z) é apresentada no espectro de massas obtido ao 0 min e aos 30 min de reação. No ensaio foram avaliadas as amostras F1 a F11 da peçonha da *A. veratra*; Branco (S + tampão); e Controle positivo (T + S), onde S= Substrato e T= Tripsina. As frações 4, 6, 7 e 10 apresentaram inibição da tripsina.

Figura 9. Fracionamento; ensaio de inibição; e análise por MALDI-TOF da Fração 4 da peçonha da *A. veratra*.

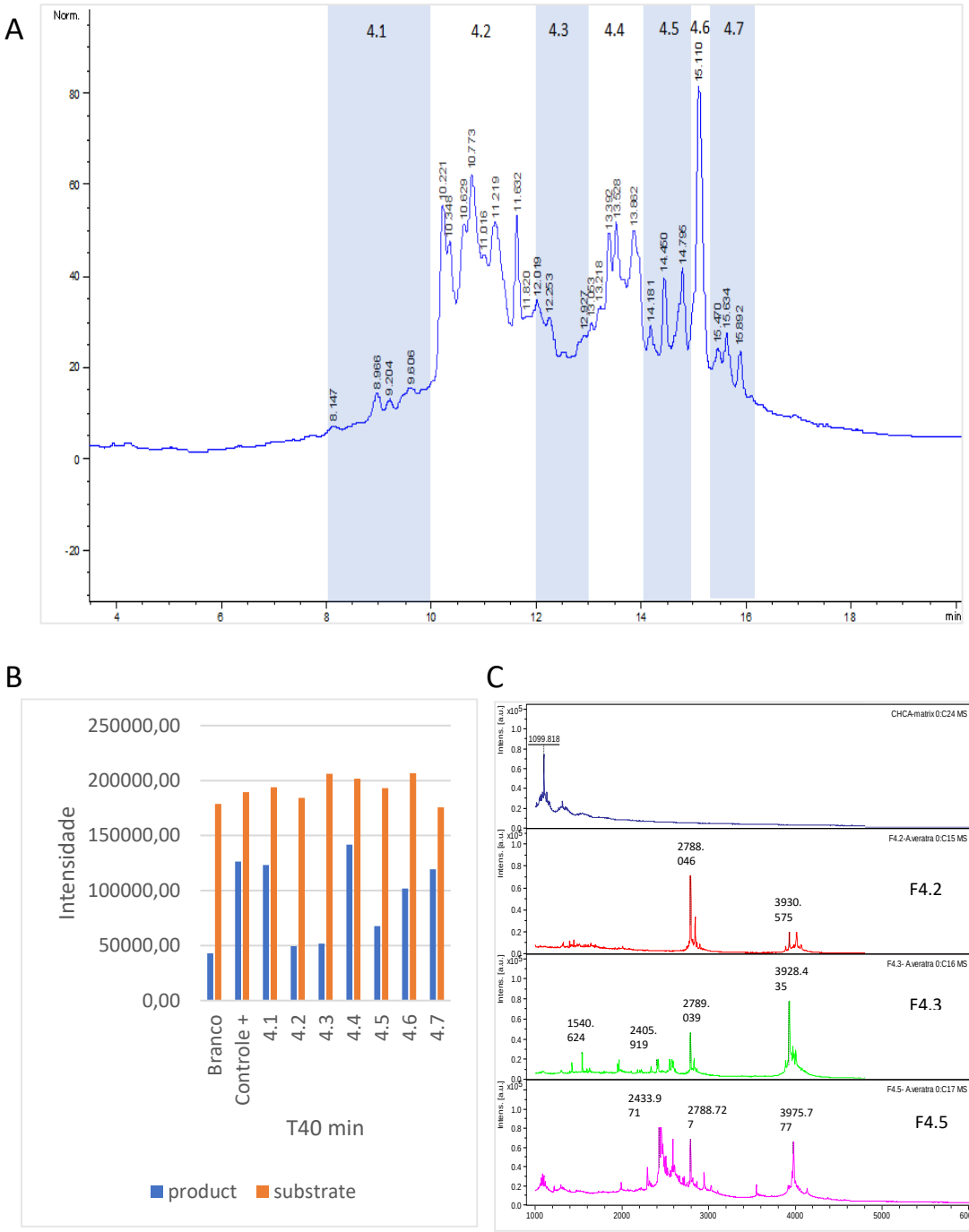

A- Fracionamento da Fração 4 da peçonha da *A. veratra*. A F4 foi submetida à separação em RP-HPLC em C18, na condição de 5-35% de B em 30 min. As frações foram divididas em F4.1 a F4.7 de acordo com o perfil cromatográfico acima. O cromatograma mostra a absorbância de moléculas no comprimento de onda de 214 nm. **B- Ensaio de inibição da tripsina por frações da F4.** Frações da F4 (1µl) foram incubadas com a tripsina (1:1) para a indução da inibição e logo após o substrato foi adicionado à amostra. A média da intensidade do produto 523 m/z em relação ao substrato (644 m/z) é apresentada após 40 min de reação. No ensaio foram avaliadas as amostras F4.1 a F4.7 da peçonha da *A. veratra*; Branco (S + tampão); e Controle positivo (T + S), onde S= Substrato e T= Tripsina. As fraçoes 4.2, 4.3 e 4.5 apresentaram inibição da tripsina. **C- Perfil de m/z presentes nas frações inibitórias (4.2, 4.3 e 4.5) por MALDI-TOF.**

Figura 10. Análise por MALDI-TOF do ensaio de inibição da tripsina por frações da F4.

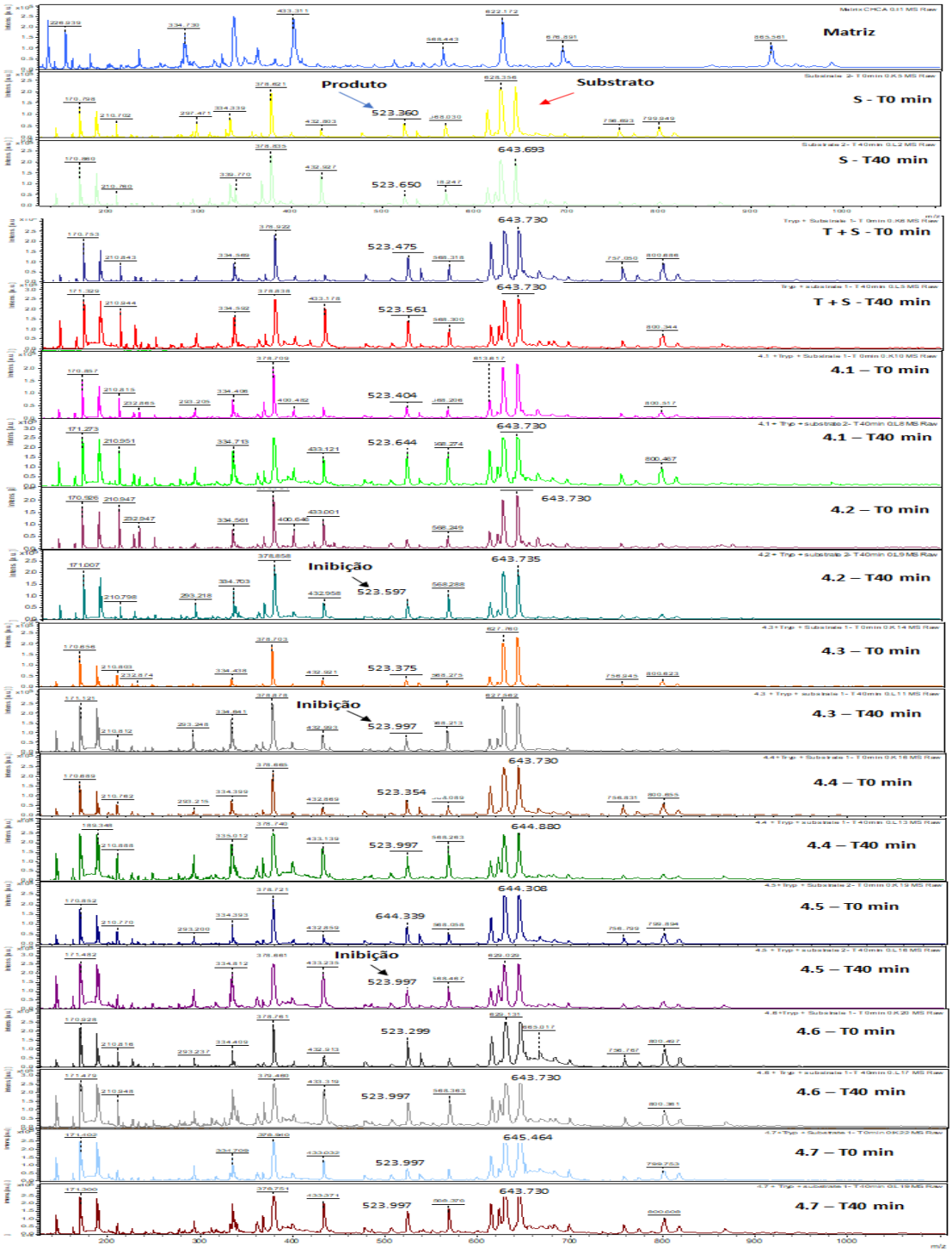

Frações da F4 (1µl) foram incubadas com a tripsina (1:1) para a indução da inibição e logo após o substrato foi adicionado à amostra. A intensidade do produto (523 m/z) em relação ao substrato (644 m/z) é apresentada no espectro de massas obtido ao 0 min e aos 40 min de reação. No ensaio foram avaliadas as amostras F4.1 a F4.7 da peçonha da *A. veratra*; Branco (S + tampão); e Controle positivo (T + S), onde S= Substrato e T= Tripsina. As frações 4.2, 4.3 e 4.5 apresentaram inibição da tripsina.

Figura 11. Fracionamento; ensaio de inibição; e análise por MALDI-TOF da Fração 6 da peçonha da *A. veratra*.

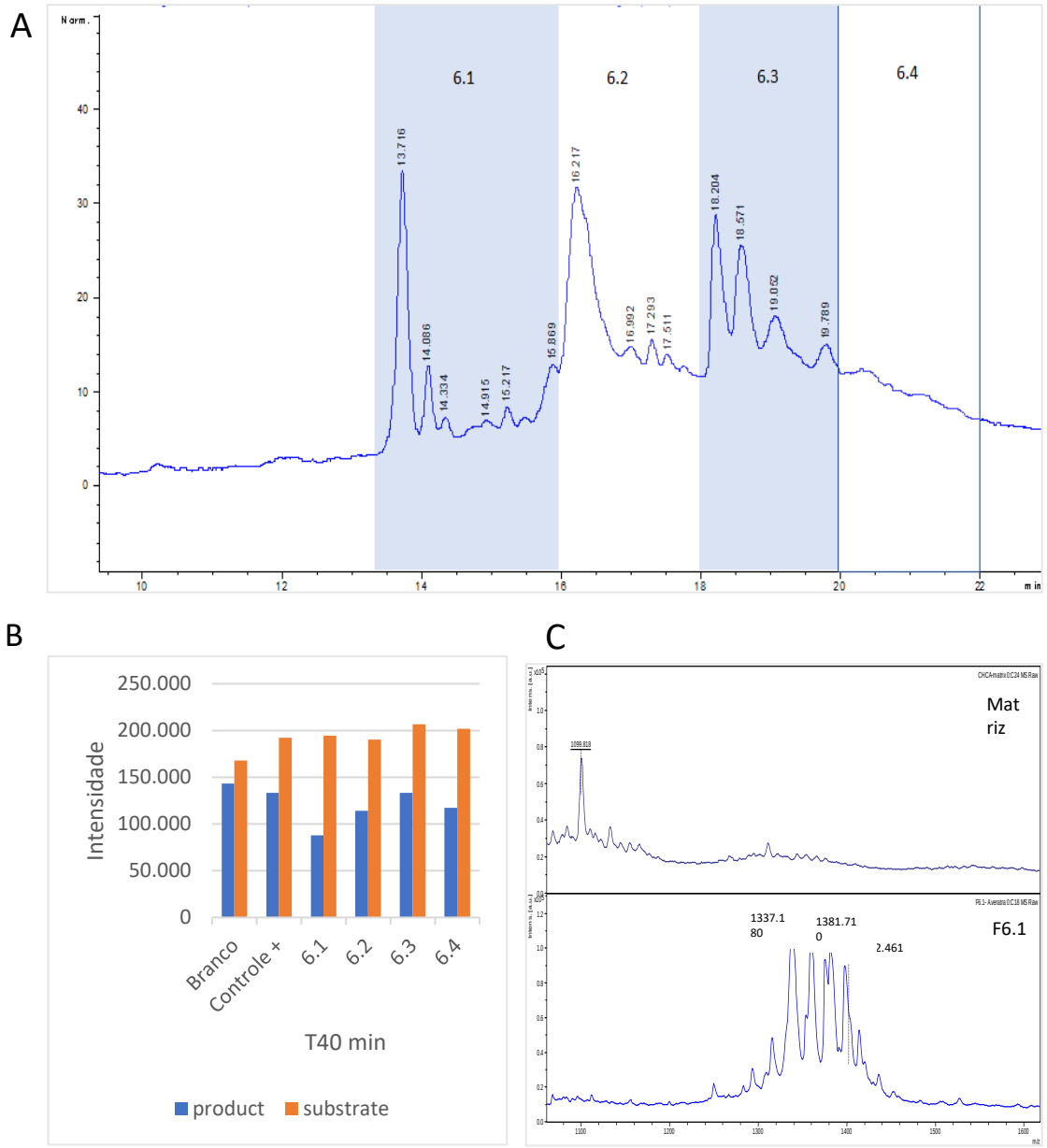

A- Fracionamento da Fração 6 da peçonha da *A. veratra*. A F6 foi submetida à separação em RP-HPLC em C18, na condição de 10-35% de B em 30 min. As frações foram divididas em F6.1 a F6.4 de acordo com o perfil cromatográfico acima. O cromatograma mostra a absorbância de moléculas no comprimento de onda de 214 nm. **B- Ensaio de inibição da tripsina por frações da F6.** Frações da F6 (1µl) foram incubadas com a tripsina (1:1) para a indução da inibição e logo após o substrato foi adicionado à amostra. A média da intensidade do produto (523 m/z) em relação ao substrato (644 m/z) é apresentada após 40 min de reação. No ensaio foram avaliadas as amostras F6.1 a F6.4 da peçonha da *A. veratra*; Branco (S + tampão); e Controle positivo (T + S), onde S= Substrato e T= Tripsina. A fração 6.1 apresentou maior inibição da tripsina. **C- Perfil de m/z presentes na fração inibitória 6.1 por MALDI-TOF.**

Figura 12. Análise por MALDI-TOF do ensaio de inibição da tripsina por frações da F6.

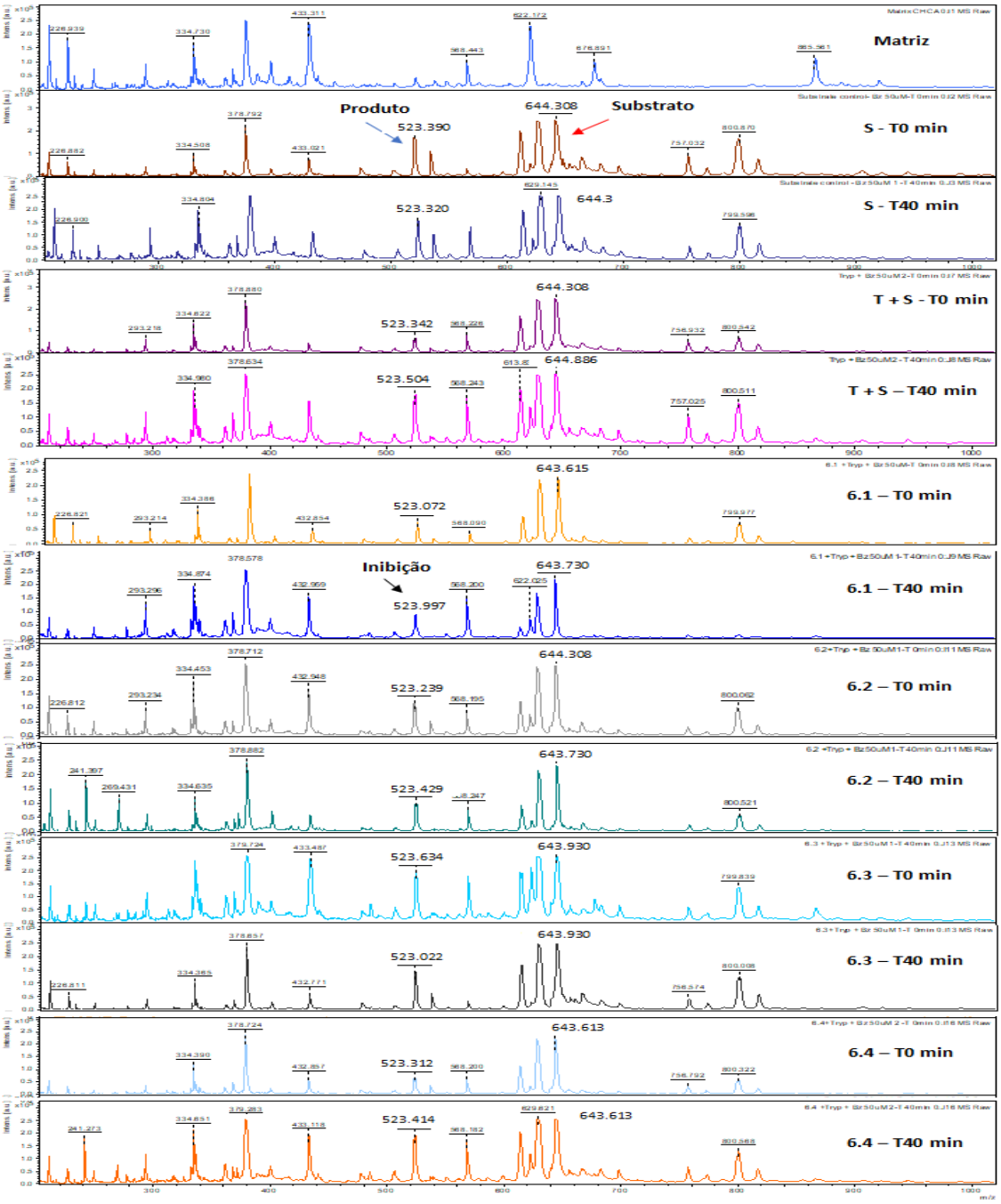

Frações da F6 (1µl) foram incubadas com a tripsina (1:1) para a indução da inibição e logo após o substrato foi adicionado à amostra. A intensidade do produto (523 m/z) em relação ao substrato (644 m/z) é apresentada no espectro de massas obtido ao 0 min e aos 40 min de reação. No ensaio foram avaliadas as amostras F6.1 a F6.4 da peçonha da *A. veratra*; Branco (S + tampão); e Controle positivo (T + S), onde S= Substrato e T= Tripsina. A fração 6.1 apresentou maior inibição da tripsina.

Figura 13. Fracionamento; ensaio de inibição; e análise por MALDI-TOF da Fração 7 da peçonha da *A. veratra*.

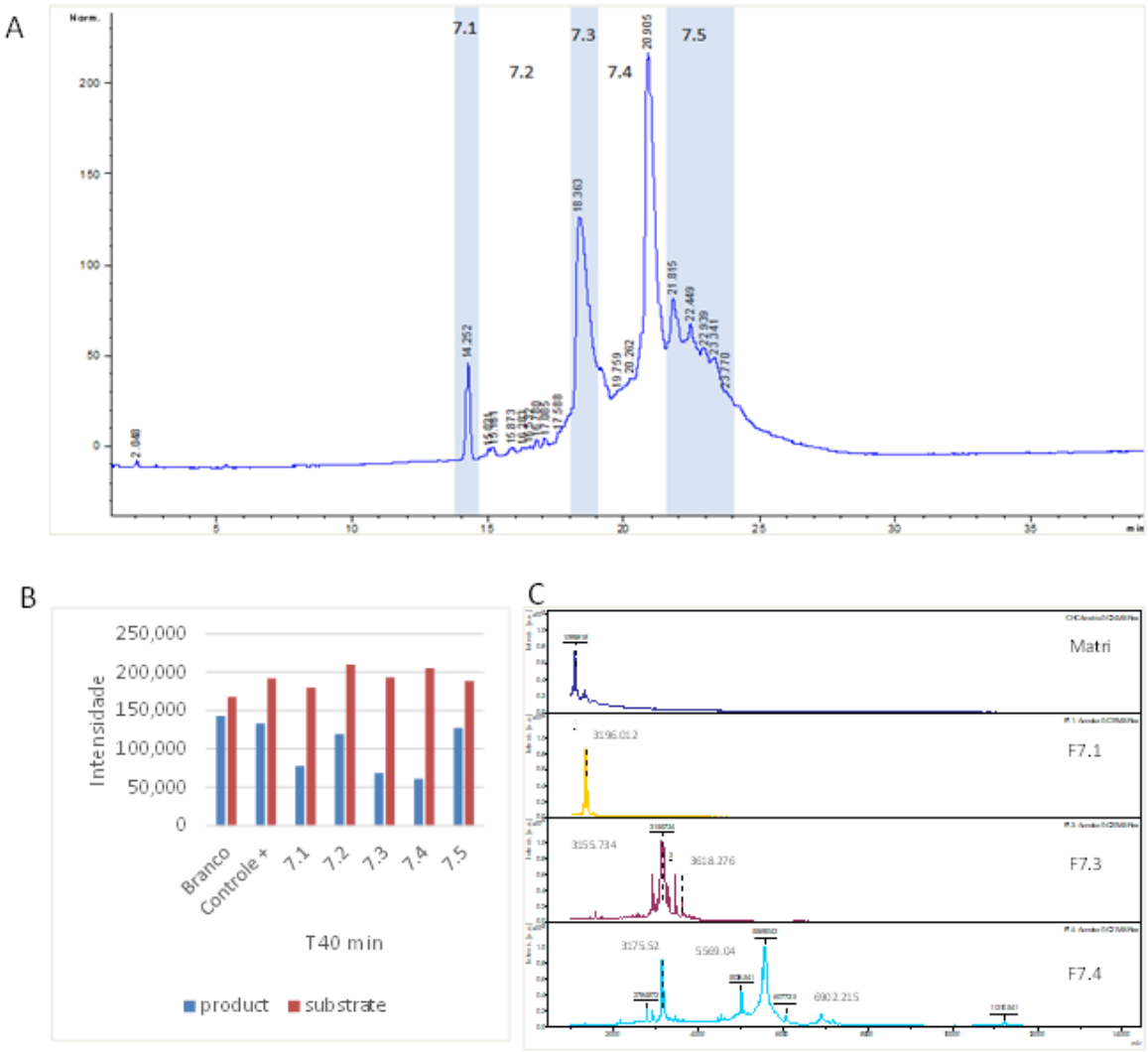

A- Fracionamento da Fração 7 da peçonha da *A. veratra*. A F7 foi submetida à separação em RP-HPLC em C18, na condição de 10-35% de B em 30 min. As frações foram divididas em F7.1 a F7.5 de acordo com o perfil cromatográfico acima. O cromatograma mostra a absorbância de moléculas no comprimento de onda de 214 nm. **B- Ensaio de inibição da tripsina por frações da F7.** Frações da F7 (1µl) foram incubadas com a tripsina (1:1) para a indução da inibição e logo após o substrato foi adicionado à amostra. A média da intensidade do produto 523 m/z em relação ao substrato (644 m/z) é apresentada após 40 min de reação. No ensaio foram avaliadas as amostras F7.1 a F7.5 da peçonha da *A. veratra*; Branco (S + tampão); e Controle positivo (T + S), onde S= Substrato e T= Tripsina. A fração 7.1, 7.3 e 7.4 apresentaram inibição da tripsina. **C- Perfil de m/z presentes nas frações inibitórias (7.1, 7.3 e 7.4) por MALDI-TOF.**

Figura 14. Análise por MALDI-TOF do ensaio de inibição da tripsina por frações da F7.

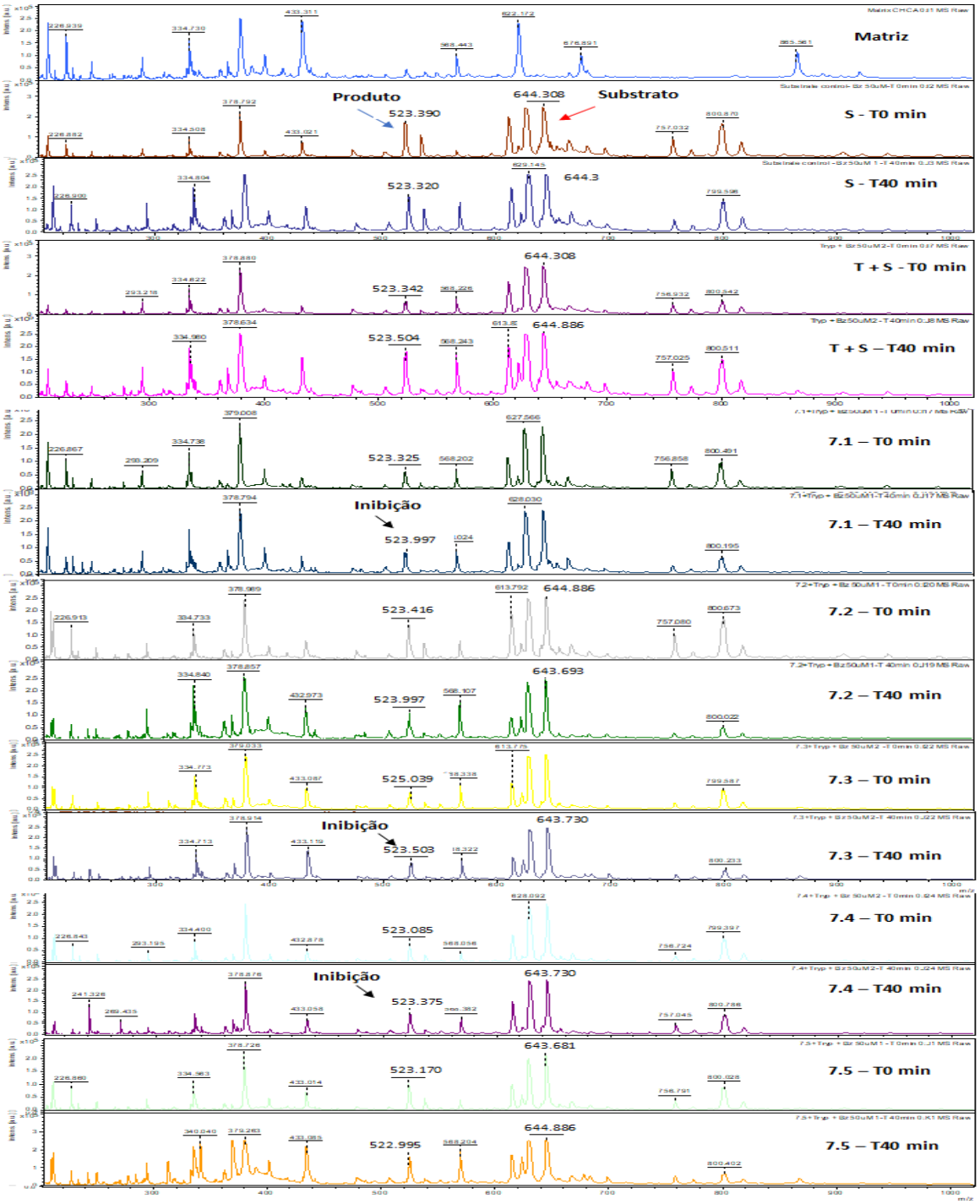

Frações da F7 (1µl) foram incubadas com a tripsina (1:1) para a indução da inibição e logo após o substrato foi adicionado à amostra. A intensidade do produto (523 m/z) em relação ao substrato (644 m/z) é apresentada no espectro de massas obtido ao 0 min e aos 40 min de reação. No ensaio foram avaliadas as amostras F7.1 a F7.5 da peçonha da *A. veratra*; Branco (S + tampão); e Controle positivo (T + S), onde S= Substrato e T= Tripsina. As frações 7.3 e 7.4 apresentaram inibição da tripsina.

Figura 15. Fracionamento; ensaio de inibição; e análise por MALDI-TOF da Fração 10 da peçonha da *A. veratra.*

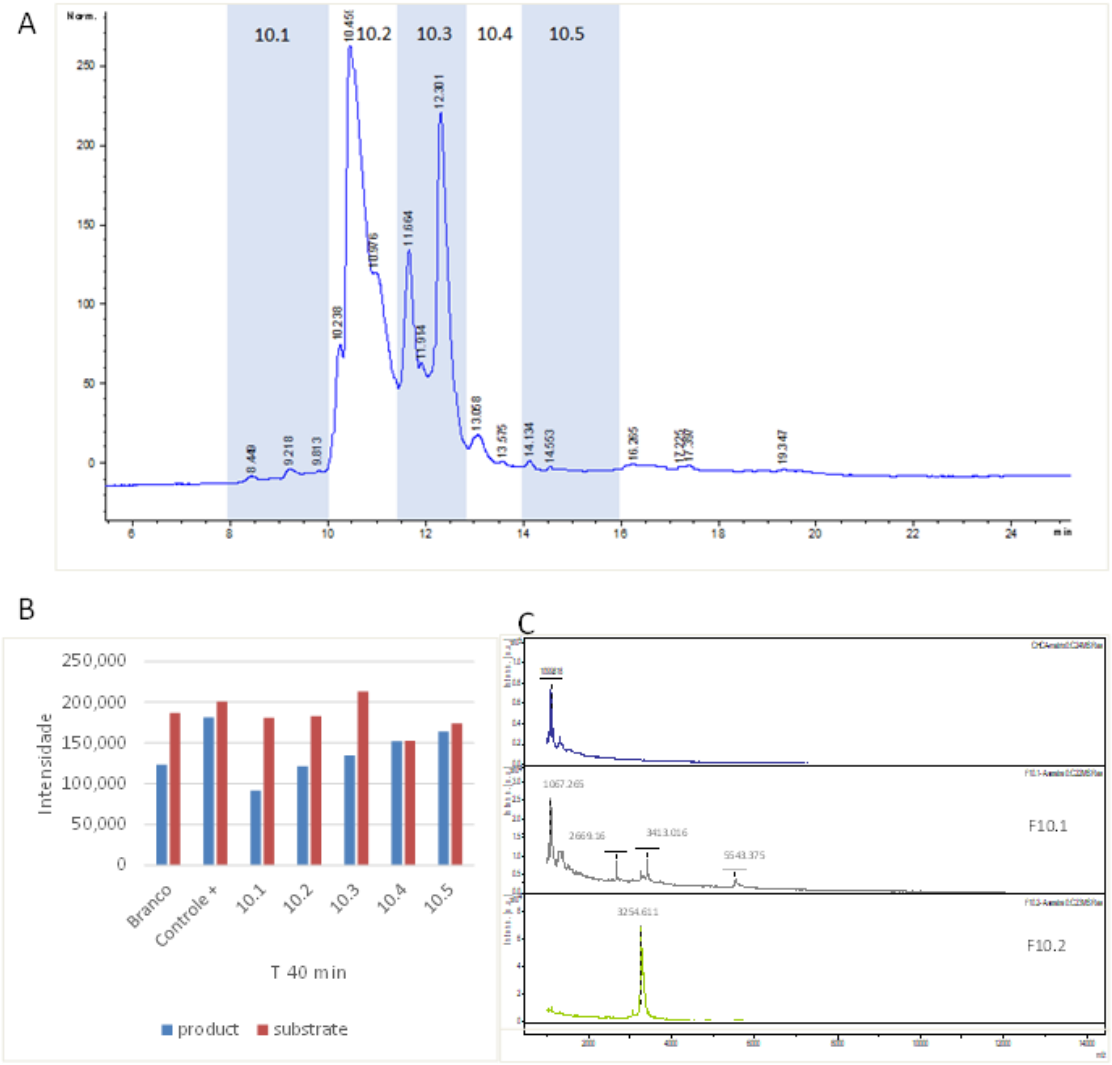

A- Fracionamento da Fração 10 da peçonha da *A. veratra*. A F10 foi submetida à separação em RP-HPLC em C18, na condição de 20-45% de B em 30 min. As frações foram divididas em F10.1 a F10.5 de acordo com o perfil cromatográfico acima. O cromatograma mostra a absorbância de moléculas no comprimento de onda de 214 nm. **B- Ensaio de inibição da tripsina por frações da F10.** Frações da F10 (1µl) foram incubadas com a tripsina (1:1) para a indução da inibição e logo após o substrato foi adicionado à amostra. A média da intensidade do produto 523 m/z em relação ao substrato (644 m/z) é apresentada após 40 min de reação. No ensaio foram avaliadas as amostras F10.1 a F10.5 da peçonha da *A. veratra*; Branco (S + tampão); e Controle positivo (T + S), onde S= Substrato e T= Tripsina. A fração 10.1 e 10.2 apresentaram maior inibição da tripsina. **C- Perfil de m/z presentes nas frações inibitórias (7.1, 7.3 e 7.4) por MALDI-TOF.**

Figura 16. Análise por MALDI-TOF do ensaio de inibição da tripsina por frações da F10.

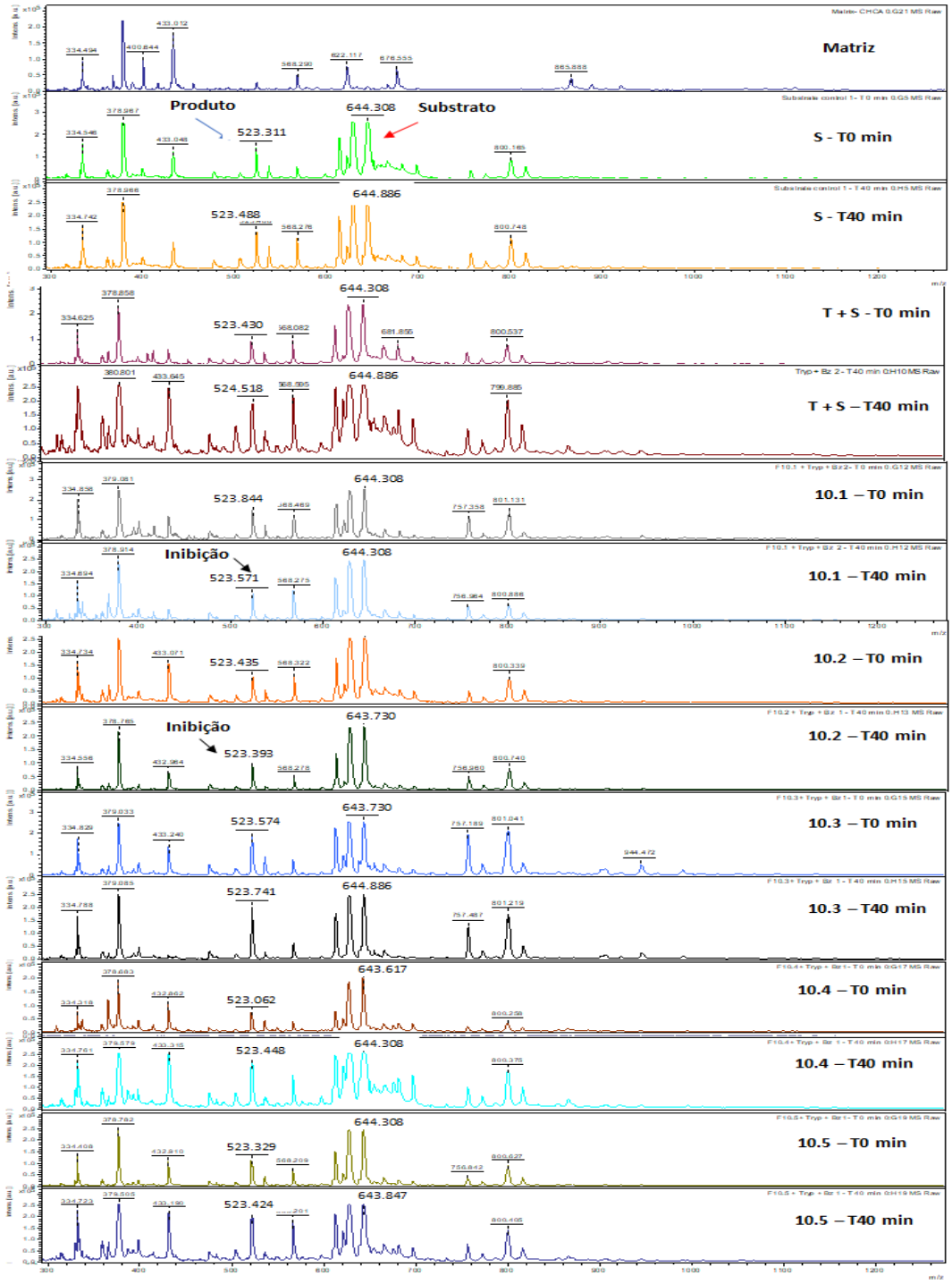

Frações da F10 (1µl) foram incubadas com a tripsina (1:1) para a indução da inibição e logo após o substrato foi adicionado à amostra. A intensidade do produto (523 m/z) em relação ao substrato (644 m/z) é apresentada no espectro de massas obtido ao 0 min e aos 40 min de reação. No ensaio foram avaliadas as amostras F10.1 a F10.5 da peçonha da *A. veratra*; Branco (S + tampão); e Controle positivo (T + S), onde S= Substrato e T= Tripsina. As frações 10.1 e 10.2 apresentaram inibição da tripsina.

Figura 17. Fracionamento das Frações 6.1, 7.1, e 7.3 da peçonha da *A. veratra*.

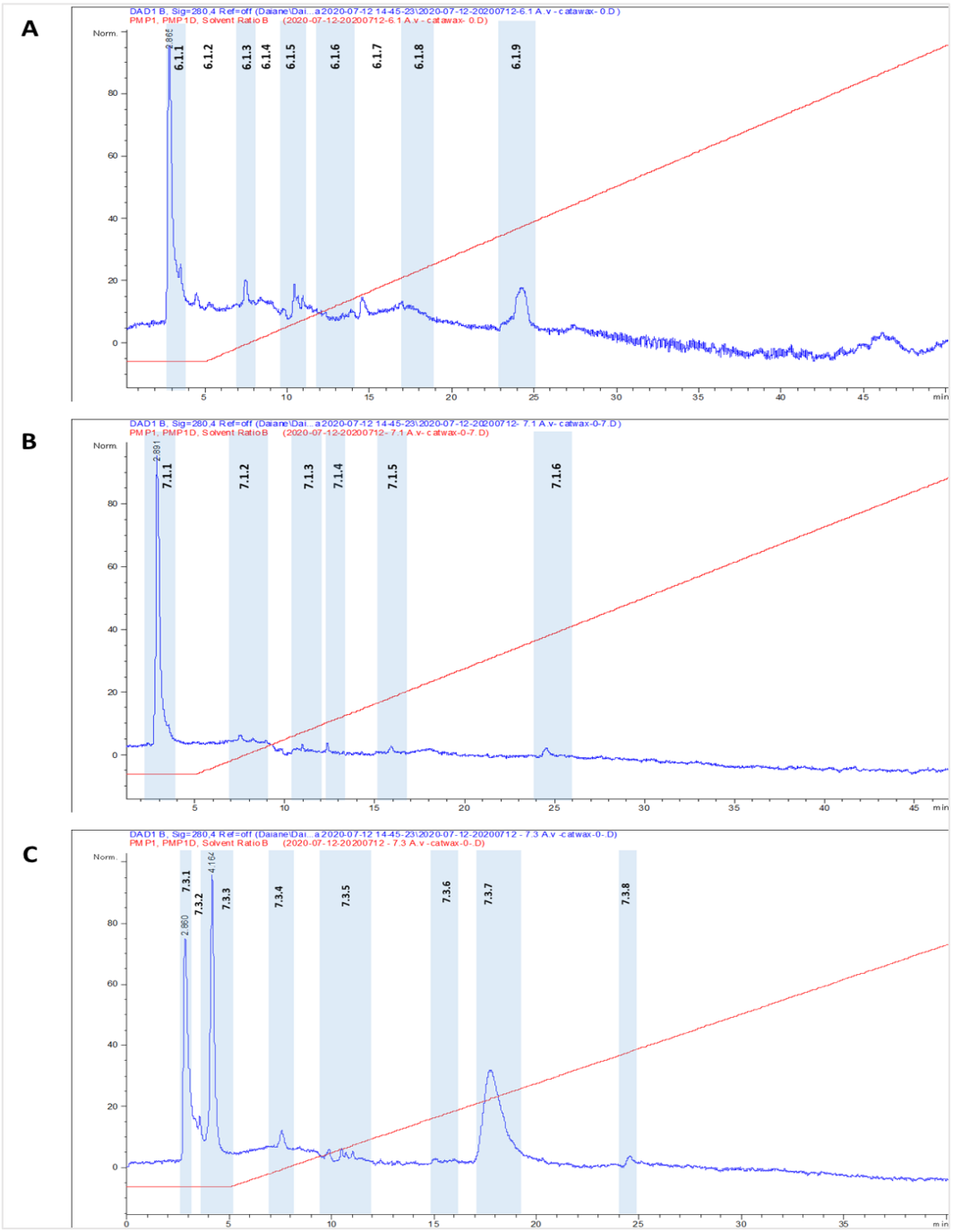

A- Fracionamento da F6.1. **B-** Fracionamento da 7.1. **C**- Fracionamento da 7.3. As frações contendo inibidores de serinopeptidases foram submetidas à separação por troca iônica, na condição de 0-70% de B em 35 min. As frações foram subdivididas de acordo com o perfil cromatográfico acima. O cromatograma mostra a absorbância de moléculas no comprimento de onda de 280 nm. Tais frações serão submetidas à análise de inibição da tripsina.

4.3 Identificação de inibidores em tecido utilizando MALDI-IMS e ensaio de inibição da tripsina no tecido da *A. veratra*

Com a disponibilização das sequências de aminoácidos das toxinas do tipo Kunitz e Kazal a partir no estudo da *A. veratra* aqui realizado, foi possível prever a massa das moléculas maduras, através da remoção do peptídeo sinal e propeptídeo das sequências (Tabela 2). A distribuição dos inibidores do tipo Kazal e Kunitz no tecido da *A. veratra* é apresentada nas Fig 18 e 19, através do uso do MALDI-IMS.

Tabela 2. Massa/carga (m/z) de inibidores de serinopeptidases encontrados no proteoma da peçonha da *A. veratra*. As sequências de aminoácidos dos inibidores tiveram o peptídeo sinal e propeptídeo removidos a fim de calcular a massa teórica das moléculas.

Accession	Type	Cod	m/z
aul_smart_877428|CDS1	Kazal	NTAv202	5210.04
aul_smart_876517|CDS28	Kazal	Av26	6228.23
aul_smart_813067|CDS1	Kazal	NTAv30	7474.51
aul_smart_687983|CDS3	Kazal	NTAv145	5090.86
aul_smart_427605|CDS2	Kazal	NTAv120	5596.56
aul_smart_426451|CDS2	Kazal	Av24	5191
aul_smart_280649|CDS1	Kazal	NTAv107	6171.18
aul_smart_1046916|CDS2	Kazal	Av133	5449.17
aul_smart_955021|CDS2	Kunitz	NTAv66	22457.94
aul_smart_886056|CDS2	Kunitz	NTAv215	16411.37
aul_smart_859108|CDS2	Kunitz	NTAv41	13851.63
aul_smart_859005|CDS1	Kunitz	NTAv189	6014.61
aul_smart_856786|CDS3	Kunitz	NTAv186	6919.06

Com a análise do tecido da *A. veratra* por MALDI-IMS tivemos o objetivo de verificar se os inibidores de serinopeptidases identificados no proteoma

apresentavam diferenças em distribuição ao longo do tecido. Na Fig. 18 é possível notar que apenas os inibidores Kunitz NTAv186 e NTAv189 foram identificados por IMS. Os demais inibidores do tipo Kunitz, com massas acima de 13 kDa, não foram detectados, provavelmente devido ao método de análise, que pode ser limitante no sentido de tornar moléculas maiores detectáveis. Entre tais inibidores, NTAv189 apresentou maior presença na região dos tentáculos da anêmona, o que pode ser um indício do local de estoque desta possível toxina. Ao contrário deste, o NTAv186 apresentou maior distribuição ao longo do mesentério.

Quanto aos oito inibidores do tipo Kazal analisados, as moléculas NTAv202, NTAv145 e Av24 apresentaram maior detecção na região dos tentáculas da anêmona, enquanto NTAv120, Av26, NTAv30, NTAv107, e Av133 apresentam distribuição mais inespecífica e muito similar ao longo de todo o tecido, principalmente no mesentério (Fig. 19).

Quanto ao teste de identificação de inibição da tripsina no tecido da anêmona, verificamos que os inibidores da *A. veratra* permanecem ativos no tecido. A figura 20 mostra a detecção do substrato (644 m/z) e do produto (523 m/z) em tecidos incubados por 2h a 37°C, com a presença ou ausência de tripsina e substrato. No tecido que recebeu apenas a matriz α-ciano (Fig 20.A) ou apenas tripsina (Fig 20.B) é possível observar que não há qualquer detecção do 644 m/z no espectro de massas, o que leva a concluir que o íon 523 m/z identificado na imagem destes grupos não pertence a um produto de reação enzimática, mas sim à matriz ou à tripsina.

Na Fig 20.C é demonstrada a presença intensa da 644 m/z, principalmente na área fora do tecido. Tais diferenças de aquisição são esperadas devido às diferenças da impregnação do substrato no tecido e na lâmina ionizável. Quanto ao produto, mais uma vez a região fora do tecido mostrou a presença do íon 523 m/z. Porém, a presença deste íon fora do tecido não é um produto de atividade enzimática da tripsina, uma vez que o tecido não recebeu a enzima. A detecção residual do íon 523 m/z também ocorreu em amostras contendo apenas o substrato no ensaio de inibição da tripsina (Fig 6).

No caso da incubação de apenas substrato com o tecido (Fig 20.C), é possível que a 523 m/z identificada seja uma massa remanescente do substrato não conjugado ao pNa, ou que este produto esteja sendo gerado por

serinopeptidases endógenas. Nesta figura é possível ver a especial detecção da 523 m/z na extremidade dos tentáculos. Proteínas semelhantes à serinopeptidases foram encontradas no proteoma da peçonha da *A. veratra* (Tabela 2).

Nas figuras 20.D, E e F é possível observar claramente a inibição da atividade da tripsina em algumas áreas do tecido da *A. veratra*. Isto pode ser observado de duas formas: 1. pelo intenso consumo do substrato fora do tecido, onde não há a presença de inibidores, levando à baixa detecção (em azul) do íon 644 m/z, e alta detecção do substrato restante no tecido (em vermelho). 2- Pela alta intensidade do íon 523 m/z (produto) fora do tecido (em vermelho) e baixa intensidade no tecido (em azul).

O modelo de detecção de inibição da tripsina em tecido ainda está sendo otimizado em nosso laboratório. Nesta primeira fase de testes, a concentração de 0,5 µM/µL de substrato parece ser a ideal para observar diferenças de intensidade do produto em regiões variadas do tecido da *A. veratra*. Isto possibilitará relacionar a inibição detectada com as localizações de inibidores (Fig. 18 e 19). Pretendemos aumentar o período de incubação do tecido com tripsina visando diferenças mais claras entre as detecções do substrato restante nas regiões de dentro e fora do tecido.

Figura 18. MALDI-IMS - Detecção de inibidores do tipo Kunitz no tecido da *A. veratra.*

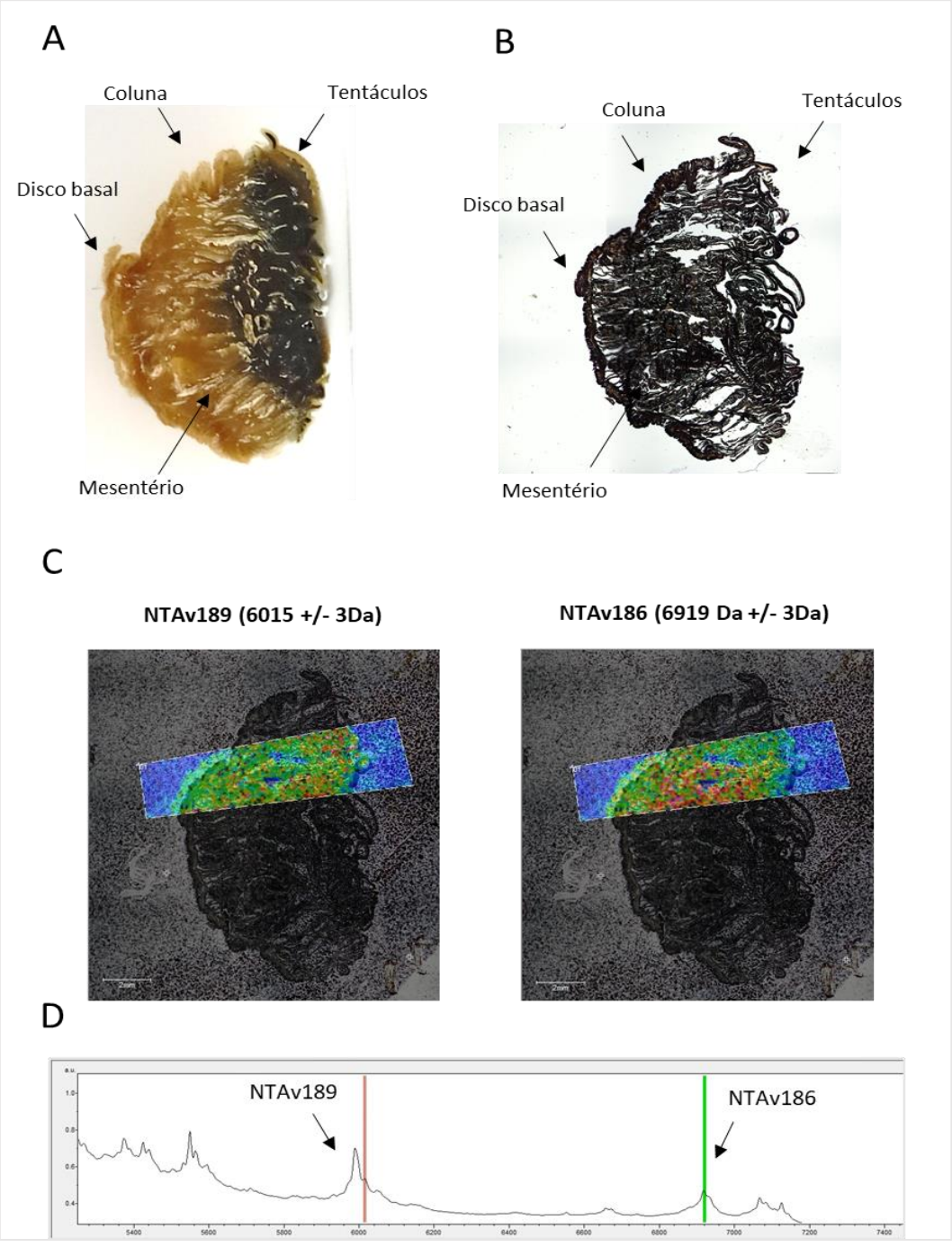

A – Imagem do corte longitudinal do tecido da *A. veratra* em parafina. **B**- Imagem do tecido desparafinizado por microscopia óptica. **C**- Distribuição dos íons correspondentes aos inibidores do tipo Kunitz ao longo do tecido. A localização pode ser identificada por 'hotspots'. Locais em vermelho representam intensa presença da m/z, locais em verde presença mediana, e locais em azul representam baixa presença da m/z. **D**- Apresenta o espectro de massas adquirido a partir do tecido. Os picos correspondentes às m/z dos inibidores Kunitz estão indicados.

Figura 19. MALDI-IMS- Detecção de inibidores do tipo Kazal no tecido da *A. veratra.*

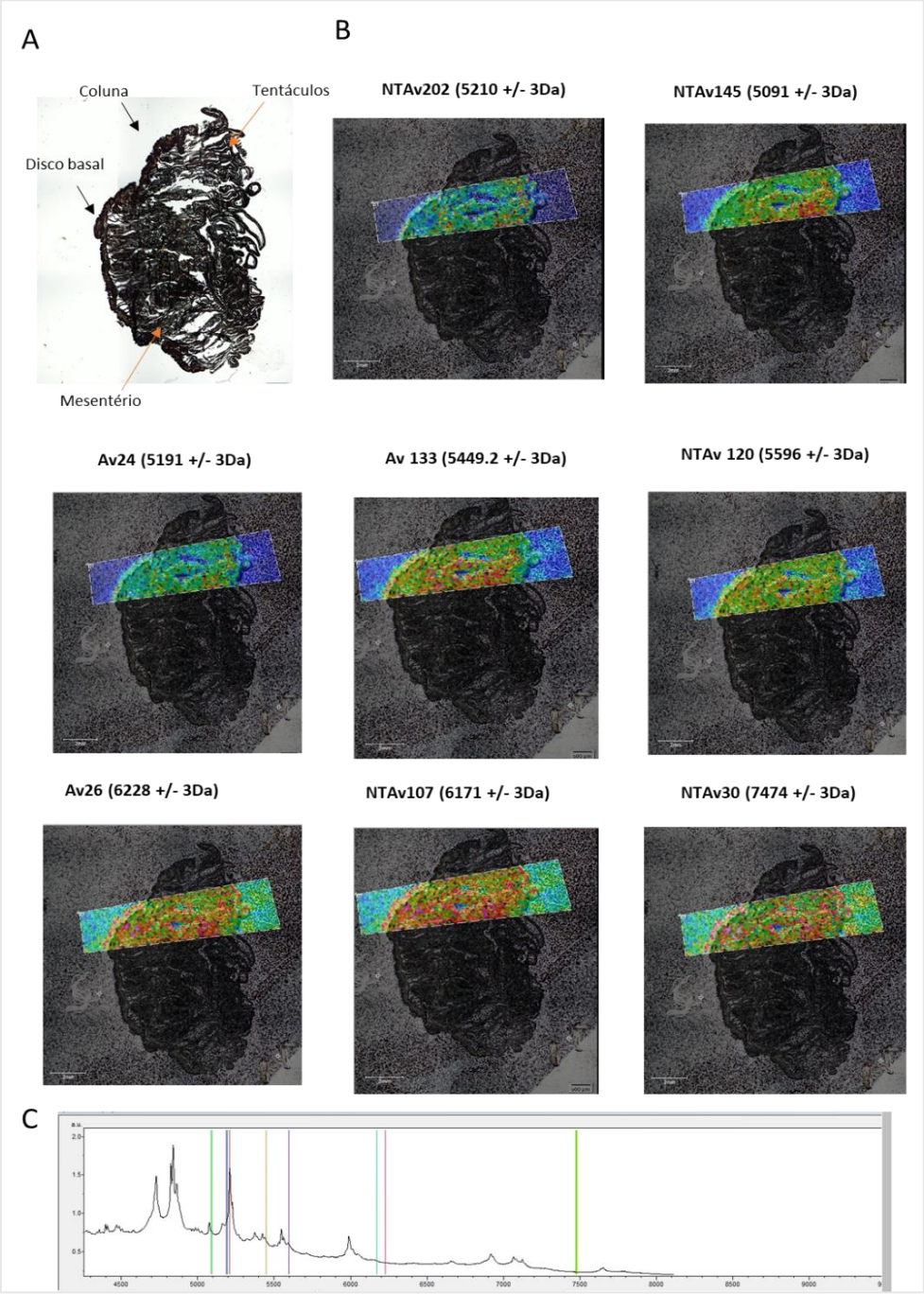

A - Imagem do tecido por microscopia óptica. **B**- Distribuição dos íons correspondentes aos inibidores do tipo Kazal ao longo do tecido. A localização dos íons pode ser identificada por 'hotspots'. Locais em vermelho representam intensa presença da m/z, locais em verde presença mediana, e locais em azul representam baixa presença da m/z. **C**- Apresenta o espectro de massas adquirido a partir do tecido. Os picos correspondentes às m/z dos inibidores Kazal estão indicados.

Figura 20. Detecção da inibição da tripsina no tecido da *A. veratra* por MALDI-IMS.

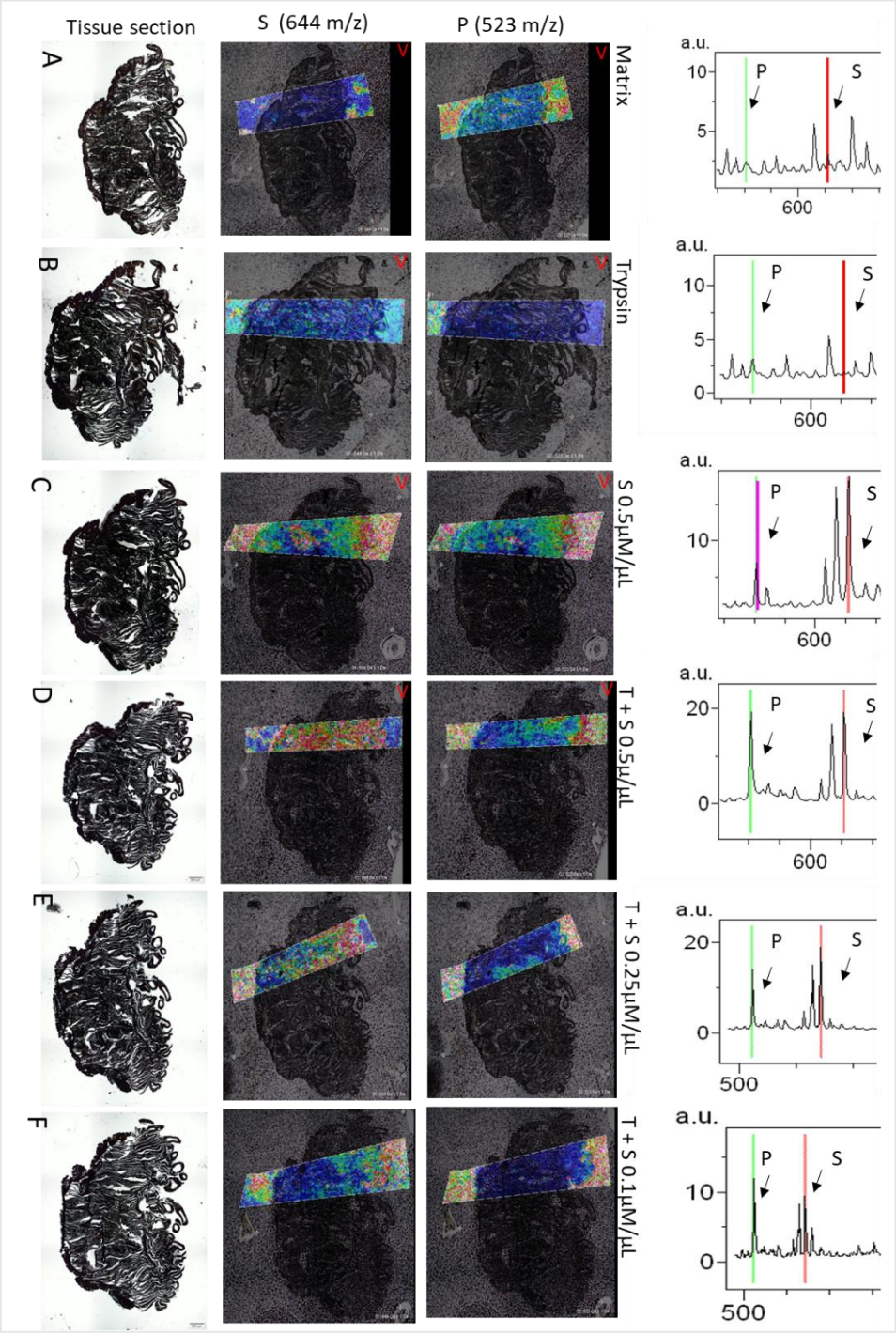

A figura mostra a identificação do substrato (644 m/z) e produto (523 m/z) no tecido da anêmona *A. veratra*. A coluna 1 representa a imagem do corte do tecido sem colorações ou deposição de material. A coluna 2 mostra a detecção do substrato. A coluna 3, a detecção do produto. A coluna 4 mostra a intensidade da m/z correspondente ao produto (P) e substrato (S). A distribuição dos íons ao longo do tecido pode ser identificada por 'hotspots'. Locais em vermelho representam intensa presença da m/z, locais em verde presença mediana, e locais em azul, baixa presença da m/z. **A** – Matriz (controle). **B**- T (controle). **C** – S (controle). **D-** T + S 0,5 µM/µL. **E -** T + S 0,25 µM/µL. **F-** T + S 0,1 µM/µL. As figuras A a F representam diferentes componentes pulverizados sobre o tecido, sendo eles M (matriz), S (substrato) e T (tripsina).

5 DISCUSSÃO

Do ponto de vista ecológico cnidários usam suas peçonhas – constituídas principalmente por citolisinas, proteases, neurotoxinas, fosfolipases e inibidores de proteases – para predação, defesa e competição intraespecífica (ASHWOOD et al., 2020; RAMÍREZ-CARRETO et al., 2019). No caso das anêmonas-do-mar, por vezes, estruturas especializadas estão diretamente relacionadas à tais papéis ecológicos. Por exemplo, acontia e nematoesferas de algumas espécies estão relacionadas à defesa contra predadores (ASHWOOD et al., 2020; LAM et al., 2017); enquanto a acrorhagi e tentáculos de captura estão relacionados à competição de anêmonas com rivais da mesma espécie (PURCELL, 1977; WILLIAMS, 1991).

A nível molecular, isto também ocorre: peptídeos do tipo Kunitz podem agir tanto como toxinas de defesa, por impedirem a degradação de toxinas da peçonha por enzimas de predadores; como podem agir como toxinas de agressão, modulando canais de potássio e levando suas presas à paralisia (FRAZÃO et al. 2012; HONMA et al., 2006).

A peçonha de anêmonas-do-mar pode conter componentes proteicos de três principais grupos: neurotoxinas, citolisinas e fosfolipases do tipo A2. Além destes, componentes não proteicos como purinas e aminas biogênicas podem ser encontrados (MADIO et al., 2017).

No presente estudo foram avaliadas as peçonhas de duas anêmonas – *A. cascaia e A. veratra* (Apêndice B – Manuscrito 2) – através de análise proteômica por LC-MS/MS. Ambas as peçonhas foram obtidas por técnicas distintas – imersão do animal em água acidificada ou eletroestimulação – que induzem o disparo de nematocistos no meio aquoso e possibilitam a obtenção de amostras mais puras; e de maneira geral, foi visto que ambas as anêmonas são detentoras de inibidores de serinopeptidases; de toxinas enzimáticas; e de citolisinas do tipo actinoporinas.

Caracterização bioquímica da peçonha da *A. cascaia*

No estudo da peçonha da anêmona *A. cascaia*, foi possível identificar apenas três proteínas similares à toxinas: Uma natterina exibindo 64% de identidade com natterin-4 de *Exaiptasia pallida;* uma PLA2 com 56% de identidade

com a fosfolipase A2 da *Exaiptasia pallida* e uma citolisina, com 100% de identidade com a Delta-actitoxina AaS1a da *Anthopleura asiatica* (Tabela 1 da tese). Tais achados destacam o fato de que esta espécie de anêmona possui uma variedade interessante de toxinas em sua peçonha, uma vez que além de neurotoxinas moduladoras de canal de potássio – AcaIII1425, AcaIII2970, e AcaIII3090 previamente descritas por MADIO, 2012 – a *A. cascaia* também possui toxinas com papel enzimático (PLA2) e citolítico (citolisina).

A presença de PLA2 e citolisinas também tem sido descrita como parte do arsenal de toxinas de outras espécies do gênero *Anthopleura*. Por exemplo, na avaliação do transcriptoma da acrorhagi de pólipos não-agressivos e agressivos da espécie *Anthopleura elegantissima* por RNA-Seq, foi demonstrada a identificação de 65 genes de toxinas candidatas, entre estes, 10 genes correspondentes à toxinas do tipo PLA2 e dois à citolisinas. A reconstrução da rede de genes de toxinas envolvendo sequências maduras resultou na identificação de pelo menos 6 tipos de PLA2 na acrorhagi, e ao menos 3 destas fazem parte do 'cluster' que inclui apenas genes de anêmonas marinhas. Tal estudo revelou a presença de candidatos a citolisinas do tipo II e IV tanto na acrorhagi de pólipos não-agressivos quanto de pólipos agressivos da anêmona (MACRANDER et al., 2015).

Em anêmonas, PLA2 são descritas como instrumentos de defesa e agressão, comumente presentes em nematocistos. Tais toxinas são descritas em cnidários da classe Anthozoa, Hydrozoa, Scyphozoa e Cubozoa (NEVALAINEN et al., 2004). Particularmente toxinas do tipo PLA2 estão amplamente presentes em peçonhas de serpentes e são conhecidas por levar à despolarização e contração de células do músculo esquelético (OWNBY, 1998).

Quanto à citolisina encontrada no proteoma da *A. cascaia*, apresentando similaridade a uma actinoporina, foi visto que tal citolisina também é descrita no proteoma de outras espécies do gênero *Anthopleura*. Actinoporinas são citolisinas com massa molecular de 20 kDa, que constituem uma das principais famílias de toxinas de anêmonas e apresentam alta afinidade por esfingomielina (PRENTIS et al., 2018; MADIO et al., 2019; VALLE et al., 2015). Estas toxinas são caracterizadas pela capacidade de formação de monômeros na superfície de células-alvo, levando à formação de poros que causam um desbalanceamento iônico, comprometendo a

integridade da membrana celular. Tais toxinas têm sido investigadas como alternativas na terapia do câncer (RAMÍREZ-CARRETO et al., 2019).

Quanto à proteína similar à natterina identificada, na literatura é descrito que tais proteínas agem como proteases não neurotóxicas e não homólogas da peçonha do peixe *Thalassophryne nattereri*. Estas proteases são capazes de clivar cininogênio, liberando cininas, que levam à vasodilatação e aumentam a distribuição sistêmica de toxinas. Estas proteases também são capazes de induzir citotoxicidade e retardar a regeneração tecidual por comprometimento da infiltração de leucócitos (LOPES-FERREIRA et al., 2014). Adicionalmente, já é descrito a presença de natterinas em anêmonas como *Exaiptasia pallida*, apesar de não destas toxinas não serem formalmente classificadas entre as famílias de toxinas de anêmonas (Tabela 1 da tese) (MADIO et al., 2019).

Adicionalmente foram identificadas proteínas da zona pelúcida no conteúdo analisado, tais proteínas são encontradas em oócitos de anêmonas como *Nematostella vectensis*, *Exaiptasia pallida*, *Anthopleura elegantissima*, e comumente estão envolvidas na maturação e fertilização de oócitos em vertebrados (LOTAN *et al*., 2014). Além destas, proteínas estruturais como glicoproteínas de superfície celular; histonas pertencentes às superfamílias H2A e H4; proteínas ricas em glicina e cisteína com domínios LIM e proteínas contendo o domínio FH1/FH2 relacionadas à organização do citoesqueleto; além de colágeno Alfa-1 também foram encontradas (LOUIS et al, 1997; PRUYNE et al., 2017). Adicionalmente, proteínas relacionadas ao metabolismo celular, como proteínas contendo domínio Zinc-finger CCCH, responsáveis por se ligar ao mRNA, remover a cauda poli(A) e levar ao RNA *turnover*; proteínas tipo NST1 relacionadas à resposta ao stress; proteínas tipo LHR, da família de receptores acoplados à proteína G, responsáveis por ligar hormônios e induzir mudanças na atividade celular; e enzimas superóxido dismutase de cobre/zinco relacionadas à atividade antioxidante, também foram identificadas (LIANG et al., 2008, EBI, 2019).

Caracterização bioquímica da peçonha da *A. veratra*

Com relação à caracterização da peçonha da *Aulactinia veratra*, foram identificados mais de 300 proteínas e peptídeos por LC-MS/MS. Destes, cerca de

59 biomoléculas foram classificadas como pertencentes a 14 famílias de toxinas de anêmonas-do-mar e mais 20 peptídeos foram classificados como detentores de novos ‘scaffolds’ de cisteínas, totalizando a identificação de 79 toxinas (Fig 2 do manuscrito 2 – Apêndice B). Além disso, a busca por sequências no transcriptoma que apresentassem a mesma arquitetura de domínios de toxinas encontradas no proteoma, possibilitou a identificação de mais de 600 toxinas putativas. Tal número de toxinas foi apenas identificado devido à associação de dados proteômicos ao banco de dados do transcriptoma, já disponível para esta espécie. Para a classificação de toxinas, não apenas a similaridade ao BLASTp hit foi utilizada como critério, mas também a assinatura de domínios característicos para cada toxina (manuscrito 2 – Apêndice B). Tal estratégia foi seguida, pois a associação de técnicas ômicas permite tanto a identificação de toxinas já conhecidas, como permite a elucidação de novos polipeptídios e a validação de toxinas putativas (BABENKO et al., 2017).

Dentro desta avaliação foi visto que a peçonha da *A. veratra* é formada principalmente por inibidores do tipo Kunitz e Kazal, e por um diverso arsenal de neurotoxinas que incluem SCRiP ‘*Small Cysteine Rich Peptides*’ e ICKs ‘*Inhibitor cystine knot*’, neurotoxinas estas que são menos comuns em anêmonas.

Inibidores de serinopeptidases e neurotoxinas

Peptídeos inibidores de serinopeptidases têm sido amplamente descritos na peçonha de anêmonas, especialmente os de tipo Kunitz (C1-C6, C2-C4, C3-C5) que exercem tal importância, que correspondem à uma das principais classes de toxinas de anêmonas – a ‘Família tipo Kunitz da Peçonha, subfamília de toxinas de canais de potássio tipo 2 de anêmonas-do-mar’ (PRENTIS et al., 2018). Estes peptídeos têm sido isolados a partir de extratos de tecidos de anêmonas; estando presentes em tentáculos, acrorhagi, muco ou diretamente na peçonha secretada por estes cnidários (SCHWEITZ et al., 1995; MINAGAWA et al., 2008; MADIO et al., 2017). Tais toxinas podem apresentar ação dupla inibindo peptidases e modulando canais de potássio. Alguns exemplos são as Kalicludinas e Kaliseptina da *Anemonia sulcate*; ShPI-1 da *Stichodactyla helianthus;* APEKTx1 da *Anthopleura elegantissima;* HCRG1 e HCRG2 da *Heteractis crispa* (SCHWEITZ et

al., 1995; GARCÍA-FERNÁNDEZ et al., 2016; PEIGNEUR et al., 2011; GLADKIKH et al.,2015; GLADKIKH et al 2020).

Por outro lado, inibidores do tipo Kazal, que tipicamente exibem pontes dissulfeto entre C1-C5, C2-C4 e C3-C6, não são classificados como as principais toxinas de anêmonas (MADIO et al., 2019), apesar de sequências de domínio kazal já terem sido descritas no transcriptoma da *Anthopleura dowii* (RAMÍREZ-CARRETO et al., 2019); no transcriptoma e proteoma de tentáculos da *Oulactis sp.* (MITCHELL et al., 2020); e até um inibidor já ter sido isolado de extratos da *Anemonia sulcata*, sendo classificado como PI-Actitoxin-Adv5a no Uniprot/SwissProt (HEMMI et al., 2005; KOLKENBROCK & TSCHESCHE; 1987). No caso da *A. veratra*, inibidores do tipo Kazal estão entre os principais componentes, correspondendo a quase 10% das toxinas encontradas na peçonha (Fig 2 do manuscrito 2 – Apêndice B).

Além destes inibidores, foi visto que a peçonha da *A. veratra* é constituída por seis tipos de neurotoxinas: ShK-like; β-defensinas tipo Nav; β-defensinas tipo Kv3; SCRiPs, EGF-like; e ICKs, correspondendo a um terço do total de toxinas desta anêmona. Tal observação é corroborada pelo fato de que uma das principais características da peçonha de anêmonas vem da sua constituição predominante por neurotoxinas (ASHWOOD et al., 2020; FRAZÃO ET AL., 2012).

A maioria das neurotoxinas encontradas na *A. veratra* estão relacionadas a função de modular canais iônicos dependentes de voltagem (manuscrito 2 – Apêndice B). Por exemplo, foram encontradas toxinas exibindo domínio característicos de ShK-like (CXDXnCXnCXnKKXnCXKXCX2C), apresentando a presença de 6 cisteínas e resíduos de lisina (K) e ácido aspártico (D) em posições conservadas (MADIO et al., 2019). Toxinas com esta assinatura são conhecidas por serem potentes bloqueadores de canais do tipo Kv1. São exemplos as toxinas BgK (*Bunodosoma granulifera*), AsKs (*Anemonia sulcata*) e ShK da *Stichodactyla helianthus* (DAUPLAIS et al., 1997; FRAZÃO et al., 2012). Adicionalmente, toxinas com domínios exibindo pontes dissulfeto entre C1-C5, C2-C4, C3-C6, classificadas como β-defensinas, são normalmente relacionadas à modulação de canais Kv3 e Nav. A maioria das β-defensinas de *A. veratra* apresentam similaridade a toxinas moduladoras de canais de potássio do tipo III da *Anemonia sulcata*. Toxinas como

BDS-I e BDS-II, têm sido aplicadas em estudos biofísicos envolvendo a elucidação do papel de canais Kv3 no sistema nervoso central (YEUNG *et al*., 2005). Além disso, apenas uma β-defensina foi classificada como inibidor de Nav e apenas uma toxina classificada como do tipo ICK (CXnCXnCCXnCXnC), representando potenciais moduladores de canais de sódio dependentes de voltagem (Nav) (MADIO et al., 2019; CARDOSO et al; 2019; POSTIC et al., 2018).

Toxinas do tipo Citolisinas (Actinoporinas e MACPF)

Além destas, citolisinas do tipo II (actinoporinas) e V (MACPF) foram identificadas na peçonha da *A. veratra* (Tabela 1 do manuscrito 2 – Apêndice B). Citolisinas são moléculas capazes de causar poros em membranas celulares. No caso das actinoporinas, é conhecido que a pré-incubação destas com a esfingomielina leva à completa inibição da atividade destas toxinas, sugerindo-se a alta afinidade das actinoporinas por membranas ricas neste lipídeo (VALLE et al., 2015). Devido à alta capacidade citolítica destas toxinas, actinoporinas têm sido empregadas na construção de imunotoxinas usadas contra células tumorais e parasitas. Estas toxinas têm sido empregadas na criação de imunocomplexos pela vantagem de não necessitarem da internalização do componente tóxico para que haja a morte celular (TEJUCA; ANDERLUH; DALLA SERRA, 2009).

Dos transcritos encontrados no proteoma e classificados como actinoporinas, apenas a toxina correspondente ao aul_smart_512597|CDS1, exibiu o completo domínio característico, tendo cerca de 75% de identidade à Delta-actitoxina da *Anthopleura asiatica* (Tabela 1 do manuscrito 2 – Apêndice B). Tal toxina, que não possui cisteínas em sua sequência, segue o que é descrito para a maioria das actinoporinas, conhecidas pela a ausência de resíduos de cisteínas em sua estrutura (VALLE et al., 2015).

As citolisinas do tipo V, caracterizadas pela presença de um domínio EGF e pela presença do domínio que caracteriza a superfamília das MACPF, são toxinas com aproximadamente 60kDa. Até 2019 apenas três toxinas desta classe tinham sido descritas, a saber a AvTx-60A da *Actineria villosa*, PsTx-60A e a PsTx-60B da anêmona *Phyllodiscus semoni* (MADIO et al., 2019; OSHIRO et al., 2004; SATOH et al., 2007). Na análise proteômica da peçonha da *A. veratra* foram identificadas duas novas citolisinas do tipo V, contendo o domínio MACPF, são elas a

aul_smart_487417|CDS2 e aul_smart_884261|CDS11 (Tabela 1 do manuscrito 2 – Apêndice B).

Enzimas

Quanto às enzimas, uma serinopeptidase exibindo 64% de identidade com quimotripsinogênio-A-like de *Actinia tenebrosa* foi encontrada (Tabela 1 do manuscrito 2 – Apêndice B). A sequência de aminoácidos desta serinopeptidase quando submetida à plataforma InterPro, apresentou a ocorrência de domínios de tripsina e quimotripsina, sendo classificada como pertencente à família de peptidases S1 e subfamília S1A, caracterizada por apresentar a tríade catalítica histidina, ácido aspártico e serina. Além desta, metalopeptidases foram encontradas (Tabela 1 – Manuscrito 2 – Apêndice B). Estas possíveis toxinas exibiram em torno de 50% de identidade com a "endothelin-converting enzyme 1-like (ECE-1-like)" de *Actinia tenebrosa* (Tabela 2 e 3). A enzima ECE-1 humana é conhecida por catalizar os passos finais da biossíntese da endotelina 1, uma importante molécula associada à asma, hipertensão pulmonar e sistêmica (SCHULZ et al., 2009). De acordo com a plataforma InterPro, as metalopeptidases da peçonha da *A. veratra* exibem a existência de domínios correspondentes à metalopeptidases da família M13, na qual o sítio ativo predito envolve o motivo HEXXH, nos quais os resíduos de histidina (H) ligam ao zinco e o ácido glutâmico (E) assume uma função catalítica (RAWLINGS & BARRETT, 2004). Como os membros da M13 possuem parte de seus resíduos ligados à membrana, as sequências das metalopeptidases encontradas serão investigadas quanto à presença de domínios transmembrana. Adicionalmente a estas, sequências correspondentes às endonucleases, CAP, CAP-ShK e WSC foram encontradas (Manuscrito 2 – Apêndice B).

SCREPS ' Secreted Cysteine-Rich REpeat Peptides' encontrados na peçonha da ***A. veratra***

A repetição em tandem de domínios tem sido descrita em várias toxinas peptídicas isoladas de secreções da peçonha de animais. Esta repetição é um evento relativamente comum na natureza, considerado uma estratégia evolutiva através do uso da duplicação intragênica ou recombinação. Recentemente chamadas de SCREPs do inglês "Secreted, Cysteine-Rich REpeat Peptides" por

Maxwell et al. 2018, tais toxinas apresentam um arranjo estrutural incomum levando a uma resposta farmacológica única (MAXWELL; UNDHEIM; MOBLI., 2018; SHIOMI et al., 2001).

Particularmente, toxinas com domínios ricos em pontes dissulfeto chamados DRDs ("*Disulfide-rich domains*"), são visadas devido à habilidade de modulação de canais iônicos. Tais toxinas de peçonhas animais assumem dobramentos específicos e são classificadas em grandes grupos como no caso de toxinas com domínios do tipo Kunitz, Kazal, ICKs e ShKT (MAXWELL; UNDHEIM; MOBLI., 2018). Quando exibem dois domínios ou mais com repetição em tandem, estas toxinas assumem uma arquitetura diferenciada que pode levá-las a um modo de ação bivalente. Este é o caso da DkTx (Double-knot toxin), isolada da tarântula *Ornithoctonus huwena*, uma toxina com dois domínios ICK em tandem, que ativam irreversivelmente canais TRPV1 através da sua ligação a resíduos da região de formação de poros do canal (BOHLEN et al., 2010).

Na análise proteômica da peçonha e do transcriptoma da *A. veratra*, a existência de SCREPs pôde ser notada nas classes de toxinas do tipo ShK, SCRiP, EGF-like, Kunitz and Kazal (Fig 4.B do manuscrito 2 – Apêndice B). A ocorrência destes SCREPs na peçonha apresenta uma interessante possibilidade de análise quanto às diferenças de atividade desempenhada entre toxinas com único domínio e repetição de domínios em tandem. Além disso, a análise das famílias gênicas às quais tais toxinas pertencem e os eventos de duplicação ou recombinação que levaram ao surgimento dos SCREPs encontrados aqui, parecem ser uma boa porta de entrada para o estudo da evolução destas toxinas.

*Novos scaffolds de cisteínas caracterizam novas toxinas na **A. veratra***

Como descrito anteriormente, a combinação de tecnologias ômicas permite a identificação de classes de toxinas bem estabelecidas, além da avalição de sequências de toxinas e a identificação possíveis novos domínios ainda não descritos para toxinas em estudos prévios (BABENKO et al., 2017). Trabalhos recentes envolvendo estas abordagens permitiram a identificação de 12 novos scaffolds de cisteína em toxinas da peçonha da anêmona *Stichodactyla haddoni*, e 3 novos identificados na peçonha da espécie *Cnidopus japonicus* (BABENKO et al., 2017; MADIO et al., 2017).

Aqui, para o estabelecimento dos 18 novos scaffolds de toxinas nunca antes descritos para anêmonas, foi de fundamental importância a associação de dados do transcriptoma e proteoma da *A. veratra*. De forma geral, para tal classificação foram consideramos 4 aspectos: 1. Proteínas/peptídeos sem similaridade a BLASTp hits. 2. Proteínas/peptídeos similares a proteínas não caracterizadas de espécies de anêmonas. 3. Ausência de domínios automaticamente identificados pelo NCBI ou InterPro. 4. Candidatos ricos em resíduos de cisteínas.

Estas novas famílias de toxinas, classificadas aqui como *scaffolds* 1 a 18, correspondem a 25% do total de toxinas da peçonha, e à 30% de todas as toxinas putativas encontradas no Transcriptoma da *A. veratra* (Fig 3 e Tabela 3 do manuscrito 2 – Apêndice B). A observação mais interessante a ser feita aqui é que boa parte dos novos scaffolds de toxinas apresentaram similaridade à BLASTp hits de proteínas não caracterizadas (‘uncharacterized protein’) ou similaridade não significativa à proteínas e peptídeos do banco de dados de anêmonas do NCBI (Tabela 1 do manuscrito 2 – Apêndice B). O mesmo foi visto para a toxina ICK e SCRiP que não apresentaram qualquer similaridade à toxinas previamente descritas para anêmonas-do-mar. Tais observações destacam o fato de que muitas toxinas podem passar desapercebidas quando apenas similaridade é usado como fator primordial para a descrição de toxinas presentes em cnidários e outros animais peçonhentos.

Isolamento e seleção de inibidores de serinopeptidases a partir da peçonha da *A. cascaia*

Inibidores de serinopeptidases têm sido descritos numa série de estudos envolvendo anêmonas-do-mar (ISHIDA et al., 1997; MINAGAWA, et al 1997; MINAGAWA et al., 1998; SINTSOVA et al., 2018; GLADKIKH et al., 2015; CHEN et al., 2019). Especialmente os inibidores do tipo Kunitz da peçonha de anêmonas, que estão entre as principais famílias de toxinas destes cnidários (PRENTIS et al., 2018).

Comumente, a presença de tais peptídeos na peçonha de anêmonas é descrita pela avaliação proteômica ou transcriptômica de moléculas secretadas ou de estruturas anatômicas relacionadas à peçonha destes animais (MITCHELL et

al., 2020, MADIO et al., 2017). Porém, estratégias para identificação de tais peptídeos também podem envolver o isolamento de tais componentes por técnicas cromatográficas a partir da peçonha ou do tecido destes animais (ISHIDA et al., 1997; MINAGAWA, et al 1997; MINAGAWA et al., 1998). Tal caracterização geralmente envolve a seleção de inibidores por sua direta influência sobre a atividade de serinopeptidases como tripsina, quimotripsina, calicreínas; e a elucidação da sequência destas moléculas (CHEN et al., 2019; SINTSOVA et al., 2018). Inibidores como a PI-stichotoxin-Hmg3a (C0HK72) da *Heteractis magnifica*; PI-stichotoxin-Hcr2g (C0HJU7) da *Heteractis crispa;* ATPI-I (A0A6P8HC43) e ATPI-II da *Actinia tenebrosa,* são alguns exemplos de inibidores do tipo Kunitz isolados a partir de anêmonas (SINTSOVA et al., 2018; GLADKIKH et al., 2015; CHEN et al., 2019).

No presente estudo, a peçonha da *A. cascaia* foi investigada quanto à presença de inibidores de serinopeptidases através do monitoramento da inibição da atividade da tripsina por ensaio enzimático em placa, utilizando um substrato fluorescente (Apêndice A – Manuscrito 1). Ao todo, três peptídeos foram isolados da peçonha (encontrados na F3.7.6; F3.8.4; F3.8.8), assim como uma fração enriquecida em peptídeos inibidores (F3.7.5). Tais componentes foram comprovadamente capazes de ligar a tripsina e inibir sua atividade, sendo classificados aqui como inibidores de serinopeptidases por apresentarem de 59% a 93% de inibição da atividade enzimática (Apêndice A – Manuscrito 1 – Fig 4 e Fig 5). Para o isolamento destes peptídeos, basicamente três passos cromatográficos por RP-HPLC foram necessários, envolvendo principalmente mudanças na concentração de solventes.

Para a espécie *Anthopleura cascaia*, além do inibidor de canal de potássio previamente descrito (Acesso: A0A6I8WFP9/ PDB Entry - 6NK9), e de três neurotoxinas identificadas como AcaIII1425, AcaIII2970 e AcaIII3090, não é bem conhecida a diversidade de toxinas da peçonha desta espécie (AMORIM et al., 2020; BERMAN et al., 2003; MADIO et al., 2012).

Por outro lado, a nível de gênero, *Anthopleura* possui mais de 30 toxinas manualmente anotadas no Swiss-Prot/UniProtKB (The UniProt Consortium, 2021- acesso em 22 de maio de 2022; JUNGO et al., 2015; MONKS et al., 1995; REIMER et al., 1985). Entre tais toxinas estão 3 inibidores do tipo Kunitz, isolados a partir do

extrato aquoso da espécie *A. aff. Xanthogrammica* (PI-actitoxin-Axm2a, PI-actitoxin-Axm2b e PI-actitoxin-Axm2b), exibindo massas entre 6341 Da e 6978 Da (MINAGAWA, et al 1997; MINAGAWA et al., 1998); 2 inibidores isolados a partir da acrorhagi de *A. fuscoviridis* (PI-actitoxin-Afv2a com 6097 Da e PI-actitoxin-Afv2b de 5995 Da) (MINAGAWA et al 2008). E um inibidor isolado da *A. elegantissima*, classificado como KappaPI-actitoxin-Ael3a por exibir atividade dupla ao inibir serinopeptidases e ao ligar canais de potássio dependentes de voltagem (Kvs) (PEIGNEUR et al., 2011).

Adicionalmente a estes estudos, transcritos com BLAST hits correspondentes a inibidores do tipo Kunitz foram altamente expressos tanto no transcriptoma de pólipos agressivos, quanto não-agressivos da espécie *Anthopleura elegantisssima* (MACRANDER et al. 2015). E no estudo do proteoma e transcriptoma do muco e tentáculos da *Anthopleura dowii*, foi revelada a presença de 12 transcritos pertencentes à família Kunitz/Kv2 de toxinas. Cinco destes transcritos apresentaram similaridade à região madura da proteína KappaPI-AITX-Ael3a da *Anthopleura elegantissima*, apresentando 37 a 80% de identidade (RAMÍREZ-CARRETO et al., 2019).

O aspecto comum entre tais inibidores isolados de espécies de *Anthopleura* é a classificação comum destes peptídeos como do tipo Kunitz, exibindo três pontes dissulfeto e sequências com 56 a 61 aminoácidos. Para a espécie *A. cascaia*, cuja peçonha foi estudada aqui, os inibidores de serinopeptidases isolados exibiram m/z entre 2617 e 4755, tanto por análises por MALDI-TOF quanto por ESI (Apêndice A – Manuscrito 1 – Fig 4, 5 e 6). Tais peptídeos possuem massas moleculares semelhantes aos inibidores do tipo Kunitz/Kv2 descritos para a espécie de anêmona *Actinia equina* (4071 Da e 4308 Da); e massas moleculares semelhantes a inibidores do tipo Kunitz da espécie de serpente *Daboia siamensis*, que exibem massas de 2050 Da and 2691 Da (ISHIDA et al., 1997; The UniProt Consortium, 2021 – acesso em 22 de maio de 2022).

Devido à direta relação ao gênero *Anthopleura* e à comprovada existência de peptídeos do tipo Kunitz nde espécies do mesmo gênero, sugere-se que os três peptídeos inibidores de serinopeptidases isolados – 4461 m/z (da F3.7.6); 2617 m/z (da F3.8.4) e 2642 m/z (da F3.8.8) – e os inibidores encontrados na F.3.7.5 sejam do tipo Kunitz. Porém, o processamento adicional e análise por LC-MS/MS destas

amostras serão necessárias para a confirmação da classe de toxina e para a elucidação da sequência de aminoácidos de tais peptídeos.

Isolamento e seleção de inibidores de serinopeptidases a partir da peçonha da *A. veratra* por MALDI-TOF

Na investigação da presença de inibidores a partir da peçonha da *Aulactinia veratra*, foi visto por análise proteômica e do banco de dados do Transcriptoma, que esta espécie é uma rica fonte de inibidores de serinopeptidases, tanto do tipo Kunitz quanto Kazal (Apêndice B – Manuscrito 2). E na busca pelo isolamento de tais peptídeos, a peçonha da *A. veratra* foi fracionada por RP-HPLC e a presença de inibidores de serinopeptidases foi monitorada por ensaio enzimático envolvendo espectrometria de massas do tipo MALDI-TOF (Fig 8).

A espectrometria de massas (MS) tem sido empregada, em suas diversas formas, em uma série de trabalhos focados na detecção de atividade e cinética enzimática, seja por ESI (electrospray ionization) ou MALDI-TOF (matrix-assisted laser desorption/ionization time-of- flight). São exemplos os ensaios realizados para a detecção simultânea de substratos e produtos oriundos da atividade proteolítica de frações da peçonha da *Bothrops moojeni* utilizando ESI-MS; ensaios empregando MALDI-TOF para detecção semiquantitativa da atividade enzimática de quinases ou para cinética enzimática (LIESENER et al., 2005; MIN et al., 2004; HOUSTON et al., 2000; KANG et al., 2000).

Ao contrário de métodos de detecção que usam UV/vis, fluorescência ou radioatividade, geralmente aplicados na detecção da atividade enzimática, ensaios envolvendo MS são baseados na detecção da razão massa/carga de compostos. Isto possibilita a detecção de múltiplos substratos e seus respectivos produtos numa mesma análise (LIESENER et al., 2005).

No entanto, com relação aos ensaios envolvendo MALDI-TOF, uma desvantagem é a não distribuição homogênea de analitos na matriz o que causa uma baixa reprodutibilidade de amostra para amostra e ‘shot-to-shot’ (KANG et al., 2000). Este fato causa diferenças entre a ionização e consequentemente a intensidade de uma m/z em diferentes pontos de uma mesma amostra. Devido a isso, para detecção da inibição enzimática, não é suficiente a comparação entre intensidades do produto de uma amostra controle em relação a uma outra contendo

inibidor, mas se faz necessária a comparação da intensidade do substrato restante e seu produto no mesmo ponto da amostra. Assim, a relação de intensidade do produto pela intensidade do substrato de cada amostra foi apresentada nas figuras 9.B, 11.B, 13.B e 15.B, permitindo a comparação das frações dententoras ou não de inibição. Nestas figuras é possível notar que a amostra contendo apenas substrato e água (Branco) e incubadas por 40 min apresentam alta intensidade da 523 m/z, tal massa identificada não corresponde ao produto gerado pela tripsina. Nós hipotetizamos que esta m/z pode ser correspondente às moléculas remanescentes do substrato que não apresentam conjugação com pNa.

Tal método de seleção de inibidores por MALDI-TOF possibilitou a seleção de várias subfrações inibitórias, todas obtidas por RP-HPLC (F4.2, F4.3; F4.5, F6.1, F7.1, F 7.3, F 7.4, F10.1 e F10.2) (Fig. 9, 11, 13 e 15); e o isolamento por troca iônica de pelo menos três candidatos a inibidores: F7.1.1; F6.1.1; F10.2 (Fig 17). Devido à comprovada existência de 8 inibidores do tipo kazal e 6 inibidores do tipo Kunitz no proteoma da *A. veratra*, e à presença de mais de 140 transcritos com tais domínios no transcriptoma da espécie, é provável que as moléculas das frações responsáveis pela inibição sejam inibidores do tipo Kazal ou Kunitz (Manuscrito 2 – Apêndice B). Para a confirmação, será realizada a análise por LC-MS/MS destas amostras e será feita uma busca por BLAStp contra o bando de dados do transcriptoma e proteoma da *A. veratra*, já elucidados no Manuscrito 2 (Apêndice B).

Identificação da localização tecidual de inibidores de serinopeptidases no tecido da *A. cascaia* e no tecido da *A. veratra*

Comumente, o estudo da composição de peçonhas envolve o processamento de tecidos ou de secreções animais, com o objetivo de investigar a diversidade molecular e consequentemente identificar toxinas e transcritos relacionados (MITCHELL et al., 2020, de OLIVEIRA et al., 2018; MADIO et al., 2017). Porém, a informação sobre a distribuição espacial de toxinas geralmente é perdida em análises como proteômica e transcriptômica, uma vez que são utilizados extratos ou secreções de tecidos para investigar tais toxinas.

Neste processo, a espectrometria de massas (MS) é considerada uma ferramenta crucial para a caracterização estrutural de moléculas, o que contribui grandemente para a investigação da função biológica destas (DON et al., 2016). Quando associada à histologia, tal técnica oferece uma interessante solução para suprir o desafio de localizar toxinas em tecidos, através do imageamento por espectrometria de massas (IMS).

O IMS tem sido aplicado na investigação de distribuição de moléculas em diferentes estágios do desenvolvimento de tecidos; permite comparar a co-localização de moléculas de interesse; e ainda visualizar em quais regiões estas moléculas podem estar estocadas (VELIČKOVIĆ et al., 2014; HAMILTON et al, 2019; UNDHEIM et al, 2014). As aplicações para o estudo de glândulas ou outras estruturas que estocam toxinas são inúmeras.

Para anêmonas-do-mar, assim como para outros cnidários, acessar a localização de toxinas pode ser desafiador, uma vez que estes animais possuem cápsulas de peçonha distribuídas por todo o corpo, em vez de um sistema centralizado de toxinas (MITCHELL et al., 2017).

Dentro deste contexto, no presente estudo a distribuição de toxinas ao longo do tecido das anêmonas *Anthopleura cascaia* e *Aulactinia veratra*, foi investigada. Pela primeira vez aqui foi demonstrada a localização direta de inibidores de serinopeptidases nos tentáculos e disco pedal de anêmonas-do-mar pelo Imageamento por espectrometria de massas (Fig 18, Fig 19 da tese; Fig 7 do Manuscrito 1 – Apêndice A). É importante salientar que a presença de toxinas do tipo Kunitz em tentáculos já foi descrita através da avaliação da composição de extratos brutos de tecidos de anêmonas (MACRANDER et al., 2016). Porém, aqui foi demonstrada a distribuição de tais inibidores em tentáculos - estruturas anatômicas utilizadas por estes cnidários para a imobilizar presas e repelir predadores (ASHWOOD et al., 2020; MACRANDER et al., 2016). Tal relação entre estrutura anatômica e localização da toxina é bastante interessante, uma vez que inibidores do tipo Kunitz também são relatados na literatura como toxinas de agressão e defesa em anêmonas (FRAZÃO et al., 2012).

Estudos prévios já demonstraram a presença de peptídeos do tipo Kunitz em filamentos mesenteriais de *Actinia tenebrosa*, além disso, o MALDI-IMS já foi aplicado na elucidação da distribuição espacial da κ-actitoxin-Ate1a em *Actinia*

tenebrosa, e na distribuição de toxinas peptídicas em *Oulactis muscosa* (CHEN et al., 2019; MITCHELL et al., 2017; MADIO et al., 2018; SURM et al., 2019).

No presente estudo, a análise por MALDI-IMS revelou que inibidores de serinopeptidases são diferentemente distribuídos tanto na anêmona *A. cascaia* (Fig 7- Manuscrito 1 – Apêndice A), quanto na anêmona *A. veratra* (Fig 18 e 19). Para ambas anêmonas foi visto que há a presença de inibidores nos filamentos mesentéricos: os inibidores 2617 m/z (da F3.8.4) e 2642 m/z (da F3.8.8) da *A. cascaia* estão especialmente presentes nesta região (Fig 7- Manuscrito 1 – Apêndice A). Assim como os inibidores do tipo Kunitz (NTAv186 de 6919 Da – Fig 18) e tipo Kazal (NTAv120, Av26, NTAv30, NTAv107 e Av133) encontrados na *A. veratra* (Fig 19). Por outro lado, os peptídeos da F3.7.5 (4518, 4685 and 4755m/z) e F3.7.6 (4461 m/z) da *A. cascaia* estão localizados principalmente na região do disco pedal e tentáculos da anêmona (Fig 7 - Manuscrito 1 – Apêndice A). Enquanto na *A. veratra*, apenas os inibidores do tipo Kunitz (NTAv189) e Kazal (NTAv202, NTAv145 e Av24) apresentam maior presença na região dos tentáculos da anêmona (Fig 18 e 19). A presença de tais toxinas nestas regiões é esperada devido à presença de nematocistos, especialmente em tentáculos envolvidos com defesa e predação. Além disso, para animais da classe Anthozoa, como anêmonas, já é descrita a presença de estruturas secretoras de toxinas como nematocistos e células ectodérmicas (‘*ectodermal gland cells*’) – na endoderme e ectoderme destes animais (FAUTIN et al., 2009; MORAN et al., 2011).

Adicionalmente, estudos anteriores mostram que há significativa variação na abundância de genes relacionados a toxinas entre tentáculos, filamentos mesentéricos e coluna de espécies de anêmonas-do mar (MACRANDER et al., 2016). Particularmente, inibidores do tipo Kunitz/Kv2 são altamente expressos em filamentos mesentéricos e tentáculos nas espécies *Anemonia sulcata*; *Heteractis crispa* e *Megalactis griffithsi*. Tais dados corroboram as diferenças em distribuição de inibidores encontrados aqui para as anêmonas *A. cascaia* e *A. veratra* (MACRANDER et al., 2016).

Além disso, quando testado se tais inibidores eram capazes de inibir a tripsina diretamente em tecido, foi constatado que tais moléculas permanecem ativas, mesmo após todo o tratamento térmico e químico envolvido no preparo da amostra de tecido da *A. veratra*. Foi revelado que após a incubação da tripsina num

tecido de anêmona coberto por substrato, há locais com menor geração do produto (523 m/z) a partir do substrato (644 m/z) utilizado. Tais regiões correspondem justamente à maior concentração de inibidores em certas áreas do tecido da *A. veratra*. Por exemplo, é muito clara a inibição da atividade da tripsina na região do mesentério da anêmona, onde há maior presença de inibidores do tipo Kazal e consequentemente menor detecção do produto (523 m/z) (Fig 20). Este tipo de estudo revela que inibidores podem ser localizados não só por meio da massa molecular conhecida, mas que estes podem ser rastreados em tecido através da atividade exercida sobre a enzima.

6 CONCLUSÕES GERAIS

O estudo aqui realizado apresentou pela primeira vez a elucidação do proteoma da peçonha da anêmona-do-mar *Anthopleura cascaia*, uma espécie endêmica brasileira, cuja peçonha contém uma interessante diversidade de toxinas: natterinas, citolisinas, fosfolipases do tipo A2 e inibidores de serinopeptidases.

Através do rastreamento da inibição da atividade da tripsina por frações da peçonha, foi revelada que a *A. cascaia* é uma interessante fonte de inibidores de serinopeptidases, potencialmente do tipo Kunitz, devido à ocorrência de tais toxinas em outras espécies do gênero como *A. elegantissima* e *A. dowii*. Tais inibidores isolados, exibem massa/carga de 4461 m/z; 2617 m/z e 2642 m/z e potente inibição da atividade da tripsina (60 a 93%), e estão diferencialmente localizados no mesentério, disco pedal e tentáculos desta anêmona, como revelado por MALDI-MSI.

Já os dados obtidos na análise da peçonha da anêmona *A. veratra* revelam que a associação das ferramentas de transcriptômica e proteômica permitiu uma análise complementar da riqueza de toxinas desta espécie. Estas abordagens levaram à caracterização da peçonha desta anêmona - composto principalmente por neurotoxinas e inibidores de serinopeptidases. A diversidade de toxinas identificada é tamanha que foram elucidadas14 famílias de toxinas de anêmonas para a peçonha da *A. veratra*. Entre estas, foram identificadas neurotoxinas como β-defensinas bloqueadoras de canais de potássio e sódio dependentes de voltagem; toxinas ShK-like; ICK; SCRiPs; Citolisinas e inibidores de

serinopeptidases do tipo Kunitz e Kazal, moléculas com potencial para investigação farmacológica. Além disso, a aplicação destas ferramentas possibilitou a identificação de 18 novos “scaffolds” de toxinas ricas em cisteínas, validadas em nível de proteínas/peptídeos.

Os dados do transcriptoma revelaram que as toxinas putativas mais abundantes são especialmente encontradas nas famílias ShK, Kazal, Kunitz, CAP e Scaffold 10; e que algumas destas famílias apresentam repetição em tandem de domínios - são os casos de algumas sequências encontradas em toxinas do tipo ShK, SCRiP, EGF-like, Kunitz, Kazal, Scaffold 10, Scaffold 13, classificadas como SCREPs. Tais toxinas são encontradas em nível de proteína e são traduzidas com domínios duplos e triplos, oferecendo uma oportunidade interessante de investigação de propriedades farmacológicas, uma vez que a maior disponibilidade de domínios pode facilitar a capacidade de ligação destas toxinas a enzimas e a canais iônicos dependentes de voltagem.

Estes dados ômicos permitiram um embasamento para a caracterização e busca da purificação dos inibidores do tipo Kazal e Kunitz. Aliado a estas últimas, aqui estabelecemos um ensaio de detecção da atividade e inibição de serinopeptidases por espectrometria de massas (MS). Apesar de tal ensaio não apresentar o consumo do substrato ao longo do tempo, o mesmo mostra ser um potencial método de seleção de inibidores com o uso mínimo de amostra.

A otimização deste método permitiu a aplicação do mesmo na detecção da inibição da tripsina em tecido, através do imageamento por espectrometria de massas. Assim, quanto ao estudo da peçonha da *A. veratra* foi possível elucidar sequências; isolar parcialmente inibidores de serinopeptidases e detectar toxinas em diferentes localizações do seu tecido.

REFERÊNCIAS

ABBENANTE, G.; FAIRLIE, D. P., Protease inhibitors in the clinic. **Journal of Medicinal Chemistry** v. *1*, n.1, p. 71-104, 22 oct. 2005. DOI:10.2174/1573406053402569

AMORIM, G.C., MADIO, B., ALMEIDA, F.C.L. Solution structure of AcaTx1, a potassium channel inhibitor from the sea anemone Antopleura cascaia. PDB DOI: 10.2210/pdb6NK9/pdb

ANDRADE, M. A.; PEREZ-IRATXETA, C.; PONTING, C. P. Protein Repeats: Structures, Functions, and Evolution. **Journal of Structural Biology**, v. 134, n. 2–3, p. 117–131, 1 maio 2001. https://doi.org/10.1006/jsbi.2001.4392

ARASTU-KAPUR S, et al. Identification of proteases that regulate erythrocyte rupture by the malaria parasite Plasmodium falciparum. **Nat Chem Biol**. v.4(3), n. p.203-213, 8 março, 2008. DOI: 10.1038/nchembio.70

ASHWOOD LM, et al. Characterising Functional Venom Profiles of Anthozoans and Medusozoans within Their Ecological Context. **Mar Drugs**. v.18(4):202, p1-19, 9 abril 2020. https://doi.org/10.3390/md18040202

AUF DEM KELLER U., DOUCET A. AND OVERAL C.M. Protease research in the era of systems biology. **Biol. Chem**., v. 388, n.11, p. 1159–1162, Nov. 2007. DOI: 10.1515/BC.2007.146

BABENKO, V. V. et al. Identification of unusual peptides with new Cys frameworks in the venom of the cold-water sea anemone Cnidopus japonicus. Scientific Reports, v. 7, n. 14534, p. 1–14, 6 Nov 2017. DOI:10.1038/s41598-017-14961-1

BASTOS DM, HADDAD V JÚNIOR, NUNES JL. Human envenomations caused by Portuguese man-of-war (Physalia physalis) in urban beaches of São Luis City, Maranhão State, Northeast Coast of Brazil. **Rev Soc Bras Med Trop.** v. 50, n.1, p. 130-134, Fev. 2017. doi.org/10.1590/0037-8682-0257-2016

BERMAN, H., HENRICK, K. & NAKAMURA, H. Announcing the worldwide Protein Data Bank. **Nat Struct Mol Biol**, v.10, n.980, Dez. 2003. DOI: 10.1038/nsb1203-980

BOHLEN, C. J. et al.,A bivalent tarantula toxin activates the capsaicin receptor, TRPV1, by targeting the outer pore domain. **Cell.** V. 141,n.5, p. 834–845, 28 maio 2010. doi: 10.1016/j.cell.2010.03.052

[1] De acordo com: ASSOCIAÇÃO BRASILEIRA DE NORMAS TÉCNICAS. NBR 6023: informação e documentação – referências – elaboração. Rio de Janeiro: ABNT, 2018.

CARDOSO FC, LEWIS RJ. Structure-Function and Therapeutic Potential of Spider Venom-Derived Cysteine Knot Peptides Targeting Sodium Channels. **Front Pharmacol.** v.10, n. 366, 11 abril 2019. doi: 10.3389/fphar.2019.00366

CARLGREN, O. **Survey of the Ptychodactiaria, Corallimorpharia and Actiniaria**. Califórnia. Almqvist & Wiksells Boktryckeri AB. v1, 1949, p.1-120.

CAVALCANTE MMES, et al. Health-risk assessment of Portuguese man-of-war (Physalia physalis) envenomations on urban beaches in São Luís city, in the state of Maranhão, Brazil. **Rev. Soc. Bras. Med**. **Trop.** v. 53, p 1-7; Julho 2020. doi.org/10.1590/0037-8682-0216-2020

CHEN X, et al.. A Versatile and Robust Serine Protease Inhibitor Scaffold from Actinia tenebrosa. **Mar Drugs.** v. 17(12), n. 701, 12 Dez 2019. doi: 10.3390/md17120701.

COLLINS AG. Recent insights into cnidarian phylogeny. **Smithsonian contributions to marine sciences**; n. 38, p. 139–149., Abril, 2009. https://www.researchgate.net/publication/265743266_Recent_Insights_into_Cnidarian_Phylogeny

DA SILVA, Janine Farias. **Ecologia trófica das anêmonas-do-mar *Anthopleura cascaia* e *Anthopleura Krebsi* (Cnidaria: Anthozoa) em duas prais de Pernambuco, Brasil.** Dissertação (Mestrado em Biologia Animal). Universidade Federal de Pernambuco. Recife, Pernambuco. p 11-13. 2009. URI: https://repositorio.ufpe.br/handle/123456789/581

DALY, M. et al. Anthopleura and the phylogeny of Actinioidea (Cnidaria: Anthozoa: Actiniaria). **Organisms Diversity and Evolution**, v. 17, n. 3, p. 545–564, 1 set. 2017. DOI 10.1007/s13127-017-0326-6

DALY, M.; FAUTIN, D. **World List of Actiniaria. Anthopleura Duchassaing de Fonbressin & Michelotti, 1860**. 2022. Acesso em: World Register of Marine Species at: https://www.marinespecies.org/aphia.php?p=taxdetails&id=100696 on 2022-05-25 ; Documented distribution of Anthopleura cascaia - Acesso em: https://www.marinespecies.org/aphia.php?p=distribution&id=1521868,1521867,1521866,1521865,1521864,1521863,1520563

DAVID, C.N.; et al. Evolution of complex structures: minicollagens shape the cnidarian nematocyst. **Trends Genet**., v. 24, n. 9 p. 431–438, Set 2008. DOI: 10.1016/j.tig.2008.07.001

DAUPLAIS M., et al. On the Convergent Evolution of Animal Toxins. Conservation of a diad of functional residues in potassium channel-blocking toxins with unrelated structures*. **The Journal of Biological Chemistry**, v. 272, n. 7, p. 4302-4309, Fev. 1997. DOI: 10.1074/jbc.272.7.4302

DONG Y., Li B. Aharoni A. More than Pictures: When MS Imaging Meets Histology.**Trends in Plant Science**, v. 21, n. 8, p.686 – 698, Ago 2016. DOI: 10.1016/j.tplants.2016.04.007

DE CAPITANI, Joana Dutilh. **Estrutura populacional e variabilidade genética de anêmonas-do-mar da região entremarés de costão rochoso**. Dissertação (Mestrado em Ecologia). Universidade Estadual de Campinas. São Paulo, p. 1-69, 2007. https://hdl.handle.net/20.500.12733/1605032

DE OLIVEIRA UC, et al., Proteomic endorsed transcriptomic profiles of venom glands from Tityus obscurus and T. serrulatus scorpions. **PLoS One.,** v. 13, n.3, Mar 2018. DOI: 10.1371/journal.pone.0193739

DI CERA, E., Serine proteases. **Intern. Union of Biochem. and Molec. Biol. Life** , v. *61*, n. 5, p. 510-515, Maio 2009. DOI: 10.1002/iub.186.

EDMANDS, S.; FAUTIN, D. G. Redescription of Aulactinia veratra n. comb. (=Cnidopus veratra) (Coelenterata: Actiniaria) from Australia. **Rec. West. Aust.**

Mus. v. 15, n. 1, p. 59-68, Jan 1991. https://www.researchgate.net/publication/42853794_Redescription_of_Aulactinia_veratra_ncomb_Cnidopus_veratra_Coelenterata_Actiniaria_from_Australia

ENGHILD J.J, et al. An examination of the inhibitory mechanism of serpins by analysing the interaction of trypsin and chymotrypsin with α 2-antiplasmin. **Biochem. J.,** v. 291, n. 3, p. 933-938, Maio 1993. doi: 10.1042/bj2910933

EBI - European Bioinformatics Institute. Link de acesso: https://www.ebi.ac.uk/QuickGO/term/GO:0016500 (Consulta em 14 de agosto de 2019).

FAUTIN, G. Reproduction of Cnidaria. **Canadian Journal of Zoology**, v. 80, n. 10, p. 1735-1754, Out 2002. https://doi.org/10.1139/z02-133

FAUTIN DG. Structural diversity, systematics, and evolution of cnidae. **Toxicon.** V. 54, n. 8. p. 1054-1064, Dez 2009. DOI: 10.1016/j.toxicon.2009.02.024

FOOX J, SIDDALL ME. The road to Cnidaria: history of phylogeny of the Myxozoa.

J Parasitol. v. 101, n. 3, p. 269–274., Jun 2015. doi: 10.1645/14-671.1.

FRAZÃO B., VASCONCELOS V.; ANTUNES A. Sea Anemone (Cnidaria, Anthozoa, Actiniaria) Toxins: An Overview. **Mar. Drugs**, v. 10, n. 8, p. 1812-1851, Ago 2012. DOI: 10.3390/md10081812

FRY, B.G.; *et al*. The toxicogenomic multiverse: Convergent recruitment of proteins into animal venoms*.* **Annu. Rev. Genomics Hum. Genet***.* v.*10*, p. 483–511, jul 2009. doi: 10.1146/annurev.genom.9.081307.164356.

GARCÍA-FERNÁNDEZ R, et al. The Kunitz-Type Protein ShPI-1 Inhibits Serine Proteases and Voltage-Gated Potassium Channels. **Toxins (Basel**). v. 8, n. 4:110, Abril 2016. doi: 10.3390/toxins8040110

GASTEIGER E., et al. ExPASy: the proteomics server for in-depth protein knowledge and analysis. **Nucleic Acids Res**. v. 31, n. 13; p. 3784-3788, Jul 2003. Expasy pI/MW- https://web.expasy.org/compute_pi/
DOI: 10.1093/nar/gkg563

GLADKIKH I, et al. New Kunitz-Type HCRG Polypeptides from the Sea Anemone Heteractis crispa. **Mar Drugs**.v.13, n. 10, p. 6038-6063, 24 Set 2015. DOI:10.3390/md13106038

GLADKIKH I, et al. Kunitz-Type Peptides from the Sea Anemone Heteractis crispa Demonstrate Potassium Channel Blocking and Anti-Inflammatory Activities. **Biomedicines**.v.8, n.11:473, Nov 2020. doi: 10.3390/biomedicines8110473

GETTINS, P.G. Serpin structure, mechanism, and function. **Chem. Rev**., v. 102, n.12, p. 4751–4804, Dez 2002. DOI: 10.1021/cr010170+

GETTINS, P.G., OLSON, S.T., 2016. Inhibitory serpins. New insights into their folding, polymerization, regulation and clearance. **Biochem. J**., v. 473, n.15 p.2273–2293, Ago 2016. DOI: 10.1042/BCJ20160014

GILLMAN J.D., KIM W.S, KRISHNAN H.B.Identification of a new soybean kunitz trypsin inhibitor mutation and its effect on bowman-birk protease inhibitor content in soybean seed. **J Agric Food Chem**., v.63, n. 5, p. 1352-1359, Jan 2015. https://doi.org/10.1021/jf505220p

GOMES, P.B. **Anêmonas-do-mar (Cnidaria, Actiniaria) de Pernambuco (Brasil). em: Diagnóstico da Biodversidade de Pernambuco.** In.: TABARELLI M., SILVA J.M.C. (CoordRecife: SECTMA, editora Massangana, v.2, p.343-364, 2002.

GROHMANN, P.A., MAGALHÃES, M.P. & HIRANO, Y.M. First record of the order Stauromedusae (Cnidaria, Scyphozoa) from the tropical southwestern Atlantic, with a review of the distribution of Stauromedusae in the southern hemisphere. **Species Divers**. v. 4, p. 381–388. Jul 1999. DOI:10.12782/specdiv.4.381

HADDAD JUNIOR V.; DA SILVEIRA F.L.; MIGOTTO A.E. Skin lesions in envenoming by cnidarians (Portuguese man-of-war and jellyfish): etiology and severity of accidents on the Brazilian coast. **Rev. Inst. Med. trop. S. Paulo**, v.52 n.1, Fev. 2010. https://doi.org/10.1590/S0036-46652010000100008

HADDAD, VIDAL; et al. Jellyfish Blooms Causing Mass Envenomations in Aquatic Marathonists: Report of Cases in S and SE Brazil (SW Atlantic Ocean). **Wilderness & Environmental Medicine**, v. 29, p. 142-145, 2018. https://www.wemjournal.org/article/S1080-6032(17)30273-9/pdf

HADDAD JUNIOR V, COSTA MAO, NAGATA R. Outbreak of jellyfish envenomations caused by the species Olindias sambaquiensis (CNIDARIA: HYDROZOA) in the Rio Grande do Sul state (Brazil). **Rev Soc Bras Med Trop**. v. 52, p.1-2, 2019. https://doi.org/10.1590/0037-8682-0137-2019

HAMILTON B.R., et al.. Mapping Enzyme Activity on Tissue by Functional Mass SpectrometryImaging. **Angew. Chem. Int. Ed.**, v. 59, n.10, p. 3855 –3858, Dez 2019. doi.org/10.1002/anie.201911390

HAMLET C, STRYCHALSKI W, MILLER L. Fluid Dynamics of Ballistic Strategies in Nematocyst Firing. **Fluids, v.** 5, n. 1:20, p.1-18, Fev. 2020. doi.org/10.3390/fluids5010020

HAND, C. **The sea anemones of Central California., Part II**. Wasman Journal of Biology, v.12, n. 3, p.37-99. 1955.

HEMMI H, et al. Structural and functional study of an Anemonia elastase inhibitor, a "nonclassical" Kazal-type inhibitor from Anemonia sulcata. **Biochemistry.** v. 44, n. 28, p. 9626-9636, Jul 2005. DOI: 10.1021/bi0472806

HONMA T, SHIOMI K. Peptide Toxins in Sea Anemones: Structural and Functional Aspects. **Marine Biotechnology**, v. 8, n.1, p. 1-10, Jan 2006. DOI: 10.1007/s10126-005-5093-2

HOUSTON C.T., et al. Investigation of Enzyme Kinetics Using Quench-Flow Techniques with MALDI-TOF Mass Spectrometry. **Anal. Chem.** v. 72, n.14, p. 3311-3319, Jun 2000. https://doi.org/10.1021/ac991499m

ISHIDA M, et al. Amino acid sequences of Kunitz-type protease inhibitors from the sea anemone Actinia equina. **Fish Sci**, v. 63, n. 5, p. 794–798, Nov 1997. https://doi.org/10.2331/fishsci.63.794

JEDINÁK A, Inhibition activities of natural products on serine proteases. **Phytother Res**., v. 20, n. 3, p. 214-217, Mar 2006. DOI: 10.1002/ptr.1836

JOUIAEI M., et al. Ancient Venom Systems: A Review on Cnidaria Toxins. **Toxins**, v.7, n.6, p. 2251-2271, Jun 2015. https://doi.org/10.3390/toxins7062251

JUNGO, F.; BAIROCH, A. Tox-Prot, the toxin protein annotation program of the Swiss-Prot protein knowledgebase. **Toxicon**, v. 45, n. 3, p. 293–301, 1 mar. 2005. DOI: 10.1016/j.toxicon.2004.10.018

KHAN R.A. Natural products chemistry: The emerging trends and prospective goals. Saudi **Pharmaceutical Journal,** v. 26, n. 5, p. 739–753, Jul 2018. https://doi.org/10.1016/j.jsps.2018.02.015

KANG M.J., THOLEY A. AND HEINZLE E. Quantitation of low molecular mass substrates and products of enzyme catalyzed reactions using matrix-assisted laser desorption/ionization timeof- flight mass spectrometry. **Rapid Commun. Mass Spectrom.** v.14, n. 21, p. 1972–1978, Set 2000. https://doi.org/10.1002/1097-0231(20001115)14:21<1972::AID-RCM119>3.0.CO;2-5

KAYAL, E.; et al. Phylogenomics provides a robust topology of the major cnidarian lineages and insights on the origins of key organismal traits. **BMC Evol**. **Biol.**, v.18, n. 68, Abr 2018. https://doi.org/10.1186/s12862-018-1142-0.

KOLKENBROCK, H. & TSCHESCHE, H. The covalent structure of the elastase inhibitor from Anemonia sulcata--a "non-classical" Kazal-type protein. **Biol Chem. Hoppe-Seyler**, v. 368, n. 10, p.1297 – 1304, Fev 1987. DOI: 10.1515/bchm3.1987.368.2.1297

KILLI N, et al., Nematocyst types and venom effects of Aurelia aurita and Velella velella from the Mediterranean Sea. **Toxicon.** v.175, p. 57-63, Fev 2020. https://doi.org/10.1016/j.toxicon.2019.12.155

KOZLOV S.A., GRISHIN E.V. The universal algorithm of maturation for secretory and excretory protein precursors. **Toxicon**, v. 49 p.721-726., Abr 2007. DOI: 10.1016/j.toxicon.2006.11.007

LAEMMLI U. K. Cleavege of structural proteins during the assembly of the head of bacteriophage T4. **Nature**, v. 227, p.680-685, Ago 1970. https://www.nature.com/articles/227680a0

LAM, J.; et al. A detailed observation of the ejection and retraction of defense tissue acontia in sea anemone (Exaiptasia pallida). **PeerJ**. v. 5, p. 1–11, Fev 2017. https://doi.org/10.7717/peerj.2996

LASKOWSKI, M. AND KATO, Protein inhibitors of proteínases I. **Annu. Rev. Biochem.** v.49, p. 593-626, Jul 1980. DOI: 10.1146/annurev.bi.49.070180.003113

LESNER A, ŁĘGOWSKA A, WYSOCKA M, ROLKA K. Sunflower trypsin inhibitor 1 as a molecular scaffold for drug discovery**. Curr Pharm Des**., v. 17, n. 38, p. 4308-4317, 2011. doi: 10.2174/138161211798999393.

LIANG J, et al. A Novel CCCH-Zinc Finger Protein Family Regulates Proinflammatory Activation of Macrophages.**The J of biolog chemist**. v.283, n. 10, p. 6337–6346, Mar 2008. DOI: 10.1074/jbc.M707861200

LIAO Q, et al. Novel Kunitz-like Peptides Discovered in the Zoanthid Palythoa caribaeorum through Transcriptome Sequencing. Send to **J Proteome Res**. v. 17, n. 2, p. 891-902, Fev. 2018. DOI: 10.1021/acs.jproteome.7b00686

LIESENER A., et al. Screening for proteolytic activities in snake venom by means of a multiplexing electrospray ionization mass spectrometry assay scheme. **Rapid Commun. Mass Spectrom**. v. 19: 2923–2928, Set 2005. https://doi.org/10.1002/rcm.2136

LOPES-FERREIRA et al. Thalassophryne nattereri fish venom: from the envenoming to the understanding of the immune system. **J Venom Anim Toxins Incl Trop Dis**. V.20, n. 35, Ago 2014. https://doi.org/10.1186/1678-9199-20-35

LÓPEZ-OTÍN C. AND BOND J. J.S. Proteases: Multifunctional Enzymes in Life and Disease. **Biol Chem**. v. 283, n. 45, p. 30433–30437, Nov 2008. doi: 10.1074/jbc.R800035200.

LOTAN T.; CHALIFA-CASPI V.; ZIV T.; BREKHMAN V.; GORDON M.M.; ADMON A.; LUBZENS E. Evolutionary conservation of the mature oocyte proteome. **EU pa Open proteomics** , v. 3, p. 27–36, Jun 2014. https://doi.org/10.1016/j.euprot.2014.01.003

LOUIS H.A., et al. Comparison of Three Members of the Cysteine-rich Protein Family Reveals Functional Conservation and Divergent Patterns of Gene Expression. **J Biol Chem**. v. 272, n. 43, p. 27484–27491, Out 1997. DOI: 10.1074/jbc.272.43.27484

MACRANDER J., BRUGLER M. R., DALY M. A RNA-seq approach to identify putative toxins from acrorhagi in aggressive and non-aggressive *Anthopleura elegantissima* polyps. **BMC Genomics**. v.16, n. 221, p 1-20, Mar 2015. DOI 10.1186/s12864-015-1417-4

MACRANDER J, BROE M, DALY M. Tissue-Specific Venom Composition and Differential Gene Expression in Sea Anemones. **Genome Biol Evol**., v.8, n. 8, p. 2358-2375, Ago 2016. https://doi.org/10.1093/gbe/evw155

MADIO, B. **Purificação e caracterização da fração neurotóxica da peçonha da anêmona do mar *Anthopleura cascaia*.** Dissertação (Mestrado em Ciências - Fisiologia Geral). Universidade de São Paulo. São Paulo, p. 65, 2012. DOI: 10.11606/D.41.2012.tde-10102012-091315

MADIO B., KING G.F., UNDHEIM E.A.B. Revisiting venom of the sea anemone *Stichodactyla haddoni*: Omics techniques reveal the complete toxin arsenal of a well-studied sea anemone genus. **Journal of Proteomics**. V.166, p. 83–92. Ago 2017. DOI: 10.1016/j.jprot.2017.07.007

MADIO B., et al. PHAB toxins: a unique family of predatory sea anemone toxins evolving via intra-gene concerted evolution defines a new peptide fold. **Cell Mol Life Sci.** v. 75, n. 24, p. 4511-4524, Dez 2018. DOI: 10.1007/s00018-018-2897-6

MADIO B, KING GF, UNDHEIM EAB. Sea Anemone Toxins: A Structural Overview. **Mar Drugs**. v.17, n.6:325, p.1-26, Jun 2019. doi: 10.3390/md17060325

MALPEZZI E.L.A, FREITAS J.C, KAMIYA K.M.H. Characterization of peptides in sea anemone venom collected by a novel procedure. **Toxicon**, v. 31, n . 7, p. 853-864, Jul 1993. DOI: 10.1016/0041-0101(93)90220-d

MARISCAL, R.N. **Nematocysts**. In: Muscatine, L., Lenhoff, H.M. (Eds.), Coelenterate Biology. Academic Press, p. 129–178, 1974.

MAXWELL, M.; UNDHEIM, E. A. B.; MOBLI, M. Secreted cysteine-rich repeat proteins “SCREPs”: A novel multi-domain architecture. **Frontiers in Pharmacology**, v. 9, p. 1–16, Nov 2018. doi: 10.3389/fphar.2018.01333

MIN D.H., SU J., AND MRKSICH M. Profiling Kinase Activities by Using a Peptide Chip and Mass Spectrometry.**Angew. Chem. Int. Ed.** v.43, n.44, p. 5973 –5977, Nov 2004. https://doi.org/10.1002/anie.200461061

MINAGAWA S, et al. Kunitz-type protease inhibitors from acrorhagi of three species of sea anemones. **Comp Biochem Physiol B Biochem Mol Biol.**, v. 150, n.2:240-5, Jun 2008. DOI: 10.1016/j.cbpb.2008.03.010

MINAGAWA S, et al.. Isolation and amino acid sequences of two Kunitz-type protease inhibitors from the sea anemone Anthopleura aff. xanthogrammica. **Comp Biochem Physiol B Biochem Mol Biol.**, v. 118, n.2, p. 381-386, Out 1997. DOI: 10.1016/s0305-0491(97)00174-0

MINAGAWA, S.; et al. Amino acid sequence and biological activities of another Kunitz-type protease inhibitor from the sea anemone Anthopleura aff. xanthogrammica. **Fish Sci.**, v. 64, n.1 p.155–159, Jul 1998. https://doi.org/10.2331/fishsci.64.155

MITCHELL, M.L. et al.. The Use of Imaging Mass Spectrometry to Study Peptide Toxin Distribution in Australian Sea Anemones. **Aust. J. Chem**. v. 70, n.11, p.1235–1237, Jan 2017. https://doi.org/10.1071/CH17228

MITCHELL ML, et al. Tentacle Transcriptomes of the Speckled Anemone (Actiniaria: Actiniidae: Oulactis sp.): Venom-Related Components and Their Domain Structure. **Mar Biotechnol** (NY). v. 22, n. 2, p. 207-219, Jan 2020. https://doi.org/10.1007/s10126-020-09945-8

MIRANDA, L.S., MARQUES, A.C. Hidden impacts of the Samarco mining waste dam collapse to Brazilian marine fauna – an example from the staurozoans (Cnidaria). **Biota Neotropica**. v. 16, n.2, Jun 2016. https://doi.org/10.1590/1676-0611-BN-2016-0169

MIRANDA, L.S., et al. Lucernariopsis capensis Carlgren, 1938 (Cnidaria, Staurozoa) in Brazil: first record outside its type locality in South Africa. **Zootaxa**. V. 3158, n. 1, p.60–64. Jan 2012. DOI: https://doi.org/10.11646/zootaxa.3158.1.5

MOLINARI, C. G.; MORANDINI, A. C . Update on Benthic Scyphozoans from the Brazilian Coast (Cnidaria: Scyphozoa: Coronatae). **Revista Brasileira de Zoociências,** v. 20, n.2, p. 1-14, Dez 2019. DOI: https://doi.org/10.34019/2596-3325.2019.v20.27610

MONKS AS. Solution structure of the cardiostimulant polypeptide anthopleurin-B and comparison with anthopleurin-A. **Structure.** v. 3, n.8, p.791-803, Aug 1995. DOI: 10.1016/s0969-2126(01)00214-3

MORAN, Y.; et al. Neurotoxin localization to ectodermal gland cells uncovers an alternative mechanism of venom delivery in sea anemones. **Proc. Biol. Sci.**, v. 279, p. 1351–1358, Nov 2012. https://doi.org/10.1098/rspb.2011.1731

NAGATA, R. M. ; et al. First description of wild-collected ephyrae of Lychnorhiza lucerna (Cnidaria, Scyphozoa). **Anais da Academia Brasileira de Ciências,** v. 93, n.2, p. 1-12, 2021. https://doi.org/10.1590/0001-3765202120190574

NEVALAINEN T.J., et al. Phospholipase A2 in cnidaria. **Comp Biochem Physiol B Biochem Mol Biol**. V.139, n. 4, p. 731-5, Dez 2004. DOI:10.1016/j.cbpc.2004.09.006

OBIS - OCEAN BIODIVERSITY INFORMATION SYSTEM. Intergovernmental Oceanographic Commission of UNESCO. Link de acesso em 11 de julho de 2022: https://obis.org/taxon/283379

OLIVEIRA, O.M.P.; et al. Census of Cnidaria (Medusozoa) and Ctenophora from South American marine waters. **Zootaxa**. V.4194, n.1 p. 1-256, Nov 2016.

ORTS, D.J.; et al. Biochemical and Electrophysiological Characterization of Two Sea Anemone Type 1 Potassium Toxins from a Geographically Distant Population of *Bunodosoma caissarum.* ***Mar. Drugs****,* v.11, n.3, p. 655–679, Mar 2013. DOI:10.3390/md11030655

OSHIRO N, et al. A new membrane-attack complex/perforin (MACPF) domain lethal toxin from the nematocyst venom of the Okinawan sea anemone Actineria

villosa. **Toxicon**. v. 43, n. 2, p.225-228, Fev 2004. DOI: 10.1016/j.toxicon.2003.11.017

OWNBY C.L. Structure, Function and Biophysical Aspects of the Myotoxins from Snake Venoms. **J. of Toxic: Toxin Reviews**.v. 17. n.2, P. 213-238,1998. https://doi.org/10.3109/15569549809009250

PAGE MJ, DI CERA E. Serine peptidases: classification, structure and function. **Cell Mol Life Sci.,** v. 65, n. 7-8, p. 1220-1236, Abr 2008. DOI: 10.1007/s00018-008-7565-9

PEIGNEUR S,et al.. A bifunctional sea anemone peptide with Kunitz type protease and potassium channel inhibiting properties. **Biochem Pharmacol**. 2011 v. 82, n. 1, p. 81-90, Jul 2011. https://doi.org/10.1016/j.bcp.2011.03.023

PESCOSOLIDO N,et al. Role of Protease-Inhibitors in Ocular Diseases. **Molecules**., v.19, n.12, p. 20557-20569, Dez 2014. DOI:10.3390/molecules191220557

PRENTIS P.J., PAVASOVIC A., NORTON R.S. Sea Anemones: Quiet Achievers in the Field of Peptide Toxins. **Toxins** (Basel), v.10, n.1, p.1-15, 2018. https://doi.org/10.3390/toxins10010036

POSTIC G., et al. KNOTTIN: the database of inhibitor cystine knot scaffold after 10 years, toward a systematic structure modelling. **Nucleic Acids Research**, v. 46, Jan 2018. DOI: 10.1093/nar/gkx1084

PRUYNE D. Probing the origins of metazoan formin diversity: Evidence for evolutionary relationships between metazoan and non-metazoan formin subtypes. **PLoS One.** V. 5, n. 12(10), p. 1-18, Out 2017. DOI: 10.1371/journal.pone.0186081

PURCELL, J.E. Aggresive function and induced development of catch tentacles in the sea anemone Metridium senile (Coelenterata, Actiniaria). **Biol. Bull.**,v. 153,n.2, p. 355–368, Out 1977. DOI:10.2307/1540441

RAMÍREZ-CARRETO S, et al. Identification of a pore-forming protein from sea anemone *Anthopleura dowii* Verrill (1869) venom by mass spectrometry. **J Venom Anim Toxins incl Trop Dis,** v. 25, p. 1-12.Fev 2019. https://doi.org/10.1590/1678-9199-JVATITD-1474-18

RAMÍREZ-CARRETO S, et al. Transcriptomic and Proteomic Analysis of the Tentacles and Mucus of Anthopleura dowii Verrill, 1869. **Mar Drugs**, v. 25; n.17 (8), Jul 2019. DOI: 10.3390/md17080436

RAWLINGS, N. D.; TOLLE, D. P.; BARRETT, A. J. Evolutionary families of peptidase inhibitors. **Biochemical Journal**, v. 378, n. 3, p. 705–716, Mar 2004 DOI: 10.1042/BJ20031825.

RAWLINGS, N.D., et al. The MEROPS database of proteolytic enzymes, their substrates and inhibitors in 2017 and a comparison with peptidases in the

PANTHER database. **Nucleic Acids Res**, v.46, n. D1, p. D624-D632, Jan 2018. https://doi.org/10.1093/nar/gkx1134
https://www.ebi.ac.uk/merops/cgi-bin/statistics_index?type=P#S

RECKZIEGEL G.C., et al. Injuries caused by aquatic animals in Brazil: an analysis of the data present in the information system for notifiable diseases. **Rev. Soc. Bras. Med. Trop.** v. 48. n. 4, p. 461-467, Ago 2015. https://doi.org/10.1590/0037-8682-0133-2015

REIMER NS, et al. Amino acid sequence of the Anthopleura xanthogrammica heart stimulant, anthopleurin-B. **J Biol Chem**. v. 260, n.15, p. 8690-3, Jul 1985. https://doi.org/10.1016/S0021-9258(17)39403-6

REMINGANTE A, et al. Impact of Scyphozoan Venoms on Human Health and Current First Aid Options for Stings. **Toxins (Basel).** v. 10, n.4, p.133, Mar 2018. DOI: 10.3390/toxins10040133

RENATUS M.,et al. Structural and Functional Analyses of Benzamidine-Based Inhibitors in Complex with Trypsin: Implications for the Inhibition of Factor Xa, tPA, and Urokinase. **J. Med. Chem.** v. 41, n.27, p. 5445–5456, Dez 1998. DOI:10.1021/jm981068g

RIMPHANITCHAYAKIT V., TASSANAKAJON A. Structure and function of invertebrate Kazal-type serine proteínase inhibitors. **Dev Comp Immunol.**, v. 34, n.4, p. 377-386, Abr 2010. DOI: 10.1016/j.dci.2009.12.004

ROBERTS R.M. et al. Regulation and regulatory roles of proteinase inhibitors. **Crit Rev Eukaryot Gene Expr**. v. 5, n. 3-4, p. 385-436, 1995. DOI:10.1615/critreveukargeneexpr.v5.i3-4.80

SATOH H, et al. Characterization of PsTX-60B, a new membrane-attack complex/perforin (MACPF) family toxin, from the venomous sea anemone Phyllodiscus semoni. **Toxicon**. v. 49, n.8, p. 1208-10, Jun 2007. DOI: 10.1016/j.toxicon.2007.01.006

SHER, D.;et al. Toxic polypeptides of the hydra–a bioinformatic approach to cnidarian allomones. **Toxicon**, v. 45, n. 7, p. 865−879, Jul 2005. DOI:10.1016/j.toxicon.2005.02.004

SHIOMI K., et al. Protein repeats: Structures, functions, and evolution. **Journal of Structural Biology**, v. 134, n. 2–3, p. 117–131, Maio 2001. DOI: 10.1006/jsbi.2001.4392

SCHULZ, H. et al. Structure of human Endothelin-converting Enzyme I Complexed with Phosphoramidon. **Journal of Molecular Biology**, v. 385, n. 1, p. 178–187, Jan 2009. https://doi.org/10.1016/j.jmb.2008.10.052

SCHWEITZ, H. et al. Kalicludines and kaliseptine: Two different classes of sea anemone toxins for voltage-sensitive K+ channels. **Journal of Biological**

Chemistry, v. 270, n. 42, p. 25121–25126, Out 1995. DOI: 10.1074/jbc.270.42.25121

SILVERMAN, G.A.,et al. The serpins are na expanding superfamily of structurally similar but functionally diverse proteins. Evolution, mechanism of inhibition, novel functions, and a revised nomenclature. **J. Biol. Chem**. v. 276, n. 36, p. 33293–33296, Set 2001. DOI: 10.1074/jbc.R100016200

SILVEIRA A.F.L. E MORANDINI, A.C. Checklist dos Cnidaria do Estado de São Paulo, Brasil. **Biota Neotrop***.* v.1., Suppl 1, Dez 2011. https://doi.org/10.1590/S1676-06032011000500016

SINTSOVA O, et al. Peptide fingerprinting of the sea anemone Heteractis magnifica mucus revealed neurotoxins, Kunitz-type proteinase inhibitors and a new β-defensin α-amylase inhibitor. **J Proteomics.** v.173, p.12-21, Fev. 2018. DOI: 10.1016/j.jprot.2017.11.019

SMITH, B.L., POTTS, D.C. Clonal and solitary anemones (Anthopleura) of western North America: population genetics and systematics. **Mar. Biol.**, v. 94, p. 537–546, Dez 1987. https://link.springer.com/article/10.1007/BF00431400

SOUTHAN, C. A genomic perspective on human proteases as drug targets. **Drug Discovery Today**, v. 6, n.13, p. 681–688,Jul 2001. DOI: 10.1016/s1359-6446(01)01793-7

SURM JM, et al. A process of convergent amplification and tissue-specific expression dominates the evolution of toxin and toxin-like genes in sea anemones. **Mol Ecol.** v. 28, n. 9, p. 2272-2289, Maio 2019. DOI: 10.1111/mec.15084

TARGINO A.K.G; GOMES A.B. Distribution of sea anemones in the Southwest Atlantic: biogeographical patterns and environmental drivers. **Mar. Biodivers**. v.50,n. 80, p. 2-17, Set 2020. https://doi.org/10.1007/s12526-020-01099-z

TEJUCA, M.; ANDERLUH, G.; DALLA SERRA, M. Sea anemone cytolysins as toxic components of immunotoxins. **Toxicon**, v. 54, n. 8, p. 1206–1214, Dez 2009. DOI: 10.1016/j.toxicon.2009.02.025

THE UNIPROT CONSORTIUM, UniProt: The universal protein knowledgebase in 2021. **Nucleic Acids Res.**, v 49, D1, p. D480–D489, Jan 2021 DOI:10.1093/nar/gkaa1100
https://www.uniprot.org/uniprot/?query=anthopleura&fil=reviewed%3Ayes&sort=score

UNDHEIM E.A.B, et al. Multifunctional warheads: Diversification of the toxin arsenal of centipedes via novel multidomain transcripts. **Journal of Proteomics**, v. 112, p.1-10, Mai 2014. https://doi.org/10.1016/j.jprot.2014.02.024

VALLE, A. et al. The multigene families of actinoporins (part I): Isoforms and genetic structure. **Toxicon**, v. 103, p. 176–187, Set 2015. https://doi.org/10.1016/j.toxicon.2015.06.028

VEGA F.J., ALBORES F.V. A four-Kazal domain protein in *Litopenaeus vannamei* hemocytes. **Develop. & Comp. Immuno**., v. 29, n.5, p. 385-391, Dez 2005. DOI: 10.1016/j.dci.2004.10.001

VELIČKOVIĆ, D. et al. New insights into the structural and spatial variability of cellwall polysaccharides during wheat grain development, as revealed through MALDI mass spectrometry imaging. **Journal of Experimental Botany**, v. 65, n. 8, p. 2079–2091, Mai 2014. DOI: 10.1093/jxb/eru065

WANG Y. The role and regulation of urokinase-type plasminogen activator receptor gene expression in cancer invasion and metastasis. **Med Res Ver.** v. 21, n.2, p. 146–170, Mar 2001. DOI: 10.1002/1098-1128(200103)21:2<146::aid-med1004>3.0.co;2-b

WAXLER, B.; RABITO, S. Aprotinin: A Serine Protease Inhibitor with Therapeutic Actions: Its Interaction with ACE Inhibitors. **Current Pharmaceutical Design**, v. 9, n. 9, p. 777–787, 2003. DOI: 10.2174/1381612033455468

WILLIAMS, R.B. Acrorhagi, catch tentacles and sweeper tentacles: a synopsis of aggression of actiniarian and scleractinian cnidaria. **Hydrobiologia**. v. 216, p. 539–545, 1991. https://link.springer.com/content/pdf/10.1007/BF00026511.pdf

WISHART D.S., et al. DrugBank 5.0: a major update to the DrugBank database for 2018. **Nucleic Acids Res**. v. 46, n. D1, Pages D1074–D1082 Nov. 2017. https://doi.org/10.1093/nar/gkx1037
Link de acesso:
https://www.drugbank.ca/unearth/q?utf8=%E2%9C%93&searcher=drugs&query=protease+inhibitors

WOLSTENHOLME J.K, WALLACE C.C. **Australian anemones Final Report. Prepared for the Department of Environment and Heritage, Heritage Division by Museum of Tropical Queensland** (Queensland Museum), 2004.https://researchonline.jcu.edu.au/52871/

XU, P.; HUANG, M. Small Peptides as Modulators of Serine Proteases. **Current Medicinal Chemistry,** v. 27, n. 22, p. 3686–3705, Out 2020. DOI: 10.2174/0929867325666181016163630

YE, S., et al. The structure of a Michaelis serpin–protease complex. **Nat. Struct. Mol. Biol.**, v.8, p. 979–983, Nov. 2001.
https://www.nature.com/articles/nsb1101-979

YEUNG S.Y.M., et al. Modulation of Kv3 Subfamily Potassium Currents by the Sea Anemone Toxin BDS: Significance for CNS and Biophysical Studies. **The Journal of Neuroscience**, v. 25, n. 38, p. 8735– 8745, Set 2005.
DOI: 10.1523/JNEUROSCI.2119-05.2005

YUN Chow Shiao. **Towards Serine Protease Inhibitors.** A thesis submitted for the degree of Doctor of Philosophy. The University of Queensland, Australia.

Institute for Molecular Bioscience. p.1-30. 2013.
https://doi.org/10.14264/uql.2017.381

ZHANG, Z. Animal biodiversity: An introduction to higher-level classification and taxonomic richness. **Zootaxa**, v. 3148, n.1, p.7–12, Dez 2011. DOI: https://doi.org/10.11646/zootaxa.3148.1.3

APÊNDICES

APÊNDICE A – MANUSCRITO 1 – Tracking serine peptidase inhibitors in the venom and tissue of the sea anemone *Anthopleura cascaia*

Daiane Laise da Silva[a,b], Rodrigo Valladão[a], Emidio Beraldo Neto[a], Guilherme Rabelo Coelho[a], Oscar Bento da Silva[a], Adriana Rios Lopes[a], Brett R. Hamilton[b], Eivind A.B. Undheim[b,c] Juliana Mozer Sciani[d], Daniel Carvalho Pimenta[a]

[a]Laboratório de Bioquímica e Biofísica, Instituto Butantan. Av. Vital Brasil, 1500, Butantã, São Paulo, Brazil.

[b]Centre for Advanced Imaging, University of Queensland, St Lucia, QLD 4072, Australia

[c]Centre for Ecological and Evolutionary Synthesis, Department of Biosciences, University of Oslo, PO Box 1066 Blindern, 0316 Oslo, Norway

[d] Laboratório de Pesquisa Multidisciplinar, Universidade São Francisco. Av. São Francisco de Assis, 218, Bragança Paulista, São Paulo, Brazil

E-mail address of authors:

Daiane Laise da Silva –daianelaise@gmail.com

https://orcid.org/0000-0002-8401-7883

Rodrigo Valladão – rodrigovalladao3@gmail.com

https://orcid.org/0000-0003-3180-0046

Emídio Beraldo Neto – emidio.beraldo@butantan.gov.br

https://orcid.org/0000-0002-4735-5162

Guilherme Rabelo Coelho – guilherme.coelho@butantan.gov.br

http://orcid.org/0000-0002-9633-7219

Oscar Bento da Silva Neto – oscar.bentoneto@gmail.com

https://orcid.org/0000-0002-1587-2691

Adriana Rios Lopes Rocha – adriana.lopes@butantan.gov.br

https://orcid.org/0000-0002-9741-2110

Brett R. Hamilton - b.hamilton@uq.edu.au

https://orcid.org/0000-0002-2921-7620

Eivind A. B. Undheim - e.a.b.undheim@ibv.uio.no

https://orcid.org/0000-0002-8667-3999

Juliana Mozer Sciani – Juliana.sciani@usf.edu.br

https://orcid.org/0000-0001-7213-206X

Daniel Carvalho Pimenta – dcpimenta@butantan.gov.br

https://orcid.org/0000-0003-2406-0860

* Daniel Carvalho Pimenta (Corresponding author) – dcpimenta@butantan.gov.br

Laboratório de Bioquímica e Biofísica, Instituto Butantan. Av. Vital Brasil, 1500, Butantã, São Paulo - SP, CEP 05503900, Brazil

Telephone number: + 55-11-26279745

ABSTRACT

Sea anemones exhibit an interesting structural diversity of toxins, spanning multiple cysteine-rich peptide scaffolds in their venoms. Between these toxins, serine peptidase inhibitors, specially from Kunitz type, represent an important toxin family that are suggested as defensive peptides employed by sea anemones for protecting other venom's components from fast degradation. Here, we report that the venom of the endemic Brazilian sea anemone *A. cascaia* is a rich source of serine peptidase inhibitors. The secreted venom was fractionated by RP-HPLC; venom's fractions were screened for inhibitory activity over trypsin, using time-course fluorescence-based kinetic assays; and the spatial distribution of these toxins across *A. cascaia* tissue was performed by Mass Spectrometry Imaging (MSI). Three peptides exhibiting 4461 m/z; 2617 m/z and 2642 m/z; and an enriched fraction F 3.7.5, were isolated from the venom. Such peptides present from 59% to up 93% inhibition of trypsin's activity, and analysis by MALDI-MSI revealed that these serine protease inhibitors show distinct tissue distributions throughout the body of *A. cascaia*, including the tentacles, pedal disc and mesenterial filaments. Due to the occurrence of Kunitz peptides in species from *Anthopleura* genus, we suggest that the isolated inhibitors obtained in this work might belong to Venom Kunitz toxin family of sea anemones.

INTRODUCTION

Animals belonging to phylum Cnidaria all share one main characteristic: the presence of cnidocytes — specialized stinging cells — that each produce and harbour a dischargeable venomous capsule called the nematocyst (Fautin, 2009; Moran et al., 2012). This phylum comprises more than 10,000 species, and around 10% of them are represented by sea anemones (Anthozoa: Actiniaria) (Prentis et al., 2018; Zhang, 2011). Sea anemones are benthic, sessile cnidarians, with a remarkably basic body plan that is covered by nematocysts (Fautin, 2009; Frazão

et al., 2012; Madio et al., 2018). These small structures release venom under mechanical or chemical stimuli and can be found in several parts of sea anemones body, including tentacles, actinopharynx, column and mesenterial filaments (Fautin, 2009; Prentis et al., 2018; Ramírez-Carreto et al., 2019).

Sea anemones exhibit an interesting structural diversity of toxins, spanning multiple cysteine-rich peptide scaffolds stabilised by multiple intra-molecular disulfide bridges (Madio et al., 2018, 2019). Such toxins can affect at least 20 types of pharmacological targets, including several subtypes of voltage-gated sodium (Nav) and potassium (Kv) channels; Acid-sensing channels; and transient receptor potential (TRP) channels, which highlights their potential for drug discovery (Madio et al., 2019; Prentis et al., 2018)However, this pharmacological potential is also a reflection of the diverse roles that these toxins play in sea anemones' day-to-day life, which include predation, defense, prey immobilisation, digestion, and intra-specific competition. While some of these toxins, such as some that target Nav and Kv channels, are known to immobilise prey by inhibiting voltage-gated ion channels (Frazão et al., 2012; Wanke et al., 2009), other toxins, like actinoporins and Membrane Attack Complex/Perforin (MACPF)-type cytolysins, create pores in cell membranes, causing necrosis in competitors (Oshiro et al., 2004; Satoh et al., 2007; Valle et al., 2015). Additionally, some of these toxins might impair the activity of target enzymes, inhibiting the peptidases that otherwise would impair the action of venom's components, acting as defense toxins (Frazão et al., 2012; Rodríguez et al., 2014).

In the case of serine peptidase inhibitors from sea anemones, it has been suggested that such toxins are ultimately employed for protecting other venom's components from fast degradation, caused by endogenous or exogenous enzymes (Frazão et al., 2012). Interestingly, several of these inhibitors have been classified as both Kunitz-type inhibitors and type 2 potassium channel toxins due to their dual ability to both inhibit serine peptidases and block Kv channels (Gladkikh et al., 2020; Madio et al., 2019; Prentis et al., 2018). AsKC11 from *Anemonia sulcata*, HCRG1 and HCRG2 from *Heteractis crispa,* and ShPI-1 from *Stichodactyla helianthus* are few examples of these Kunitz peptide toxins (An et al., 2022; García-Fernández et al., 2016; Gladkikh et al., 2015). The bifunctional activity of such peptides suggest

that these toxins might be used for defense and aggression, e.g. by deactivating exogenous enzymes and paralysing prey, respectively (Frazão et al., 2012; Honma & Shiomi, n.d.).

Anthopleura is among the most familiar genera from sea anemones, known for their accessible species, frequently found between rocky intertidal communities in both temperate and tropical zones worldwide (Daly et al., 2017). This genus comprises more than 50 reviewed species according to World Register of Marine Species – WoRMS (accessed on 25 of May 2022) (Daly & Fautin, 2022), that present two common morphological aspects: The presence of verrucae (adhesive structures) throughout the entire column, and acrorhagi – dense bulbous structures filled with nematocysts – commonly used for intraspecific competition (Ashwood et al., 2020; Daly et al., 2017). Interestingly, these species are morphologically differentiated both by the abundance and distribution of verrucae on columns and by the distribution and types of nematocysts (Hand, 1955; Smith & Potts, 1987)

In the Southwest Atlantic region, *Anthopleura* species are found in shallow-waters at Brazilian and Caribbean provinces. Brazil shelters three of the five species found: *A. krebsi*, *A. varioarmata* and *A. cascaia* (Targino & Gomes, 2020). Of these, *A. cascaia* is endemic to Brazil, where it can be easily found between rocky shores, more specifically in mid and inferior eulittoral and infralittoral; over and under rocks, sand, tide channels, tide pools, caves and clefts as described under their documented distribution at WORMS (Daly & Fautin, 2022). During low tide periods, this species is easily spotted by the presence of gravels and small rocks attached to its adhesive verrucae (Fig 1).

To date, studies involving *A. cascaia* have typically been related to trophic ecology and biogeographical distribution (da Silva J.F., 2009; de Capitani, 2007; Targino & Gomes, 2020), with only a single study reporting the characterization of neurotoxic fractions from this species (Madio, 2012). This biochemical study revealed that the venom of this sea anemone possesses three peptides that selectively inhibit different Nav and Kv channels expressed on *Xenopus* oocytes: AcaIII1425 (3337 Da), AcaIII2970 (4881 Da) and AcaIII3090 (4880 Da) (Madio, 2012). Thus, despite being such a common species, the venom of *A. cascaia* remains underexplored (Prentis et al., 2018)

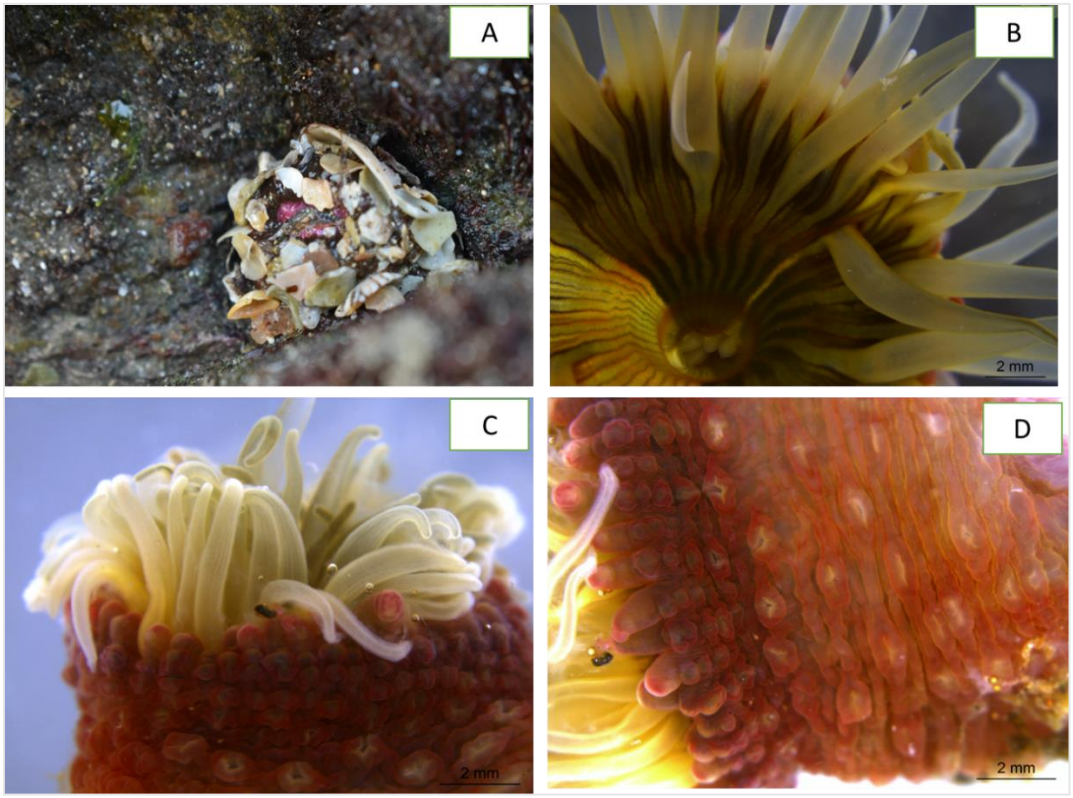

Fig 1. A- *Anthopleura cascaia* sea anemone covered by rocks and shells, at the intertidal zone of Cigarras beach, at São Sebastião district - São Paulo - Brazil. **B-** Superior image of oral disc and tentacles from *A. cascaia*. **C, D-** External morphology of a living specimen of *A. cascaia*. Tentacles are visible at superior region of the animal and adhesive vesicles are distributed throughout the body. **B**, **C** and **D** images were acquired using a stereo microscope Leica M205 A attached to DMC2900 camera and LAS V4.6 software.

Here, for the first time, we report that the venom of the Brazilian sea anemone *A. cascaia* is a rich source of serine peptidase inhibitors. Such toxins, that were fractionated from the secreted venom by RP-HPLC, show molecular masses ranging between 2.6 kDa and 4.7 kDa, as assessed by MALDI-TOF/MS and ESI-IT-TOF/MS. In this work, venom's fractions were screened for inhibitory activity over trypsin, using time-course fluorescence-based kinetic assays. Furthermore, the evaluation of spatial distribution of these toxins across *A. cascaia* by Mass Spectrometry Imaging (MSI) revealed that these inhibitors are mainly present in the tentacles, the pedal disc and in the mesenterial filaments from *A. cascaia*.

MATERIAL AND METHODS

2.1 Obtention of ***Anthopleura cascaia***´s venom

Adult individuals from *A. cascaia* species were collected between the rocky shores from Cabelo Gordo and Cigarras beaches at São Sebastião district, north coastline from São Paulo state, under authorization n° 72666-1 from SISBIO (Sistema de Autorização e Informação em Biodiversidade). Specimens (n=10) were collected in the intertidal zone, during low tide periods and immediately put in tubes containing sea water. Specimens were led to the Centro de Biologia Marinha (CEBIMar) from Universidade de São Paulo and washed with artificial sea water. For inducing nematocytes discharge, animals were immersed in ultra-pure acidified water (0.1% acetic acid). The obtained venom solution (50 mL) was recovered, lyophilized, resuspended in ultrapure water and kept at -20°C for posterior analysis.

2.2 Purification of inhibitors

The fractionation of venom components was performed through RP- HPLC (Reversed-Phase High-Performance Liquid Chromatography) using a LC-20A Prominence *HPLC* system, Shimadzu Co. Kyoto, Japan; and a C18 column (Luna C18(2), 5 µm particle size ,100 Å pore size, 250 x 4.6 mm). The initial chromatographic profile of the venom was obtained by using a linear gradient from 0-100% of Solvent B in 30 min and a flow rate of 1 $mL.min^{-1}$. The solvents used were: Solvent B (0.1% acetic acid in 90% acetonitrile) and solvent A (0.1% acetic acid in water). The elution of components from stationary phase was monitored by a Shimadzu detector SPD-M20A PDA, selecting the wavelength of 214 and 280 nm for monitoring the eluate. Fractions of the venom were collected every 5 min, being initially divided in 6 fractions, manually collected, freeze dried and posteriorly tested for trypsin inhibition.

For posterior fractionations, the separation conditions were optimized. For the inhibitory fraction F3, a gradient of 5-40% of B in 40 min was selected. The subsequent fractionations followed the gradient condition of 5-60% of B in 35 min for F3.7 and F3.8.

2.3 SDS-PAGE analysis of venom's fractions

The venom and the fractions obtained by RP-HPLC had the electrophoretic profiles elucidated by SDS-PAGE, under reducing conditions,

according to Laemmli (1970) (*Laemmli,* n.d.). Proteins were loaded in polyacrylamide gels – stacking gel (5%); resolving gel (12%) – and submitted to electrophoresis under 100 V for 1 h. 'Amersham Low Molecular Weight Calibration Kit for SDS Electrophoresis' (GE Healthcare) was used for molecular mass estimation. The resulting gel was stained with Coomassie brilliant blue.

2.4 Trypsin activity inhibition by venom's fractions

For determining the activity of Trypsin, the peptidase was serially diluted and incubated with a fixed amount (0.1 mM) of the fluorogenic substrate N-alpha-Carboxybenzyl L-Arginine 7-amido-4-methylcoumarin hydrochloride (Z-L-ARG-MCA) dissolved in DMSO (Dimethyl sulfoxide) and diluted in assay buffer (0.1 M Tris-Cl, pH 8.5). For selecting venom fractions containing potential inhibitors, inhibitory effects of fractions over the substrate hydrolysis by Trypsin were evaluated.

Once determined the ideal standard conditions for the assay (reading time and enzyme saturation with substrate), 15 µL of each venom fraction were incubated with Trypsin (40 ng/µL) (1:1) for 30 min in 96-well microplate used for fluorescence assays. After incubation, 125µL of substrate at 0.1 mM was added to the samples. The enzymatic assays were conducted at 30°C and the substrate hydrolysis rates were determined by measuring the change in fluorescence every 5 min for 30 min. The reaction was measured by using the SpectraMax M2 (Molecular Devices), λ_{ex} 330 nm, λ_{em} 430 nm. The relative inhibitory activity of venom fractions was determined by the calculating the percentage of inhibition related to the enzymatic activity of the control sample (Enzyme + substrate). All assays were performed in duplicate and the mean of fluorescence value was used. Negative fluorescence values were considered equal to 0.

2.5 Mass determination by MALDI-TOF/MS and ESI--MS

For Matrix Assisted Laser Desorption Ionization -Time of flight (MALDI-TOF) analysis, 1µL of the venom/ inhibitory fractions were spotted with 1 µL of saturated CHCA in 50% ACN, containing 0,1% TFA (α-cyano-4-hydroxycinnamic acid) or

Sinapinic acid matrix on a MALDI plate and analysed in a AXIMA series MALDI-TOF/MS (Shimadzu, Co. Kyoto, Japan). Peptide mass spectra data was acquired in positive ion linear mode in the range of 500–15000 m/z.

For LC-MS, previously lyophilized fractions from *A. cascaia* venom were dissolved into 50µL of acidified water containing 0.1% Trifluoroacetic acid (TFA). Samples were deposited into the 96 well plate of the SIL-20A autosampler for LC-MS analysis in an ion trap time of flight (IT-TOF) mass spectrometer system (Shimadzu, Co. Kyoto, Japan). 0 µL of sample aliquots were injected and subject to a RP-HPLC (20A Prominence system) separation by a Discovery C18 1.5 (2 x 50 mm) column. Solvent A containing (0.1% Formic acid in water) and Solvent B (0.1% Formic acid in 90 % acetonitrile), were used in a linear gradient from 0 to 100% of B in 6 minutes, under a constant flow rate of 0.2 mL.min-1. The interface was kept at 4.5 kV and 200°C. Detector was operated at 1.95 kV. MS spectra were acquired in positive mode, in the 350-1400 m/z range. Instrument control, data acquisition and processing were performed by the LCMS Solution suite (Shimadzu).

2.6 Mass Spectrometry Imaging (MSI) by MALDI-TOF

A specimen of *A. cascaia* was divided by longitudinal sectioning and left in fixative (5mL) and ethanol 100% (3mL) solution, for 16h at 8°C. The formalin-free fixative used was prepared in-house as previously published protocols (Stefanits et al., 2016). For dehydration, the tissue was submitted to gradual concentrations of xylene/ethanol (10 to 100%) with intervals of 30 min at each concentration, until the tissue was completely immersed in 100% xylene. Subsequently, the tissue was submitted to gradual baths (10 to 100%) of Paraplast® (manufactured by Oxford Labware, St. Louis, MO, USA), until be completely embedded. The sample was kept at -20°C.

For preparing samples for MALDI-MSI, the tissue was sectioned longitudinally at 7µm thickness on a microtome. Sections were placed on ITO (Indium Tin Oxide) coated glass slides and heated at 58°C on a heat block for melting paraffin. Sequentially, tissue sections were gently washed with 100% xylene for paraffin removal and images of the tissue were acquired on optical microscope. A Bruker ImagePrep equipment was used for automatically spraying α-cyano-4-

hydroxycinnamic acid (CHCA) matrix solution (105 mg CHCA, 8 mL acetonitrile, 7 mL ultrapure water and 30 µL TFA) over tissue. The slides were placed on Bruker SCiLS™ Lab MTP Slide Adapter II and analyzed in a MALDI-TOF/TOF Ultraflex III mass spectrometer (Bruker, Germany). The MSI analysis was performed under linear positive mode, with the range set to 1000–10,000 m/z, using the software FlexControl 3.3 to operate the mass spectrometer and to acquire individual spectra. For the analysis, the following parameters were used: spatial resolution of 60 µm; Laser 3- medium; laser power of 48%; 400 laser shots; matrix ion suppression up to 980 m/z. FlexImaging 4.0 (Bruker, Germany), was used for determining the geometry and location for data acquisition over tissue; comprising mainly the tentacles, mesenteric tissue and pedal disc of the animal. SciLS™ Lab MS software (Bruker, Germany) was used for visualisation of two-dimensional (2D) ion-intensity maps data. Baseline convolution and root mean square normalization parameters were applied to the spectra acquired. After MSI analysis, CHCA matrix was removed from tissues and samples were stained with hematoxylin and eosin, according to previously described protocol (Undheim et al., 2015).

RESULTS

Here, we proposed the investigation of the presence of serine peptidase inhibitors in the venom of *A. cascaia* and the isolation of such components by reverse phase liquid chromatography. For screening these peptides, a rational path was taken, basically involving three steps: 1. Fractionation of the venom by RP-HPLC; 2. Trypsin activity inhibition detection; 3. Mass spectrometry analysis of inhibitory fractions by MALDI-TOF and LC-MS.

In this work, trypsin was used as the serine peptidase model for tracking such molecules. At first stage, *A. cascaia* venom was tested for trypsin inhibition and it was seen that the positive control, composed by enzyme and substrate, showed a linear consumption of substrate throughout time. On the opposite side, samples containing trypsin and previously incubated with the venom, showed no product release, reflecting the complete inhibition of the enzyme and the presence of serine peptidase inhibitors in this biological sample (Supplementary material 1). Additionally, the previous analysis of the venom by SDS-page and MALDI-TOF

revealed that this venom is mainly composed of proteins with molecular masses ranging from 14 to 97 kDa (Fig 2. B) and lower molecular mass components with 3–10 kDa (Supplementary material 1).

Taking further steps on tracking serine peptidase inhibitors, *A. cascaia* venom was fractionated by RP-HPLC. Fig 2. A shows the chromatographic profile of the venom, divided in 6 fractions (F1 to F6), every 5 min, according to the elution time. Most venom components eluted between 30 and 60% B in the interval of 15 to 22 min, corresponding mainly to F3 (Fig 2. A). Venom's fractions were later tested against trypsin inhibition and analysed by SDS-PAGE and MALDI-TOF (Fig 2. B and C). From the 6 fractions analysed, only F3 and F4 exhibited the presence of serine peptidase inhibitors, exhibiting 100% and 28% of inhibition, respectively (Supplementary material 2.A). As F3 attained the complete inhibition of the enzyme, this fraction was chosen as the main source for inhibitors isolation (Fig 2. A). The evaluation of F3 by SDS-PAGE revealed that the majority of its components are concentrated between 20 and 14 kDa (Fig 2. B). MALDI-TOF analysis showed F3 contained ions with m/z 4486, 4902, 5095, 6663 (Fig 2. C).

Figure 3. A shows the fractionation model used for the inhibitory fraction F3, separated in 9 fractions (F3.1 a F3.9), according to the chromatographic profile. Fractions 3.7 and 3.8 showed complete trypsin inhibition (100%) (Fig 3; Supplementary material 2.B), and the m/z profile of these fraction's components are shown in Figure 3. B. These inhibitory fractions were later fractionated under a gradient of 5-60% B in 40 min. The fractionation of F3.7 and F3.8 are shown in Figure 4.A and Figure 5.A, respectively. Subfractions were tested against trypsin and it was found that all of them exhibited some inhibition level of trypsin activity (41% to 93%), although the inhibitors exhibiting > 90 % inhibition against trypsin were found in F3.7.5 and 3.7.6 (Fig 4B). The complete table exhibiting the remaining enzymatic activity of trypsin for all fractions tested are presented in Supplementary material 2.C. These fractions were evaluated by MALDI-TOF, showing that F3.7.6 contained a single peptide with m/z of 4461, while F3.7.5 contained three main components of similar m/z: 4518, 4685 and 4755 (Fig 4.C).

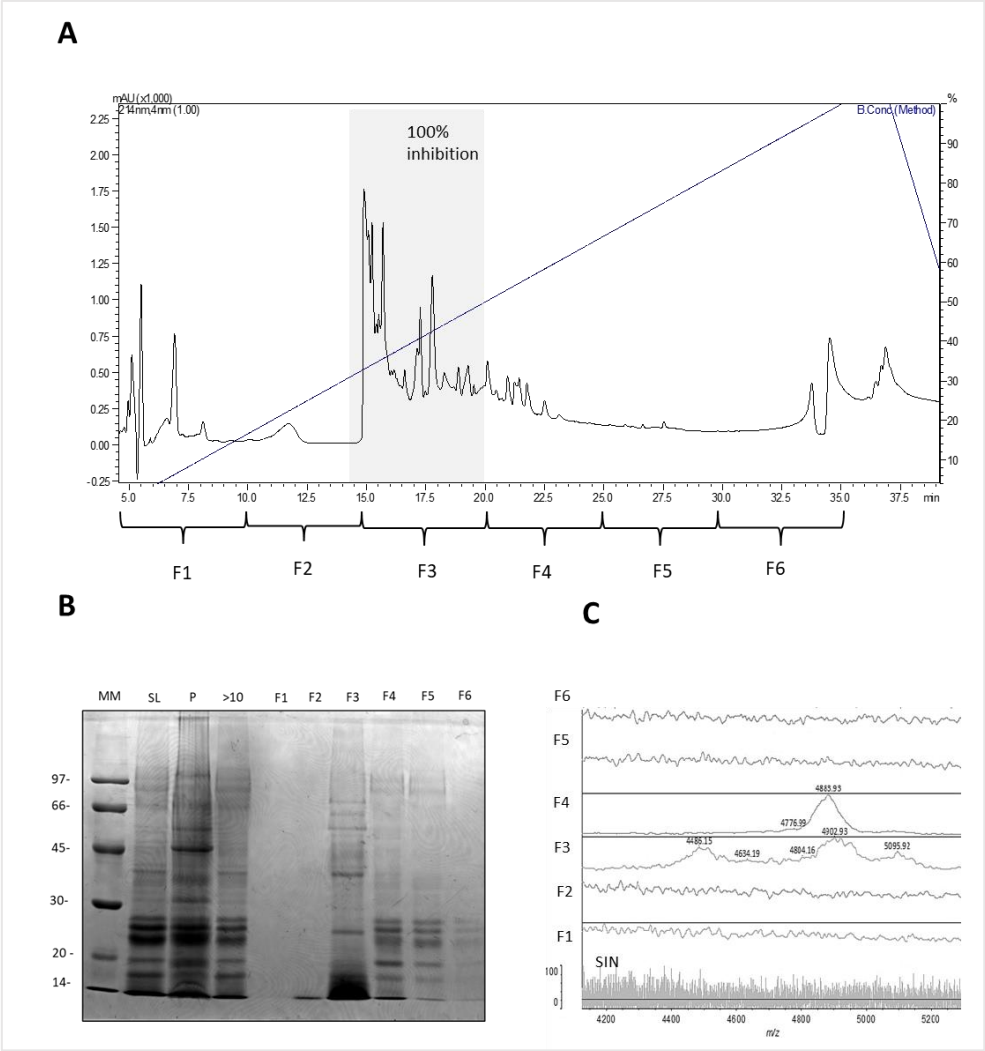

Figure 2- A- Chromatographic profile of *A. cascaia*'s venom. The venom was separated by RP-HPLC under a gradient of 5 to 40% of B in 40 min. Fractions (F1 to F6) were tested regarding trypsin activity and F3 presented 100% inhibition. **B- SDS-PAGE analysis.** Samples (20µL) were analysed by SDS-PAGE (12 %) and stained with Comassie brilliant blue. The gel presents the pattern of proteins found in the soluble fraction (SL) of the venom; venom precipitate (P); Fraction higher than 10kDa; and HPLC fractions (F1-F6) from *A. cascaia*'s venom. **C- MALDI-TOF analysis of venom's fractions from *A. cascaia* venom.** The mass spectra show m/z ranging from 4200 to 5200, with peaks of 4486, 4902, 5095, 6663 m/z corresponding to the most abundant ions in F3 and the peak m/z 4883 corresponding to the most abundant ion in F4. The profile of the Sinapinic acid (SIN) matrix is shown as the spectrum below F1.

Additionally, the three subfractions from F 3.8 (F3.8.4, F3.8.6 and F3.8.8), exhibiting the most isolated components, presented 85%, 65% and 59% inhibition of trypsin, respectively (Fig 5B). MALDI-TOF analysis revealed that the isolated peaks from F3.8.4 presents three main masses (2617, 2633 and 2649 m/z), corresponding likely to a unique peptide that presents a 16 m/z variation in the

spectrum. F3.8.8 and 3.8.6 did not show ionization of peptides. A complete table exhibiting the remaining enzymatic activity of trypsin for all fractions tested is presented in Supplementary material 2.D.

LC-MS analysis using an ESI-IT-TOF mass spectrometer revealed a more detailed mass profile of the serine peptidase inhibitors isolated from the venom fractions. Figure 6 shows a complete table of peptides identified by LC-MS in each inhibitory fraction. Particularly, F3.7.6 exhibited the presence of a unique peptide (4466 Da); F3.8.4 shows the presence of a 2652 peptide and F3.8.8 shows a peptide exhibiting 2642 Da. F3.7.5 is the only fraction that seems to contain two main peptide inhibitors (4645 Da and 4690 Da).

We next wanted identify the ecological roles of these serine peptidase inhibitors, which in sea anemone correlates well with the distribution across functionally distinct tissues and regions. We therefore investigated their distribution across the sea anemone body using MALDI mass spectrometry imaging. Figure 7 shows the distribution of inhibitors throughout *A. cascaia*. The inhibitors from F3.7.5, showed to be mainly localized in the tentacles (4685 and 4755 m/z) and pedal disc region (4518 m/z) of the animal, suggesting these are involved in predation and substrate adhesion, respectively. Meanwhile, the serine peptidase inhibitor found in F3.7.6 (4461 m/z) showed a moderate distribution in the pedal disc and mesenteric tissue, indicating potential functions in adhesion and digestion. The peptide isolated from 3.8.4, exhibiting three possible oxidized m/z (2617, 2633 and 2649 m/z) was detected in the mesenteries and tentacles of the sea anemone—a distribution shared with the peptide found in 3.8.8 (2642 m/z)—indicating that these are probably involved in prey capture and digestion.

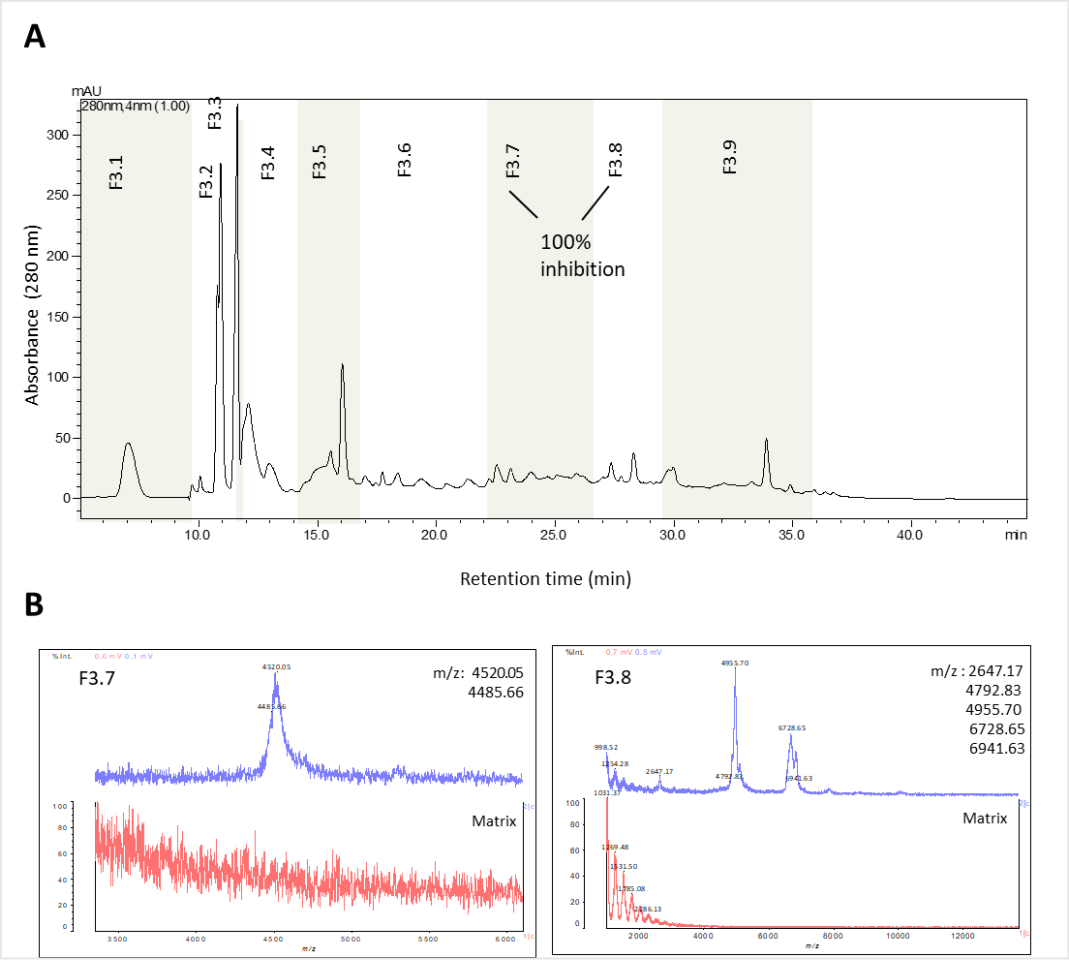

Figure 3- A- Chromatographic profile of Fraction 3 from *A. cascaia*'s venom. The inhibitory fraction was separated by RP-HPLC using a C18 column and a gradient of 5-40% of B in 40 min, leading to the obtention of 9 fractions (3.1 to 3.9). The fractions were tested regarding trypsin inhibition and F3.7 and F3.8 exhibited 100% enzyme activity inhibition. **B-** MALDI-TOF analysis of inhibitory fractions (3.7 and 3.8) from *A. cascaia* venom. Fraction 3.7 shows mainly he existence of two components 4520 and 4485 m/z, and F3.8 shows m/z ranging from 2647 to 6941 m/z. The profile of the Sinapinic acid matrix (red spectrum) is shown below each fraction spectrum.

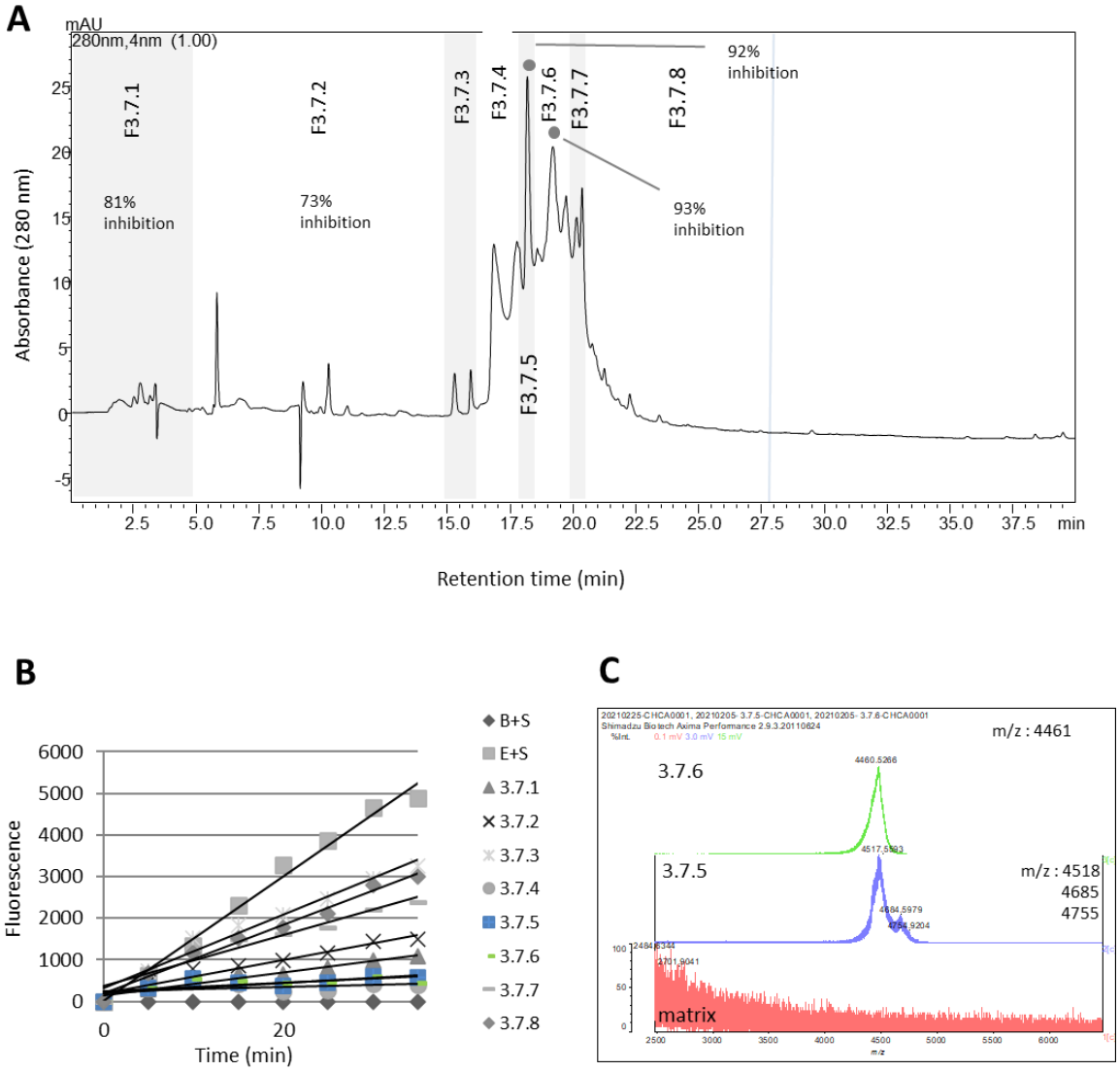

Figure 4. A- Chromatographic profile of Fraction 3.7 from *A. cascaia*'s venom. The fraction was separated by RP-HPLC using a C18 column and a gradient of 5-60% of B in 35 min. The separation led to the obtention of 8 fractions (3.7.1 to 3.7.8) that were subsequently tested regarding trypsin inhibition. F3.7.5 and F3.7.6 presented more than 90% of activity inhibition. **B- Trypsin Inhibition Assay.** F3.7 subfractions (5µl) were incubated for 30 min with trypsin (1:1), and afterwards substrate was added to the samples. Substrate consumption in Arbitrary Units of Fluorescence (Y axis) was read every 5 min for 35 min (X axis). In the test, samples F3.7.1 to F3.7.8 representing venom fractions from *A. cascaia*; Blank (B + S); and Positive Control (E + S), were analysed. B = Buffer, S = Substrate and E = Enzyme. The subfractions F3.7.5 and 3.7.6 exhibited the highest enzyme inhibition (>90%), reflecting lower substrate consumption over time. **C- MALDI-TOF analysis of *A. cascaia* venom fractions.** The spectra of F3.7.5 (blue) by positive mode shows the existence of three main components: 4518, 4685 and 4755m/z. Fraction 3.7.6 (blue) shows the presence of a unique peptide of 4461 m/z. The profile of the CHCA matrix (in red) is shown below each fraction spectrum.

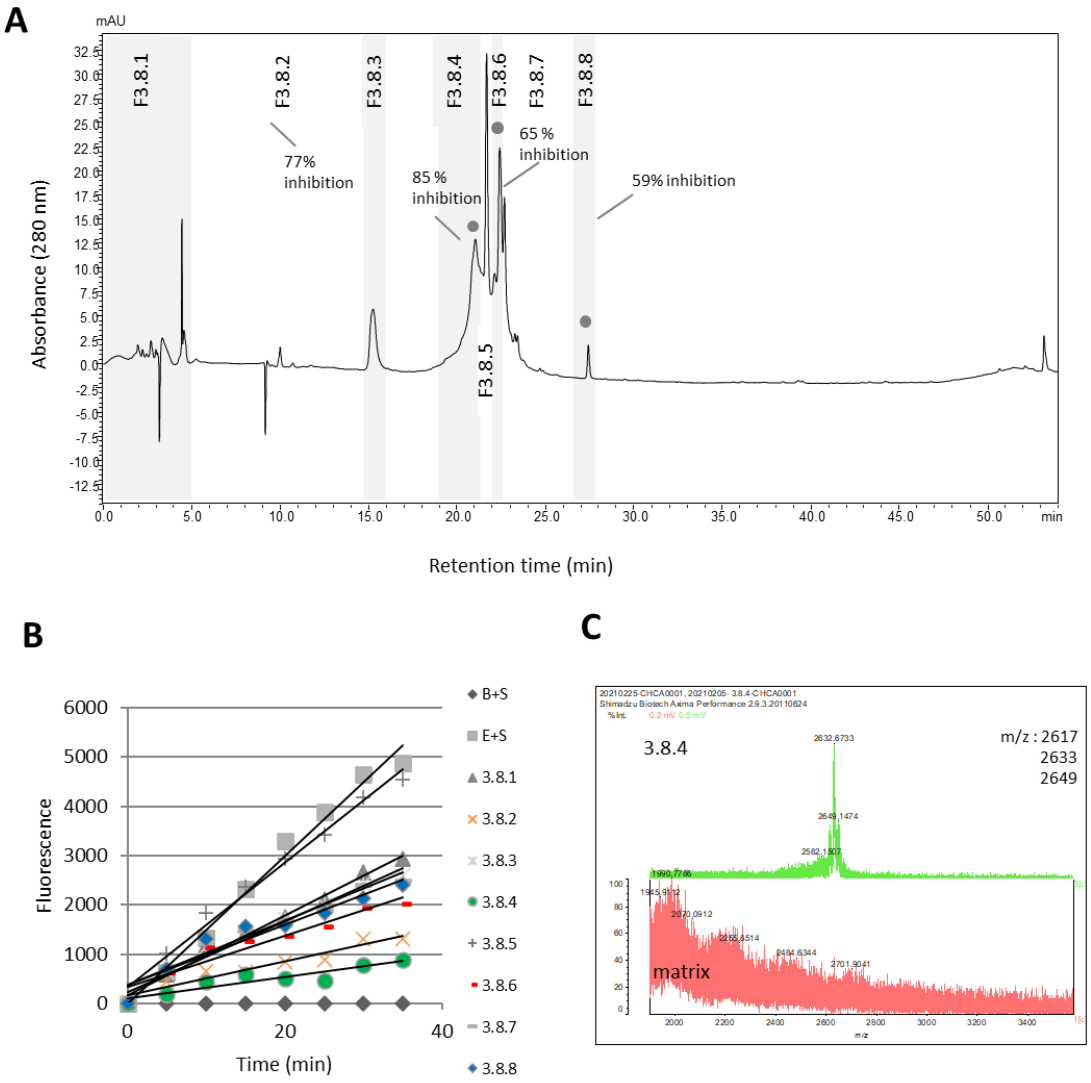

Figure 5. A- Chromatographic profile of Fraction 3.8 from *A. cascaia*'s venom. The fraction was separated by RP-HPLC using a C18 column and a gradient of 5-60% of B in 35 min. The separation led to the obtention of 8 fractions (3.8.1 to 3.8.8). Fractions exhibiting trypsin inhibition are highlighted with a symbol (°) above the peaks. **B- Trypsin Inhibition Assay.** F3.8 subfractions (5µl) were incubated for 30 min with trypsin (1:1), and afterwards substrate was added to the samples. Substrate consumption in Arbitrary Units of Fluorescence (Y axis) was read every 5 min for 35 min (X axis). In the test, samples F3.8.1 to F3.8.8 representing venom fractions from *A. cascaia*; Blank (B + S); and Positive Control (E + S), were analysed. B = Buffer, S = Substrate and E = Enzyme. F3.8.4; F3.8.6 and 3.8.8 exhibited the highest enzyme inhibition, reflecting lower substrate consumption over time. **C- MALDI-TOF analysis of *A. cascaia* venom fractions**. The spectra of F3.8.4 by positive linear mode shows the existence of 2617, 2633 and 2649 m/z. Fraction 3.8.8 shows the presence of a unique mass of 2642 m/z. The profile of the Sinapinic acid matrix is shown below each fraction spectra.

A

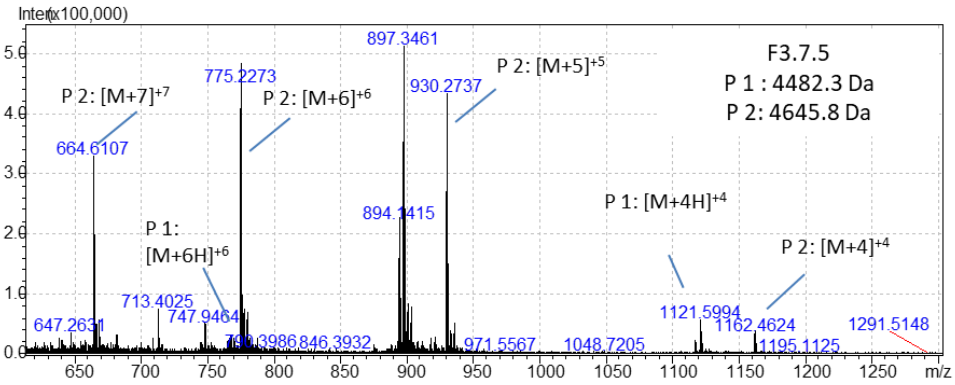

B

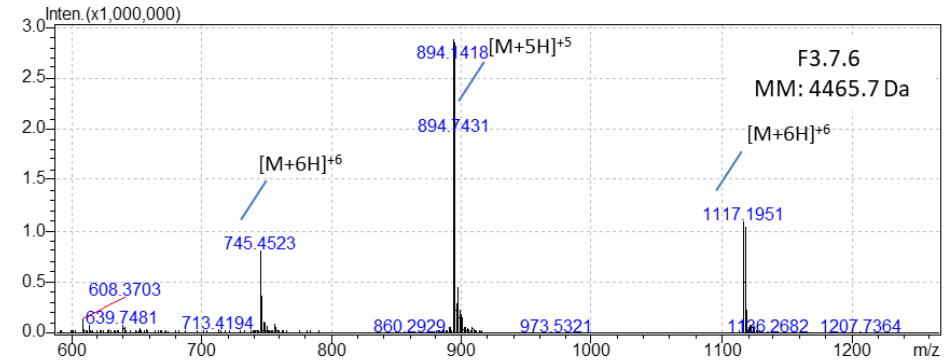

C

Fraction	Peptide Mass (Da) by LC-MS
F3.7.5	4645.84
	4690.3
F 3.7.6	4465.7
F3.8.4	2652.45
	2668.6
F3.8.8	2641.97

Figure 6. Mass profile of serine peptidase inhibitors isolated from venom's fractions by ESI-IT-TOF. A- Shows two peptide inhibitors found by LC-MS in F3.7.5. P1 (Peptide 1) and P2 (Peptide 2) are used for highlighting the supporting m/z identified. **B-** Shows the purified inhibitor from F3.7.6 from *A. cascaia* venom. **C** – Shows the peptide masses found in each fraction by LC-MS using ESI-IT-TOF. Fraction 3.8.4 presents the existence of two masses with 16 Da difference (oxidation), likely corresponding to the same inhibitor.

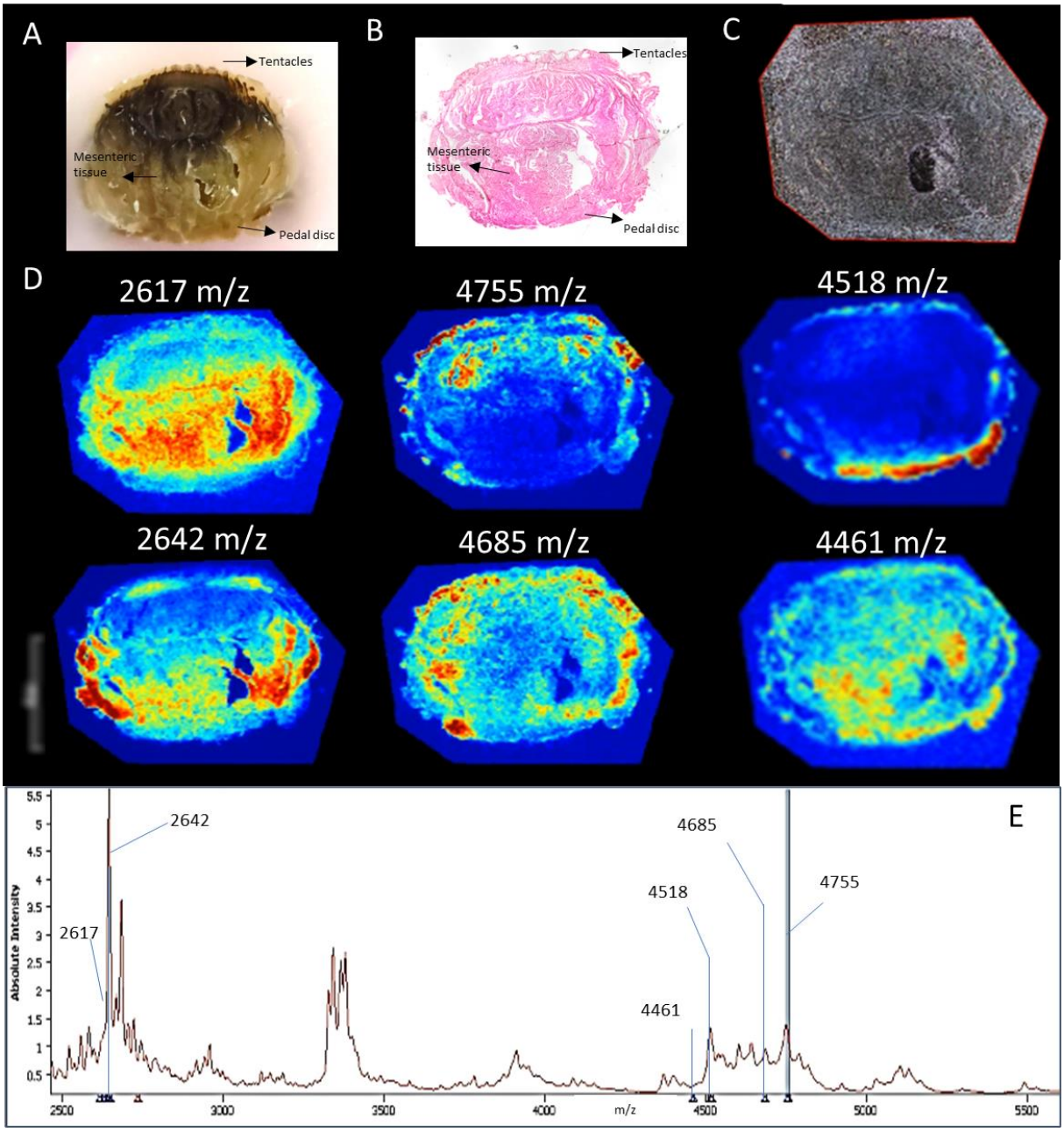

Figure 7. A- MALDI-MS Imaging – Spatial distribution of serine peptidase inhibitors on *A. cascaia's* tissue. **A** – Image of paraffinized tissue from *A. cascaia*. **B**- Histological image of the sea anemone longitudinal section used for MSI, stained with hematoxylin and eosin. **C-** Tissue section sprayed with matrix CHCA. **D-** Heat map showing the distribution of serine peptidase inhibitors ions across *A.* cascaia's tissue. The ions localization is represented by hotspots. **E**- Positive mode average spectra acquired in the longitudinal section from the animal. Y axis correspond to the signal intensity. X axis shows the corresponding m/z.

DISCUSSION

In the current study three peptides (found in F3.7.6; F3.8.4; F3.8.8) from the venom of the sea anemone *A. cascaia* were isolated, and an enriched fraction (F3.7.5) capable of binding trypsin and impairing its activity was identified. Such peptides, classified here as serine peptidase inhibitors, showed from 59% to up 93% inhibition of trypsin's activity. To achieve purification, basically three chromatographic steps by RP-HPLC were needed, mainly involving changes in solvents percentages for isolation.

Serine peptidase inhibitors have been described before in sea anemones; in fact, the Venom Kunitz-type family represent one of the four main toxin families found in these animals (Prentis et al., 2018). Commonly, the presence of these peptides in the venom is described by proteomics or transcriptomics analysis of secreted molecules or venom-related structures (Madio et al., 2017; Mitchell et al., 2020). However, in some cases, strategies for elucidating such inhibitors may involve the individual characterization of components previously isolated by chromatographic techniques, from venom or extracts of related-structures (Ishida et al., 1997; Minagawa et al., 1997, 1998). This characterization generally involves testing their direct influence over serine peptidase representants like trypsin, chymotrypsin, kallikreins; and the elucidation of their amino acid sequence (Chen et al., 2019; Sintsova et al., 2018). PI-stichotoxin-Hmg3a (entry - C0HK72) from *Heteractis magnifica*; PI-stichotoxin-Hcr2g (entry - C0HJU7) from *Heteractis crispa;* ATPI-I (entry - A0A6P8HC43) and ATPI-II from *Actinia tenebrosa,* are few of the already characterized Kunitz-type serine protease inhibitors isolated from sea anemones (Chen et al., 2019; Gladkikh et al., 2015; Sintsova et al., 2018).

For *Anthopleura cascaia*, beyond the potassium channel inhibitor Acatoxin 1 (accession- A0A6I8WFP9/ PDB Entry - 6NK9), and the three neurotoxins named as AcaIII1425, AcaIII2970 and AcaIII3090, not much is known about the venom of this species(Amorim et al., 2019; *Berman, H., Henrick, K. & Nakamura, 2003,* n.d.; Madio, 2012). However, at genus level, more than 30 toxins have been already annotated for *Anthopleura* in Swiss-Prot/UniProtKB, including Delta-actitoxin-Axm1a

(Anthopleurin A) and Delta-actitoxin-Axm1b (Anthopleurin B) – accessed 2 may of 2022 (D480-D489, 2021; Jungo & Bairoch, 2005; Monks et al., n.d.; Reimers et al., 1985).

Between the toxins found in this genus, 6 reviewed Kunitz-type protease inhibitors were isolated from three species: PI-actitoxin-Axm2a (P81547), PI-actitoxin-Axm2b (P81548) and PI-actitoxin-Axm2b (P0DMX0) were isolated from the aqueous extract of *A. aff. Xanthogrammica*; and exhibit average masses between 6341.13 Da and 6979.68 Da (Minagawa et al., 1997, 1998). Additionally, PI-actitoxin-Afv2a with 6096.98 Da (P0DMJ3) and PI-actitoxin-Afv2b of 5994.93 Da (P0DMJ4) were isolated from the acrorhagi of *A. fuscoviridis.* These inhibitors exhibited a strong antitryptic activity and the presence of a basic residue (Arg or Lys) at position 17 in its sequences was considered essential for protease inhibition (Minagawa et al., 2008). Furthermore, the most recent Kunitz inhibitor described for this genus, with molecular mass (MM) of 7484.5 Da, was isolated from *A. elegantissima* and classified as KappaPI-actitoxin-Ael3a (entry-P86862) for exhibiting a dual activity. Such inhibitor targets voltage-gated potassium channels (Kvs) and is capable of inhibiting serine peptidases (Peigneur et al., 2011).

The common aspect between such inhibitors isolated from *Anthopleura* species relies on their classification as Kunitz type, exhibiting 3 disulfide bridges and mature chains of 56 to 61 residues**.** For *A. cascaia*, the serine peptidase inhibitors evaluated here showed m/z between 2617 and 4755 by MALDI-TOF and ESI analysis. These peptides exhibit mass differences of almost 4000 Da (considering 2617 m/z and 2642 m/z), if compared to the Kunitz inhibitors already found for this genus species (Minagawa et al., 1997, 1998, 2008; Peigneur et al., 2011). However, inhibitors with similar molecular masses (MM)to the peptides found here, have been described for the sea anemone *Actinia equina* and the snake *Daboia siamensis*: Two toxins belonging to Venom Kunitz-type family - Sea anemone type 2 potassium channel toxin subfamily, with MM of 4071 Da (P0DMW8) and 4308 Da (P0DMW9) have been described for *Actinia equina* (Ishida et al., 1997). For *Daboia siamensis*, two Kunitz inhibitors with MM of 2050 Da (P85040) and 2691 Da (P85039) have also been found in the venom - accessed 20 may of 2022 (D480-D489, 2021).

The presence of serine peptidase inhibitors also has been described by transcriptome and proteome analysis of *Anthopleura elegantissima* and

Anthopleura dowii. For *A. elegantissima,* the transcriptome analysis of aggressive and non-aggressive polyps revealed that venom Kunitz/Kv2 toxins transcripts are found for both types of polyps, but that these toxins are highly expressed in the acrorhagi of aggressive polyps (Macrander et al., 2015). Additionally, twelve transcripts belonging to the venom Kunitz/Kv2 toxin family were identified in the tentacle's transcriptome of *A. dowii.* Five of these transcripts presented similarity to the mature KappaPI-AITX-Ael3a from *A. elegantissima*, presenting from 37 to 80% identity with this toxin. Another five transcripts showed similarity to serine peptidase inhibitors described for the snake's species *Walterinnesia aegyptia*, *Daboia russelii* and *Vipera ammodytes ammodytes.* At proteome level, only the transcript c14874_g1 presenting similarity to KappaPI-actitoxin-Ael3a (P86862) from *A. elegantissima* was identified in the mucus (Ramírez-Carreto et al., 2019). Beyond these Kunitz type inhibitors, two Kazal-type transcripts were identified in the transcriptome of *A. dowii*, exhibiting 41% identity with a turripeptide LoI9.1 (P0DKM7) of the sea snail *Lophiotoma olangoensis* and 75% identity to PI-actitoxin-Avd5a from *Anemonia sulcata* (P16895) (Ramírez-Carreto et al., 2019).

Due to the genus relationship, and the proved existence of Kunitz inhibitors in the venom of such sea anemones, we suggest that the three isolated serine peptidase inhibitors – 4461 m/z (from F3.7.6); 2617 m/z (from F3.8.4) and 2642 m/z (from F3.8.8) – and the inhibitors present in F3.7.5, might belong to Kunitz family. Further LC-MS/MS analysis will be necessary for confirming this hypothesis and for elucidating the amino acid sequences of such peptides.

Regarding the distribution of such toxins across *A. cascaia's* tissue; for the first time here, the localization of serine peptidase inhibitors was visualised in the tentacles and pedal disc of a sea anemone by MSI. It is important to highlight that type Kunitz toxins have been described in the tentacles of sea anemones before, by the evaluation of the composition of crude extracts (Macrander et al., 2016). However, as far as our knowledge goes, this is the first data that shows these inhibitors in their 'expected' tissue; as tentacles are used for immobilizing preys and are also involved in repelling potential predators (Ashwood et al., 2020; Macrander et al., 2016).

Previous studies have shown the presence of Kunitz peptides by MSI in mesenterial filaments of *Actinia tenebrosa* and MALDI-MSI have been applied on the elucidation of spatial distribution of κ-actitoxin-Ate1a in *Actinia tenebrosa,* and on localizing peptide toxins from *Oulactis muscosa* sea anemone (Chen et al., 2019; Madio et al., 2018; Mitchell et al., 2017; Surm et al., 2019).

Usually, secretions or tissue extracts are used for elucidating the proteome or transcriptome profile of venomous animals. These approaches commonly allow revealing the diversity of venoms by the identification of toxins or toxin-like transcripts (de Oliveira et al., 2018; Madio et al., 2017; Mitchell et al., 2020). However, the sample processing involved by these techniques usually loses the spatial distribution of toxins, and the association of MSI and histology seems to be an interesting alternative to overcome this problem. For sea anemones, like other cnidarians, accessing the localization of toxins can be challenging, once these animals possess venomous capsules distributed throughout their bodies, instead of a centralised venom system (Mitchell et al., 2017). These 'thread capsules' – cnidocysts – produced by Golgi apparatus of specialised cells – cnidocytes – can present variations in toxin composition according to the tissue where they are found (Fautin, 2009; Macrander et al., 2016).

Here, MSI analysis revealed that serine peptidase inhibitors are differently distributed on *A. cascaia* body. Interestingly, the inhibitors presenting 2617 m/z (from 3.8.4) and 2642 m/z (from 3.8.8) are notably present in mesenteric tissue region, meanwhile, peptides from F3.7.5 fraction (4518, 4685 and 4755m/z) and 3.7.6 fraction (4461 m/z) are mainly present in tentacles and pedal disc regions of *A. cascaia*. Such distribution of toxins is expected for sea anemones, once these animals regularly present nematocysts in the tentacles involved in predation and defense. Beyond that, Anthozoa animals may have nematocytes and gland cells, considered toxins reservoirs, in the ectoderm and endoderm (Fautin, 2009; Moran et al., 2012). Particularly, the presence of venom components has been recorded in mesenterial filaments, which are involved in digestion but also related with competition and defense (Basulto et al., 2006; Macrander et al., 2016). Additionally, a significant variation in abundance of toxin-like genes across tentacles, mesenterial filaments and columns of sea anemones species have been reported (Macrander

et al., 2016). Particularly, Kunitz protease inhibitors/type II KTx are highly expressed in mesenteric filaments and tentacles of sea anemones, as shown on a study involving *Anemonia sulcata*; *Heteractis crispa* and *Megalactis griffithsi* species (Macrander et al., 2016).

CONCLUSIONS

In this work we show that the endemic Brazilian species *A. cascaia*, relies on serine peptidase inhibitors toxins as part of its venom arsenal. The three isolated inhibitors (4461 m/z; 2617 m/z and 2642 m/z) and the inhibitors found in the fraction 3.7.5 (4518, 4685 and 4755m/z) showed potent inhibition (from 60 to 93%) against trypsin. The most potent inhibitor peptide found in F3.7.6 (4461 m/z; exhibiting 93% inhibition), suggest that this is an interesting molecule for further properties characterization. Here, it is suggested that these toxins belong to Venom Kunitz family due to the presence of these serine peptidase inhibitors representants in *Anthopleura* genus; to confirm this hypothesis, LC-MS/MS analysis will be performed. Although widely considered to be primarily used by sea anemones for defensive purposes, these serine protease inhibitors show distinct tissue distributions throughout the body of *A. cascaia*, including the tentacles, pedal disc and mesenterial filaments. Given that these animals do not have a centralized venom system, but instead have nematocysts over the whole body, these distinct tissue distributions indicate venom serine proteases serve a range of ecological roles in *A. cascaia*.

ACKNOWLEDGEMENTS

The authors acknowledge the financial support provided by Comissão de Aperfeiçoamento de Pessoal do Nível Superior (CAPES) and Conselho Nacional de Desenvolvimento Científico e Tecnológico (CNPq) from Brazil, for this study development. The authors also thank Dr. André Carrara Morandini from Laboratório de Cultivo e Estudos de Cnidaria - Universidade de São Paulo, for the identification of sea anemones species collected at São Sebastião beach and for all orientation for ideal location for collecting the animals. We also thank Dr. Pedro Luiz Mailho Fontana (Laboratório de Biologia Estrutural-Instituto Butantan) for *A. cascaia*

images kindly acquired using the stereo microscope Leica M205 A. DCP is a CNPq fellow (#301974/2019-5).

REFERENCES

Amorim, G. C. , Madio, B. , & Almeida, F. C. L. (2019). Solution structure of AcaTx1, a potassium channel inhibitor from the sea anemone Antopleura cascaia. In *PDB DOI: 10.2210/pdb6NK9/pdb*. Protein Data Bank.

An, D., Pinheiro-Junior, E. L., Béress, L., Gladkikh, I., Leychenko, E., Undheim, E. A. B., Peigneur, S., & Tytgat, J. (2022). AsKC11, a Kunitz Peptide from Anemonia sulcata, Is a Novel Activator of G Protein-Coupled Inward-Rectifier Potassium Channels. *Marine Drugs*, *20*(2). https://doi.org/10.3390/md20020140

Ashwood, L. M., Norton, R. S., Undheim, E. A. B., Hurwood, D. A., & Prentis, P. J. (2020). Characterising functional venom profiles of anthozoans and medusozoans within their ecological context. In *Marine Drugs* (Vol. 18, Issue 4). MDPI AG. https://doi.org/10.3390/md18040202

Basulto, A., Pérez, V. M., Noa, Y., Varela, C., Otero, A. J., & Pico, M. C. (2006). Immunohistochemical targeting of sea anemone cytolysins on tentacles, mesenteric filaments and isolated nematocysts of Stichodactyla helianthus. *Journal of Experimental Zoology Part A: Comparative Experimental Biology*, *305*(3), 253–258. https://doi.org/10.1002/jez.a.256

Berman, H., Henrick, K. & Nakamura, 2003. (n.d.).

Chen, X., Leahy, D., van Haeften, J., Hartfield, P., Prentis, P. J., van der Burg, C. A., Surm, J. M., Pavasovic, A., Madio, B., Hamilton, B. R., King, G. F., Undheim, E. A. B., Brattsand, M., & Harris, J. M. (2019). A Versatile and Robust Serine Protease Inhibitor Scaffold from Actinia tenebrosa. *Marine Drugs*, *17*(12). https://doi.org/10.3390/md17120701

D480-D489. (2021). UniProt: the universal protein knowledgebase in 2021 The UniProt Consortium. *Nucleic Acids Research*, *49*. https://doi.org/10.1093/nar/gkaa1100

da Silva J.F. (2009). *Ecologia trófica das anêmonas-do-mar Anthopleura cascaia e Anthopleura krebsi (Cnidaria: Anthozoa) em duas praias de Pernambuco, Brasil.* [Master thesis]. Universidade Federal de Pernambuco. .

Daly, M., Crowley, L. M., Larson, P., Rodríguez, E., Heestand Saucier, E., & Fautin, D. G. (2017). Anthopleura and the phylogeny of Actinioidea (Cnidaria: Anthozoa: Actiniaria). *Organisms Diversity and Evolution*, *17*(3), 545–564. https://doi.org/10.1007/s13127-017-0326-6

Daly, M., & Fautin, D. (2022). *World List of Actiniaria. Anthopleura Duchassaing de Fonbressin & Michelotti, 1860*. https://www.marinespecies.org/aphia.php?p=taxdetails&id=100696

de Capitani, J. D. (2007). *Estrutura populacional e variabilidade genética de anêmonas-do-mar da região entremarés de costão rochoso* [Master thesis]. UNIVERSIDADE ESTADUAL DE CAMPINAS.

de Oliveira, U. C., Nishiyama, M. Y., dos Santos, M. B. V., de Paula Santos-Da-Silva, A., de Menezes Chalkidis, H., Souza-Imberg, A., Candido, D. M., Yamanouye, N., Dorce, V. A. C., & Junqueira-de-Azevedo, I. de L. M. (2018). Proteomic endorsed transcriptomic profiles of venom glands from Tityus obscurus and T. serrulatus scorpions. *PLoS ONE*, *13*(3). https://doi.org/10.1371/journal.pone.0193739

Fautin, D. G. (2009). Structural diversity, systematics, and evolution of cnidae. *Toxicon*, *54*(8), 1054–1064. https://doi.org/10.1016/j.toxicon.2009.02.024

Frazão, B., Vasconcelos, V., & Antunes, A. (2012). Sea anemone (cnidaria, anthozoa, actiniaria) toxins: An overview. In *Marine Drugs* (Vol. 10, Issue 8, pp. 1812–1851). MDPI AG. https://doi.org/10.3390/md10081812

García-Fernández, R., Peigneur, S., Pons, T., Alvarez, C., González, L., Chávez, M. A., & Tytgat, J. (2016). The kunitz-type protein ShPI-1 inhibits serine proteases and voltage-gated potassium channels. *Toxins*, *8*(4). https://doi.org/10.3390/toxins8040110

Gladkikh, I., Monastyrnaya, M., Zelepuga, E., Sintsova, O., Tabakmakher, V., Gnedenko, O., Ivanov, A., Hua, K. F., Kozlovskaya, E., & Jacobson, P. B. (2015). New kunitz-type HCRG polypeptides from the sea anemone heteractis crispa. *Marine Drugs*, *13*(10), 6038–6063. https://doi.org/10.3390/md13106038

Gladkikh, I., Peigneur, S., Sintsova, O., Pinheiro-Junior, E. L., Klimovich, A., Menshov, A., Kalinovsky, A., Isaeva, M., Monastyrnaya, M., Kozlovskaya, E., Tytgat, J., & Leychenko, E. (2020). Kunitz-type peptides from the sea anemone heteractis crispa demonstrate potassium channel blocking and anti-inflammatory activities. *Biomedicines*, *8*(11), 1–17. https://doi.org/10.3390/biomedicines8110473

Hand, C. H. (1955). *The sea anemones of Central California: Vol. Part II*. San Francisco University, Wasmann Biological Society.

Honma, T., & Shiomi, K. (n.d.). *Peptide Toxins in Sea Anemones: Structural and Functional Aspects*. https://doi.org/10.1007/s10126-005-5093-2

Ishida, M., Minagawa, S., Miyauchi, K., Shimakura, K., Nagashima, Y., & Shiomi, K. (1997). Amino Acid Sequences of Kunitz-type Protease Inhibitors from the Sea Anemone Actinia equina. In *Fisheries Science* (Vol. 63, Issue 5).

Jungo, F., & Bairoch, A. (2005). Tox-Prot, the toxin protein annotation program of the Swiss-Prot protein knowledgebase. *Toxicon*, *45*(3), 293–301. https://doi.org/10.1016/j.toxicon.2004.10.018

Laemmli. (n.d.).

Macrander, J., Broe, M., & Daly, M. (2016). Tissue-specific venom composition and differential gene expression in sea anemones. *Genome Biology and Evolution*, *8*(8), 2358–2375. https://doi.org/10.1093/gbe/evw155

Macrander, J., Brugler, M. R., & Daly, M. (2015). A RNA-seq approach to identify putative toxins from acrorhagi in aggressive and non-aggressive Anthopleura elegantissima polyps. *BMC Genomics*, *16*(1). https://doi.org/10.1186/s12864-015-1417-4

Madio, B. (2012). *Purificação e caracterização da fração neurotóxica da peçonha da anêmona do mar Anthopleura cascaia* [Master thesis]. Universidade de São Paulo. .

Madio, B., King, G. F., & Undheim, E. A. B. (2019). Sea anemone toxins: A structural overview. In *Marine Drugs* (Vol. 17, Issue 6). MDPI AG. https://doi.org/10.3390/md17060325

Madio, B., Peigneur, S., Chin, Y. K. Y., Hamilton, B. R., Henriques, S. T., Smith, J. J., Cristofori-Armstrong, B., Dekan, Z., Boughton, B. A., Alewood, P. F., Tytgat, J., King, G. F., & Undheim, E. A. B. (2018). PHAB toxins: a unique family of predatory sea anemone toxins evolving via intra-gene concerted evolution defines a new peptide fold. *Cellular and Molecular Life Sciences*, *75*(24), 4511–4524. https://doi.org/10.1007/s00018-018-2897-6

Madio, B., Undheim, E. A. B., & King, G. F. (2017). Revisiting venom of the sea anemone Stichodactyla haddoni: Omics techniques reveal the complete toxin arsenal of a well-studied sea anemone genus. *Journal of Proteomics*, *166*, 83–92. https://doi.org/10.1016/j.jprot.2017.07.007

Minagawa, S., Ishida, M., Shimakura, K., Nagashima, Y., & Shiomi, K. (1997). Isolation and Amino Acid Sequences of Two Kunitz-Type Protease Inhibitors From the Sea Anemone Anthopleura aff. xanthogrammica. In *Biochem. Physiol* (Vol. 118, Issue 2).

Minagawa, S., Ishida, M., Shimakura, K., Nagashima, Y., & Shiomi, K. (1998). Amino Acid Sequence and Biological Activities of Another Kunitz-type Protease Inhibitor isolated from the Sea Anemone Anthopleura aff. xanthogrammica. In *Fisheries Science* (Vol. 64, Issue 1).

Minagawa, S., Sugiyama, M., Ishida, M., Nagashima, Y., & Shiomi, K. (2008). Kunitz-type protease inhibitors from acrorhagi of three species of sea anemones. *Comparative Biochemistry and Physiology - B Biochemistry and Molecular Biology*, *150*(2), 240–245. https://doi.org/10.1016/j.cbpb.2008.03.010

Mitchell, M. L., Hamilton, B. R., Madio, B., Morales, R. A. V., Tonkin-Hill, G. Q., Papenfuss, A. T., Purcell, A. W., King, G. F., Undheim, E. A. B., & Norton, R. S. (2017). The use of imaging mass spectrometry to study peptide toxin distribution in Australian sea anemones. *Australian Journal of Chemistry*, *70*(11), 1235–1237. https://doi.org/10.1071/CH17228

Mitchell, M. L., Tonkin-Hill, G. Q., Morales, R. A. V., Purcell, A. W., Papenfuss, A. T., & Norton, R. S. (2020). Tentacle Transcriptomes of the Speckled Anemone (Actiniaria: Actiniidae: Oulactis sp.): Venom-Related Components and Their Domain Structure. *Marine Biotechnology*, *22*(2), 207–219. https://doi.org/10.1007/s10126-020-09945-8

Monks, S. A., Pallaghy, P. K., Scanlon, M. J., & Norton, R. S. (n.d.). *Solution structure of the cardiostimulant polypeptide anthopleurin-B and comparison with anthopleurin-A*.

Moran, Y., Genikhovich, G., Gordon, D., Wienkoop, S., Zenkert, C., Özbek, S., Technau, U., & Gurevitz, M. (2012). Neurotoxin localization to ectodermal gland cells uncovers an alternative mechanism of venom delivery in sea anemones. *Proceedings of the Royal Society B: Biological Sciences*, *279*(1732), 1351–1358. https://doi.org/10.1098/rspb.2011.1731

Oshiro, N., Kobayashi, C., Iwanaga, S., Nozaki, M., Namikoshi, M., Spring, J., & Nagai, H. (2004). A new membrane-attack complex/perforin (MACPF) domain lethal toxin from the nematocyst venom of the Okinawan sea anemone Actineria villosa. *Toxicon*, *43*(2), 225–228. https://doi.org/10.1016/j.toxicon.2003.11.017

Peigneur, S., Billen, B., Derua, R., Waelkens, E., Debaveye, S., Béress, L., & Tytgat, J. (2011). A bifunctional sea anemone peptide with Kunitz type protease and potassium channel inhibiting properties. *Biochemical Pharmacology*, *82*(1), 81–90. https://doi.org/10.1016/j.bcp.2011.03.023

Prentis, P. J., Pavasovic, A., & Norton, R. S. (2018). Sea anemones: Quiet achievers in the field of peptide toxins. In *Toxins* (Vol. 10, Issue 1). MDPI AG. https://doi.org/10.3390/toxins10010036

Ramírez-Carreto, S., Vera-Estrella, R., Portillo-Bobadilla, T., Licea-Navarro, A., Bernaldez-Sarabia, J., Rudiño-Piñera, E., Verleyen, J. J., Rodríguez, E., & Rodríguez-Almazán, C. (2019). Transcriptomic and Proteomic Analysis of the Tentacles and Mucus of Anthopleura dowii Verrill, 1869. *Marine Drugs*, *17*(8). https://doi.org/10.3390/md17080436

Reimers, N. S., Yasunobus, C. L., Yasunobusq, K. T., & Nortonll, T. R. (1985). *THE JOURNAL OF BIOLOGICAL CHEMISTRY Amino Acid Sequence of the Anthopleura xanthogrammica Heart Stimulant, Anthopleurin-B** (Vol. 260, Issue 15).

Rodríguez, A. A., Salceda, E., Garateix, A. G., Zaharenko, A. J., Peigneur, S., López, O., Pons, T., Richardson, M., Díaz, M., Hernández, Y., Ständker, L., Tytgat, J., & Soto, E. (2014). A novel sea anemone peptide that inhibits acid-sensing ion channels Dedicated to professor Lászlo Béress, a pioneer in the research on sea anemone toxins, for his contributions to this field. *Peptides*, *53*, 3–12. https://doi.org/10.1016/j.peptides.2013.06.003

Satoh, H., Oshiro, N., Iwanaga, S., Namikoshi, M., & Nagai, H. (2007). Characterization of PsTX-60B, a new membrane-attack complex/perforin (MACPF) family toxin, from the venomous sea anemone Phyllodiscus semoni. *Toxicon*, *49*(8), 1208–1210. https://doi.org/10.1016/j.toxicon.2007.01.006

Sintsova, O., Gladkikh, I., Chausova, V., Monastyrnaya, M., Anastyuk, S., Chernikov, O., Yurchenko, E., Aminin, D., Isaeva, M., Leychenko, E., & Kozlovskaya, E. (2018). Peptide fingerprinting of the sea anemone Heteractis magnifica mucus revealed neurotoxins, Kunitz-type proteinase inhibitors and a new β-defensin α-amylase inhibitor. *Journal of Proteomics*, *173*, 12–21. https://doi.org/10.1016/j.jprot.2017.11.019

Smith, B. L., & Potts, D. C. (1987). Clonal and solitary anemones (Anthopleura) of western North America: population genetics and systematics. In *Marine Biology* (Vol. 94).

Stefanits, H., Bienkowski, M., Galanski, M., Mitulovic, G., Ströbel, T., Gelpi, E., Ribalta, T., Broholm, H., Hartmann, C., Kros, J. M., Preusser, M., & Hainfellner, J. A. (2016). KINFix-A formalin-free non-commercial fixative optimized for histological, immunohistochemical and molecular analyses of neurosurgical tissue specimens. *Clinical Neuropathology*, *35*(1), 3–12. https://doi.org/10.5414/NP300907

Surm, J. M., Smith, H. L., Madio, B., Undheim, E. A. B., King, G. F., Hamilton, B. R., van der Burg, C. A., Pavasovic, A., & Prentis, P. J. (2019). A process of convergent amplification and tissue-specific expression dominates the evolution of toxin and toxin-like genes in sea anemones. *Molecular Ecology*, *28*(9), 2272–2289. https://doi.org/10.1111/mec.15084

Targino, A. K. G., & Gomes, P. B. (2020). Distribution of sea anemones in the Southwest Atlantic: biogeographical patterns and environmental drivers. *Marine Biodiversity*, *50*(5). https://doi.org/10.1007/s12526-020-01099-z

Undheim, E. A. B., Hamilton, B. R., Kurniawan, N. D., Bowlay, G., Cribb, B. W., Merritt, D. J., Fry, B. G., King, G. F., & Venter, D. J. (2015). Production and packaging of a biological arsenal: Evolution of centipede venoms under morphological constraint. *Proceedings of the National Academy of Sciences of the United States of America*, *112*(13), 4026–4031. https://doi.org/10.1073/pnas.1424068112

Valle, A., Alvarado-Mesén, J., Lanio, M. E., Álvarez, C., Barbosa, J. A. R. G., & Pazos, I. F. (2015). The multigene families of actinoporins (part I): Isoforms and genetic structure. *Toxicon*, *103*, 176–187. https://doi.org/10.1016/J.TOXICON.2015.06.028

Wanke, E., Zaharenko, A. J., Redaelli, E., & Schiavon, E. (2009). Actions of sea anemone type 1 neurotoxins on voltage-gated sodium channel isoforms. *Toxicon*, *54*(8), 1102–1111. https://doi.org/10.1016/j.toxicon.2009.04.018

Zhang, Z.-Q. (2011). Animal biodiversity: An introduction to higher-level classification and taxonomic richness. *Zootaxa*, *3148*, 7–12. www.mapress.com/zootaxa/

Supplementary Material 1

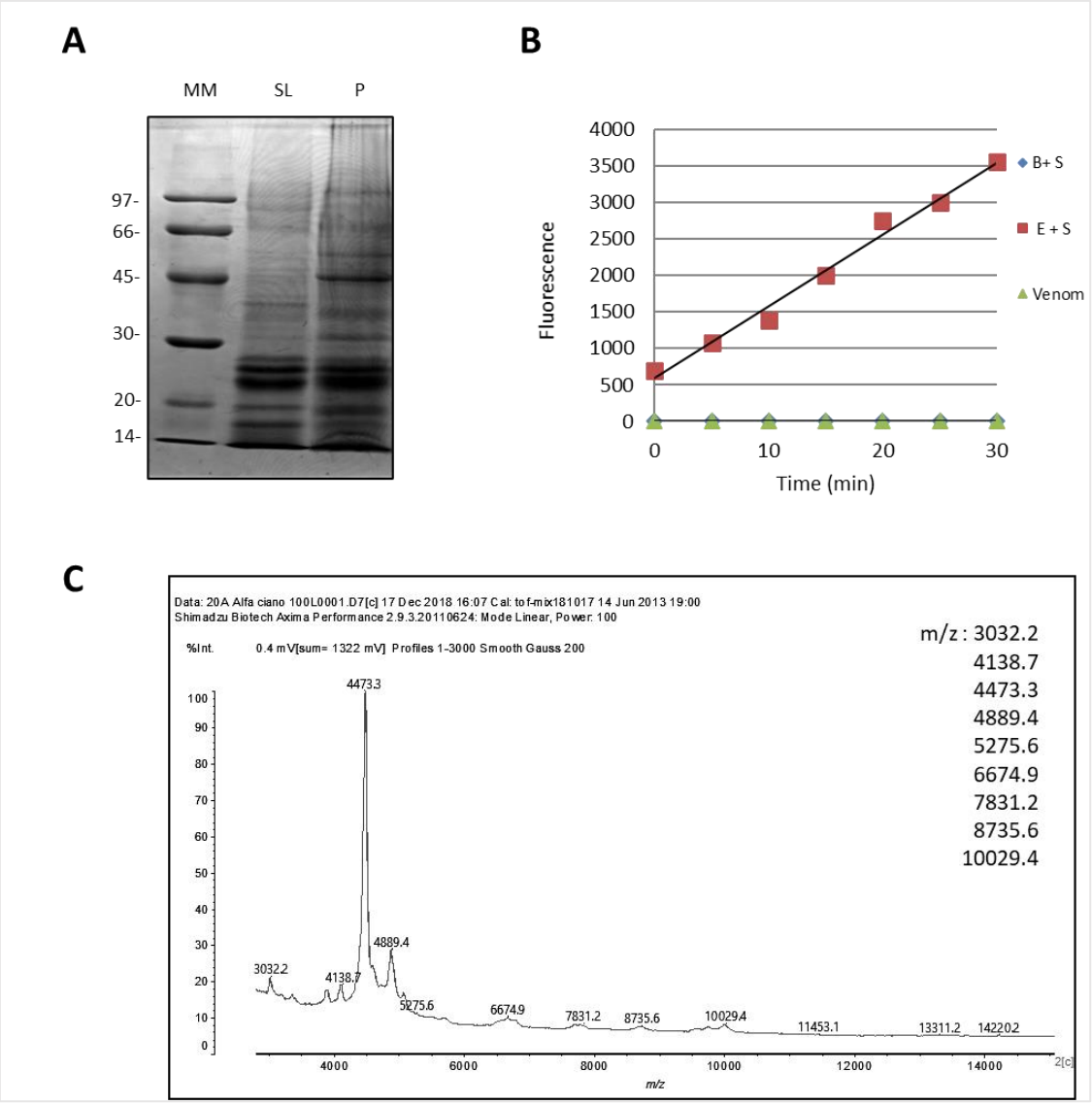

Supplementary material 1. SDS-PAGE analysis of soluble fraction (SL) of the venom and precipitate fraction of the venom (P). Samples (20µL) were analysed by SDS-PAGE (12 %) and stained with Comassie brilliant blue. The venom possesses a wide variety of proteins ranging from 14 to 97kDa. **B- Trypsin Inhibition Assay.** The venom (15 µl) was preincubated for 30 min with trypsin (1:1), and afterwards substrate was added to the samples. Substrate consumption in Arbitrary Units of Fluorescence (Y axis) was read every 5 min for 35 min (X axis). In the test, the sea anemone *A. cascaia* venom; Blank (B + S); and Positive Control (E + S), were analysed. B = Buffer, S = Substrate and E = Enzyme. The venom shows the presence of inhibitor components by complete inhibition of Trypsin activity. **C- MALDI-TOF analysis of *A. cascaia's* venom by positive mode**. The mass spectrum shows that *A. cascaia* venom is also composed by low molecular mass components ranging from 3032 to 14202 m/z.

Supplementary Material 2

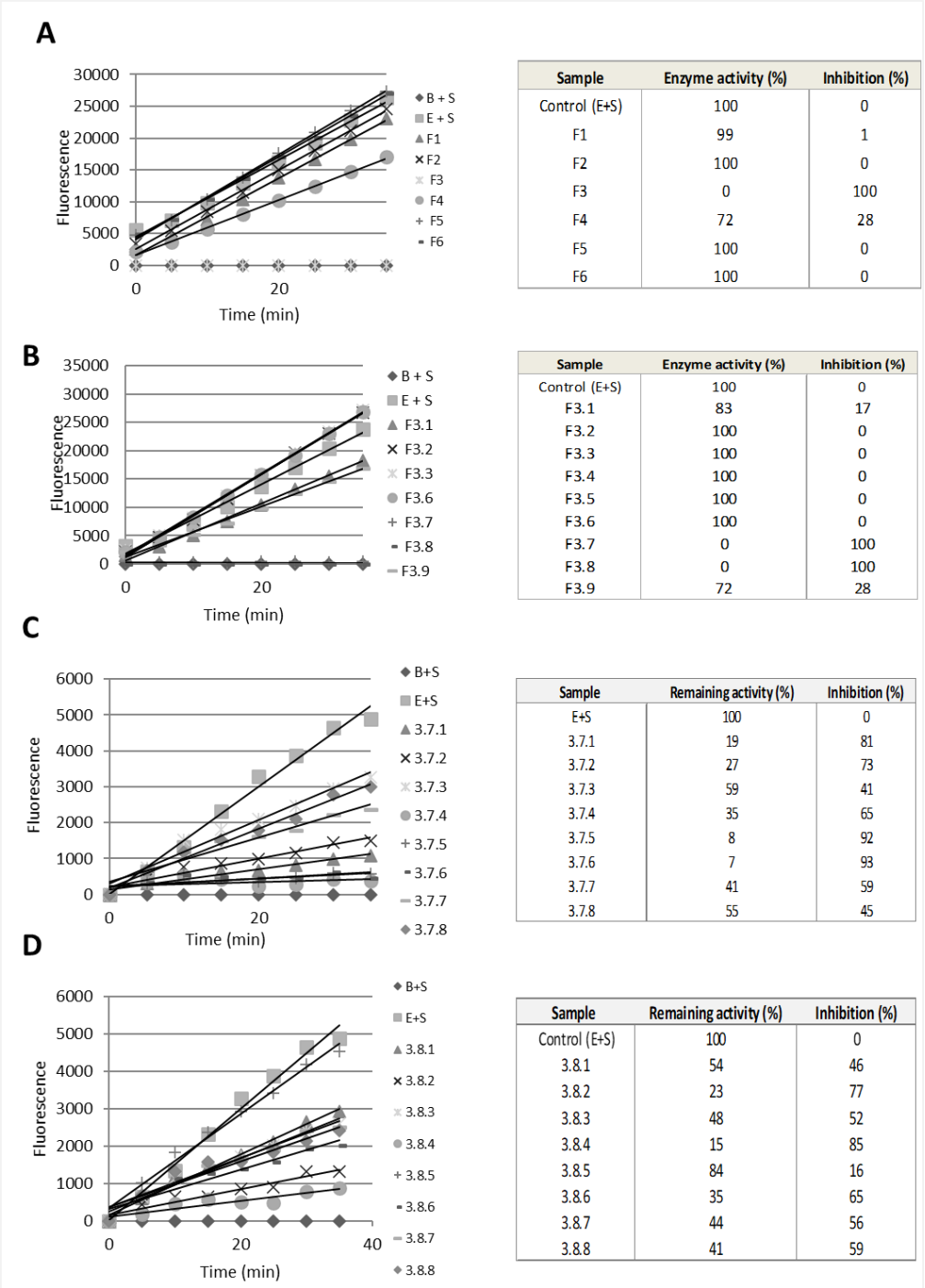

Sample	Enzyme activity (%)	Inhibition (%)
Control (E+S)	100	0
F1	99	1
F2	100	0
F3	0	100
F4	72	28
F5	100	0
F6	100	0

Sample	Enzyme activity (%)	Inhibition (%)
Control (E+S)	100	0
F3.1	83	17
F3.2	100	0
F3.3	100	0
F3.4	100	0
F3.5	100	0
F3.6	100	0
F3.7	0	100
F3.8	0	100
F3.9	72	28

Sample	Remaining activity (%)	Inhibition (%)
E+S	100	0
3.7.1	19	81
3.7.2	27	73
3.7.3	59	41
3.7.4	35	65
3.7.5	8	92
3.7.6	7	93
3.7.7	41	59
3.7.8	55	45

Sample	Remaining activity (%)	Inhibition (%)
Control (E+S)	100	0
3.8.1	54	46
3.8.2	23	77
3.8.3	48	52
3.8.4	15	85
3.8.5	84	16
3.8.6	35	65
3.8.7	44	56
3.8.8	41	59

Supplementary material 2. Trypsin Inhibition Assay. Fractions (5 to 15 µl) were preincubated for 30 min with trypsin (1:1), and afterwards substrate was added to the samples. Substrate consumption in Arbitrary Units of Fluorescence (Y axis) was read every 5 min for 35 min (X axis). In the test, samples representing venom fractions from *A. cascaia*; Blank (B + S); and Positive Control (E + S), were analysed. B = Buffer, S = Substrate and E = Enzyme. **A- Shows the graph and resulting table of the inhibition assay performed with fractions (F1-F6) from the venom.** F3 and F4 were the only fractions capable of inhibiting trypsin, presenting 100% (F3) and 28% (F4) of inhibition. **B- Shows the graph and resulting table of the inhibition assay performed with fractions from F3.** The subfractions F3.7 and F3.8 presented complete inhibition (100%) of the enzyme activity. **C- Shows the graph and resulting table of the assay performed with fractions from F3.7.** The subfractions F3.7.5 and 3.7.6 presented 90% of inhibition of the enzymatic activity. **D- Shows the**

graph and resulting table of the assay performed with fractions from F3.8. A wide variety of subfractions presented inhibitory activity, however F3.8.4; F 3.8.6; F3.8.8 were considered the best candidates due to the quality of isolation of peaks, that exhibited 85%; 65% and 59 % of trypsin inhibition.

APÊNDICE B – MANUSCRITO 2 – *Aulactinia veratra*'s venom reveals a rich arsenal of toxins containing 18 new cysteine scaffolds: A multiomics analysis

Daiane L. da Silva[1,2], Zachary K. Stewart[3], Hayden L. Smith[3], Alun Jones[4], Peter J. Prentis[3], Daniel C. Pimenta[1], Eivind A. B. Undheim[2,5,6]

[1] Laboratório de Bioquímica e Biofísica, Instituto Butantan. Av. Vital Brasil, 1500, Butantã, São Paulo, Brazil

[2]Centre for Advanced Imaging, University of Queensland, St Lucia, QLD 4072, Australia

[3]School of Earth, Environmental and Biological Sciences, Queensland University of Technology

[4] Institute for Molecular Bioscience, The University of Queensland, Brisbane, QLD 4072, Australia.

[5]Centre for Biodiversity Dynamics, Department of Biology, Norwegian University of Science and Technology, 7491 Trondheim, Norway

[6]Centre for Ecological and Evolutionary Synthesis, Department of Biosciences, University of Oslo, PO Box 1066 Blindern, 0316 Oslo, Norway

E-mail address of authors:

Daiane Laise da Silva – daianelaise@gmail.com

https://orcid.org/0000-0002-8401-7883

Zachary K. Stewart – pro_zac@hotmail.com

https://orcid.org/0000-0002-1852-9733

Hayden L. Smith – h49.smith@qut.edu.au

https://orcid.org/0000-0003-3312-4555

Alun Jones – a.jones@imb.uq.edu.au

https://orcid.org/0000-0002-9819-9163

Peter J. Prentis – p.prentis@qut.edu.au

https://orcid.org/0000-0001-6587-8875

Eivind A. B. Undheim – e.a.b.undheim@ibv.uio.no

https://orcid.org/0000-0002-8667-3999

Daniel Carvalho Pimenta – dcpimenta@butantan.gov.br

https://orcid.org/0000-0003-2406-0860

* Eivind A. B. Undheim (Corresponding author) – e.a.b.undheim@ibv.uio.no

Centre for Ecological and Evolutionary Synthesis, Department of Biosciences, University of Oslo, PO Box 1066 Blindern, 0316 Oslo, Norway

ABSTRACT

Sea anemones are underexplored sources of molecules, possessing structurally diverse toxins that can act over a diverse range of pharmacological targets, including voltage-gated ion channels – Nav, Kv, ASIC – and enzymes. These animals represent almost 96% of the manually annotated toxins from phylum Cnidaria, but until now only 4% of it's species have been studied about their toxin content. In the present work, for the first time, the venom of the Australian sea anemone *Aulactinia veratra* was studied and accessed through proteomic and transcriptomic analysis. A classification based on blastp hit similarity and relying on domain architecture of the toxin's sequences (translated transcripts) was performed. The thorough examination over toxins sequences led to the identification of 59 proteins and peptides belonging to 14 known toxin's families of sea anemones and to the acknowledge of 20 peptides presenting 18 new cysteine scaffolds. Besides, such sequences found at protein level, were searched against the transcriptome and this revealed that more than 600 putative transcripts exhibit the same domains architectures. The venom of this sea anemone mainly relies on neurotoxins from ShK-like, β-defensins, SCRiP, ICK, EGF-like types and on serine peptidase inhibitors from Kazal and Kunitz types, representing respectively 25% and 18% of the venom's toxins. The analysis of *A. veratra's* toxin-like transcripts shows that ShK-like, SCRiP, EGF-like, Kunitz, Kazal, Scaffold 10, Scaffold 13 families present repetition of domains. Such toxins, found at protein level and classified as SCREPs 'Small Cysteine Rich Peptides' are translated as double or even triple domain

repeats and represent interesting molecules for future pharmacological properties investigation.

1. INTRODUCTION

Phylum Cnidaria, considered the most ancient venomous animal lineage, emerged approximately 650 million years ago (JOUIAE et al., 2015; VAN ITEN et al., 2016) and comprises more than 10,000 species (ZHANG et al., 2011). Such animals are characterized for not possessing a central venomous apparatus, instead their bodies are covered by cnidocysts, highly specialized venomous organelles that can inject toxins directly into preys or predators (BECKMANN et al., 2012; MADIO et al., 2019). Although studied for years, until now only 93 of Cnidaria species had their proteins/peptides curated at UniprotKB. Such data reflects a total of 609 reviewed molecules in Swiss-Prot, from which 284 are toxins (accessed 25 January 2022 -The UniProt Consortium, 2021; JUNGO et al.,2015).

The ‘Animal toxin annotation project’ clearly shows that by far, in terms of toxin content, Anthozoa is the best well studied class of Cnidaria. Sea anemones alone represent 96% of the cnidarian toxins manually annotated to date (accessed 26 January 2022, JUNGO et al., 2015; COELHO et al., 2021). However, this group has a long way to go on representing the richness of toxins scaffolds of its nearly 1200 species. Until now it is estimated that only 4% of the sea anemones species have been studied about their toxin content (MADIO et al., 2019; PRENTIS et al., 2018).

Like another venomous species, sea anemones use their incredible arsenal of toxins, basically for one main purpose: Survival. These animals usually face environmental pressures living in ecological challenging niche. They can be found in the depths of oceans or in intertidal zones, where they can face abrasive changes of weather, being exposed to atmospheric changes; solar irradiation and dehydration throughout the day (CHEN et al., 2019).

Defense, predation and intraspecific competition are the three main reasons by which these animals use their toxins (ASHWOOD et al., 2020). Even though, at first glance, these animals might seem anatomically simple, sea anemones pass through complex life stages (COLUMBUS-SHENKAR et al., 2018) and develop such variety of specialized venom-related structures– tentacles; achroragi; acontia; different types of nematocysts – that they end up presenting an exquisite arsenal of toxins at

its disposal (ASHWOOD et al., 2020; ASHWOOD et al., 2021; MACRANDER et al., 2016).

Studies developed for over a century on the field of sea anemones toxins has led to the awareness of the scientific community that these animals possess not only structurally diverse toxins, but these molecules can act over specific targets: Voltage-gated ion channels – Nav, Kv, ASIC – and TRPV1 receptors are few of them (MADIO et al., 2017; MADIO et al., 2019). But far from being limited to these already named pharmacological groups of action, toxins from sea anemones influence such diverse targets that they have been classified into at least 15 families according to Tox-Prot database (PRENTIS et al., 2018); nomenclature rules for these toxins have been proposed (OLIVEIRA et al., 2012; KOZLOV & GRINSHIM; 2012) and structure-based classifications have been made, leading to the most recent categorization of such toxins into 15 major structural families and at least 20 pharmacological groups of action (MADIO et al., 2019).

Omics technologies have been considered helpful tools on revealing the evolution and complexity of venoms (VON REUMONT, 2018). Whilst Proteomics shows the repertoire of agents that represent the endpoint of information pathway (BAER & MILLER, 2016); Transcriptomics gives a landscape view of which genes are being currently expressed, exhibiting a prospect of what is potentially translated (SUNAGAR et al., 2016). In a step back, genomics shows a complete panorama of the main targets of evolution: Genes. Through this strategic analysis, observations related to single-gene co-option; duplications; splicing patterns; and the rising of multidomain proteins can be made (SUNAGAR et al., 2016; VON REUMONT, 2018).

These three main pillars – Genes, Transcripts, Proteins – of what is called ‘evolutionary venomics’ can help answering questions related to the composition of toxins; the processes involved in venom evolution; and the biology of venomous species, oftenly unknown (VON REUMONT, 2018).

The integrative approach of two or more of these omics’ strategies have been shown in a plethora of venom studies, mainly involving terrestrial venomous animals (HANEY et al., 2016; ROKYTA & WARD., 2017; de OLIVEIRA et al., 2018; CID-URIBE et al., 2019; CAMPOS et al., 2016). For Cnidaria, considered the most ancient venomous animal lineage, these integrative studies are still timid. However,

the number of efforts towards revealing the complexity of such ancient successful venoms have increased in the last few years.

Mostly, the association of transcriptomics and proteomics is the common choice for elucidating Cnidaria venoms diversity. This holistic view has been applied for a series of Cnidaria species belonging to mainly three classes: Scyphozoa, Cubozoa and Anthozoa. Multiomics studies involving the jellyfishes *Chrysaora fuscescens, Cyanea nozakii, Cyanea capillata* and *Nemopilema nomurai* from Scyphozoa class (PONCE et al., 2016; LI et al., 2016; WANG et al., 2019); the box jellysifh *Chironex fleckeri* from Cubozoa class (BRINKMAN et al., 2015)*;* the zoanthid *Zoanthus natalensis;* and the sea anemones *Stichodactyla haddoni; Cnidopus japonicus; Anthopleura dowii; Oulactis sp. and Telmatactis stephensoni* from Anthozoa class, have been reported in literature (LIAO et al., 2019; MADIO et al., 2017; BABENKO et al., 2017; RAMÍREZ-CARRETO et al., 2019; MITCHELL et al., 2020; ASHWOOD et al., 2021).

In this study, the venom of the Australian sea anemone *Aulactinia veratra* was assessed and the diversity of its toxins elucidated through the association of transcriptomics and proteomics data. The classification of toxins was based not only on similarity with BLASTp database, but the amino acid sequences of such toxins was analysed regarding the presence of characteristic toxin domain. Such approach allowed the identification of Secreted Cysteine-rich REpeat Peptides (SCREPs) and 18 new cysteine scaffolds of toxins in the venom.

2. MATERIAL E METHODS

2.1 *Aulactinia veratra* venom obtention

A. veratra specimens housed in the aquarium of School of Earth, Environmental and Biological Sciences, Queensland University of Technology (QUT), were collected and submitted to electrical stimulation (1V) for venom extraction. Animals (n= 4) were individually stimulated once a week for a month. The venom, obtained in artificial sea water, was kept at -80°C and lyophilised. The venom was suspended in ultrapure water (70mL) and centrifuged at 7000 rcf/ 30 min. The obtained fractions (soluble and precipitate) were dyalised using Pur-A-lyzer Mega Dialysis- 1kDa cut-

off tubes (Merck KGaA, Darmstadt, Germany) and ultrapure water under constant stirring (250 rpm) and temperature (5°C). The venom was recovered, lyophilised and kept at -20°C for further analysis.

2.2 SDS-PAGE

The soluble and precipitate desalted fractions of the venom had their electrophoretic profiles elucidated by SDS-PAGE, under non-reducing and reducing conditions, according to Laemmli (1970). Proteins were loaded in precast gels Bolt™ 4- 12%, Bis-Tris, 1.0 mm (Invitrogen/Thermo Fisher Scientific -USA) and electrophoresed under 100 V for 1 h. Novex™ Sharp Pre-stained Protein Standard (Invitrogen) was used for molecular weight estimation. The resulting gel was stained with Coomassie brilliant blue G250.

2.3 Venom profile by RP-HPLC

The soluble fraction of *A. veratra* venom was submitted to RP-HPLC (Reversed-Phase High-Performance Liquid Chromatography) analysis using Agilent 1100 Series HPLC System and the Chem Station software (Agilent Technologies, California, USA). The venom was fractionated using a C18 column (Gemini NX-C18, 3 µm particle size 110 Å pore size, 250 x 4.6 mm), and a flow rate of 1 mL/min. The fractionation was conducted using a gradient of 5-50% of Solvent B in 45 min. The following solvents were used: Solvent B (0.05% trifluoroacetic acid (TFA) in 90% ACN) and solvent A (0.05% TFA in water). The elution of components from stationary phase was followed by Diod Array Detector G1316A (Agilent), using wavelength of 214 and 280 nm. The soluble fraction of the venom was divided in 11 fractions that were manually collected, freeze dried and prepared for LC-MS/MS analysis.

2.4 Proteomic analysis by LC-MS/MS

2.4.1 In-solution digestion

Fractions (F1-F11) collected from HPLC and the precipitated fraction of the venom, at concentrations of 0,7 to 3,6 µg (10 µL), were placed in microtubes and 8

µL of 100 mM Ammonium Bicarbonate containing 10% of Acetonitrile were added to the samples. Proteins and peptides were reduced by addition of 1µL of 50 mM DTT, and heated at 70°C/10 minutes using a thermoblock. The samples were alkhylated by addition of 1µL of 100mM iodoacetamida and incubated at 30°C/30 minutes in the dark. Molecules were digested by addition of 2uL of Trypsin (250 ng/µL) from porcine pancreas (Proteomics Grade, BioReagent, Dimethylated – SIGMA-ALDRICH), and samples were inbubated overnight at 30°C. After digestion, reduced/alkylated samples were concentrated in a *speed vac* system for 10 min at 45 °C.

2.4.2 Mass Spectrometry and Protein Identification

Tryptic peptides from the digested fractions were analysed by LC-MS/MS using a uHPLC Shimadzu Nexera system (Japan) coupled with a Triple TOF 5600 Electrospray Quadrupole-quadrupole-Time of Flight Mass Spectrometer (AB SCIEX, Canada). Solvent A (0.1% formic acid in water) and Solvent B (90% acetonitrile, 0.1% formic acid), were used as mobile phase. Each fraction (5 µL) was injected in a Zorbax C18 column (1.8 µm, 2.1 mm x 100 mm - Agilent), using a flow rate of 200 µL/min. For elution of tryptic peptides, a linear gradient (1-40% of solvent B in 32 min), followed by a gradient of 40% to 98% of Solvent B in 6 min was used. Solvent B at 98% was used during 3 min for column wash; and between samples injections the column was reequilibrated with 1% of solvent B.

For data acquisition, the following parameters were used: A voltage of 5.500 V was used for ion spray; decomposition potencial (DP) of 100V; gas flow 25; GS1 at 50; GS2 at 60; the interface was heated to 150°C and Turbo V ion source heated to 500 °C. The mass spectrometer acquired a complete scan of TOF-MS data for 200 ms followed by 10 to 200ms of complete scan of product ions using IDA (Information Dependant Acquisition) mode. The scan of precursor ions (TOF/MS) data was acquired using a range of 300-2000 m/z. For MS/MS a range of 100-1800 m/z was selected. The precursor ions exceeding a 100 limit and presenting charge states of +2 to +5 were selected product ions generation. The 10 most intense ions resulted in the MS/MS spectra.

The mass spectra acquired was processed using Protein Pilot 5.0 software (AB SCIEX, Canada). The ‘Paragon thorough’ analysis method was selected with

the following parameters: 1. Post tradutional modifications induced (carbamidomethylation and oxidation), 2. Enzyme used for cleavage (Trypsin); 3. Amino acid substitutions; 4. Unused Proscore (Conf) > 0.05 (10%); 5. False Discovery Rate analysis (1%). The mass spectra generated were searched against the predicted Coding Sequences (CDSs) from *A. veratra* assembled transcriptome, kindly provided by the researcher Peter Prentis from School of Earth, Environmental and Biological Sciences, Queensland University of Technology (QUT). The nucleotide sequences of each transcript were translated into amino acid sequences using a 'Find CDS Tool'. The translated transcriptome was used as a database.

2.4.3 Functional annotation of Venom Proteome

After identification of the corresponding CDSs from *A. veratra* transcriptome, translated sequences were submitted to Blastp search (Basic Local Alignment Search Tool for Proteins) from NCBI platform, using ‘non-redundant protein sequences’ as database and ‘Sea Anemone Taxid 6103’ as organism. Proteins and peptides were identified by similarity and classified according to the domains found in the corresponding Blastp hit. All proteins and peptides classified as ‘toxins’ had their sequences submitted to Interpro- Classification of Protein families from European Bioinformatics Institute, for confirmation of the toxin’s domains existence (MITCHELL et al., 2019). Toxins were classified according to predicted structure and/or function (MADIO et al., 2019). Sequences presenting ‘no significant similarity found’ with Sea anemone taxid; or sequences without known function or structural motifs were classified as ‘unknown’ (MADIO et al., 2017). Such molecules were investigated regarding the presence of new cysteine scaffolds. For categorizing sequences of interest as ‘New cysteine scaffolds’ of putative toxins, seven aspects were considered: 1. Proteins/peptides with no significant similarity to Blastp hit. 2. Proteins/ peptides presenting similarity to uncharacterized Blasp hits by NCBI. 3. Absence of toxin domains automatically identified by NCBI or InterPro. 4. Sequences rich in cysteine residues. 5. Absence of these cysteine scaffolds in the venom of sea anemones according to previous literature. 6. Complete sequences, exhibiting signal peptide. 7. Absence of Transmembrane domains.

2.4.4 Functional annotation of Transcriptome

The sequences of transcripts found in the proteome were used as 'Protein query sequences' for searching putative toxins in the translated transcriptome from *A. veratra*. A BLAST database of the transcriptome was created using Galaxy Australia and an expectation value cut off of 1e-06 was set. CDSs belonging to the same putative toxin category were subjected to sequence alignments using MAFFT (Multiple alignment program for amino acid or nucleotide sequences) and accuracy method L-INS-i from Galaxy Version 7.221.3 (AFGAN et al., 2018). JALVIEW software (WATERHOUSE et al., 2009) was used for finalization of amino acids alignments and visualization of toxins motifs/domains. Sequences with absence of signal peptide; absence of the characteristic toxin domain; or incomplete sequences were removed from the alignment.

3. RESULTS

3.1 *A. veratra* venom: RP-HPLC, electrophoresis and mass spectrometry

The soluble fraction of *A. veratra* venom presented a wide diversity of molecules eluted between 5-50% of B by RP-HPLC analysis (Fig 1.A). Electrophoresis analysis (Fig 1.B) from soluble fraction and precipitate shows that the venom presents high molecular mass proteins (up to 260 kDa), although the main components of the venom seem to be proteins with molecular masses below 20 kDa, mainly between 3.5 and 10 kDa.

The proteome analysis of *A. veratra* venom by mass spectrometry showed an identification of 312 proteins and peptides (Supplementary material 1), classified in superfamilies according to conserved domains presented by the BLASTp hit. These molecules were classified in 9 categories following the molecular function: 1. Enzymes (15%); 2. Structural proteins (14%); 3. Binding (16%); 4. Inhibitors (2%) 5. Regulatory (10%); 6. Ion transport (2%); 7. Phosphoproteins (0.5%); 8. Toxins (including inhibitors and enzymes previously described as toxins) (20%); 9. Unknown (21%) (Fig 2A; Supplementary material 1). All sequences classified as toxins according to BLASTP hit were submitted to InterPro online plattform for identification of conserved domains (Fig 2B; Table 1). The toxins classification was

based on the structure of the molecule and the pharmacological group of action, according to the review work published by MADIO et al., 2019.

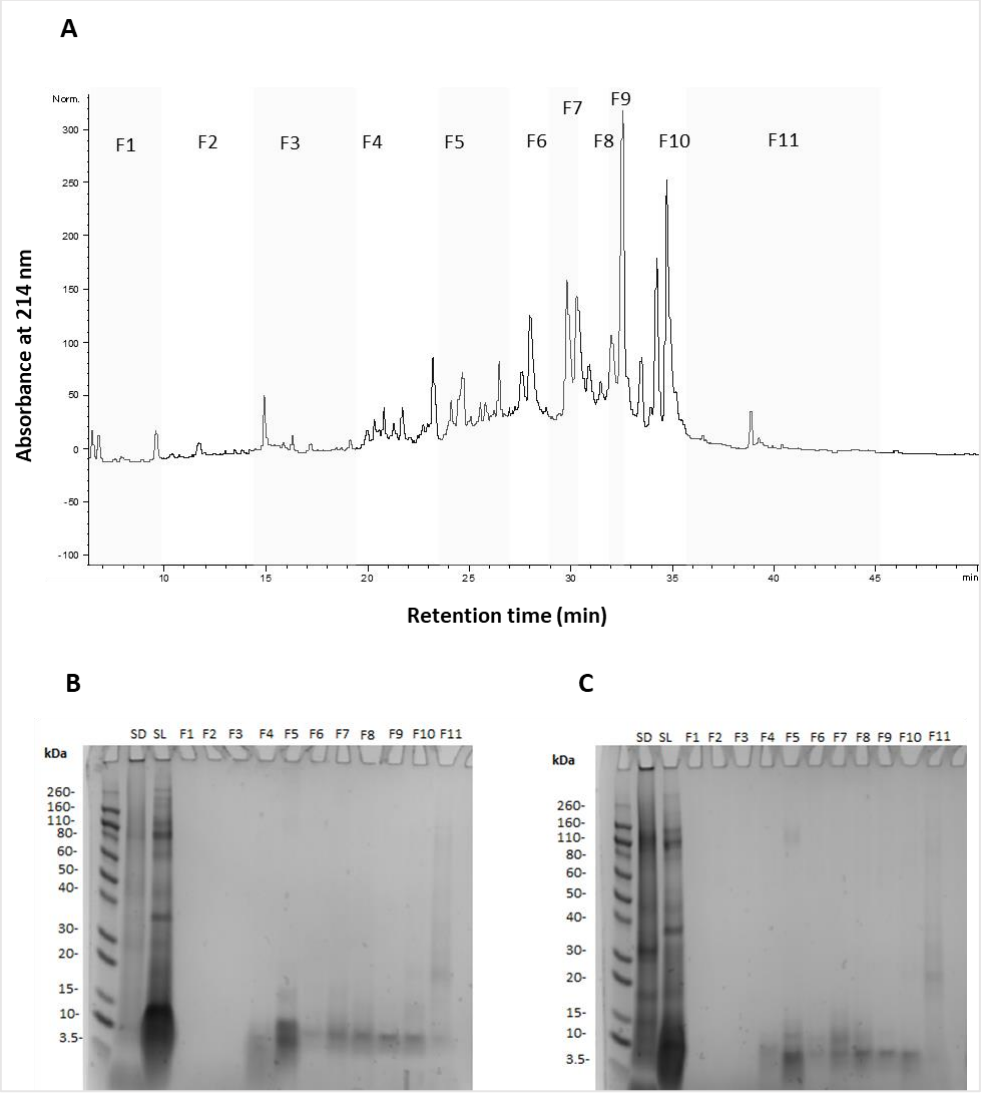

Figure 1. A- Chromatographic profile of *Aulactinia veratra's venom*. The soluble fraction of the venom (50µL) was submitted to RP-HPLC fractionation using C18 column. The chromatogram shows the profile of molecules at 214 nm absorbance, using a gradient of 5 to 50% of B in 45 min. **B, C- SDS-PAGE of *A. veratra's* venom fractions.** Samples (10 µL) from the precipitate fraction (SD), soluble fraction (SL) and obtained fractions from RP-HPLC (F1-F11) were submitted to electrophoresis by SDS-PAGE (12,5%) under not reducing (B) and reducing conditions (C). The gel, stained with Comassie Blue, shows the distribution of proteins found.

In terms of toxin content, 79 components were identified in the venom (59 toxins from 14 known families and 20 toxins exhibiting new cysteine scaffolds) (Fig

2.B, Table 1). The venom from *Aulactinia veratra* is mainly divided in 5 parts: 1. Neurotoxins (29%): including ShK (11%), β-defensins (9%), 'Small Cysteine-Rich Peptides'- SCRIPs (4%); 'Epidermal Growth Factor' - EGF-like (4%); and 'Inhibitor Cystine Knot Fold'- ICK (1%). 2. Non enzymatic components (19 %): 'Membrane-attack complex/perforin' (MACPF) toxins (3%), Actinoporins (1%), WSC (11%), Cysteine Rich Secretory Proteins- CAP (4%). 3. Serine peptidase inhibitors (18%): Kazal (10%) and Kunitz types (8%); 4. Enzymes (9%): Serine peptidase S1 (1%); Endonuclease (4%); Metallopeptidase classes (4%) 5. New cysteine scaffolds (25%) (Fig 2.B).

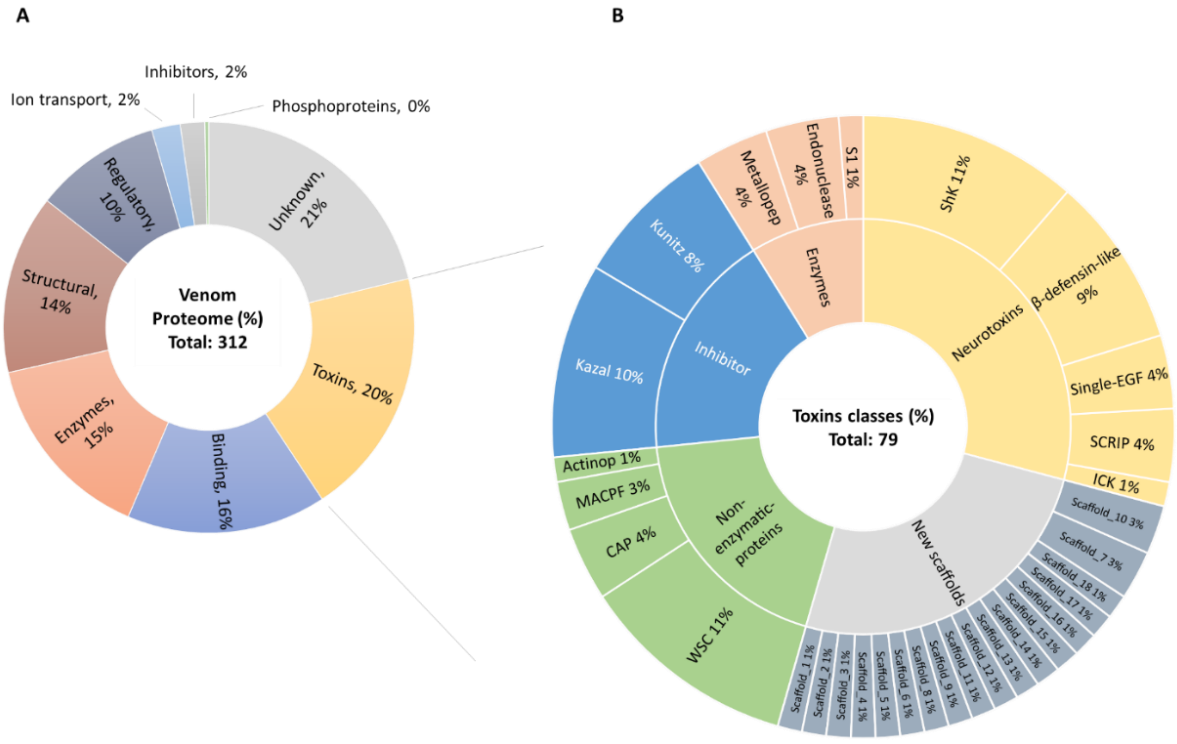

Figure 2. *A. veratra's* venom proteome. **A**- General composition of *A. veratra*'s venom based on molecular function of identified proteins. Proteins were classified according to the conserved domains presented by the corresponding BLASTp hit at NCBI online platform. **B-** Toxin families found in *A. veratra*'s venom. Toxins were classified into the respective families based on conserved domains identified in the amino acid sequences from translated transcripts submitted to Interpro-Classification of Protein Families-EMBL-EBI. Both graphs show the protein classification followed by its representativity (%).

Table 1. The venom proteome of *A. veratra*. Below it is presented the classification of toxins based on the presence of conserved domains. Each putative toxin (transcript ID) found at proteome level and the corresponding identified peptides are presented. Toxins exclusively found in the precipitate fraction of the venom are highlighted with (*) at the end of transcript ID. Identified peptides (in grey) with D1, D2 or D3 between (), represent peptides found exclusively in the first, second or third domain

of the toxin repeat. When a peptide is found between two domains, it's represented by 'Link D1-D2'. Proteins presenting 'no significant similarity' to any BLASTp hit or presenting similarity to uncharacterized proteins with absence of toxin-related domains were categorized into 18 new cysteine scaffolds.

Type	Structural family	Transcript	Identified peptides (Conf: 99)	Blastp hit [species]	E_value	Per Id	Accession
Enzymes	Endonuclease	aul_smart_249271|CDS1	DVYIFTGTGGQAK; FNGGNWAGVENAIR; TLPTPVLSSDVK; APNPQADPK; AVCDPVAK; TLIPEFTGNMIK; WYWKAVCDPVA	uncharacterized protein LOC116298347 [Actinia tenebrosa]	4.00E-79	54.05%	XP_031562623.1
		aul_smart_878853|CDS1	APNPQADPK; AVCDPVAK; DVYVFTGTSGQAK; DYNPSQQIIENPAWNDK; EMTFIVTNAAPQWQK; ESIVFVAQNNVGDQTNK; FNGGNWAGVEK; GTFLDTFLK; ITGCDGIK; LPPFHATNCK; QTTELGIIFCYSLDAASK; TLIPEFTGNMIK; TLSTPVLSSDVK; VVAPEWFWK; QTTELGIIFCYSLDAASKK	uncharacterized protein LOC116298347 [Actinia tenebrosa]	3.00E-102	52.36%	XP_031562623.1
		aul_smart_878854|CDS1	GTFLDTFLK	uncharacterized protein LOC116298347 [Actinia tenebrosa]	7.00E-101	51.69%	XP_031562623.1
	M13	aul_smart_939726|CDS1*	TWVLPGLK	endothelin-converting enzyme 1-like [Actinia tenebrosa]	6.00E-86	58.65%	XP_031563523.1
		aul_smart_939847|CDS2*	ENINSLTWLDDFTR; IQDLGGWNMIEGSR; AIENLGDAPLR; LSLEELQR; SLTWLDDFTR; DAVTYTEHAK; DNIQGITKPAIR; ISGLIYEETR; VFLENVIR	endothelin-converting enzyme 1-like [Actinia tenebrosa]	5.00E-134	49.40%	XP_031564967.1
		aul_smart_939848|CDS1*	IDAMAGNVGYPDYILDSK; ENINSLTWLDDFTR; SLTWLDDFTR	endothelin-converting enzyme 1-like [Actinia tenebrosa]	2.00E-62	47.66%	XP_031563523.1
	S1	aul_smart_839293|CDS2	AILPIADNNHCSAR; HDVALLLLDQK; IINGQNANLHEFPWQVSLR; IPAGTQCSLSGWGR; TVPGGSSAYILQK; VTYSSGIQAIGLPTSGSR	chymotrypsinogen A-like [Actinia tenebrosa]	6.00E-125	64.15%	XP_031568088.1
Inhibitors	Kazal	aul_smart_1046916|CDS2	FCTLEYAPVCSSDGVTYGNACMLR; SDTNIELVHR; GVTYGNACMLR;TNIELVHR	PI-actitoxin-Avd5a [Anemonia sulcata]	2E-20	73.91%	P16895.1
		aul_smart_426451|CDS2	IEFVHGGPC; MFAPVCGSYGVTYANECLLR; SDSKIEFVHGGPC; KHCPEHCNR; GVTYANECLLR	PI-actitoxin-Avd5a [Anemonia sulcata]	4E-11	52.17%	P16895.1
		aul_smart_876517|CDS28	YQVAVLASCPGGCPITYEPVCGSDGETYK; MTIDHYGNC; NTCWFR; TYEPVCGSDGETYK	uncharacterized protein LOC110241796 [Exaiptasia pallida]	0.00000005	46.67%	XP_020903357.2
		aul_smart_813067|CDS1	GADCSSNNNIELVHQGPC; FCTLEYAPVCSSDGVTYGNACMLR; GVTYGNACMLR	PI-actitoxin-Avd5a [Anemonia sulcata]	9.00E-18	67.39%	P16895.1
		aul_smart_280649|CDS1	YQVAVLASCPGGCPITYEPVCGSDGETYK; MTIDHHGSC; NTCWFR	uncharacterized protein LOC110241796 [Exaiptasia diaphana]	1.00E-08	38.98%	XP_020903357.2
		aul_smart_427605|CDS2	FCAPLYTPLCGSDGVTYDNDCLLR; CGSDGVTYDNDCLLR	predicted protein [Nematostella vectensis]	2.00E-11	36.25%	EDO42282.1
		aul_smart_687983|CDS3	HVAECK; IGLAHVGPC	PI-actitoxin-Avd5a; Short=PI-AITX-Avd5a [Anemonia sulcata]	2.00E-09	53.49%	P16895.1
		aul_smart_877428|CDS1*	IEFVHGGPC; MFAPVCGSYGVTYANECLLR; VTYANECLLR; ANECLLR; SYGVTYANECLLR	PI-actitoxin-Avd5a; Short=PI-AITX-Avd5a [Anemonia sulcata]	5.00E-11	52.17%	P16895.1
	Kunitz	aul_smart_859108|CDS2	AMVTGNCK (D1); DCQDACMGK (D1); DECLR (D2); FYYTGCQGNANNFETR (D1); GFCLFPPATGPCK (Link D1-D2); KDCQDACMGK (D1); NNFETKDECLR (D2); TFTYGGCEGNK (D2); YYYDNEGGK (D2)	kappaPI-actitoxin-Avd3e-like [Actinia tenebrosa]	1.00E-68	69.34%	XP_031558603.1
		aul_smart_955021|CDS2	CEEFFYGGCGGNANNFHTQNECEQK (D1 and D2); CSGYLAGYSGTSDICHLQSVTGFCR (Link D1-D2); FYFNVDTR (D1 and D2); GNANNFHTQK (D3); RCEEFFYGGCGGNANNFHTQNECEQK; SGTSDICHLQSVTGFCR (D2 and D3); CEEFIYGGCR (D3); TSGICELQSVTGFCR (D1)	carboxypeptidase inhibitor SmCI-like [Exaiptasia diaphana]	7.00E-49	40.27%	XP_020904664.1
		aul_smart_856786|CDS3	QFIYGGCQGNENNFK; YHYDESIGTCR;	PI-actitoxin-Aeq3a-like [Actinia tenebrosa]	1.00E-41	78.67%	XP_031550082.1
		aul_smart_859005|CDS1	AVGSCQAAFPR; CEPFTYGGCGGNANNFQSEEECNK; FYYNSGSGK	BPTI/Kunitz domain-containing protein-like [Actinia tenebrosa]	3.00E-33	69.62%	XP_031567285.1
		aul_smart_886056|CDS2	CEEFFYGGCWGNANNFHTQK (D2); CSGYLAGYSGTSDICHLQSVTGFCR (Link D1-D2); FYFNVDTR (D1-D2); GNANNFHTQK (D2);TSGICELQSVTGFCR (D1)	BPTI/Kunitz domain-containing protein-like [Actinia tenebrosa]	5.00E-38	46.04%	XP_031567285.1
		aul_smart_684611|CDS2	CESFIYGGCGGNR; NNFHSFNECR; YYYNTEAGR; ETGMPSFCHLPSEVGR	KappaPI-stichotoxin-Shd2a; Short=KappaPI-SHTX-Shd2a [Stichodactyla haddoni]	1.00E-25	63.08%	B1B5I8.1

Table 1 (continued)

Type	Structural family	Transcript	Identified peptides (Conf: 99)	Blastp hit [species]	E_value	Per Id	Accession
Neurotoxins	B-defensin-like_Kv3	aul_smart_420607|CDS1	GDWWIWR	type III potassium channel toxin protein [Anemonia sulcata]	1.00E-15	49.35%	ALL34550.1
		aul_smart_270533|CDS2	GDCPSGHGYKNSCK; IGFNMCCYPR; SSQGDFWLLR	type III potassium channel toxin protein [Anemonia sulcata]	1E-20	52.56%	ALL34533.1
		aul_smart_904166|CDS1	GAPCTCR; GESGIYWFSGK; TYCNFVIGLCCVK	type III potassium channel toxin protein [Anemonia sulcata]	3.00E-32	67.57%	ALL34555.1
		aul_smart_846342|CDS2	ALACYCK; GDKWILR; STCPGGYGYSSGCTQSGYR; CCYPQYY	type III potassium channel toxin protein [Anemonia sulcata]	6.00E-33	65.43%	ALL34531.1
		aul_smart_870725|CDS2	AVFGICCYK; CEGGFSGTYWFAR; GSCPGGHGYNGVCR	type III potassium channel toxin protein [Anemonia sulcata]	1.00E-17	50.00%	ALL34555.1
		aul_smart_914904|CDS2	AVFGVCCYK; GGFSGTYWFAR; GSCPGGHGYNGVCR	type III potassium channel toxin protein [Anemonia sulcata]	9.00E-18	50.00%	ALL34555.1
	B-defensin-like_Nav	aul_smart_802345|CDS9	GLLSDCCKQ; GNIGCPSGWNLCADR; GVPCKCDSDGPTVHGNHLSGTIWMK; TPGYGNIGCPSGWNLCADRYLCADR; RGLLSDCCK	Delta-actitoxin-Ave sodium channel inhibitory toxin [Aulactinia veratra]	2.00E-52	84.69%	ATY39984.1
	ICK	aul_smart_887805|CDS26	SQVQGCYHSSECCSPLVCK; YCLKF; AYCNYDAGGCTNAR	Predicted protein NvePTx1; Flags: Precursor [Nematostella vectensis]	0.0002	31.51%	A7RMN1.2
	SCRIP	aul_smart_34921|CDS3	CSASCGWNAK; GSCLPK; LQACYAGTR; GSCLPKLQACYAGTR	No_significant_similarity_found			
		aul_smart_760423|CDS2	ACSGANHYCSVSTNK (D1); CYGASNHCTLSTNK (D2)	small cysteine-rich protein 2-like [Actinia tenebrosa]	2.00E-08	41.75%	XP_031553817.1
		aul_smart_9946|CDS1	VGLLTR	uncharacterized protein LOC116308971 isoform X1 [Actinia tenebrosa]	3.00E-60	54.97%	XP_031575359.1
	ShK	aul_smart_206650|CDS2	ACEDNLPAPTCR; ANNICDSEK; DNLPAPTCR	U-actitoxin-Oulsp2 [Oulactis sp. MM-2018]	9.00E-24	52.44%	A0A330KUG5.1
		aul_smart_333142|CDS1	SDCGWILEGKDPAGYCYQYR (D1); TCGFCKPPAPPQVHCEDTR (Link D1-D2); HQNDAFIQDCK (D2); NDCSWIAQHNNDVAEYCDR (D2); NDPEVK (D1);	uncharacterized protein LOC116305581 [Actinia tenebrosa]	1.00E-67	67.53%	XP_031571380.1
		aul_smart_540526|CDS2	YENVLCR	Kappa-stichotoxin-Hmg1a [Heteractis magnifica]	2.00E-11	48.00%	O16846.2
		aul_smart_677929|CDS2	LLQSQCTQYR	Kappa-actitoxin-Aer3a [Anemonia erythraea]	2.00E-10	70.59%	Q0EAE5.1
		aul_smart_68364|CDS1	AACGICEAPPPPYATAEK; AIGHFTQVVWK; HGVPSLVWDSTLASESADWALHLAQR; IPDCESGYTESSGCTQWK; LVHSDANSAYGENLYYAGTSAIGSLASCTNAVK; NGWTYTFVAAR; SWYSEIDDYDFNNPGTSTNGK; VGVGIAAVTK; DFENSATK; YTPPGNQAGQYAENVPNVVSN	uncharacterized protein LOC116288443 [Actinia tenebrosa]	1.00E-91	58.75%	XP_031551091.1
	Single-EGF-domain	aul_smart_835448|CDS1	WITALDTPSCICATGYEGQR; NDGHFSPCPESHEHYCLNGGTCR	U-actitoxin-Avd12a [Anemonia viridis]	4.00E-09	37.88%	P0DMY9.1
		aul_smart_685108|CDS3	GSAGVACTGQHATSFCLNGGECR; HIESLGEYYCICHGDYTGLR (D1); HIESLGK (D2)	OMEGA-stichotoxin-Shd4a [Stichodactyla haddoni]	2.00E-27	64.37%	B1B5J0.1
		aul_smart_997952|CDS1	HIESLGK; YYCICYDDYIGLR	OMEGA-stichotoxin-Shd4a [Stichodactyla haddoni]	1.00E-23	60.24%	B1B5J0.1
Non-enzymatic -proteins	Actinop.	aul_smart_512597|CDS1*	ALLYDGK; NEGPVATGVVGVLAYHITGGHTLAVMFSVPFDYNLY QNWWNVK; VILPHNVDSGK; ADQSMYEDLYYSSNPFR	DELTA-actitoxin-Aas1a [Anthopleura asiatica]	7.00E-61	74.78%	C5NSL2.1
	CAP	aul_smart_464302|CDS2*	EGENIVISPSPDCK; EIPGTDVAPGKPLPICPPPSSGEGM	ectin-like [Actinia tenebrosa]	1.00E-72	70.42%	XP_031569962.1
		aul_smart_860615|CDS2	EAVNAWYAQEK; GNVQPFFYYQR; NDWTYTFVVAR; VGVGIAAVTR; VLSVNTAECLAAHNAK	uncharacterized protein LOC116288443 [Actinia tenebrosa]	5.00E-61	44.98%	XP_031551091.1
		aul_smart_414628|CDS1	EGENIVISPSPDCK; LGVGISGNWLVAR; WDATLAAHAQK; EAVEEWSDEAYDYDDWGYCAKPPR; IPSFAASCLK	ectin-like [Actinia tenebrosa]	9.00E-91	72.29%	XP_031569962.1
	MACPF	aul_smart_487417|CDS2*	IVGLPTLNQYTICFWIEFSNVKPR; ANDLFPDENIDWGCEK; FDPSDTGGK; FLMGSIADLVDLR; FYSFGNGEDPAQIVDSHVISR; GTLYVVLSAVPSNTDSWYYVEISSFGVGIYK; ILDYYNK; NMIDGAAFIGVGFDGR; TEMDVLLR; VAPVVAGALSK	uncharacterized protein LOC116292765 [Actinia tenebrosa]	0	70.42%	XP_031555977.1
		aul_smart_884261|CDS11*	ANDLFPDENIDWGCEK; DSISGETNFFADGVVQR; FDPSDTGGK; FLMGSIADLVDLR; FYSFGNGEDPAQIVDSHVISR; GADMETLR; GTLYVVLSAVPSNTDSWYYVEISSFGVGIYK; ILDYYNK; IVGLPTLNQYTICFWIEFSNSK; LLTNDEIAK; NMIDGAAFIGVGFDGR; TEMDVLLR; VAPVVAGALSK	uncharacterized protein LOC116292765 [Actinia tenebrosa]	0	65.72%	XP_031555977.1

Table 1 (continued)

Type	Structural family	Transcript	Identified peptides (Conf: 99)	Blastp hit [species]	E_value	Per_Id	Accession
Non- enzymatic -proteins	Actinop.	aul_smart_512597|CDS1*	ALLYDGK; NEGPVATGVVGVLAYHITGGHTLAVMFSVPFDYN LYQNWWNVK; VILPHNVDSGK; ADQSMYEDLYYSSNPFR	DELTA-actitoxin-Aas1a [Anthopleura asiatica]	7.00E-61	74.78%	C5NSL2.1
	CAP	aul_smart_464302|CDS2*	EGENIVISPSPDCK; EIPGTDVAPGKPLPICPPPSSGEGM	ectin-like [Actinia tenebrosa]	1.00E-72	70.42%	XP_031569962.1
		aul_smart_860615|CDS2	EAVNAWYAQEK; GNVQPFFYYQR; NDWTYTFVVAR; VGVGIAAVTR; VLSVNTAECLAAHNAK	uncharacterized protein LOC116288443 [Actinia tenebrosa]	5.00E-61	44.98%	XP_031551091.1
		aul_smart_414628|CDS1	EGENIVISPSPDCK; LGVGISGNWLVAR; WDATLAAHAQK; EAVEEWSDEAYDYDDWGYCAKPPR; IPSFAASCLK	ectin-like [Actinia tenebrosa]	9.00E-91	72.29%	XP_031569962.1
	MACPF	aul_smart_487417|CDS2*	IVGLPTLNQYTICFWIEFSNVKPR; ANDLFPDENIDWGCEK; FDPSDTGGK; FLMGSIADLVDLR; FYSFGNGEDPAQIVDSHVISR; GTLYVVLSAVPSNTDSWYYVEISSFGVGIYK; ILDYYNK; NMIDGAAFIGVGFDGR; TEMDVLLR; VAPVVAGALSK	uncharacterized protein LOC116292765 [Actinia tenebrosa]	0	70.42%	XP_031555977.1
		aul_smart_884261|CDS11*	ANDLFPDENIDWGCEK; DSISGETNFFADGVVQR; FDPSDTGGK; FLMGSIADLVDLR; FYSFGNGEDPAQIVDSHVISR; GADMETLR; GTLYVVLSAVPSNTDSWYYVEISSFGVGIYK; ILDYYNK; IVGLPTLNQYTICFWIEFSNSK; LLTNDEIAK; NMIDGAAFIGVGFDGR; TEMDVLLR; VAPVVAGALSK	uncharacterized protein LOC116292765 [Actinia tenebrosa]	0	65.72%	XP_031555977.1
	WSC	aul_smart_186432|CDS2	FPAVEAVSK	uncharacterized protein LOC116308716 [Actinia tenebrosa]	5E-166	0.7432	XP_031575055.1
		aul_smart_6042|CDS2*	TVNVGSTVEFK; CPSYNVK; GYEYFGIQHK; LGCYEDASDR; MFEECKK; QDTCYK; SECWGSSNGQEITYNK; YDDSPGGYKR	uncharacterized protein LOC116305510 [Actinia tenebrosa]	3.00E-118	59.09%	XP_031571305.1
		aul_smart_143517|CDS1	SDDGFGVGSIWSNFVYRK; CPSYNVK; GYEYFGIQHK; SECWGSSNGQEITYNK; YDDSPGGYK	uncharacterized protein LOC116305510 [Actinia tenebrosa]	1.00E-83	69.36%	XP_031571305.1
		aul_smart_761274|CDS2*	SLPIPYK; GYEYFGIQHK; LGCYEDASDR; LGCYEDTSDR; MFEECKK; VTVVSAGWEK; YDDSPGGYKR	uncharacterized protein LOC116305510 [Actinia tenebrosa]	2.00E-32	51.35%	XP_031571305.1
		aul_smart_879797|CDS2	LGCYEDTSDR; SDDGFGVGSNFSNFVYR; ASHTNTYK; ASPKPSLLNVEYNPSTPNLGDEVSK; CPSYNVK; GYEYFGIQHK; SECWGSSNGQEITYNK; SVSFIGNLK; YDDSPGGYK	uncharacterized protein LOC116305510 [Actinia tenebrosa]	8.00E-110	56.21%	XP_031571305.1
		aul_smart_879937|CDS4	SDDDFGVGSNWSNFVYR; ASHTNTYK; EGKPWFR; GTQYDR; GYEYFGIQHK; LGCYEDASDR; MFEECKK; SECWGSSNGQEITYNK; SVSFIGNLK; VTVGSGWEK; YDDSPGGYKR	uncharacterized protein LOC116305510 [Actinia tenebrosa]	8.00E-110	54.86%	XP_031571305.1
		aul_smart_879959|CDS2	SDDGFGVGSNWSNFVYR; ASHTNTYK; ASPKPSLLNVEYNPSTPNLGDEVSK; CPSYNVK; FHYYALLK; GYEYFGIQHK; LGCYEDASDR; SECWGSSNGQEITYNK; SVSFIGNLK; VTVVSAGWEK; YDDSPGGYK	uncharacterized protein LOC116305510 [Actinia tenebrosa]	5.00E-113	56.94%	XP_031571305.1
		aul_smart_879960|CDS2*	LGCYEDTSDR; QDTCYECPSYNVK; VTVGSGWEK; SDDGFGVGSNFSNFVYRK; NPNLGVIVSK; INPTPSILIAQY; CPSYNVK; ASHTNTYK; EGKPWFR; GYEYFGIQHK; MFEECKK; SECWGSSNGQEITYNK; SVSFIGNLK; YDDSPGGYKR	uncharacterized protein LOC116305510 [Actinia tenebrosa]	1.00E-110	55.56%	XP_031571305.1
		aul_smart_1033576|CDS2	ASHTNTYK; ASPKPSLLNVEYNPSTPNLGDEVSK; CPSYNVK; FHYYALLK; GYEYFGIQHK; LGCYEDASDR; SECWGSSNGQEITYNK; SVSFIGNLK; VTVVSAGWEK; YDDSPGGYK; SDDGFGVGSNLSNFVYRK	uncharacterized protein LOC116305510 [Actinia tenebrosa]	5.00E-111	61.15%	XP_031571305.1
Unknown	Scaffold_1	aul_smart_34342|CDS1	VGVGIAAVTK	No_significant_similarity_found			
	Scaffold_2	aul_smart_1012536|CDS1	HTFDVYYFR; LPPALHTVICAK; HTTVYDCVRK	No_significant_similarity_found			
	Scaffold_3	aul_smart_983271|CDS1	DVPGGSCK; FVCCVTI; INCDSR; KGFTVNK; SGDCKDVDVR	uncharacterized protein LOC5508728 isoform X2 [Nematostella vectensis]	0.94	43.33%	XP_032233414.1
	Scaffold_4	aul_smart_963082|CDS3	AGQCCPCPKP; LQCCPCGAK	predicted protein [Nematostella vectensis]	4.6	62.50%	EDO29841.1
	Scaffold_5	aul_smart_73591|CDS2	ACDVCSSK; ANTKPQVLQCGKEDEICR; ICQENCLNEK; TCYDNCNTK; TNCMSLCTQAK; VACVDGIK; KTCSLNCTT	chymotrypsinogen B-like isoform X1 [Actinia tenebrosa]	0.047	31.76%	XP_031550563.1
	Scaffold_6	aul_smart_828408|CDS2	DGNAVCRPL; FGNNCECSK; TVQCTYGSVTYEPGDR	uncharacterized protein LOC116604574 [Nematostella vectensis]	0.008	33.87%	XP_032223012.1
	Scaffold_7	aul_smart_418125|CDS1	SEEIPCNEEDLEKLR; AMGLQVDHAR; CYPKPQAR; DTNLCCGPECK	uncharacterized protein LOC116304236 [Actinia tenebrosa]	2E-37	57.01%	XP_031569802.1
	Scaffold_7	aul_smart_188645|CDS1	DTNLCCGPECK; LTAMGLQVDHAR; CYPKPQAR; REIPCNEEALEK	uncharacterized protein LOC116304236 [Actinia tenebrosa]	9.00E-37	56.19%	XP_031569802.1
	Scaffold_8	aul_smart_219023|CDS3	AQTDIIACRDPCAVK; DPCAVKDANGK; AQTDIIACR	uncharacterized protein LOC116301422 isoform X1 [Actinia tenebrosa]	1.00E-09	41.67%	XP_031566334.1
	Scaffold_9	aul_smart_955171|CDS3	ERPCPTDK; YCHSIQEDCWWTDDKDSEACK	hypothetical protein AC249_AIPGENE18232 [Exaiptasia pallida]	2E-13	43.24%	KXJ05374.1
	Scaffold_10	aul_smart_128724|CDS3	KVPVAESDGR (D1); STTCDVGGVTYNVGETFVTK (D2); TTCEPLCIPPPPLLCPPGEK (D1); TYNAGEEFIDGLCFGR (D1); EDSCVFGGK (D1)	cysteine-rich motor neuron 1 protein-like [Actinia tenebrosa]	1.00E-54	52.35%	XP_031549053.1
	Scaffold_10	aul_smart_954616|CDS2	ACTIYCR; CVSLCPPSIVACEPGER; EAGCVFEGK	cysteine-rich motor neuron 1 protein-like isoform X6 [Actinia tenebrosa]	2.00E-22	43.64%	XP_031549072.1
	Scaffold_11	aul_smart_502041|CDS2	FCSLDGQVLHIMA; WYNAGEIIFER; GCEYEGK; GSGGTYEIK	mucin-2 [Nematostella vectensis]	0.002	35.42%	XP_032230364.1
	Scaffold_12	aul_smart_838698|CDS3	GRCQTIHSCV; CQTIHSCV; DIIDGGGCPHCYEPDPEGNCR	precusor of biologically active peptides MS9.2 [Metridium senile]	0.22	32.05%	SBO16029.1
	Scaffold_13	aul_smart_978781|CDS2	EACDLLGDPCTTDK; QCPGDCDGFPLFCYR; SECAMNVESNPY	transmembrane cell adhesion receptor mua-3 [Nematostella vectensis]	0.000004	40.00%	XP_001636659.1
	Scaffold_14	aul_smart_94777|CDS1	NACASDFNK; NVIDSSQYDNCVIK	uncharacterized protein LOC116307697 [Actinia tenebrosa]	5.00E-36	50.00%	XP_031573854.1
	Scaffold_15	aul_smart_798440|CDS8*	ATDCGSSGESEGSFSR; ESEGSFSR	uncharacterized protein LOC116306945 [Actinia tenebrosa]	5.00E-16	78.05%	XP_031572946.1
	Scaffold_16	aul_smart_869134|CDS1	TIMHLFDVNNCK; VDPGYCEDYGDQPFCR	uncharacterized protein LOC116297886 [Actinia tenebrosa]	1.00E-65	68.94%	XP_031562063.1
	Scaffold_17	aul_smart_92667|CDS2	LMYCEIYDVPLPGPIGR	uncharacterized protein LOC116308711 [Actinia tenebrosa]	0.48	27.03%	XP_031575053.1
	Scaffold_18	aul_smart_944968|CDS3*	GCGGDSDCPCPGWHCPSPGGR	hypothetical protein AC249_AIPGENE28876 [Exaiptasia pallida]	0.93	21.74%	KXJ20930.1

3.2 Transcripts and correspondent toxins found in the venom

Aulactinia veratra's transcriptome is composed by a total of 627 transcripts containing domains from 11 known toxin families. For this analysis, enzymatic components from transcriptome were not included. Beyond that, the transcriptome showed the presence of new toxin's domains, classified here as 18 new cysteines scaffolds. Taking in consideration *A. veratra's* transcripts, it was found that putative neurotoxins are correspondent to 21% of the toxin-like transcripts, including β-defensins, ICK, SCRIP, ShK, Single-EGF families; putative non-enzymatic components to 19% (Actinoporins, CAP, CAP, ShK, MACPF and WSC); putative inhibitors represent 25%, comprising Kazal and Kunitz families; and the putative new cysteine scaffolds correspond to 31% of the toxin-like transcripts (Scaffolds 1 to 18). The representativity (%) of toxin-like transcripts is shown in Fig 3.

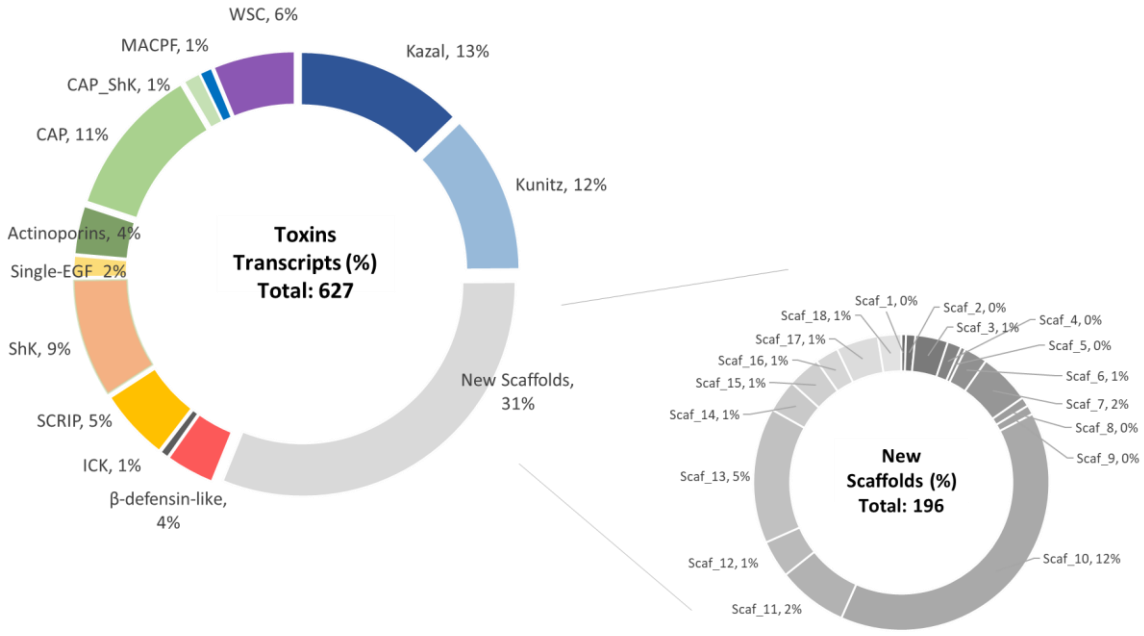

Figure 3. The arsenal of putative toxins found in *A. veratra*. Putative toxins sequences found at protein level in the venom were used as query sequences for looking for homologues into *A. veratra*'s translated transcriptome database. The Blastp hit sequences were assessed and the existence of the respective toxin domain confirmed. It was found that the transcriptome is composed by a total of 627 transcripts (unique CDSs) containing toxin-like domains characteristic of 11 known toxin families from sea anemones. Additionally, 18 new cysteine scaffolds of toxins were found. The Graph shows the putative toxin family followed by its representativity (%).

A comparison between the toxin-like transcripts found in the venom proteome *versus* transcriptome is shown in Fig 4. The graph shows that the five most abundant toxins families found between the CDSc (blue bars) correspond to serine peptidase inhibitors (Kazal and Kunitz types); CAP proteins; ShK and Scaffold 10. Following this pattern, at proteome level, serine peptidase inhibitors once more correspond to the major part of the proteome; but at this level, β-defensins and WSC -like toxins take the place of CAP and Scaffold 10, as the most abundant toxins (Fig 4. A). Fig 4B shows the families of putative toxins that exhibit the existence of repeat domains and the relative proportion of the toxin-like transcripts exhibiting single, double or more domains.

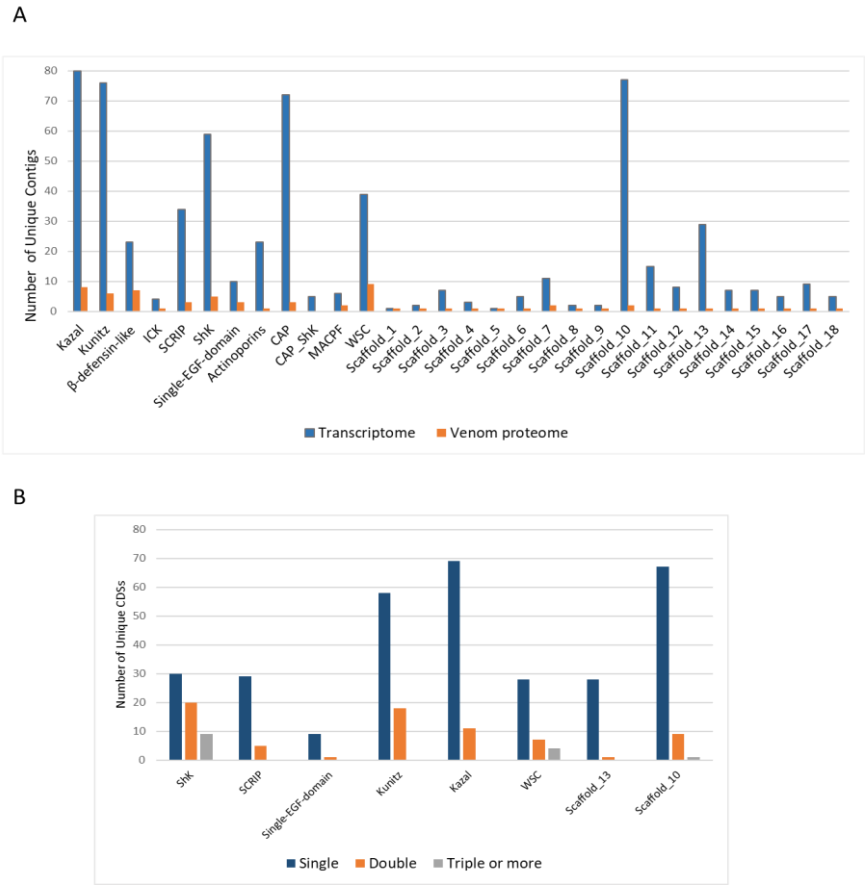

Figure 4. A- Unique CDSs found in the Transcriptome vs Venom proteome. This figure shows the diversity of unique protein/ peptides sequences found for each toxin class identified in the transcriptome (blue) and venom proteome (red) of *A. veratra*. **B-**Toxins families that present sequences exhibiting repetition of domains. This graph shows the number of unique transcripts (CDSs) exhibiting single, double, triple (or more) domains for each toxin family.

3.2.1 Putative neurotoxins

ShK-like

Aulactinia veratra's transcriptome shows the presence of 6 types of putative neurotoxins: ShK-like; SCRIPs; β-defensins-Kv3; β-defensins-Nav; Single domain EGF-like and ICKs. Between these, ShK-like putative toxins are the most abundant components exhibiting 59 homologues, corresponding to 9% of total toxin-like transcripts (Fig 3, Table 2). From ShK-like transcripts, 30 sequences possess a single domain while 20 sequences have double ShK domain; and 9 sequences have 3 or more domains (Table 2). The alignment of amino acid (aa) sequences of five ShK-like toxins identified in the proteome (blue color sequences) and their correspondent homologues are shown in Supplementary material 2.1). From the five CDSs found in the proteome, a unique transcript aul_smart_333142|CDS1 showed a triple ShK domain in its sequence. For better visualisation of the alignments, sequences presenting domain repeat were split into the number of domains found (D1 to D5). Such homologues can be identified in Supplementary material 2.1) with D1 to D5 at the end of the sequence ID (identification).

SCRIP

Taking the second place in the most frequent putative neurotoxins, transcripts holding SCRIP domain correspond to 5% of the toxin-like transcripts found (Fig 3). *A. veratra* transcriptome shows the existence of 34 homologues of this family, three of them found in the venom (blue color sequences) (Table 2; Supplementary material 2.2). Interestingly one of the SCRIP sequences found in the proteome (aul_smart_760423|CDS2), shows the existence of a double SCRIP domain. Additionally, another 4 homologues with double SCRIP domains were found in the transcriptome (Table 2). Such sequences were split in two domains (D1 and D2) for better visualisation of the alignments. These homologues can be found in Supplementary material 2.2). with CDSs with D1 or D2 at the end of ID.

β-*defensins*

Following the arsenal of putative neurotoxins, β-defensins corresponding to 4% of the toxin-like transcripts were found (Fig 3), totalizing 23 homologues, all of them with single domains (Table 2; Supplementary material 2.3). Six of these transcripts,

were found in the proteome level and are Kv3-like β-defensins (Table 1). Additionally, a unique β-defensin corresponding to a voltage-gated sodium channel inhibitor (Nav) from *A. veratra*, was found. The aa sequence alignments of the 7 β-defensins found in the proteome (sequences in blue color) and their homologues sequences are presented in the Supplementary material 2.3).

Table 2. The following table presents the number of unique CDSs found in the Venom Proteome and Transcriptome of *A. veratra.* The presence of the toxin-like domain characteristic for each structural family was confirmed by BLASTp search and MAFFT alignment of sequences. The number of CDSs that presented sequences exhibiting repetition of domains (double, triple or more) are presented below.

Structural family	Proteome confirmed by domain (n)	Transcriptome homologs (n)	Single domain (n)	Double domain (n)	Triple or more domains (n)
ShK	5	59	30	20	9
Kunitz	6	76	58	18	
Kazal	8	80	69	11	
Scaffold_10	2	77	67	9	1
WSC	9	39	28	7	4
SCRIP	3	34	29	5	
Single-EGF-like	3	10	9	1	
Scaffold_13	1	29	28	1	
B-defensin-like	7	23	23		
ICK	1	4	4		
Actinoporins	1	23	23		
CAP	3	72	72		
CAP_ShK	0	5	5		
MACPF	2	6	6		
Scaffold_1	1	1	1		
Scaffold_2	1	2	2		
Scaffold_3	1	7	7		
Scaffold_4	1	3	3		
Scaffold_5	1	1	1		
Scaffold_6	1	5	5		
Scaffold_7	2	11	11		
Scaffold_8	1	2	2		
Scaffold_9	1	2	2		
Scaffold_11	1	15	15		
Scaffold_12	1	8	8		
Scaffold_14	1	7	7		
Scaffold_15	1	7	7		
Scaffold_16	1	5	5		
Scaffold_17	1	9	9		
Scaffold_18	1	5	5		

Single domain EGF-like

Single domain EGF-like putative toxins were also found in the transcriptome, corresponding to 2% of toxin-like transcripts (Fig 3), and totalizing 10 homologues, from which 3 were found in the venom (Table 2). Exceptionally, just one of these transcripts (aul_smart_685108|CDS3) carries a double EGF-like domain. Supplementary material 2.4 shows the CDS sequence divided in two domains, identified by D1 and D2 at the end of the ID.

ICK

Putative ICKs correspond to 1% of the total toxin-like transcripts (Fig 3). Specifically, a unique ICK toxin identified corresponding to aul_smart_887805|CDS26 was found in the venom. The aa sequences alignments of the four putative ICK homologues are shown in Supplementary material 2.5.

3.2.2 Putative Inhibitors

Corresponding to a quarter of the toxin-like transcripts of *A. veratra*, serine peptidase inhibitors from Kazal and Kunitz types hold respectively 13% and 12% of total CDSs (Fig3). A total of 80 homologues corresponding to Kazal peptides, were found (Table 2, Supplementary material 2.6). About 10% of them were found in the venom (see Table 1). Although presenting Kazal-like transcripts with double domains, only Kazal inhibitors with single domain were found in the venom (sequences in blue color) (Supplementary material 2.6). Differently, Kunitz-like transcripts (n=76) presented homologues with up three domains (Supplementary material 2.7) and Kunitz inhibitors with single, double (aul_smart_859108|CDS2) or triple domains (aul_smart_955021|CDS2) were found in the venom (Table 2, Supplementary material 2.7). The 6 Kunitz inhibitors found in the venom proteome are presented at Table 1 and Supplementary material 2.7) (blue color sequences).

3.2.3 Putative non-enzymatic components

Cytolysins (Actinoporins and MACPF toxins)

Type II and type V cytolysins-like CDSs were identified in *A. veratra's* transcriptome, corresponding to 5% of the total toxin-like transcripts (Fig 3). Two sequences of cytolysins type II were found at protein level, however, only the

transcript aul_smart_512597|CDS1 showed a complete actinoporin domain, exhibiting 75% of identity with Delta-actitoxin from *Anthopleura asiatica* (Table 1). Supplementary material 2.8 shows sequences alignments of the 23 homologues of actinoporins found and the toxin found in the venom (highlighted in blue) (Table 2). All actinoporins candidates presented absence of cysteine residues in its structure. Additionally, 6 transcripts containing membrane attack complex component/perforin (MACPF), classified as cytolysins type V, were found. Two of these, aul_smart_487417|CDS2 and aul_smart_884261|CDS11, were found in the venom (Table 2). Supplementary material 2.9 presents the sequences alignments of MACPF-like transcripts found, including the ones found at protein level (blue color sequences). Due the extension of the sequences, only the central regions of the transcripts exhibiting the conserved toxin domain are highlighted.

CAP and CAP-ShK

Toxin-like transcripts belonging to CAP protein superfamily were found in *A. veratra*. The nomenclature of this superfamily stands for the three major groups: Cysteine-rich secretory proteins, Allergen-5 and Pathogenesis-related 1 proteins, from which, CRISPs are the most common in animal venoms, particularly in snake venoms, acting as L-type Ca^{2+} channel blockers or cyclic nucleotide-gated (CNG) channel-blocking toxins (TADOKORO et al., 2020; YAMAZAKI & MORITA., 2004). Corresponding to 12% of the total toxin-like transcripts evaluated (Fig 3), CAP representants found in *A. veratra* presented at least one of three possible motif signatures (CAP1, CAP3 and CAP4) in its sequences, excepting the motif CAP2 (Supplementary material 2.10). The majority of the CAP putative toxins presented all three motifs (Supplementary material 2.10). From the 72 CDSs exhibiting exclusively CAP motifs (Table 2), three transcripts (aul_smart_464302|CDS2, aul_smart_414628|CDS1, aul_smart_860615|CDS2) were found at protein level (sequences highlighted in blue) (Table 1, Supplementary material 2.10). Such proteins show the existence of HNKIR or HNAKR residues for CAP3 motif; and GENI or GENL residues for CAP4 motif. For CAP1 motif, characterized by the presence of 11 amino acids, the CDSs found at protein level show the presence of MH or RD at first two positions followed by FTQLVWKST. On the other hand, the majority of the transcripts that did not achieve protein level, exhibit GH at first two

positions, and a variation between KS, ND, KD at positions 9th and 10th for CAP1 motif.

Interestingly, five CAP putative toxins exhibiting an additional ShK domain (CX**D**XnCXnCXn**KK**XnCX**K**XCX2C) were found (Table 2, Supplementary material 2.11). These transcripts were classified as CAP-ShK putative toxins, presenting double CAP1 and CAP4 motifs followed by ShK domain. These putative toxins, classified as CAP-ShK are shown in Supplementary material 2.11. None of these transcripts were found at protein level. The presence of multidomain putative toxins containing CAP and Shk domains have been also described in the transcriptome of the sea anemone *Oulactis sp.* and in the vampire snail *Cumia reticulata* (MITCHELL et al., 2020; GERDOL et al., 2019).

WSC

Corresponding to 6% of toxin-like transcripts, toxin candidates (n= 39) presenting a carbohydrate binding domain (WSC), characterized by eight cysteines in conserved positions were found in the transcriptome (Fig3, Table 2). WSC putative toxins were also found in the venom (9 toxins); 8 of them with single WSC domain, identified as blue color sequences Supplementary material 2.12, and a unique toxin with a double WSC, identified under transcript aul_smart_186432_CDS2 (Supplementary material 2.11). Sequences that have '**NCBI'** at the end of the ID in Supplementary material 2.12, are proteins that did not have WSC domain recognised by Interpro, but presented 55 to 69% of similarity with the amino acid sequence of an uncharacterized protein LOC116305510 from *Actinia tenebrosa* (accession: XP_031571305.1/1-285), exhibiting WSC domain characterized by $CX_{31}CX_{19}CX_{15}CX_{3}CX_{26}CX_{14}CX_{2}CX_{15}C$. Differently, the remaining transcript (aul_smart_186432_CDS2), identified at protein level and having WSC domain recognised by InterPro, presented a triple motif of four cysteines $CX_{25}CX_{19}CX_{18}CX_{22}$, totalizing 12 cysteine residues. This respective sequence and its 10 homologues were split into the number of motifs identified (D1 to D4) shown in Supplementary material 2.12.

3.2.4 Enzymatic components of the Venom

Representing 9% of *A. veratra*'s venom, a total of 7 enzymes related to toxin function were found at protein level (Table 1). A serine peptidase (transcript ID: aul_smart_839293|CDS2), exhibiting 64% of identity with chymotrypsinogen A-like from *Actinia tenebrosa* was found. When submitted to InterPro, the amino acid sequence of this enzyme presented the existence of trypsin and chymotrypsin domains, being classified as a S1 peptidase, belonging to the subfamily S1A, characterized by the presence of a catalytic triad formed by histidine, aspartic acid and serine residues.

Additionally, three metallopeptidases (Table 1) exhibiting around 50% of identity with 'endothelin-converting enzyme 1-like (ECE-1-like)' from *Actinia tenebrosa* were found at protein level. The correspondent transcripts IDs of these enzymes can be visualised in Table 1. According to InterPro, the amino acid sequences of these metallopeptidases exhibit domains that classify them as components of M13 family. Beyond these components, three proteins, classified as endonucleases (Table 1) presented more than 50% of similarity to a BLASTp hit predicted by automated computational analysis (NCBI Reference Sequence: XP_031562623.1). Such hit, called uncharacterized protein LOC116298347 from *A. tenebrosa,* exhibits a predicted conserved domain corresponding to a DNA/RNA non-specific endonuclease, according to NCBI database (Table 1).

3.2.5 New cysteine scaffolds found in the venom and transcriptome of ***A. veratra***

The proteomics analysis conducted on *A. veratra* venom led to the identification of several proteins and peptides presenting 'no significant similarity' to any Blastp hit, or some level of similarity with uncharacterized proteins. The common "issue" about these sequences, classified as unknowns, is that none of them presented the existence of known domains/function related when submitted to NCBI/InterPro databases. The only exception is scaffold 10, presenting a VWF domain related to protein binding (Table 1, Table 3). These peptides were further selected for inspection about the amount of cysteine residues present in their

sequences, once that sea anemones toxins usually present rich cysteine structures. Table 3 presents the 18 new cysteine scaffolds found in 20 peptides identified in *A. veratra's* venom. Such peptides were used as query sequences for a search against the transcriptome. They present a length between 39 to 126 aa, a number of cysteine residues that can vary between of 4 and 16 and predicted m/z of 4,200 to 15,000 (see table 3). Such data corroborates with the electrophoresis presented in Fig1 and the MALDI analysis (Supplementary material 3) that shows the soluble fraction of the venom as source of low mass molecules (between 2000 to 9000 m/z). Turns out that these 18 new cysteine scaffolds correspond to 31% (n=185) of the toxin-like transcripts (Fig 3) found in *A. veratra*, representing 25% of the venom's toxins (Fig 2). The sequences alignments for each one of the new scaffolds found are shown between Supplementary material 2.13 and 2.30 figures. Sequences found in the venom are highlighted in blue.

Particularly toxins having scaffolds 1 and 5 in the proteome don't present homologues in the transcriptome. These scaffolds were found in only one CDS each. Exceptionally, between the new cysteine scaffolds, scaffold 10 and scaffold 13 presented transcript sequences with double domains. Scaffold 10 showed the existence of two toxins at protein level (Table 1), one of them presenting a double domain (aul_smart_128724|CDS3). The sequences alignments for Scaffold 10 putative toxins can be visualized in Fig 30 (single domain) and Fig 31 (double domain sequences).

Table 3. New cysteine scaffolds found in *A. veratra*'s venom. Proteins presenting 'no significant similarity' to any BLASTp hit or presenting similarity to uncharacterized proteins with absence of domains related with toxin function were categorized into 18 new cysteine scaffolds.

Structural family	Cysteine scaffold	N of Cysteines	Transcript ID	N of homologues	Mature Chain (aa)	Length	m/z
Scaf_1	X31CX21CX5CX33CX7	4	aul_smart_34342|CDS1	1	24-149	126	14532.01
Scaf_2	CX21CX5C34CX4	4	aul_smart_1012536|CDS1	2	19-130	112	12731.66
Scaf_3	X3CX8CX5CX13CX8CCX3	6	aul_smart_983271|CDS1	7	20-83	64	7255.35
Scaf_4	X10CCXCX10CCXCX3	6	aul_smart_963082|CDS3	3	23-63	41	4431.38
Scaf_5	X5CX3CX6CX12CX6CX3CX3CX6CX3CX6CX3CX5CX2CX6CX3CX3CX3	16	aul_smart_73591|CDS2	1	23-116	94	10512.24
Scaf_6	X5CX16CXCX7CX4	4	aul_smart_828408|CDS2	5	23-61	39	4295.77
Scaf_7	XnCX19CX18CCX3CX15CX3	6	aul_smart_418125|CDS1 aul_smart_188645|CDS1	11	21-106 21-102	86 82	9674.03 9089.49
Scaf_8	X7CX3CX8CX5CX6	4	aul_smart_219023|CDS3	2	19-75	57	6427.52
Scaf_9	X15CX7CX6CX10CX5CXC	6	aul_smart_955171|CDS3	2	21-70	50	5857.57
Scaf_10*	X3CX17CX3CXCX6CX3CX6CX18CXCX4CXn	10	aul_smart_954616|CDS2 aul_smart_128724|CDS3	77	25-97 25-173	73 149	8174.5 15711.03
Scaf_11	X16CX26CX10	2	aul_smart_502041|CDS2	15	31-85	55	6021.74
Scaf_12	X7CX2CX8CX5CX17CX5CX	6	aul_smart_838698|CDS3	8	31-81	51	5701.52
Scaf_13	X2CX6CX5CX3CX6CX4CX12	6	aul_smart_978781|CDS2	29	23-82	60	6834.84
Scaf_14	X19CX3X6CX3CX10CX3CX6CX21CX23	8	aul_smart_94777|CDS1	7	20-121	102	11130.14
Scaf_15	X3CX13CX3CX13CX5	4	aul_smart_798440|CDS8	7	14-60	47	5137.66
Scaf_16	X19CX10CX10CX8CX3CX2CX13CX6CX11CX10CX3CX2CX10	12	aul_smart_869134|CDS1	5	25-149	125	14373.5
Scaf_17	X4CX6CX5CX3CX6CX13CX3	6	aul_smart_92667|CDS2	9	18-84	67	7772
Scaf_18	XCX3CX5CXCX4CX6CX2	6	aul_smart_944968|CDS3	5	23-68	46	4930.25

4. DISCUSSION

In the present work, for the first time, *A. veratra's* venom was studied and accessed through proteomic and transcriptomic analysis. Such strategy was followed because the use of multiomics analysis allows not only the identification of already known toxin families, but allows the elucidation of new polipeptides and the validation of putative toxins through proteomic analysis of venoms (BABENKO et al., 2017). Here, more than 300 proteins and peptides were found in the secreted venom of *A. veratra*, however, hardly all the molecules identified execute a toxin-related function. Therefore, to overcome the challenge of knowing which components from the venom were real toxins, a classification based on blastp hit similarity and relying on domain architecture of the toxin's sequences (translated transcripts) was performed. This thorough examination over toxins sequences led to the identification of 59 proteins and peptides belonging to 14 known toxin's families and to the acknowledge of 18 new cysteine scaffolds of toxins. Besides, such sequences found at protein level were searched against the transcriptome and this revealed that more than 600 putative transcripts exhibit the same domains architectures.

Aulactinia veratra's venom is mainly composed by serine peptidase inhibitors and neurotoxins

Considering the ecological context, cnidarians have used their venoms for predation, defense and intraspecific competition (ASHWOOD et al., 2020). In the case of some sea anemones, specialized structures are directly related with these functions: Nematospheres (spherical tentacles) and acontia (long thin threads) have been associated with a defensive role against predators (ASHWOOD et al., 2020; LAM et al., 2017); while acrorhagi and catch tentacles have been used in aggressive encounters, causing necrosis in rival sea anemones and being specifically used for intraspecific competition (PURCELL, 1977; WILLIAMS, 1991).

At the molecular level, some toxins also have been associated with such functions. Potassium channel toxins with inhibitory activity over proteases, serve as both defensive and offensive substances. When injected into predators such molecules can protect other toxins from rapid degradation (defensive role), or can assume an offensive function, affecting prey through paralysis (FRAZÃO et al. 2012; HONMA et al., 2006).

Interestingly most of *A. veratra's* venom relies on serine peptidase inhibitors from kazal and kunitz types and in a diverse range of neurotoxins, including small cysteine rich peptides (SCRiP) and Inhibitor cystine knot (ICKs).

Serine peptidase inhibitors have been documented in several studies involving sea anemones. The most common is the kunitz type, found in whole body extracts; in specialized structures like tentacles and acrorhagi; mucus; or directly in the venom of these cnidarians (SCHWEITZ et al., 1995; Minagawa et al., 2008; MADIO et al., 2017). In fact, these inhibitors represent such importance to sea anemones that they correspond to one of the four most common toxins families found in these animals: the 'Venom Kunitz-type family, sea anemone type 2 potassium channel toxin subfamily' (PRENTIS et al., 2018). Such peptides are described as bifunctional molecules, being capable of inhibiting several serine peptidase representants at the same time that they can efficiently block voltage-gated potassium channels, specially Kv1.1, Kv1.2, and Kv1.6 (SCHWEITZ et al., 1995; GLADKIKH et al., 2020). Kalicludines and Kaliseptine from *Anemonia sulcate*; ShPI-1 from *Stichodactyla helianthus;* APEKTx1 from *Anthopleura elegantissima;* HCRG1 and HCRG2 from *Heteractis crispa* are few of them (SCHWEITZ et al., 1995; GARCÍA-FERNÁNDEZ et al., 2016; PEIGNEUR et al., 2011; GLADKIKH et al.,2015; GLADKIKH et al 2020).

On the other hand, Kazal inhibitors that typically show three typical disulfide bridges between C1-C5, C2-C4 e C3-C6, have not been classified as the main components of sea anemone venoms (MADIO et al., 2019). Sequences containing kazal domains have been identified in the transcriptome of *Anthopleura dowii* (RAMÍREZ-CARRETO et al., 2019); in the transcriptome and tentacle proteome of *Oulactis sp.* (MITCHELL et al., 2020); and even isolated from *Anemonia sulcata* whole body extracts, being classified as a 'Non classical' Kazal type elastase inhibitor, named as PI-Actitoxin-Adv5a at Uniprot/SwissProt. For *A. veratra*, Kazal inhibitors are amongst the main components of the venom, totalizing 8 peptides found in the proteome (HEMMI et al., 2005; KOLKENBROCK & TSCHESCHE; 1987).

A main characteristic of sea anemone venoms is that they are predominantly composed by neurotoxins (ASHWOOD et al., 2020; FRAZÃO et al., 2012). For *A. veratra* species this is a confirmed fact and neurotoxins correspond to almost a third of this sea anemone venom, comprising fundamentally 6 types: ShK-like; type Nav β-defensins; Type Kv3 β-defensins; SCRiPs, EGF-like; and ICKs.

Most part of the neurotoxins found here present domain structures similar to toxins that act as modulators of voltage-gated ion channels. For example, ShK-like toxins, exhibiting the domain CXDXnCXnCXnKKXnCXKXCX2C, are characterized by the presence of 6 cysteines; lysine (K) and aspartic acid (D) residues in conserved positions (MADIO et al., 2019). These toxins are known for being potent Kv1 blockers. The toxins BgK (*Bunodosoma granulifera*), AsKs (*Anemonia sulcata*) and ShK from *Stichodactyla helianthus* have been described as blockers of several subtypes of Kv1 channels. Such toxins present structural characteristics that seem to be directly involved in their functional role: BgK and ShK possess Lys and Tyr residues in similar positions (Lys^{22} or Lys^{25} and Tyr^{26}) and an extended strand, a loop and a helix in different locations of its structures (DAUPLAIS et al., 1997; FRAZÃO et al., 2012).

In addition, β-defensins found here exhibit similar domain architectures (C1-C5, C2-C4, C3-C6) to toxins that can modulate Kv3 and Nav channels. Most of the β-defensins from *A. veratra* presented similarity to a type III Potassium channel toxin from *Anemonia sulcata*. Kv3 channels have a critical role in the induction of fast-spiking neurons and the interruption of electrical signal in these cells can lead to

epilepsy and mental disorders (GU *et al*., 2018). Therefore, Kv3 β-defensins like BDS-I e BDS-II, have been applied in biophysics studies focused in investigating the role of Kv3 channels in central nervous system disorders (YEUNG *et al*., 2005).

Furthermore, the unique β-defensin corresponding to a Nav inhibitor and the ICK toxin from *A. veratra* found, represent interesting molecules that potentially could modulate Voltage-gated sodium channels (Nav). The cysteine pattern of ICKs, with classical signature CXnCXnCCXnCXnC, exhibit three disulfide bridges and form a special knot, making these peptides highly stable molecules, resistant to enzymatic degradation and high temperatures. Typical ICKs from spiders exhibiting C1–C4, C2–C5, and C3–C6, are broadly known as potent Nav channel modulators (MADIO et al., 2019; CARDOSO et al; 2019; POSTIC et al., 2018). On the other hand, the β-defensin-Nav found here (aul_smart_802345|CDS9) was identified for the first time at protein level corresponding to Delta-actitoxin-Ave sodium channel inhibitory toxin from *Aulactinia veratra* deposited in NCBI database.

Toxins found exclusively in the precipitate fraction of the venom

Interestingly proteins from three toxin families – metallopeptidase, actinoporins and MACPF – were exclusively found in the precipitate fraction of *A. veratra*'s venom.

Metallopeptidases are not between the main structural families of sea anemone venoms (MADIO et al., 2019), but some studies have shown the presence of putative toxins belonging to the families M12, M13, M14, M15 or M16 in the transcriptomes of the sea anemones *Oulactis* sp (MITCHELL et al., 2020); *Stichodactyla haddoni* and *Anthopleura dowii* (MADIO et al., 2017; RAMÍREZ-CARRETO et al., 2019). For *Telmatactis stephensoni and Anthopleura dowii,* the Peptidase M12A family was found in the secreted venom or in venom-related structures by proteomic analysis (ASHWOOD et al., 2021; RAMÍREZ-CARRETO et al., 2019). For *A. veratra*, the metallopeptidase sequences found at protein level showed similarity to 'endothelin-converting enzyme 1-like (ECE-1-like)' from *Actinia tenebrosa*, and domains corresponding to M13 family were found. Metallopeptidases from this family have a predicted active site formed by HEXXH

motif, in which histidine (H) residues bind zinc; and the glutamic acid (E) has catalytic function (RAWLINGS & BARRETT, 2004). As members of this family may have some residues attached to the transmembrane region, the sequences found here might have a housekeeping function instead of a toxin role. The function of these metallopeptidases should be investigated posterior studies.

Additionally, all pore forming toxins from *A. veratra* were exclusively found in the precipitate fraction of the venom. Actinoporins, which constitute a major toxin family in sea anemones, have molecular masses around 20 kDa and present high affinity for sphingomyelin (PRENTIS et al., 2018; MADIO et al., 2019; VALLE et al., 2015). These cytolysins type II can cause pores on the surface of target-cells, compromising the integrity of cellular membranes and leading to ionic imbalance. Due to such properties, these toxins have been used in immunocomplexes and applied against parasites and tumour cells (RAMÍREZ-CARRETO et al., 2019; TEJUCA; ANDERLUH; DALLA SERRA, 2009). On the other hand, MACPF-cytolysins found in *A. veratra* are less common toxins. Classified as type V cytolysins, these toxins are characterized by the presence of an EGF and MACPF domains and have molecular masses around 60 kDa. So far, only three cytolysins from this type have been described in literature: AvTx-60A from *Actineria villosa*, PsTx-60A and PsTx-60B from *Phyllodiscus semoni* (OSHIRO et al., 2004; SATOH et al., 2007). Here it has been revealed that the venom of *A. veratra* presents two novel cytolysin type V, containing the membrane-attack complex/perforin (MACPF) domain, at protein level (Table 1).

Putative toxins found in the venom

For *A. veratra*, not all transcripts found for each putative toxin family was found in the venom. For some toxins families, like kazal and kunitz inhibitors, only 10% of the transcripts were found in the venom. This is expected, once that not all putative inhibitors represent potential toxins and instead might play a housekeeping function. However, for toxins families that have a clear role in envenomation, this scenario changed, and the proportion between putative toxins and real toxins identified became closer.

For some neurotoxins families from *A. veratra*, for example, almost 30% of the available transcripts end up as peptides in the venom. These are the cases of β-defensins; Single EGF-like and ICK toxins. For cytolysins (MACPF) this number increased to 33%. Differently, for ShK and SCRIP putative toxins, only 8% of the transcripts were available at the venom.

It is known that venomous animals can change their toxin profile in response to environmental stimuli (ASHWOOD et al., 2020). Toxin expression is variable and this might be directly related to dietary shifts, geographical location; stages of development; localization in specialized tissues; and sexes (Surm & Moran; 2021; CIPRIANI et al., 2017; SALDARRIAGA et al., 2003).

For sea anemones, changes in toxin expression can vary according to the stage of development or tissue specialization (ASHWOOD et al; 2020; COLUMBUS-SHENKAR et al., 2018). These animals, like other cnidarians, pass through a complex life cycle, interacting differently with prey and predators at different stages of life – egg, swimming planulae or adult polyp (COLUMBUS-SHENKAR et al., 2018). For *Nematostella verctensis*, a studied model sea anemone, it was seen that the venom changes according to maturation of the organism. At egg stage, these anemones express only defensive toxins and at the very early stage of larvae, these animals are already capable of killing preys larger than themselves. Therefore, along with morphological changes, biochemical shifts are made and the toxin arsenal of these sea anemones is updated (COLUMBUS-SHENKAR et al., 2018; SURM & MORAN, 2021).

The variations between toxin expression at the transcriptional level and protein level observed in this study, have also been reported previously for the sea anemones *Stichodactyla haddoni* and *Oulactis sp*. (MADIO et al., 2017; MITCHELL et al., 2020). In the current study, the adult individuals from *A. veratra* species used for the extraction of the venom were different from the ones used for building the transcriptome database. This, for sure, is a factor to be considered in the differences between putative toxins expressed and toxins found in the venom. Another factor that should be taken in consideration is that the venom collected by electro stimulation is from individuals kept at controlled conditions in the laboratory. Therefore, the toxin profile of this species might change according to the environment or stage of life.

Secreted Cysteine-Rich REpeat Peptides (SCREPS) *found in A. veratra venom*

The repetition of residues or domains within proteins is a relatively common event in nature, considered an evolutive strategy through the use of intragenic duplication or recombination. Between the advantages of repetition is the improved binding capacity of a protein and the consequent expansion of its cellular functions. As a selective advantage can be offered to the organism, the repetition might remain conserved in a population (ANDRADE; PEREZ-IRATXETA; PONTING, 2001).

The tandem repeat domains have been described in peptide toxins isolated from animal venoms (BOHLEN et al., 2010; VASSILEVSKI et al., 2010; CHASSAGNON et al., 2017). Recently categorised as SCREPs 'Secreted Cysteine-Rich REpeat Peptides' by Maxwell et al. 2018, such toxins present an uncommon structural arrangement that can lead to a unique pharmacological response. Particularly, the majority of SCREPs execute a bivalent interaction and have as main targets ion channels and serine peptidases (MAXWELL et al., 2018).

Along with the data analysis of the putative toxins sequences from *A. veratra*, it was noticed that SCREPs are present in 6 toxins families and in 2 types of new cysteine scaffolds (Scaf10 and Scaf13). The occurrence of such sequences with double, triple or more domains for the same toxin, was found in ShK, SCRiP, EGF-like, Kunitz and Kazal families, coincidentally the same toxin groups – neurotoxins and serine peptidase inhibitors – abundant in the venom proteome. The most interesting part of this is that these putative toxins are not a frustrated attempt of nature towards enhancing its venom; these molecules are actually found at protein level by MS/MS and they are translated as double or triple repeat domain toxins. At table 1 is possible to notice the peptides identified in each one of the domains of SCREPs found, including peptides that represent a link between D1 and D2. Examples of such repeat domain toxins found at protein level are: aul_smart_333142|CDS1 (ShK-like); aul_smart_760423|CDS2 (SCRip); aul_smart_859108|CDS2 (Kunitz), aul_smart_955021|CDS2 (Kunitz -triple domain), aul_smart_886056|CDS2 (Kunitz); aul_smart_685108|CDS3 (EGF-like) and aul_smart_128724|CDS3 (Scaffold 10).

New cysteine scaffolds discovered in the venom of A. veratra

A relatively recent work, published by MADIO et al., 2017, revealed that a well-studied sea anemone, *Stichodactyla haddoni*, had several new domain toxins discovered when its venom was revisited and looked under the light of transcriptomics and proteomics association. To be more precise, 12 new cysteine scaffolds of toxins were found in this specific venom (MADIO et al., 2017). This is just one of few studies that have shown the emerging new toxins present in cnidarian venoms (CASSOLI et al., 2013; BABENKO et al., 2017).

In the present study, the elucidation of such variety of new toxins was possible due to the availability of the transcriptome database and MS/MS data. This approach allowed the identification of 18 new cysteine scaffolds of toxins not described before. These new toxins families correspond not only to a quarter of all toxins found in the venom, but also represent 30% of all putative-toxins found. The most striking observation from this is that a considerable part of these toxins presented sequence similarity to uncharacterized proteins from sea anemones taxid database, or no significant similarity at all with any previously described protein or peptide. The same happened for SCRIP and ICK toxins found in this study. This, of course, highlights the fact that some new toxins may pass unnoticed in analysis that consider only similarity as a main factor for classifying new molecules as toxins.

5. CONCLUSIONS

The association of omics technologies used here allowed a holistic view over the venom of *Aulactinia veratra*, possibiliting the identification of 14 toxin families of sea anemones and revealing the existence of 18 new scaffolds of toxins, validated by proteomic level confirmation.

A. veratra's venom possess an interesting diversity of molecules, relying mainly on neurotoxins and serine peptidase inhibitors. This is clearly shown by the diversity of toxins that exhibit domains characteristic of ion channels modulators like ShK, β-defensins (Kv3 and Nav types); ICK; SCRiPs; EGF-like toxins; beyond kazal and kunitz type inhibitors. Some of the toxin's families (metallopeptidases and

cytolysins type II and V) were exclusively found in the precipitated fraction of the venom.

The transcriptome data shows that a series of homologues are found for each type of toxin family, but not all of them were in the venom. The most abundant homologues were specially found for ShK, Kazal, Kunitz, CAP and Scaffold 10 families. The analysis of *A. veratra* toxin-like transcripts shows that the toxin families ShK-like, SCRIP, EGF-like, Kunitz, Kazal, Scaffold 10, Scaffold 13 present repetition of domains. Such toxins, found at protein level and classified as SCREPs are translated as double or even triple domain repeats. The SCREPs toxins offer an interesting possibility for pharmacological properties investigation; specially ShK, SCRiP, EGF-like and Kunitz, as they might have a higher binding capacity to enzymes or voltage gated ion channels.

REFERENCES

JOUIAEI M., YANAGIHARA A. A., MADIO B, NEVALAINEN T.J., ALEWOOD P.F. E FRY B.G. Ancient Venom Systems: A Review on Cnidaria Toxins. **Toxins**, v.7, p. 2251-2271, 2015

VAN ITEN, H.; LEME, J.M.; PACHECO, M.L.A.F.; SIMÕES, M.G.; FAIRCHILD, T.R.; RODRIGUES, F.; GALANTE, D.; BOGGIANI, P.C.; MARQUES, A.C. Origin and Early Diversification of Phylum Cnidaria: Key Macrofossils from the Ediacaran System of North and South America. In The Cnidaria, Past, Present and Future; Springer: Berlin/Heidelberg, Germany, 2016; pp. 31–40.

ZHANG, Z. Animal biodiversity: An introduction to higher-level classification and taxonomic richness. **Zootaxa**, v. 3148, p.7–12, 2011

BECKMANN, A.; ÖZBEK, S. The Nematocyst: A molecular map of the Cnidarian stinging organelle. Int. J. Dev. Biol. 2012, 56,577–582.

MADIO B, KING GF, UNDHEIM EAB. Sea Anemone Toxins: A Structural Overview. **Mar Drugs**. V.17(6):325, p.1-26, 2019.

THE UNIPROT CONSORTIUM, UniProt: The universal protein knowledgebase in 2021. Nucleic Acids Res. 2021, 49, D480–D489. https://www.uniprot.org/biocuration_project/Toxins/statistics

JUNGO, F.; BAIROCH, A. Tox-Prot, the toxin protein annotation program of the Swiss-Prot protein knowledgebase. **Toxicon**, v.45, p. 293–301, 2005.

COELHO GR, DA SILVA DL, BERALDO-NETO E, VIGERELLI H, DE OLIVEIRA LA, SCIANI JM, PIMENTA DC. Neglected Venomous Animals and Toxins:

Underrated Biotechnological Tools in Drug Development. Toxins (Basel). 2021 Nov 29;13(12):851. doi: 10.3390/toxins13120851. PMID: 34941689; PMCID: PMC8708286.

PRENTIS P.J., PAVASOVIC A., NORTON R.S. Sea Anemones: Quiet Achievers in the Field of Peptide Toxins. **Toxins** (Basel), v.10, p.1-15, 2018.

CHEN X, LEAHY D, VAN HAEFTEN J, HARTFIELD P, PRENTIS PJ, VAN DER BURG CA, SURM JM, PAVASOVIC A, MADIO B, HAMILTON BR, KING GF, UNDHEIM EAB, BRATTSAND M, HARRIS JM. A Versatile and Robust Serine Protease Inhibitor Scaffold from Actinia tenebrosa. **Mar Drugs.** 2019.

ASHWOOD LM, NORTON RS, UNDHEIM EAB, HURWOOD DA, PRENTIS PJ. Characterising Functional Venom Profiles of Anthozoans and Medusozoans within Their Ecological Context. Mar Drugs. 2020 Apr 9;18(4):202.

COLUMBUS-SHENKAR YY, SACHKOVA MY, MACRANDER J, FRIDRICH A, MODEPALLI V, REITZEL AM, SUNAGAR K, MORAN Y. Dynamics of venom composition across a complex life cycle. Elife. 2018 Feb 9;7:e35014.

ASHWOOD LM, UNDHEIM EAB, MADIO B, HAMILTON BR, DALY M, HURWOOD DA, KING GF, PRENTIS PJ. Venoms for all occasions: The functional toxin profiles of different anatomical regions in sea anemones are related to their ecological function. **Mol Ecol.** 2021 Nov 27.

MACRANDER J, BROE M, DALY M. Tissue-Specific Venom Composition and Differential Gene Expression in Sea Anemones. **Genome Biol Evol.** v. 25;8(8):2358-2375, 2016.

MADIO B., KING G.F., UNDHEIM E.A.B. Revisiting venom of the sea anemone *Stichodactyla haddoni*: Omics techniques reveal the complete toxin arsenal of a well-studied sea anemone genus. Journal of Proteomics 166 (2017) 83–92.

OLIVEIRA, J.S.; FUENTES-SILVA, D.; KING, G.F. Development of a rational nomenclature for naming peptide and protein toxins from sea anemones. **Toxicon** 2012, 60, 539–550.

KOZLOV S, GRISHIN E. Convenient nomenclature of cysteine-rich polypeptide toxins from sea anemones. **Peptides.** 2012 Feb;33(2):240-4.

VON REUMONT, B.M. Studying Smaller and Neglected Organisms in Modern Evolutionary Venomics Implementing RNASeq (Transcriptomics)—A Critical Guide. **Toxins** 2018, *10*, 292.

BAER B, Millar AH. Proteomics in evolutionary ecology. J Proteomics. 2016 Mar 1;135:4-11.

SUNAGAR K, MORGENSTERN D, REITZEL AM, MORAN Y. Ecological venomics: How genomics, transcriptomics and proteomics can shed new light on the ecology and evolution of venom. **J Proteomics**. 2016 Mar 1;135:62-72.

HANEY RA, AYOUB NA, CLARKE TH, HAYASHI CY, GARB JE. Dramatic expansion of the black widow toxin arsenal uncovered by multi-tissue transcriptomics and venom proteomics. BMC **Genomics.** 2014 Jun 11;15(1):366.

ROKYTA DR, WARD MJ. Venom-gland transcriptomics and venom proteomics of the black-back scorpion (Hadrurus spadix) reveal detectability challenges and an unexplored realm of animal toxin diversity. **Toxicon.** 2017 Mar 15;128:23-37

DE OLIVEIRA UC, NISHIYAMA MY JR, DOS SANTOS MBV, SANTOS-DA-SILVA AP, CHALKIDIS HM, SOUZA-IMBERG A, CANDIDO DM, YAMANOUYE N, DORCE VAC, JUNQUEIRA-DE-AZEVEDO ILM. Proteomic endorsed transcriptomic profiles of venom glands from Tityus obscurus and T. serrulatus scorpions. PLoS One. 2018 Mar 21;13(3):e0193739.

CID-URIBE, J.I.; MENESES, E.P.; BATISTA, C.V.F.; ORTIZ, E.; POSSANI, L.D. Dissecting Toxicity: The Venom Gland Transcriptome and the Venom Proteome of the Highly Venomous Scorpion *Centruroides limpidus* (Karsch, 1879). *Toxins* **2019**, *11*, 247.

CAMPOS, P.F; ANDRADE-SILVA D., ZELANIS A., LEME A.F.P, ROCHA M.M. T., MENEZES, M.C., , SERRANO S.M.T., JUNQUEIRA-DE-AZEVEDO I.L.M., Trends in the Evolution of Snake Toxins Underscored by an Integrative Omics Approach to Profile the Venom of the Colubrid Phalotris mertensi, Genome Biology and Evolution, Volume 8, Issue 8, August 2016, Pages 2266–2287.

PONCE D, BRINKMAN DL, POTRIQUET J, MULVENNA J. Tentacle Transcriptome and Venom Proteome of the Pacific Sea Nettle, Chrysaora fuscescens (Cnidaria: Scyphozoa). Toxins (Basel). 2016 Apr 5;8(4):102.

LI R, YU H, YUE Y, LIU S, XING R, CHEN X, LI P. Combined proteomics and transcriptomics identifies sting-related toxins of jellyfish Cyanea nozakii**. J Proteomics**. 2016 Oct 4;148:57-64.

WANG C, WANG B, WANG B, WANG Q, LIU G, WANG T, HE Q, ZHANG L. Unique Diversity of Sting-Related Toxins Based on Transcriptomic and Proteomic Analysis of the Jellyfish Cyanea capillata and Nemopilema nomurai (Cnidaria: Scyphozoa). **J Proteome** Res. 2019 Jan 4;18(1):436-448.

BRINKMAN DL, JIA X, POTRIQUET J, KUMAR D, DASH D, KVASKOFF D, MULVENNA J. Transcriptome and venom proteome of the box jellyfish Chironex fleckeri**. BMC Genomics**. 2015 May 27;16(1):407.

LIAO Q, GONG G, POON TCW, ANG IL, LEI KMK, SIU SWI, WONG CTT, RÁDIS-BAPTISTA G, LEE SM. Combined transcriptomic and proteomic analysis reveals a diversity of venom-related and toxin-like peptides expressed in the mat anemone

Zoanthus natalensis (Cnidaria, Hexacorallia). **Arch Toxicol.** 2019 Jun;93(6):1745-1767.

CASSOLI JS, VERANO-BRAGA T, OLIVEIRA JS, MONTANDON GG, COLOGNA CT, PEIGNEUR S, PIMENTA AM, KJELDSEN F, ROEPSTORFF P, TYTGAT J, DE LIMA ME. The proteomic profile of Stichodactyla duerdeni secretion reveals the presence of a novel O-linked glycopeptide. J Proteomics. 2013 Jul 11;87:89-102.

BABENKO, V.V., MIKOV, A.N., MANUVERA, V.A. *et al.* Identification of unusual peptides with new Cys frameworks in the venom of the cold-water sea anemone *Cnidopus japonicus* . *Sci Rep* **7,** 14534 (2017).

RAMÍREZ-CARRETO S, VERA-ESTRELLA R, PORTILLO-BOBADILLA T, LICEA-NAVARRO A, BERNALDEZ-SARABIA J, RUDIÑO-PIÑERA E, et al. Transcriptomic and Proteomic Analysis of the Tentacles and Mucus of Anthopleura dowii Verrill, 1869. **Marine Drugs**. 2019; 17: 436.

MITCHELL ML, TONKIN-HILL GQ, MORALES RAV, PURCELL AW, PAPENFUSS AT, NORTON RS. Tentacle Transcriptomes of the Speckled Anemone (Actiniaria: Actiniidae: Oulactis sp.): Venom-Related Components and Their Domain Structure. Mar Biotechnol (NY). 2020 Apr;22(2):207-219.

LAEMMLI U. K. Cleavege of structural proteins during the assembly of the head of bacteriophage T4. **Nature**, v. 227, p.680-685, 1970.

MITCHELL A.L, ATTWOOD T.K.,BABBITT P.C. et al.InterPro in 2019: improving coverage, classification and access to protein sequence annotations. Nucleic Acids Research, Jan 2019. InterPro- classification of protein families - https://www.ebi.ac.uk/interpro/

AFGAN E., BAKER D., BATUT B., VAN DEN BEEK M., BOUVIER D, ČECH M.,et al. The Galaxy platform for accessible, reproducible and collaborative biomedical analyses: 2018 update, **Nucleic Acids Research**, v. 46, Issue W1, W537–W544, 2018.

WATERHOUSE, A.M., PROCTER, J.B., MARTIN, D.M.A, CLAMP, M. AND BARTON, G. J. (2009) "Jalview Version 2 - a multiple sequence alignment editor and analysis workbench" **Bioinformatics** 25 (9) 1189-1191 doi: 10.1093/bioinformatics/btp033

MADIO B, UNDHEIM EAB, KING GF. Revisiting venom of the sea anemone Stichodactyla haddoni: Omics techniques reveal the complete toxin arsenal of a well-studied sea anemone genus. **J Proteomics.** 2017 Aug 23;166:83-92.

YAMAZAKI Y, MORITA T. Structure and function of snake venom cysteine-rich secretory proteins. **Toxicon**. 2004 Sep 1;44(3):227-31.

TADOKORO T, MODAHL CM, MAENAKA K, AOKI-SHIOI N. Cysteine-Rich Secretory Proteins (CRISPs) From Venomous Snakes: An Overview of the

Functional Diversity in A Large and Underappreciated Superfamily. **Toxins** (Basel). 2020 Mar 12;12(3):175.

GERDOL M, CERVELLI M, MARIOTTINI P, OLIVERIO M, DUTERTRE S, MODICA MV. A Recurrent Motif: Diversity and Evolution of ShKT Domain Containing Proteins in the Vampire Snail Cumia reticulata. Toxins (Basel). 2019 Feb 12;11(2):106.

LAM, J.; CHENG, Y.W.; CHEN, W.U.; LI, H.H.; CHEN, C.S.; PENG, S.E. A detailed observation of the ejection and retraction of defense tissue acontia in sea anemone (Exaiptasia pallida). **PeerJ** 2017, 5, 1–11.

PURCELL, J.E. Aggresive function and induced development of catch tentacles in the sea anemone Metridium senile (Coelenterata, Actiniaria). **Biol. Bull.** 1977, 153, 355–368.

WILLIAMS, R.B. Acrorhagi, catch tentacles and sweeper tentacles: a synopsis of aggression of actiniarian and scleractinian cnidaria. **Hydrobiologia** 1991, 216, 539–545.

FRAZÃO, B.; VASCONCELOS, V.; ANTUNES, A. Sea anemone (Cnidaria, Anthozoa, Actiniaria) toxins: na overview. **.Mar. Drugs** 2012, 10, 1812–1851.

HONMA, T.; SHIOMI, K. Peptide toxins in sea anemones: Structural and functional aspects. **Mar. Biotechnol**. 2006, 8, 1–10.

SCHWEITZ, H.; BRUHN, T.; GUILLEMARE, E.; MOINIER, D.; LANCELIN, J.-M.M.; BÉRESS, L.; LAZDUNSKI, M.; BERESS, L.;LAZDUNSKI, M.; BÉRESS, L.; et al. Kalicludines and Kaliseptine: Two different classes of sea anemone toxins for voltage sensitive K+ cannels**. J. Biol. Chem.** 1995, 270, 25121–25126.

MINAGAWA S, SUGIYAMA M, ISHIDA M, NAGASHIMA Y, SHIOMI K. Kunitz-type protease inhibitors from acrorhagi of three species of sea anemones. **Comp Biochem Physiol B Biochem Mol Biol**. 2008 Jun;150(2):240-5.

GLADKIKH I, MONASTYRNAYA M, ZELEPUGA E, SINTSOVA O, TABAKMAKHER V, GNEDENKO O, IVANOV A, HUA KF, KOZLOVSKAYA E. New Kunitz-Type HCRG Polypeptides from the Sea Anemone Heteractis crispa. **Mar Drugs**.v.13(10), p. 6038-6063, 2015.

GLADKIKH I, PEIGNEUR S, SINTSOVA O, LOPES PINHEIRO-JUNIOR E, KLIMOVICH A, MENSHOV A, KALINOVSKY A, ISAEVA M, MONASTYRNAYA M, KOZLOVSKAYA E, TYTGAT J, LEYCHENKO E. Kunitz-Type Peptides from the Sea Anemone Heteractis crispa Demonstrate Potassium Channel Blocking and Anti-Inflammatory Activities. **Biomedicines**.v.8(11):473, 2020.

GARCÍA-FERNÁNDEZ R, PEIGNEUR S, PONS T, ALVAREZ C, GONZÁLEZ L, CHÁVEZ MA, TYTGAT J. The Kunitz-Type Protein ShPI-1 Inhibits Serine Proteases and Voltage-Gated Potassium Channels. **Toxins (Basel**). V. 8(4):110, 2016.

PEIGNEUR S, BILLEN B, DERUA R, WAELKENS E, DEBAVEYE S, BÉRESS L, TYTGAT J. A bifunctional sea anemone peptide with Kunitz type protease and potassium channel inhibiting properties. **Biochem Pharmacol.** 2011 Jul 1;82(1):81-90.

HEMMI H, KUMAZAKI T, YOSHIZAWA-KUMAGAYE K, NISHIUCHI Y, YOSHIDA T, OHKUBO T, KOBAYASHI Y. Structural and functional study of an Anemonia elastase inhibitor, a "nonclassical" Kazal-type inhibitor from Anemonia sulcata. **Biochemistry.** 2005 Jul 19;44(28):9626-36.

KOLKENBROCK, H. & TSCHESCHE, H. (1987) Biol Chem. Hoppe-Seyler 368, 93-99. 25 13 Hirs, C.H.W. (1956)/. **Biol. Chem.** 247,611.

DAUPLAIS M., LECOQ A., SONG J. et al. On the Convergent Evolution of Animal Toxins. Conservation of a diad of functional residues in potassium channel-blocking toxins with unrelated structures*. The Journal of Biological Chemistry, v. 272, p. 4302-4309.

GU Y, SERVELLO D, HAN Z, LALCHANDANI RR, DING JB, HUANG K, GU C. Balanced Activity between Kv3 and Nav Channels Determines Fast-Spiking in Mammalian Central Neurons. iScience. 2018 Nov 30;9:120-137.

YEUNG SY, THOMPSON D, WANG Z, FEDIDA D, ROBERTSON B. Modulation of Kv3 subfamily potassium currents by the sea anemone toxin BDS: significance for CNS and biophysical studies. J Neurosci. 2005 Sep 21;25(38):8735-45.

CARDOSO FC, LEWIS RJ. Structure-Function and Therapeutic Potential of Spider Venom-Derived Cysteine Knot Peptides Targeting Sodium Channels. **Front Pharmacol**. 2019 Apr 11;10:366.

POSTIC G., GRACY J, PÉRIN LAURENT CHICHE L., GELLY J.C. KNOTTIN: the database of inhibitor cystine knot scaffold after 10 years, toward a systematic structure modelling. Nucleic **Acids Research**, v. 46, 2018.

RAWLINGS, N. D.; TOLLE, D. P.; BARRETT, A. J. Evolutionary families of peptidase inhibitors. **Biochemical Journal**, v. 378, n. 3, p. 705–716, 1995.

TEJUCA, M.; ANDERLUH, G.; DALLA SERRA, M. Sea anemone cytolysins as toxic components of immunotoxins. **Toxicon**, v. 54, n. 8, p. 1206–1214, 2009.

OSHIRO N, KOBAYASHI C, IWANAGA S, NOZAKI M, NAMIKOSHI M, SPRING J, NAGAI H. A new membrane-attack complex/perforin (MACPF) domain lethal toxin from the nematocyst venom of the Okinawan sea anemone Actineria villosa. **Toxicon.** 2004 Feb;43(2):225-8

SATOH H, OSHIRO N, IWANAGA S, NAMIKOSHI M, NAGAI H. Characterization of PsTX-60B, a new membrane-attack complex/perforin (MACPF) family toxin, from the venomous sea anemone Phyllodiscus semoni. **Toxicon**. 2007 Jun 15;49(8):1208-10

SURM JM, MORAN Y. Insights into how development and life-history dynamics shape the evolution of venom. **Evodevo**. 2021 Jan 7;12(1):1.

CIPRIANI V, DEBONO J, GOLDENBERG J, JACKSON TNW, ARBUCKLE K, DOBSON J,Et al. Correlation between ontogenetic dietary shifts and venom variation in Australian brown snakes (Pseudonaja). **Comp Biochem Physiol C: Toxicol Pharmacol.** 2017;197:53–60.

SALDARRIAGA MM, OTERO R, NÚNEZ V, TORO MF, DÍAZ A, GUTIÉRREZ JM. Ontogenetic variability of Bothrops atrox and Bothrops asper snake venoms from Colombia. **Toxicon.** 2003;42:405–11.

ANDRADE, M. A.; PEREZ-IRATXETA, C.; PONTING, C. P. Protein repeats: Structures, functions, and evolution. Journal of Structural Biology, v. 134, n. 2–3, p. 117–131, 2001.

BOHLEN, C. J., PRIEL, A., ZHOU, S., KING, D., SIEMENS, J., AND JULIUS, D. A bivalent tarantula toxin activates the capsaicin receptor, TRPV1, bytargeting the outer pore domain. Cell v. 141, p. 834–845, 2010.

VASSILEVSKI, A. A., FEDOROVA, I. M., MALEEVA, E. E., KOROLKOVA, Y. V., EFIMOVA, S. S., SAMSONOVA, O. V., et al. (2010). Novel class of spider toxin: active principle from the yellow sac spider Cheiracanthium punctorium venom is a unique twodomain polypeptide. **J. Biol. Chem.** 285, 32293–32302.

CHASSAGNON, I. R., MCCARTHY, C. A., CHIN, Y. K., PINEDA, S. S., KERAMIDAS, A., MOBLI, M., et al. (2017). Potent neuroprotection after stroke afforded by a double-knot spider-venom peptide that inhibits acid-sensing ion channel 1a. **Proc. Natl. Acad. Sci**. U.S.A. 114, 3750–3755.

MAXWELL, M.; UNDHEIM, E. A. B.; MOBLI, M. Secreted cysteine-rich repeat proteins “SCREPs”: A novel multi-domain architecture. **Frontiers in Pharmacology**, v. 9, n. NOV, p. 1–16, 2018.

Supplementary Material 1

Supplementary material 1. General Venom proteome from *A. veratra*. The following table shows the classification of toxins based on the presence of conserved domains according to Blastp hit from ‘Sea anemone Taxid (6103)’ from NCBI database.

Superfamily based on Conserved Domains (NCBI/InterPr	Transcript	BLAST hit (Name/Species)	E_value	Per_Ident	Accession	Mol_Functi
Adenylate_cyclase_associated	aul_smart_61445|CDS2	adenylyl cyclase-associated protein 1-like isoform X1 [Actinia tenebrosa]	2E-98	80.81%	XP_031559161.1	Binding
Adenylate_cyclase_associated	aul_smart_724959|CDS2	adenylyl cyclase-associated protein 1-like [Actinia tenebrosa]	1.00E-33	75.68%	XP_031555439.1	Binding
Annexin	aul_smart_880196|CDS9	annexin A7-like [Actinia tenebrosa]	0	87.13%	XP_031574768.1	Binding
CLECT_C-type_lectin_C-type_lectin-like-CTLD	aul_smart_69509|CDS2	C-type mannose receptor 2-like [Actinia tenebrosa]	1.00E-65	44.22%	XP_031563187.1	Binding
CLECT_C-type_lectin_C-type_lectin-like-CTLD	aul_smart_130501|CDS2	perlucin-like protein [Actinia tenebrosa]	4.00E-79	65.84%	XP_031571012.1	Binding
CLECT_C-type_lectin_C-type_lectin-like-CTLD	aul_smart_895619|CDS1	C-type mannose receptor 2-like [Actinia tenebrosa]	2.00E-37	50.38%	XP_031563187.1	Binding
C-type_lectin	aul_smart_864663|CDS2	perlucin-like protein [Actinia tenebrosa]	2.00E-55	61.76%	XP_031561983.1	Binding
C-type_lectin	aul_smart_864761|CDS2	perlucin-like protein [Actinia tenebrosa]	2.00E-55	61.76%	XP_031561983.1	Binding
C-type_lectin	aul_smart_498792|CDS2	perlucin-like protein [Actinia tenebrosa]	2.00E-50	58.02%	XP_031561983.1	Binding
C-type_lectin	aul_smart_1006387|CDS1	perlucin-like protein [Actinia tenebrosa]	2.00E-36	58.33%	XP_031561983.1	Binding
Efh	aul_smart_904722|CDS2	CnidEF [Anthopleura artemisia]	4.00E-22	46.15%	ABD16203.1	Binding
EF-hand	aul_smart_93641|CDS1	EF-hand calcium-binding domain-containing protein 1-like [Actinia tenebrosa]	2.00E-57	65.19%	XP_031572947.1	Binding
Ezrin_radixin_moesin_superfamily	aul_smart_983651|CDS5	radixin-like [Actinia tenebrosa]	0	74.29%	XP_031554104.1	Binding
FA58C	aul_smart_463795|CDS1	uncharacterized protein LOC116291022 [Actinia tenebrosa]	1.00E-62	62.05%	XP_031554005.1	Binding
Folate_receptor	aul_smart_936223|CDS1	riboflavin-binding protein-like [Actinia tenebrosa]	2.00E-82	56.31%	XP_031575470.1	Binding
Folate_receptor	aul_smart_1074279|CDS1	riboflavin-binding protein-like [Actinia tenebrosa]	5.00E-83	55.83%	XP_031575470.1	Binding
Folate_receptor	aul_smart_255309|CDS1	riboflavin-binding protein-like [Actinia tenebrosa]	5.00E-78	53.57%	XP_031575470.1	Binding
Folate_receptor	aul_smart_775591|CDS1	riboflavin-binding protein-like [Actinia tenebrosa]	2.00E-65	64.58%	XP_031563985.1	Binding
Folate_receptor	aul_smart_936226|CDS1	riboflavin-binding protein-like [Actinia tenebrosa]	6.00E-77	52.91%	XP_031575470.1	Binding
Folate_receptor	aul_smart_832688|CDS2	riboflavin-binding protein-like [Actinia tenebrosa]	6.00E-83	54.07%	XP_031575470.1	Binding
Folate_receptor	aul_smart_135906|CDS2	riboflavin-binding protein-like [Actinia tenebrosa]	2.00E-82	56.52%	XP_031575470.1	Binding
Gal_Lectin	aul_smart_381427|CDS2	collectin-46 [Exaiptasia pallida]	2E-137	88.10%	XP_020912057.1	Binding
Gal_Lectin	aul_smart_344603|CDS1	complement C1q subcomponent subunit B-like isoform X1 [Actinia tenebrosa]	0	96.58%	XP_031564242.1	Binding
Ig_superfamily	aul_smart_956418|CDS3	fasciclin-2-like isoform X1 [Actinia tenebrosa]	0	61.48%	XP_031567368.1	Binding
Ig_superfamily	aul_smart_761275|CDS3	uncharacterized protein LOC116286621 [Actinia tenebrosa]	2.00E-15	44.44%	XP_031549028.1	Binding
Laminin_G	aul_smart_905601|CDS1	neuronal pentraxin-1-like [Actinia tenebrosa]	7.00E-74	56.04%	XP_031566952.1	Binding
Laminin_G	aul_smart_889815|CDS1	uncharacterized protein LOC116289442 [Actinia tenebrosa]	0	80.25%	XP_031552244.1	Binding
LU_Ly-6_antigen-uPA_receptor	aul_smart_606980|CDS1	lymphocyte antigen 6 complex locus protein G6d-like [Actinia tenebrosa]	5.00E-13	46.97%	XP_031567565.1	Binding
MAM	aul_smart_502751|CDS4	putative tyrosinase-like protein tyr-3 [Exaiptasia diaphana]	6.00E-30	45.45%	XP_028518481.1	Binding
PhosphatidylEthanolamine_PEBP	aul_smart_943810|CDS1	uncharacterized protein LOC116291200 [Actinia tenebrosa]	6.00E-66	58.38%	XP_031554197.1	Binding
PhosphatidylEthanolamine_PEBP	aul_smart_404904|CDS2	protein D2-like [Actinia tenebrosa]	1.00E-86	75.76%	XP_031554151.1	Binding
PROF	aul_smart_721914|CDS1	profilin [Exaiptasia diaphana]	5.00E-63	77.87%	XP_020903662.1	Binding
Profilin	aul_smart_67928|CDS3	profilin-like [Actinia tenebrosa]	6.00E-88	85.71%	XP_031559793.1	Binding
PTZ00184	aul_smart_859621|CDS2	calmodulin isoform X2 [Nematostella vectensis]	4.00E-105	100.00%	XP_001638581.1	Binding
PTZ00184	aul_smart_465228|CDS1	calmodulin-like [Actinia tenebrosa]	5.00E-79	71.43%	XP_031564677.1	Binding
S1_like_superfamily-Cold-shock_DNA_binding	aul_smart_557721|CDS2	protein lin-28 [Exaiptasia pallida]	4E-20	54.05%	XP_020896672.1	Binding
SAC6	aul_smart_506039|CDS3	plastin-2-like [Actinia tenebrosa]	0	87.60%	XP_031572293.1	Binding
Scavenger_receptor_Cys-rich	aul_smart_466234|CDS2	LOW QUALITY PROTEIN: scavenger receptor cysteine-rich domain superfamily protein-like	0	61.27%	XP_031550216.1	Binding
Smc_superfamily	aul_smart_42678|CDS6	major antigen-like [Actinia tenebrosa]	0	87.40%	XP_031567644.1	Binding
SRPBCC	aul_smart_895169|CDS3	FK506-binding protein 5-like [Actinia tenebrosa]	0	67.94%	XP_031553808.1	Binding
TGFb_propeptide	aul_smart_915247|CDS1	uncharacterized protein LOC116286705 [Actinia tenebrosa]	5.00E-33	44.79%	XP_031549132.1	Binding
TSP1	aul_smart_859952|CDS1	coadhesin-like isoform X5 [Actinia tenebrosa]	1.00E-29	82.09%	XP_031569447.1	Binding
vWD_superfamily	aul_smart_187102|CDS1	mucin-2-like [Exaiptasia pallida]	7E-123	60.38%	XP_020897325.1	Binding
vWFA_subfamily_ECM	aul_smart_688615|CDS2	uncharacterized protein LOC116307005 [Actinia tenebrosa]	2.00E-46	67.77%	XP_031573008.1	Binding
TSP1	aul_smart_877372|CDS1	hemicentin-1-like [Actinia tenebrosa]	0	67.26%	XP_031571781.1	Binding
Three-EGF-domain	aul_smart_86799|CDS3	fibropellin-1-like [Actinia tenebrosa]	2.00E-49	44.24%	XP_031566184.1	Binding
TSP1	aul_smart_196320|CDS2	coadhesin-like [Actinia tenebrosa]	0	69.74%	XP_031554933.1	Binding
Disintegrin_snake_EGF-like	aul_smart_983271|CDS1	uncharacterized protein LOC5508728 isoform X2 [Nematostella vectensis]	0.94	43.33%	XP_032233414.1	Binding
TSP1_vWF_typeA	aul_smart_883941|CDS3	coadhesin-like [Actinia tenebrosa]	0	68.19%	XP_031563116.1	Binding
Amino_oxidase	aul_smart_947026|CDS1	L-amino-acid oxidase-like [Actinia tenebrosa]	0	68.15%	XP_031558114.1	Enzyme
AmyAc_family	aul_smart_24138|CDS4	uncharacterized protein LOC116290231 [Actinia tenebrosa]	0	89.10%	XP_031553097.1	Enzyme
An_peroxidase	aul_smart_935043|CDS1	peroxidasin homolog [Actinia tenebrosa]	0	65.02%	XP_031551641.1	Enzyme
Animal_haem_peroxidase	aul_smart_870010|CDS1	peroxidasin homolog [Actinia tenebrosa]	0	66.67%	XP_031551641.1	Enzyme
Aspartate_aminotransferase	aul_smart_954807|CDS4	Cubilin [Exaiptasia diaphana]	0	69.73%	KXJ23981.1	Enzyme
CAP_ED	aul_smart_691948|CDS4	cAMP-dependent protein kinase type II regulatory subunit [Exaiptasia diaphana]	2.00E-108	78.53%	KXJ14771.1	Enzyme
Carbonic_anhydrase_alpha_superfamily	aul_smart_204889|CDS2	carbonic anhydrase 2-like [Actinia tenebrosa]	5.00E-132	62.29%	XP_031572154.1	Enzyme
Carbonic_anhydrase_alpha_superfamily	aul_smart_99612|CDS1	carbonic anhydrase 2-like [Actinia tenebrosa]	6.00E-134	64.36%	XP_031572154.1	Enzyme
Cu-Zn_Superoxide_Dismutase	aul_smart_64708|CDS1	copper/zinc superoxide dismutase CuZnSODb [Anemonia viridis]	1.00E-88	94.08%	AAN85727.2	Enzyme
Cyclophilin	aul_smart_347155|CDS3	peptidyl-prolyl cis-trans isomerase-like [Actinia tenebrosa]	5.00E-80	71.95%	XP_031555456.1	Enzyme
Cyclophilin	aul_smart_849571|CDS3	peptidyl-prolyl cis-trans isomerase-like [Actinia tenebrosa]	2.00E-86	76.22%	XP_031555456.1	Enzyme
EHN	aul_smart_653215|CDS1	epoxide hydrolase 1-like [Actinia tenebrosa]	7.00E-98	76.92%	XP_031572871.1	Enzyme
Flavoprotein	aul_smart_570080|CDS3	phosphopantothenoylcysteine decarboxylase-like [Actinia tenebrosa]	2.00E-75	73.83%	XP_031553514.1	Enzyme
Glutathione_peroxidase	aul_smart_397961|CDS6	gluthatione peroxidase [Anemonia viridis]	3.00E-82	66.10%	AOW71504.1	Enzyme
Glutathione_S_transferase	aul_smart_541217|CDS6	failed axon connections homolog [Actinia tenebrosa]	0	90.42%	XP_031556073.1	Enzyme
Gluzincin	aul_smart_963082|CDS3	predicted protein [Nematostella vectensis]	4.6	62.50%	EDO29841.1	Enzyme
Gluzincin	aul_smart_842869|CDS2	endothelin-converting enzyme 1-like [Actinia tenebrosa]	2.00E-171	48.76%	XP_031556633.1	Enzyme
Glyco_hydro	aul_smart_849253|CDS2	uncharacterized protein LOC116287299 [Actinia tenebrosa]	7.00E-162	63.17%	XP_031549826.1	Enzyme
Glyco_tranf_GTA_type	aul_smart_839456|CDS3	predicted protein [Nematostella vectensis]	3.1	25.74%	EDO40882.1	Enzyme
Lysozyme_like	aul_smart_760219|CDS3	lysozyme-like [Actinia tenebrosa]	4.00E-68	71.64%	XP_031553937.1	Enzyme
MDH_cytoplasmic_cytosolic	aul_smart_795760|CDS4	malate dehydrogenase, cytoplasmic-like [Actinia tenebrosa]	2.00E-168	90.61%	XP_031551010.1	Enzyme
NHL_Cu2_monooxygen	aul_smart_915608|CDS1	peptidyl-glycine alpha-amidating monooxygenase B-like isoform X3 [Actinia tenebrosa]	0	78.21%	XP_031553480.1	Enzyme
Pancreat_lipase_like	aul_smart_870137|CDS1	inactive pancreatic lipase-related protein 1-like [Actinia tenebrosa]	0	71.84%	XP_031553932.1	Enzyme
Peptidase_M17	aul_smart_945427|CDS2	putative aminopeptidase W07G4.4 [Actinia tenebrosa]	0	88.13%	XP_031567573.1	Enzyme
Phosphoenolpyruvate_carboxykinase_PEPCK	aul_smart_254731|CDS2	phosphoenolpyruvate carboxykinase, cytosolic [GTP]-like isoform X1 [Actinia tenebrosa]	0	87.46%	XP_031568381.1	Enzyme
PLN00052_prolyl-4-hydroxylase	aul_smart_721825|CDS1	putative tyrosinase-like protein tyr-3 [Exaiptasia diaphana]	6.00E-13	39.47%	KXJ20687.1	Enzyme
PLN00052_prolyl-4-hydroxylase	aul_smart_560524|CDS2	putative tyrosinase-like protein tyr-3 [Exaiptasia diaphana]	2.00E-08	40.32%	KXJ20687.1	Enzyme
PLN00052_prolyl-4-hydroxylase	aul_smart_45485|CDS2	uncharacterized protein LOC5502283 isoform X1 [Nematostella vectensis]	1.00E-19	44.14%	XP_032226437.1	Enzyme
PLN00052_prolyl-4-hydroxylase	aul_smart_932039|CDS1	putative tyrosinase-like protein tyr-3 [Actinia tenebrosa]	2E-12	70.00%	XP_031558727.1	Enzyme
PLN02272	aul_smart_917614|CDS2	glyceraldehyde-3-phosphate dehydrogenase-like [Actinia tenebrosa]	0	93.73%	XP_031564793.1	Enzyme
PLN02337	aul_smart_358191|CDS2	arachidonate 5-lipoxygenase-like [Actinia tenebrosa]	0	65.54%	XP_031570634.1	Enzyme
PLN02337_enzyme	aul_smart_875107|CDS3	uncharacterized protein LOC116308077 [Actinia tenebrosa]	0	70.79%	XP_031574298.1	Enzyme
PLN02338	aul_smart_12409|CDS1	uncharacterized protein LOC116308077 [Actinia tenebrosa]	0	61.21%	XP_031574298.1	Enzyme
PLN02338	aul_smart_875112|CDS3	uncharacterized protein LOC116308077 [Actinia tenebrosa]	0	73.58%	XP_031574298.1	Enzyme
PLN02339	aul_smart_20834|CDS2	arachidonate 5-lipoxygenase-like [Actinia tenebrosa]	0	62.10%	XP_031570634.1	Enzyme
PRK05901	aul_smart_606211|CDS1	uncharacterized protein LOC116617359 [Nematostella vectensis]	3.00E-49	78.23%	XP_032235896.1	Enzyme
Rib_hydrolase	aul_smart_881546|CDS3	ADP-ribosyl cyclase/cyclic ADP-ribose hydrolase-like [Actinia tenebrosa]	6.00E-118	61.94%	XP_031554780.1	Enzyme
Thioredoxin_like	aul_smart_361479|CDS2	SH3 domain-binding glutamic acid-rich-like protein 3 [Actinia tenebrosa]	8.00E-41	66.32%	XP_031568530.1	Enzyme
Thioredoxin_like	aul_smart_864445|CDS5	SH3 domain-binding glutamic acid-rich-like protein 3 [Actinia tenebrosa]	2E-37	81.91%	XP_031568536.1	Enzyme
TIM-triose_phosphate_isomerase	aul_smart_141564|CDS2	uncharacterized protein LOC116306116 [Actinia tenebrosa]	0	81.00%	XP_031572021.1	Enzyme
TIM-triose_phosphate_isomerase	aul_smart_869899|CDS2	fructose-bisphosphate aldolase A-like [Actinia tenebrosa]	0	93.31%	XP_031551456.1	Enzyme
Tyrosinase	aul_smart_948168|CDS4	uncharacterized protein LOC116305035 [Actinia tenebrosa]	0	62.84%	XP_031570716.1	Enzyme
Tyrosinase	aul_smart_828873|CDS2	uncharacterized protein LOC116297103 [Actinia tenebrosa]	0	78.68%	XP_031561123.1	Enzyme
Metallopeptidase	aul_smart_529157|CDS2	zinc metalloproteinase nas-13-like [Actinia tenebrosa]	0	74.82%	XP_031557474.1	Enzyme
Metallopeptidase	aul_smart_459329|CDS3	uncharacterized protein LOC116297953 [Actinia tenebrosa]	0	59.72%	XP_031562135.1	Enzyme
S1	aul_smart_73591|CDS2	chymotrypsinogen B-like isoform X1 [Actinia tenebrosa]	0.047	31.76%	XP_031550563.1	Enzyme
S1	aul_smart_846509|CDS1	transmembrane protease serine 2-like [Actinia tenebrosa]	0	76.62%	XP_031552036.1	Enzyme
TSP1_LU_superfamily	aul_smart_876585|CDS4	A disintegrin and metalloproteinase with thrombospondin motifs adt-2-like [Actinia tene	2.00E-81	50.83%	XP_031549934.1	Enzyme
Alpha_amylase_inhibitor	aul_smart_896615|CDS1	RecName: Full=Alpha-amylase inhibitor magnificamide [Heteractis magnifica]	2.00E-15	70.73%	C0HK71.1	Inhibitor
Cystatin-like_domain	aul_smart_90038|CDS1	cystatin-like [Actinia tenebrosa]	6.00E-45	52.76%	XP_031563705.1	Inhibitor
Thyroglobulin_superfamily	aul_smart_452043|CDS2	equistatin [Actinia tenebrosa]	3E-13	44.12%	XP_031562748.1	Inhibitor
TY_superfamily	aul_smart_690582|CDS3	uncharacterized protein LOC110232652 isoform X2 [Exaiptasia diaphana]	1.00E-13	52.17%	XP_028512983.1	Inhibitor
TY_superfamily	aul_smart_429408|CDS2	Equistatin [Exaiptasia diaphana]	8.00E-15	52.17%	KXJ18222.1	Inhibitor
TY_superfamily	aul_smart_767063|CDS3	Equistatin [Exaiptasia diaphana]	3.00E-13	50.72%	KXJ18222.1	Inhibitor

ASC_superfamily	aul_smart_821180|CDS1	uncharacterized protein LOC5519438 isoform X1 [Nematostella vectensis]	1.00E-04	38.89%	XP_032220228.1	Ion_transport
ASC_superfamily	aul_smart_895970|CDS1	uncharacterized protein LOC116307851 [Actinia tenebrosa]	0	85.36%	XP_031574028.1	Ion_transport
Association_with_the_SNF1_complex_ASC	aul_smart_898516|CDS1	predicted protein [Nematostella vectensis]	10	53.33%	EDO30894.1	Ion_transport
ATPase-IIB_Ca	aul_smart_898618|CDS1	plasma membrane calcium-transporting ATPase 4 [Exaiptasia diaphana]	6.00E-05	36.96%	XP_020905291.1	Ion_transport
Cation_Antiporter_Caca	aul_smart_859963|CDS3	uncharacterized protein LOC116303960 [Actinia tenebrosa]	0	54.11%	XP_031569460.1	Ion_transport
Cation_Antiporter_Caca	aul_smart_859956|CDS4	uncharacterized protein LOC116303960 [Actinia tenebrosa]	0	62.25%	XP_031569460.1	Ion_transport
Heavy-metal-associated_domain-HMA	aul_smart_851545|CDS2	metal homeostasis factor ATX1-like [Actinia tenebrosa]	1.00E-40	87.14%	XP_031575119.1	Ion_transport
green_fluorescent_protein	aul_smart_532699|CDS2	blue chromoprotein aeCP597 [Actinia equina]	5E-129	71.12%	ABA41382.1	Phosphoprote
P-loop-NTPase	aul_smart_805701|CDS5	cell division control protein 42 homolog [Exaiptasia diaphana]	1.00E-71	87.39%	XP_020916996.1	Regulatory
14-3-3_superfamily	aul_smart_933939|CDS2	14-3-3-like protein 2 [Actinia tenebrosa]	2.00E-141	78.49%	XP_031566012.1	Regulatory
ADF_gelsolin	aul_smart_260161|CDS2	gelsolin-like protein 1 [Actinia tenebrosa]	0	90.49%	XP_031564935.1	Regulatory
ADF_gelsolin	aul_smart_336905|CDS3	gelsolin-like protein 1 [Actinia tenebrosa]	0	87.57%	XP_031564933.1	Regulatory
ADF_gelsolin	aul_smart_883910|CDS2	gelsolin-like protein 1 isoform X1 [Actinia tenebrosa]	0	88.89%	XP_031564936.1	Regulatory
ADF_gelsolin	aul_smart_925384|CDS3	cofilin-like [Actinia tenebrosa]	5.00E-38	48.41%	XP_031566064.1	Regulatory
ADF_gelsolin	aul_smart_186558|CDS2	gelsolin-like protein 1 [Actinia tenebrosa]	0	87.57%	XP_031564933.1	Regulatory
CysPc	aul_smart_524311|CDS2	calpain-B-like isoform X1 [Actinia tenebrosa]	0	84.95%	XP_031555932.1	Regulatory
EF-hand	aul_smart_523175|CDS1	aequorin-1-like [Actinia tenebrosa]	1.00E-67	48.91%	XP_031565692.1	Regulatory
EF-hand	aul_smart_523175|CDS1	aequorin-1-like [Actinia tenebrosa]	1.00E-67	48.91%	XP_031565692.1	Regulatory
EF-hand	aul_smart_306821|CDS1	uncharacterized protein LOC110244290 [Exaiptasia pallida]	3.00E-13	33.33%	XP_020906153.1	Regulatory
EF-hand	aul_smart_505264|CDS1	CnidEF [Anthopleura elegantissima]	2E-34	46.10%	ABD16201.1	Regulatory
Ependymin	aul_smart_851787|CDS2	uncharacterized protein LOC116306046 [Actinia tenebrosa]	1.00E-78	66.27%	XP_031571939.1	Regulatory
FHA	aul_smart_774489|CDS3	proliferation marker protein Ki-67 [Nematostella vectensis]	9.2	43.48%	XP_001628947.2	Regulatory
PRP40_superfamily_WW_domain	aul_smart_860116|CDS2	transcription elongation regulator 1-like [Actinia tenebrosa]	0.62	50.00%	XP_031574967.1	Regulatory
PTZ00141	aul_smart_900807|CDS1	elongation factor 1-alpha-like [Actinia tenebrosa]	0	93.42%	XP_031557559.1	Regulatory
SAM_superfamily	aul_smart_917514|CDS2	polyhomeotic-like protein 2 [Actinia tenebrosa]	2.00E-61	91.58%	XP_031564435.1	Regulatory
Tetraspanin	aul_smart_392030|CDS2	CD151 antigen isoform X1 [Exaiptasia diaphana]	9.00E-130	83.54%	XP_020913364.1	Regulatory
Trefoil	aul_smart_798779|CDS2	trefoil factor 2 [Exaiptasia diaphana]	9.00E-18	46.88%	XP_020915722.1	Regulatory
Trefoil	aul_smart_349365|CDS1	integumentary mucin C.1-like [Actinia tenebrosa]	2.00E-55	48.65%	XP_031563222.1	Regulatory
Trefoil	aul_smart_860933|CDS3	trefoil factor 2 [Exaiptasia diaphana]	6.00E-18	46.88%	XP_020915722.1	Regulatory
Trefoil	aul_smart_855409|CDS2	integumentary mucin C.1-like [Actinia tenebrosa]	1.00E-54	47.57%	XP_031563222.1	Regulatory
Trypan_PARP	aul_smart_921580|CDS2	mucin-2 [Nematostella vectensis]	0.004	33.93%	XP_032230364.1	Regulatory
TSP1_vWF_typeA	aul_smart_153792|CDS2	hemicentin-1-like [Actinia tenebrosa]	0	73.68%	XP_031561318.1	Regulatory
TSP1_vWF_typeA	aul_smart_406926|CDS2	hemicentin-1-like [Actinia tenebrosa]	0	74.08%	XP_031561318.1	Regulatory
TSP1_vWF_typeA	aul_smart_481987|CDS2	hemicentin-1-like [Actinia tenebrosa]	9.00E-132	65.84%	XP_031561318.1	Regulatory
TSP1_vWF_typeA	aul_smart_97400|CDS2	hemicentin-1-like [Actinia tenebrosa]	1.00E-89	53.71%	XP_031561318.1	Regulatory
Ubiquitin_like_fold	aul_smart_77569|CDS1	ubiquitin-60S ribosomal protein L40 [Actinia tenebrosa]	2.00E-91	99.22%	XP_031566518.1	Regulatory
Ubiquitin_like_fold	aul_smart_881675|CDS3	ubiquitin [Nematostella vectensis]	1.00E-40	98.44%	XP_001623355.1	Regulatory
vWC_superfamily	aul_smart_56293|CDS1	uncharacterized protein LOC116287167 [Actinia tenebrosa]	9.00E-126	59.02%	XP_031549669.1	Regulatory
vWF_typeD	aul_smart_346632|CDS2	mucin-5AC-like [Actinia tenebrosa]	0	81.93%	XP_031556696.1	Regulatory
COLFI	aul_smart_892174|CDS2	uncharacterized protein LOC116301896 [Actinia tenebrosa]	9.00E-128	75.85%	XP_031566923.1	Structural
COLFI	aul_smart_963107|CDS1	uncharacterized protein LOC116301896 [Actinia tenebrosa]	2.00E-150	73.17%	XP_031566923.1	Structural
COLFI	aul_smart_963106|CDS1	uncharacterized protein LOC116301896 [Actinia tenebrosa]	2.00E-105	74.11%	XP_031566923.1	Structural
Collagen	aul_smart_471858|CDS1	collagen triple helix repeat-containing protein 1 [Exaiptasia diaphana]	8.00E-07	34.71%	XP_020897757.1	Structural
Collagen	aul_smart_988849|CDS1	collagen triple helix repeat-containing protein 1 [Nematostella vectensis]	1.00E-12	37.06%	XP_001628048.2	Structural
Collagen	aul_smart_857972|CDS3	collagen triple helix repeat-containing protein 1-like [Actinia tenebrosa]	4.00E-32	83.33%	XP_031574730.1	Structural
Fibronectin _type 3-Immunoglobulin_superfamily	aul_smart_90307|CDS1	fibronectin type III domain-containing protein-like [Actinia tenebrosa]	0	71.88%	XP_031548961.1	Structural
Galaxin	aul_smart_876177|CDS2	uncharacterized protein LOC116617139 isoform X1 [Nematostella vectensis]	0	51.69%	XP_032235427.1	Structural
Galaxin	aul_smart_846024|CDS2	uncharacterized protein LOC116610131 isoform X3 [Nematostella vectensis]	4.00E-115	38.50%	XP_032226720.1	Structural
H2B	aul_smart_99283|CDS2	late histone H2B.L4 [Actinia tenebrosa]	4.00E-77	93.55%	XP_031558499.1	Structural
H4	aul_smart_970440|CDS3	histone H3 [Nematostella vectensis]	3.00E-96	100.00%	XP_001618211.1	Structural
Myosin_tail_1_superfamily	aul_smart_26019|CDS4	myosin-10-like [Actinia tenebrosa]	0	93.74%	XP_031573966.1	Structural
MYSc_class_II	aul_smart_544318|CDS3	myosin heavy chain, striated muscle-like isoform X1 [Actinia tenebrosa]	0	92.51%	XP_031564040.1	Structural
NBD_sugar-kinase_HSP70_actin	aul_smart_978806|CDS4	actin, cytoplasmic-like [Actinia tenebrosa]	0	98.93%	XP_031566947.1	Structural
NBD_sugar-kinase_HSP70_actin	aul_smart_858216|CDS2	actin, cytoplasmic-like [Actinia tenebrosa]	0	98.66%	XP_031566947.1	Structural
NBD_sugar-kinase_HSP70_actin	aul_smart_997212|CDS3	uncharacterized protein LOC116302627 [Actinia tenebrosa]	4.8	30.61%	XP_031567825.1	Structural
Nucleotide-Binding-Domain-of-the-sugar kinase_HSP70_ac	aul_smart_471251|CDS2	actin, cytoplasmic [Exaiptasia diaphana]	0	99.20%	XP_020916414.1	Structural
Nucleotide-Binding-Domain-of-the-sugar kinase_HSP70_ac	aul_smart_902471|CDS3	actin, cytoplasmic [Exaiptasia diaphana]	0	98.94%	XP_020916414.1	Structural
PHA03247	aul_smart_656660|CDS11	uncharacterized protein LOC116295118 isoform X2 [Actinia tenebrosa]	1.5	28.57%	XP_031558715.1	Structural
PLN00035	aul_smart_941195|CDS2	histone H4 [Nematostella vectensis]	7.00E-68	100.00%	XP_001618258.1	Structural
PLN00220	aul_smart_982608|CDS3	tubulin beta-4B chain [Exaiptasia diaphana]	0	99.33%	XP_020913509.1	Structural
PTZ00017	aul_smart_967346|CDS1	histone H2A [Exaiptasia pallida]	1E-85	99.20%	XP_020899546.1	Structural
PTZ00335	aul_smart_191481|CDS2	tubulin alpha-1A chain [Nematostella vectensis]	0	99.49%	XP_001630130.1	Structural
PTZ00335	aul_smart_991528|CDS4	tubulin alpha-1A chain [Nematostella vectensis]	0	97.56%	XP_032237826.1	Structural
PTZ00335	aul_smart_796551|CDS4	tubulin alpha-1 chain [Exaiptasia diaphana]	2.00E-09	90.91%	XP_028513327.1	Structural
SCP1_superfamily	aul_smart_863628|CDS2	muscle-specific protein 20-like [Actinia tenebrosa]	2.00E-126	87.18%	XP_031553101.1	Structural
SCP1_superfamily	aul_smart_291280|CDS1	muscle-specific protein 20-like [Actinia tenebrosa]	1.00E-105	77.44%	XP_031553101.1	Structural
Spectrin	aul_smart_848020|CDS1	spectrin beta chain-like isoform X1 [Actinia tenebrosa]	0	68.38%	XP_031552903.1	Structural
Spectrin	aul_smart_834420|CDS1	spectrin alpha chain, non-erythrocytic 1-like [Actinia tenebrosa]	0	68.44%	XP_031574403.1	Structural
Tetraspanin	aul_smart_802573|CDS3	CD63 antigen-like [Actinia tenebrosa]	1.00E-121	78.41%	XP_031567640.1	Structural
Thymosin_superfamily	aul_smart_425045|CDS2	microtubule-associated protein futsch-like [Actinia tenebrosa]	0	84.01%	XP_031563437.1	Structural
Tropomyosin	aul_smart_893565|CDS1	tropomyosin-like [Actinia tenebrosa]	2.00E-126	93.80%	XP_031569061.1	Structural
Vitelline_membrane_outer_layer_protein-I-VMO-I	aul_smart_287776|CDS1	vitelline membrane outer layer protein 1 homolog isoform X2 [Actinia tenebrosa]	2.00E-56	46.77%	XP_031555991.1	Structural
Vitelline_membrane_outer_layer_protein-I-VMO-I	aul_smart_89210|CDS4	vitelline membrane outer layer protein 1 homolog isoform X2 [Actinia tenebrosa]	3.00E-57	47.26%	XP_031555991.1	Structural
vWA_collagen	aul_smart_858141|CDS1	uncharacterized protein LOC5519642 [Nematostella vectensis]	3.00E-176	39.12%	XP_032220340.1	Structural
vWF_typeA	aul_smart_414493|CDS4	collagen alpha-1(XII) chain-like [Actinia tenebrosa]	4.00E-117	69.20%	XP_031565266.1	Structural
vWF_typeA	aul_smart_97388|CDS1	vegetative cell wall protein gp1-like [Exaiptasia diaphana]	9.00E-80	52.42%	XP_028515505.1	Structural
vWF_typeA	aul_smart_877638|CDS5	collagen alpha-1(XII) chain-like [Actinia tenebrosa]	2.00E-163	72.78%	XP_031565266.1	Structural
vWF_typeA	aul_smart_982045|CDS1	uncharacterized protein LOC116289889 [Actinia tenebrosa]	2E-155	59.37%	XP_031552692.1	Structural
vWF_typeA	aul_smart_801124|CDS2	ZP domain-containing protein-like [Actinia tenebrosa]	8E-38	67.02%	XP_031557419.1	Structural
vWF_typeA	aul_smart_879849|CDS1	putative uncharacterized protein DDB_G0290521 [Actinia tenebrosa]	2.00E-119	58.12%	XP_031574008.1	Structural
Zona_pellucida	aul_smart_524456|CDS4	ZP domain-containing protein-like [Actinia tenebrosa]	0	77.61%	XP_031548860.1	Structural
Zona_pellucida	aul_smart_989823|CDS2	ZP domain-containing protein-like [Actinia tenebrosa]	8E-38	67.02%	XP_031566714.1	Structural
Zona_pellucida	aul_smart_990043|CDS2	ZP domain-containing protein-like isoform X1 [Actinia tenebrosa]	0	67.86%	XP_031566719.1	Structural
Actinoporins	aul_smart_512597|CDS1	RecName: Full=DELTA-actitoxin-Aas1a; Short=DELTA-AITX-Aas1a; AltName: Full=Bandapor	7.00E-61	74.78%	C5NSL2.1	Toxin
Actinoporins	aul_smart_893955|CDS2	actinoporin [Heteractis crispa]	1.00E-08	47.46%	APQ32106.1	Toxin
B-defensin-like	aul_smart_802345|CDS9	Delta-actitoxin-Ave sodium channel inhibitory toxin [Aulactinia veratra]	2.00E-52	84.69%	ATY39984.1	Toxin
B-defensin-like_Kv3	aul_smart_270533|CDS2	type III potassium channel toxin protein [Anemonia sulcata]	1E-20	52.56%	ALL34533.1	Toxin
B-defensin-like_Kv3	aul_smart_870725|CDS2	type III potassium channel toxin protein [Anemonia sulcata]	1.00E-17	50.00%	ALL34555.1	Toxin
B-defensin-like_Kv3	aul_smart_904166|CDS1	type III potassium channel toxin protein [Anemonia sulcata]	3.00E-32	67.57%	ALL34555.1	Toxin
B-defensin-like_Kv3	aul_smart_914904|CDS2	type III potassium channel toxin protein [Anemonia sulcata]	9.00E-18	50.00%	ALL34555.1	Toxin
B-defensin-like_Kv3	aul_smart_846342|CDS2	type III potassium channel toxin protein [Anemonia sulcata]	6.00E-33	65.43%	ALL34531.1	Toxin
B-defensin-like_Kv3	aul_smart_420607|CDS1	type III potassium channel toxin protein [Anemonia sulcata]	1.00E-15	49.35%	ALL34550.1	Toxin
CAP	aul_smart_860615|CDS2	uncharacterized protein LOC116288443 [Actinia tenebrosa]	5.00E-61	44.98%	XP_031551091.1	Toxin
CAP	aul_smart_464302|CDS2	ectin-like [Actinia tenebrosa]	1.00E-72	70.42%	XP_031569962.1	Toxin
CAP	aul_smart_414628|CDS1	ectin-like [Actinia tenebrosa]	9.00E-91	72.29%	XP_031569962.1	Toxin
CAP_ShK	aul_smart_68364|CDS1	uncharacterized protein LOC116288443 [Actinia tenebrosa]	1.00E-91	58.75%	XP_031551091.1	Toxin

Endonuclease	aul_smart_878853|CDS1	uncharacterized protein LOC116298347 [Actinia tenebrosa]	3.00E-102	52.36%	XP_031562623.1	Toxin
Endonuclease	aul_smart_249271|CDS1	uncharacterized protein LOC116298347 [Actinia tenebrosa]	4.00E-79	54.05%	XP_031562623.1	Toxin
Endonuclease	aul_smart_878854|CDS1	uncharacterized protein LOC116298347 [Actinia tenebrosa]	7.00E-101	51.69%	XP_031562623.1	Toxin
ICK	aul_smart_887805|CDS26	RecName: Full=Predicted protein NvePTx1; Flags: Precursor [Nematostella vectensis]	0.0002	31.51%	A7RMN1.2	Toxin
Kazal	aul_smart_426451|CDS2	RecName: Full=PI-actitoxin-Avd5a; Short=PI-AITX-Avd5a; AltName: Full=Non-classical Kaz	4E-11	52.17%	P16895.1	Toxin
Kazal	aul_smart_1046916|CDS2	RecName: Full=PI-actitoxin-Avd5a; Short=PI-AITX-Avd5a; AltName: Full=Non-classical Kaz	2E-20	73.91%	P16895.1	Toxin
Kazal	aul_smart_876517|CDS28	uncharacterized protein LOC110241796 [Exaiptasia pallida]	0.00000005	46.67%	XP_020903357.2	Toxin
Kazal	aul_smart_877428|CDS1	RecName: Full=PI-actitoxin-Avd5a; Short=PI-AITX-Avd5a; AltName: Full=Non-classical Kaz	5.00E-11	52.17%	P16895.1	Toxin
Kazal	aul_smart_427605|CDS2	predicted protein [Nematostella vectensis]	2.00E-11	36.25%	EDO42282.1	Toxin
Kazal	aul_smart_280649|CDS1	uncharacterized protein LOC110241796 [Exaiptasia diaphana]	1.00E-08	38.98%	XP_020903357.2	Toxin
Kazal	aul_smart_687983|CDS3	RecName: Full=PI-actitoxin-Avd5a; Short=PI-AITX-Avd5a; AltName: Full=Non-classical Kaz	2.00E-09	53.49%	P16895.1	Toxin
Kazal	aul_smart_813067|CDS1	RecName: Full=PI-actitoxin-Avd5a; Short=PI-AITX-Avd5a; AltName: Full=Non-classical Kaz	9.00E-18	67.39%	P16895.1	Toxin
Kunitz	aul_smart_859108|CDS2	kappaPI-actitoxin-Avd3e-like [Actinia tenebrosa]	1.00E-68	69.34%	XP_031558603.1	Toxin
Kunitz	aul_smart_955021|CDS2	carboxypeptidase inhibitor SmCI-like [Exaiptasia diaphana]	7.00E-49	40.27%	XP_020904664.1	Toxin
Kunitz	aul_smart_886056|CDS2	BPTI/Kunitz domain-containing protein-like [Actinia tenebrosa]	5.00E-38	46.04%	XP_031567285.1	Toxin
Kunitz	aul_smart_859005|CDS1	BPTI/Kunitz domain-containing protein-like [Actinia tenebrosa]	3.00E-33	69.62%	XP_031567285.1	Toxin
Kunitz	aul_smart_856786|CDS3	PI-actitoxin-Aeq3a-like [Actinia tenebrosa]	1.00E-41	78.67%	XP_031550082.1	Toxin
Kunitz_venoKv2	aul_smart_684611|CDS2	RecName: Full=KappaPI-stichotoxin-Shd2a; Short=KappaPI-SHTX-Shd2a; AltName: Full=Ku	1.00E-25	63.08%	B1BSI8.1	Toxin
MACPF	aul_smart_884261|CDS11	uncharacterized protein LOC116292765 [Actinia tenebrosa]	0	65.72%	XP_031555977.1	Toxin
MACPF	aul_smart_487417|CDS2	uncharacterized protein LOC116292765 [Actinia tenebrosa]	0	70.42%	XP_031555977.1	Toxin
S1	aul_smart_839293|CDS2	chymotrypsinogen A-like [Actinia tenebrosa]	6.00E-125	64.15%	XP_031568088.1	Toxin
SCRIPs	aul_smart_34921|CDS3	No_significant_similarity_found	0	0	0	Toxin
SCRIPs	aul_smart_760423|CDS2	small cysteine-rich protein 2-like [Actinia tenebrosa]	2.00E-08	41.75%	XP_031553817.1	Toxin
Shk	aul_smart_333142|CDS1	uncharacterized protein LOC116305581 [Actinia tenebrosa]	1.00E-67	67.53%	XP_031571380.1	Toxin
ShK	aul_smart_206650|CDS2	RecName: Full=U-actitoxin-Oulsp2; Short=U-AITX-Oulsp2; AltName: Full=OspTx2b; Flags: F	9.00E-24	52.44%	A0A330KUG5.1	Toxin
ShK	aul_smart_802442|CDS2	RecName: Full=U-actitoxin-Oulsp2; Short=U-AITX-Oulsp2; AltName: Full=OspTx2b; Flags: F	1.00E-22	51.85%	A0A330KUG5.1	Toxin
ShK	aul_smart_596170|CDS2	RecName: Full=U-actitoxin-Oulsp2; Short=U-AITX-Oulsp2; AltName: Full=OspTx2b; Flags: F	4.00E-19	75.00%	A0A330KUG5.1	Toxin
ShK	aul_smart_677929|CDS2	RecName: Full=Kappa-actitoxin-Aer3a; Short=Kappa-AITX-Aer3a; AltName: Full=AnerK; Al	2.00E-10	70.59%	Q0EAE5.1	Toxin
ShK	aul_smart_456681|CDS1	U-actitoxin-Avd11a-like [Actinia tenebrosa]	3.00E-27	52.00%	XP_031557495.1	Toxin
ShK	aul_smart_560713|CDS3	RecName: Full=U-actitoxin-Oulsp2; Short=U-AITX-Oulsp2; AltName: Full=OspTx2b; Flags: F	2.00E-19	75.00%	A0A330KUG5.1	Toxin
ShK	aul_smart_540526|CDS2	RecName: Full=Kappa-stichotoxin-Hmg1a; Short=Kappa-SHTX-Hmg1a; AltName: Full=Pota	2.00E-11	48.00%	O16846.2	Toxin
Single-EGF-domain	aul_smart_685108|CDS3	RecName: Full=OMEGA-stichotoxin-Shd4a; Short=OMEGA-SHTX-Shd4a; AltName: Full=EGF	2.00E-27	64.37%	B1BSJ0.1	Toxin
Single-EGF-domain	aul_smart_997952|CDS1	RecName: Full=OMEGA-stichotoxin-Shd4a; Short=OMEGA-SHTX-Shd4a; AltName: Full=EGF	1.00E-23	60.24%	B1BSJ0.1	Toxin
Single-EGF-domain	aul_smart_835448|CDS1	RecName: Full=U-actitoxin-Avd12a; Short=U-AITX-Avd12a; AltName: Full=Gigantoxin-4; Sh	4.00E-09	37.88%	P0DMY9.1	Toxin
WSC	aul_smart_1033576|CDS2	uncharacterized protein LOC116305510 [Actinia tenebrosa]	5.00E-111	61.15%	XP_031571305.1	Toxin
WSC	aul_smart_879959|CDS2	uncharacterized protein LOC116305510 [Actinia tenebrosa]	5.00E-113	56.94%	XP_031571305.1	Toxin
WSC	aul_smart_879960|CDS2	uncharacterized protein LOC116305510 [Actinia tenebrosa]	1.00E-110	55.56%	XP_031571305.1	Toxin
WSC	aul_smart_879937|CDS4	uncharacterized protein LOC116305510 [Actinia tenebrosa]	8.00E-110	54.86%	XP_031571305.1	Toxin
WSC	aul_smart_6042|CDS2	uncharacterized protein LOC116305510 [Actinia tenebrosa]	3.00E-118	59.09%	XP_031571305.1	Toxin
WSC	aul_smart_186432|CDS2	uncharacterized protein LOC116308716 [Actinia tenebrosa]	5E-166	0.7432	XP_031575055.1	Toxin
WSC	aul_smart_761274|CDS2	uncharacterized protein LOC116305510 [Actinia tenebrosa]	2.00E-32	51.35%	XP_031571305.1	Toxin
WSC	aul_smart_879797|CDS2	uncharacterized protein LOC116305510 [Actinia tenebrosa]	8.00E-110	56.21%	XP_031571305.1	Toxin
WSC	aul_smart_143517|CDS1	uncharacterized protein LOC116305510 [Actinia tenebrosa]	1.00E-83	69.36%	XP_031571305.1	Toxin
WSC	aul_smart_521871|CDS3	Pancreatic secretory granule membrane major glycoprotein GP2 [Exaiptasia diaphana]	3.00E-52	43.64%	KXJ29524.1	Toxin
WSC	aul_smart_985047|CDS3	uncharacterized protein LOC116288606 [Actinia tenebrosa]	0	65.60%	XP_031551276.1	Toxin
Metallopeptidase_Gluzincin_M13domain	aul_smart_939847|CDS2	endothelin-converting enzyme 1-like [Actinia tenebrosa]	5.00E-134	49.40%	XP_031564967.1	Toxin
Metallopeptidase_Gluzincin_M13domain	aul_smart_939848|CDS1	endothelin-converting enzyme 1-like [Actinia tenebrosa]	2.00E-62	47.66%	XP_031563523.1	Toxin
Metallopeptidase_Gluzincin_M13domain	aul_smart_939726|CDS1	endothelin-converting enzyme 1-like [Actinia tenebrosa]	6.00E-86	58.65%	XP_031563523.1	Toxin
not_predicted	aul_smart_1012536|CDS1	No_significant_similarity_found				Unknown
not_predicted	aul_smart_927781|CDS1	No_significant_similarity_found	0	0	0	Unknown
not_predicted	aul_smart_34342|CDS1	No_significant_similarity_found	0	0	0	Unknown
not_predicted	aul_smart_312129|CDS6	No_significant_similarity_found	0	0	0	Unknown
not_predicted	aul_smart_828408|CDS2	uncharacterized protein LOC116604574 [Nematostella vectensis]	0.008	33.87%	XP_032223012.1	Unknown
Domain_of_unknown_function-DUF4430	aul_smart_251703|CDS1	uncharacterized protein CG3556-like [Actinia tenebrosa]	2.00E-67	74.22%	XP_031557458.1	Unknown
DUF3421	aul_smart_39272|CDS1	natterin-4-like [Actinia tenebrosa]	1E-65	56.52%	XP_031572047.1	Unknown
FHY3_superfamily	aul_smart_781769|CDS5	Protein FAR1-RELATED SEQUENCE 7 [Exaiptasia diaphana]	0.37	47.37%	KXJ13099.1	Unknown
not_predicted	aul_smart_875469|CDS1	uncharacterized protein LOC116303478 isoform X2 [Actinia tenebrosa]	2.00E-90	74.15%	XP_031568906.1	Unknown
not_predicted	aul_smart_42307|CDS1	hypothetical protein AC249_AIPGENE16961 [Exaiptasia pallida]	0	53.59%	KXJ29233.1	Unknown
not_predicted	aul_smart_920775|CDS1	uncharacterized protein LOC116616129 [Nematostella vectensis]	2.00E-145	67.32%	XP_032233916.1	Unknown
not_predicted	aul_smart_883556|CDS2	uncharacterized protein LOC116289711 [Actinia tenebrosa]	4.00E-05	30.95%	XP_031552515.1	Unknown
not_predicted	aul_smart_850752|CDS4	uncharacterized protein LOC116306321 [Actinia tenebrosa]	0	75.89%	XP_031572215.1	Unknown
not_predicted	aul_smart_933490|CDS2	uncharacterized protein LOC116303204 [Actinia tenebrosa]	3.00E-85	59.11%	XP_031568559.1	Unknown
not_predicted	aul_smart_857219|CDS2	uncharacterized protein LOC116303204 [Actinia tenebrosa]	1.00E-85	58.62%	XP_031568559.1	Unknown
not_predicted	aul_smart_725241|CDS2	uncharacterized protein LOC116306945 [Actinia tenebrosa]	1.00E-15	65.22%	XP_031572946.1	Unknown
not_predicted	aul_smart_418125|CDS1	uncharacterized protein LOC116304236 [Actinia tenebrosa]	2E-37	57.01%	XP_031569802.1	Unknown
not_predicted	aul_smart_219023|CDS3	uncharacterized protein LOC116301422 isoform X1 [Actinia tenebrosa]	1.00E-09	41.67%	XP_031566334.1	Unknown
not_predicted	aul_smart_188645|CDS1	uncharacterized protein LOC116304236 [Actinia tenebrosa]	9.00E-37	56.19%	XP_031569802.1	Unknown
not_predicted	aul_smart_2957|CDS2	uncharacterized protein LOC116304268 [Actinia tenebrosa]	1.00E-100	76.24%	XP_031569834.1	Unknown
not_predicted	aul_smart_446350|CDS2	hypothetical protein AC249_AIPGENE26472 [Exaiptasia pallida]	9.00E-36	31.19%	KXJ07949.1	Unknown
not_predicted	aul_smart_382660|CDS2	uncharacterized protein LOC116306924 isoform X3 [Actinia tenebrosa]	2.00E-28	42.78%	XP_031572924.1	Unknown
not_predicted	aul_smart_395041|CDS2	hypothetical protein AC249_AIPGENE22923 [Exaiptasia diaphana]	3.00E-53	44.50%	KXJ19357.1	Unknown
not_predicted	aul_smart_481574|CDS3	uncharacterized protein LOC116290938 [Actinia tenebrosa]	0	82.45%	XP_031553922.1	Unknown
not_predicted	aul_smart_778565|CDS1	uncharacterized protein LOC116303204 [Actinia tenebrosa]	2.00E-49	49.12%	XP_031568559.1	Unknown
not_predicted	aul_smart_934756|CDS3	uncharacterized protein LOC116294264 [Actinia tenebrosa]	1E-43	68.69%	XP_031557684.1	Unknown
not_predicted	aul_smart_955171|CDS3	hypothetical protein AC249_AIPGENE18232 [Exaiptasia pallida]	2E-13	43.24%	KXJ05374.1	Unknown
not_predicted	aul_smart_870187|CDS3	uncharacterized protein LOC116290938 [Actinia tenebrosa]	0	80.53%	XP_031553922.1	Unknown
not_predicted	aul_smart_798440|CDS3	uncharacterized protein LOC116306945 [Actinia tenebrosa]	3.00E-15	74.42%	XP_031572946.1	Unknown
not_predicted	aul_smart_607133|CDS4	uncharacterized protein LOC116294264 [Actinia tenebrosa]	4.00E-71	67.10%	XP_031557684.1	Unknown
not_predicted	aul_smart_848252|CDS1	MAM and LDL-receptor class A domain-containing protein 2-like [Actinia tenebrosa]	0	73.95%	XP_031568759.1	Unknown
not_predicted	aul_smart_140570|CDS4	hypothetical protein AC249_AIPGENE22923 [Exaiptasia diaphana]	4.00E-30	54.00%	KXJ19357.1	Unknown
not_predicted	aul_smart_133147|CDS2	uncharacterized skeletal organic matrix protein 5-like [Actinia tenebrosa]	5E-105	71.72%	XP_031569043.1	Unknown
not_predicted	aul_smart_838698|CDS3	precusor of biologically active peptides MS9.2 [Metridium senile]	0.22	32.05%	SBO16029.1	Unknown
not_predicted	aul_smart_839458|CDS3	predicted protein [Nematostella vectensis]	1.5	32.26%	EDO30729.1	Unknown
not_predicted	aul_smart_954404|CDS2	cysteine-rich motor neuron 1 protein-like [Actinia tenebrosa]	3.00E-21	48.31%	XP_031549053.1	Unknown
not_predicted	aul_smart_954616|CDS2	cysteine-rich motor neuron 1 protein-like isoform X6 [Actinia tenebrosa]	2.00E-22	43.64%	XP_031549072.1	Unknown
not_predicted	aul_smart_537804|CDS5	neurofilament heavy polypeptide-like [Actinia tenebrosa]	5E-60	78.42%	XP_031555506.1	Unknown
not_predicted	aul_smart_978781|CDS2	transmembrane cell adhesion receptor mua-3 [Nematostella vectensis]	0.000004	40.00%	XP_001636659.1	Unknown
not_predicted	aul_smart_655777|CDS1	uncharacterized protein LOC5514703 [Nematostella vectensis]	4.00E-12	46.97%	XP_001634867.1	Unknown
not_predicted	aul_smart_801984|CDS3	uncharacterized protein LOC110248864 [Exaiptasia diaphana]	3.00E-15	79.41%	XP_020911082.1	Unknown
not_predicted	aul_smart_879877|CDS4	uncharacterized protein ZK643.6-like [Actinia tenebrosa]	1.00E-41	48.12%	XP_031564778.1	Unknown
not_predicted	aul_smart_94777|CDS1	uncharacterized protein LOC116307697 [Actinia tenebrosa]	5.00E-36	50.00%	XP_031573854.1	Unknown
not_predicted	aul_smart_537788|CDS1	uncharacterized protein LOC116299719 [Actinia tenebrosa]	2E-68	56.21%	XP_031564297.1	Unknown
not_predicted	aul_smart_729693|CDS1	uncharacterized protein LOC116307044 [Actinia tenebrosa]	8.00E-06	38.60%	XP_031573043.1	Unknown
not_predicted	aul_smart_798440|CDS8	uncharacterized protein LOC116306945 [Actinia tenebrosa]	5.00E-16	78.05%	XP_031572946.1	Unknown
not_predicted	aul_smart_887641|CDS5	uncharacterized protein LOC116297541 [Actinia tenebrosa]	4.00E-170	77.24%	XP_031561646.1	Unknown
not_predicted	aul_smart_618124|CDS2	uncharacterized protein LOC116290938 [Actinia tenebrosa]	1.00E-44	80.22%	XP_031553922.1	Unknown
not_predicted	aul_smart_839488|CDS2	uncharacterized protein LOC116286868 [Actinia tenebrosa]	5.00E-72	45.27%	XP_031549315.1	Unknown
not_predicted	aul_smart_869134|CDS1	uncharacterized protein LOC116297886 [Actinia tenebrosa]	1.00E-65	68.94%	XP_031562063.1	Unknown
not_predicted	aul_smart_6116|CDS4	uncharacterized protein LOC116294264 [Actinia tenebrosa]	4.00E-50	75.27%	XP_031557684.1	Unknown
not_predicted	aul_smart_53068|CDS1	hypothetical protein AC249_AIPGENE27263 [Exaiptasia diaphana]	2.00E-130	59.18%	KXJ07853.1	Unknown
not_predicted	aul_smart_91044|CDS4	uncharacterized protein LOC116296924 [Actinia tenebrosa]	4.00E-97	65.27%	XP_031560904.1	Unknown
not_predicted	aul_smart_92667|CDS2	uncharacterized protein LOC116308711 [Actinia tenebrosa]	0.48	27.03%	XP_031575053.1	Unknown
not_predicted	aul_smart_83228|CDS1	uncharacterized protein LOC116290232 [Actinia tenebrosa]	2E-142	78.90%	XP_031553099.1	Unknown
not_predicted	aul_smart_944968|CDS3	hypothetical protein AC249_AIPGENE28876 [Exaiptasia pallida]	0.93	21.74%	KXJ20930.1	Unknown
not_predicted	aul_smart_756128|CDS1	uncharacterized protein LOC116299739 [Actinia tenebrosa]	2.00E-38	51.88%	XP_031564316.1	Unknown
not_predicted	aul_smart_837956|CDS2	uncharacterized protein LOC116296995 [Actinia tenebrosa]	5.00E-104	58.87%	XP_031560985.1	Unknown
not_predicted	aul_smart_850753|CDS4	uncharacterized protein LOC116306321 [Actinia tenebrosa]	5.00E-76	64.50%	XP_031572215.1	Unknown
not_predicted	aul_smart_976448|CDS1	basic proline-rich protein-like [Actinia tenebrosa]	1.00E-129	79.30%	XP_031570185.1	Unknown
not_predicted	aul_smart_885416|CDS4	uncharacterized protein LOC116302789 [Actinia tenebrosa]	0	67.38%	XP_031568018.1	Unknown
not_predicted	aul_smart_9946|CDS1	uncharacterized protein LOC116308971 isoform X1 [Actinia tenebrosa]	3.00E-60	54.97%	XP_031575359.1	Unknown
PT	aul_smart_41006|CDS2	uncharacterized protein LOC110245270 [Exaiptasia diaphana]	9.00E-79	39.67%	XP_020907189.1	Unknown
ShK repeat	aul_smart_116802|CDS7	uncharacterized protein LOC116291117 [Actinia tenebrosa]	2.00E-156	62.12%	XP_031554099.1	Unknown
Trypan_PARP	aul_smart_502041|CDS2	mucin-2 [Nematostella vectensis]	0.002	35.42%	XP_032230364.1	Unknown
VWC (IPR001007, two recognised SMART domains SM00214)	aul_smart_128724|CDS3	cysteine-rich motor neuron 1 protein-like [Actinia tenebrosa]	1.00E-54	52.35%	XP_031549053.1	Unknown

Supplementary Material 2

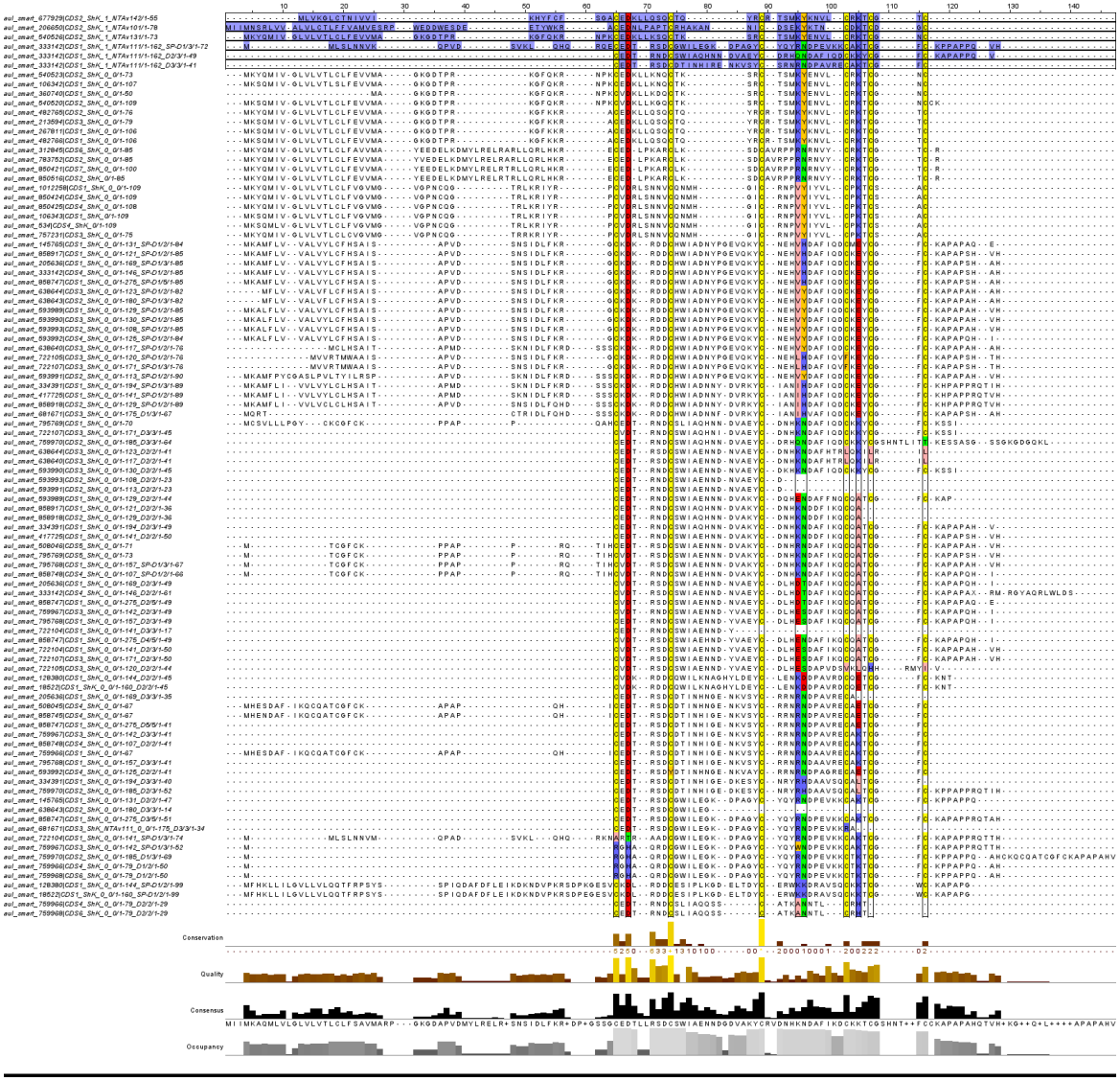

Supplementary 2.1. Amino acid sequences from ShK-like putative toxins found in the proteome (blue) and transcriptome from *A. veratra*. The residues (**C**X**D**Xn**C**Xn**C**Xn**KK**Xn**C**X**K**X**C**X2**C**) characteristic of ShK domain are highlighted. C represents cysteine residues; D- aspartic acid residues; K-Lysin residues; X correspond to any amino acid; and n correspond to a variable number (3 - 6) of amino acids. Sequences presenting double, triple or more ShK domains were split into the number of domains found (D1 to D5). Such homologues can be identified with D1 to D5 at the end of the sequence ID (identification).

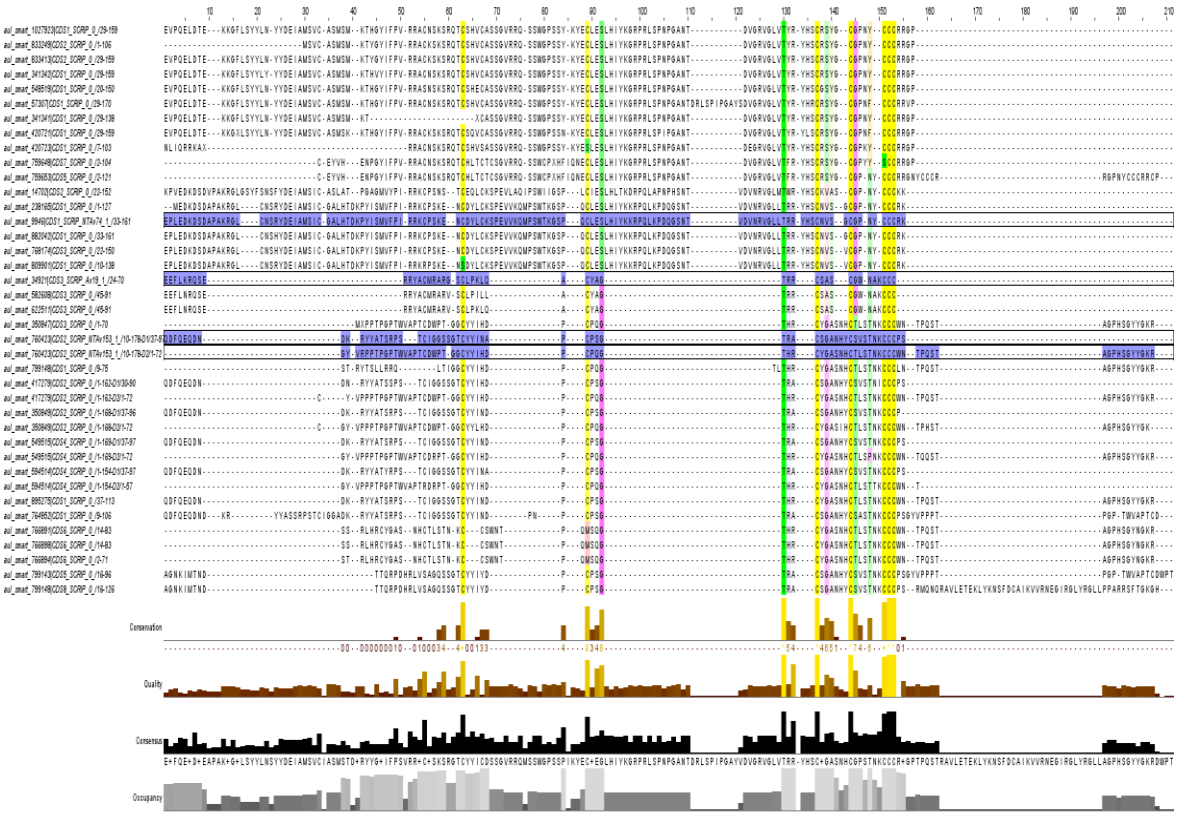

Supplementary 2.2. Amino acid sequences from SCRiP putative toxins found in the proteome (blue) and transcriptome from *A. veratra*. The six cysteine residues characteristic from SCRiP domain (CX6CX6CX6CXnCXnCCC) are highlighted. C represents cysteine residues; X correspond to any amino acid; n represents a variable number (3 - 6) of amino acids. Sequences presenting double domains were split in two parts (D1 and D2). Such homologues can be identified with D1 and D2 at the end of the sequence ID. The signal peptide from sequences was removed for better visualization.

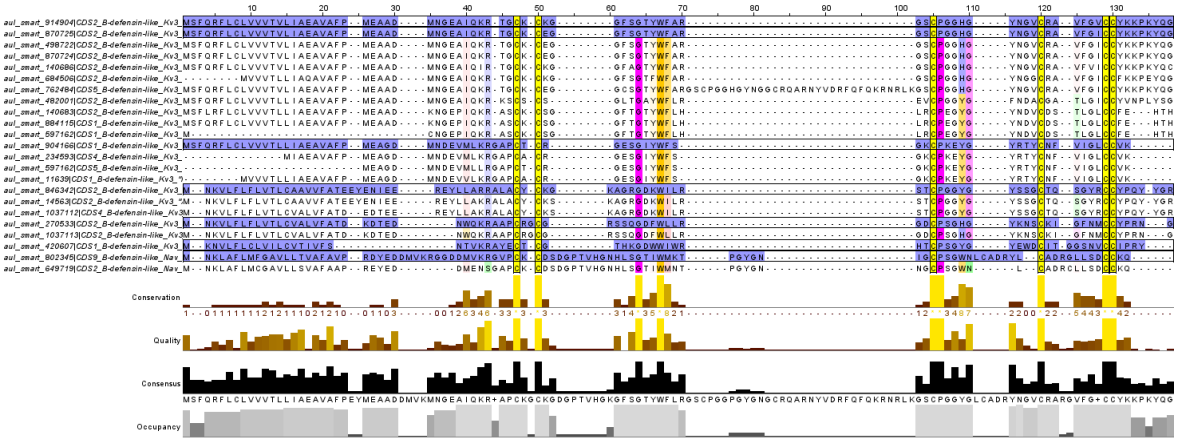

Supplementary 2.3. Amino acid sequences from putative β-desensins found in the proteome (blue) and transcriptome from *A. veratra*. The six cysteine residues (C1-C5, C2-C4, C3-C6) characteristic from the domain are highlighted.

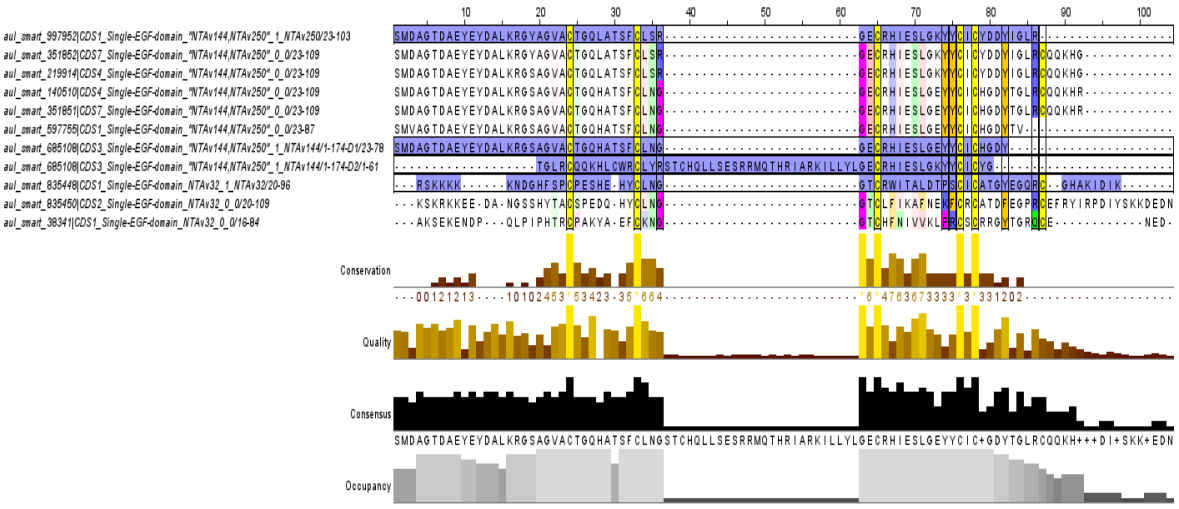

Supplementary 2.4. Amino acid sequences from EGF-like putative toxins found in the proteome (blue) and transcriptome from *A. veratra*. The conserved amino acids characteristics of EGF-like domain are highlighted. Sequences presenting double domains were split in two parts (D1 and D2). Such homologues can be identified with D1 and D2 at the end of the sequence ID. The signal peptide from sequences was removed for better visualization.

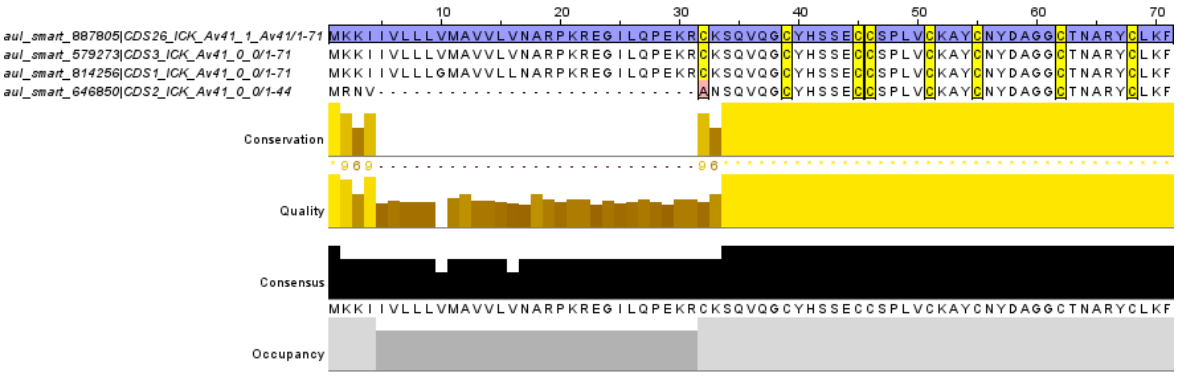

Supplementary material 2.5. Amino acid sequences from ICK putative toxins found in the proteome (blue) and transcriptome from *A. veratra*. The six cysteine residues (CXnCXnCCXnCXnC) characteristic of ICK domain are highlighted. C represents cysteine residues; X correspond to any amino acid; and n represents a variable number (3 - 6) of amino acids.

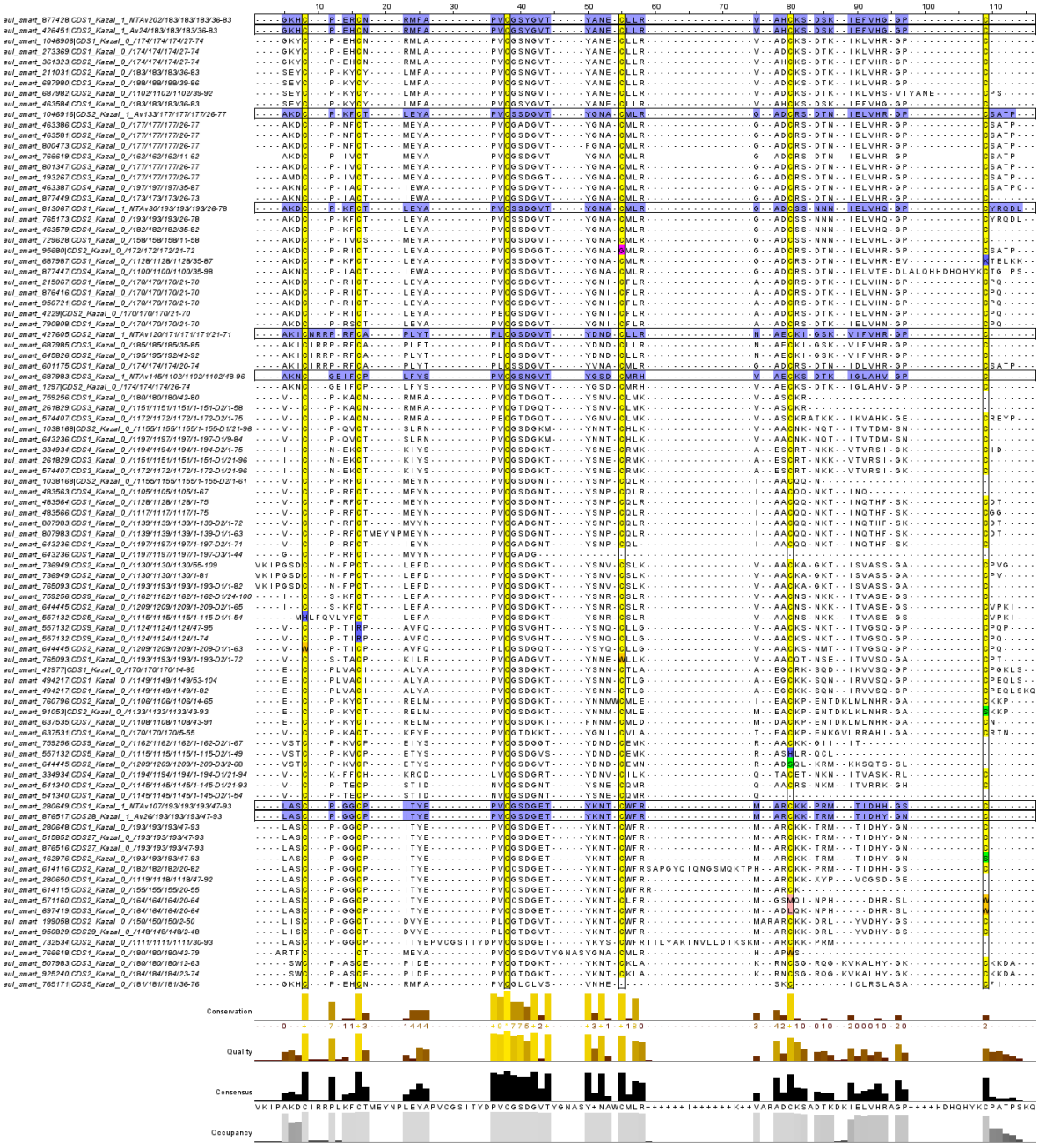

Supplementary material 2.6. Amino acid sequences of putative Kazal inhibitors found in the proteome (blue) and transcriptome from *A. veratra*. The six cysteine residues responsible for forming the disulfide bridges (C1-C5, C2-C4 e C3-C6) characteristic of Kazal domain are highlighted. Sequences presenting repeat domains were split into the number of domains found (D1 to D3). Such homologues can be identified with D1 to D3 at the end of the sequence ID. The signal peptide and C- terminal from sequences were removed for better visualization.

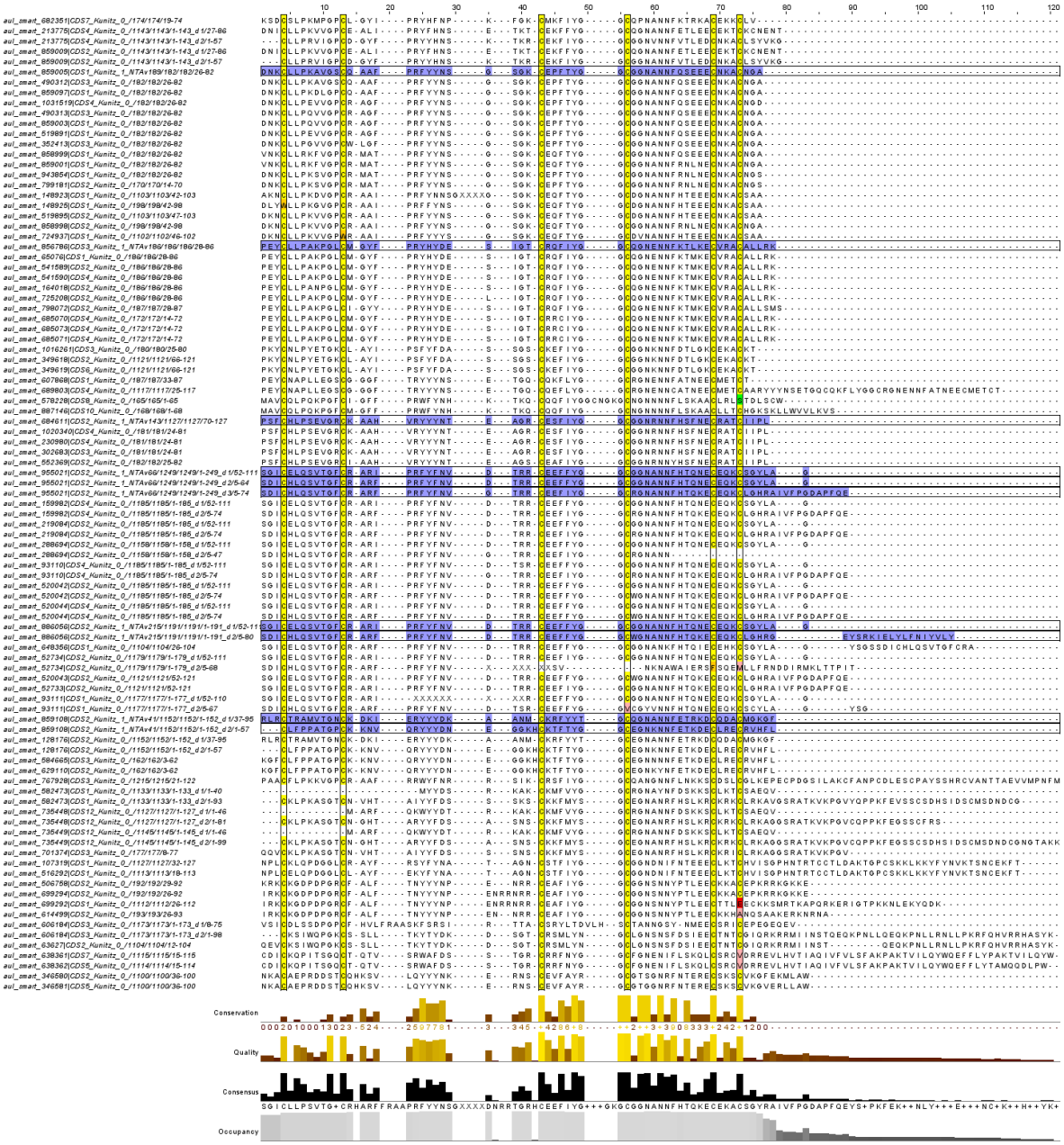

Supplementary material 2.7. Amino acid sequences of putative Kunitz inhibitors found in the proteome (blue) and transcriptome from *A. veratra*. The six cysteine residues responsible for forming the disulfide bridges (C1-C6, C2-C4, C3-C5) characteristic of Kunitz domain are highlighted. Sequences presenting repeat domains were split into the number of domains found (D1 to D3). Such homologues can be identified with D1 to D3 at the end of the sequence ID The signal peptide and C- terminal from sequences were removed for better visualization.

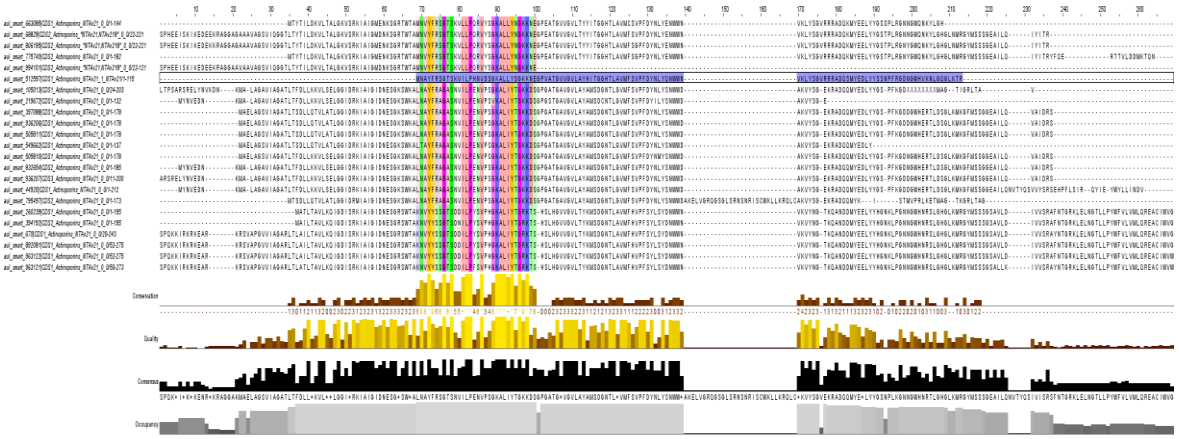

Supplementary material 2.8. Amino acid sequences of putative Actinoporins found in the proteome (blue) and transcriptome from *A. veratra*. The conserved residues characteristics of these toxins domains are highlighted. The signal peptide and C- terminal from sequences were removed for better visualization.

Supplementary material 2.9. Amino acid sequences from MACPF-cytolysins found in the proteome (blue) and transcriptome from *A. veratra*. The conserved residues characteristic these toxins are highlighted. The signal peptide and C- terminal from sequences were removed for better visualization.

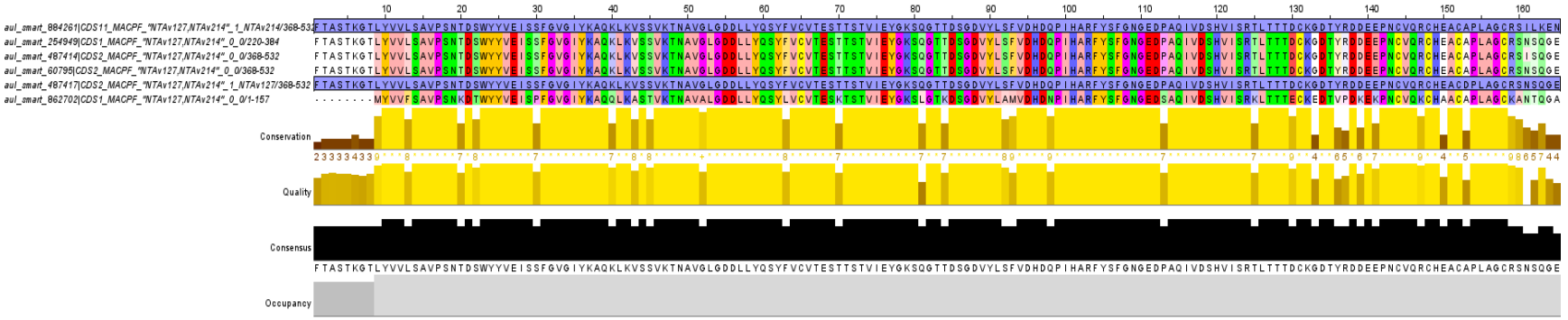

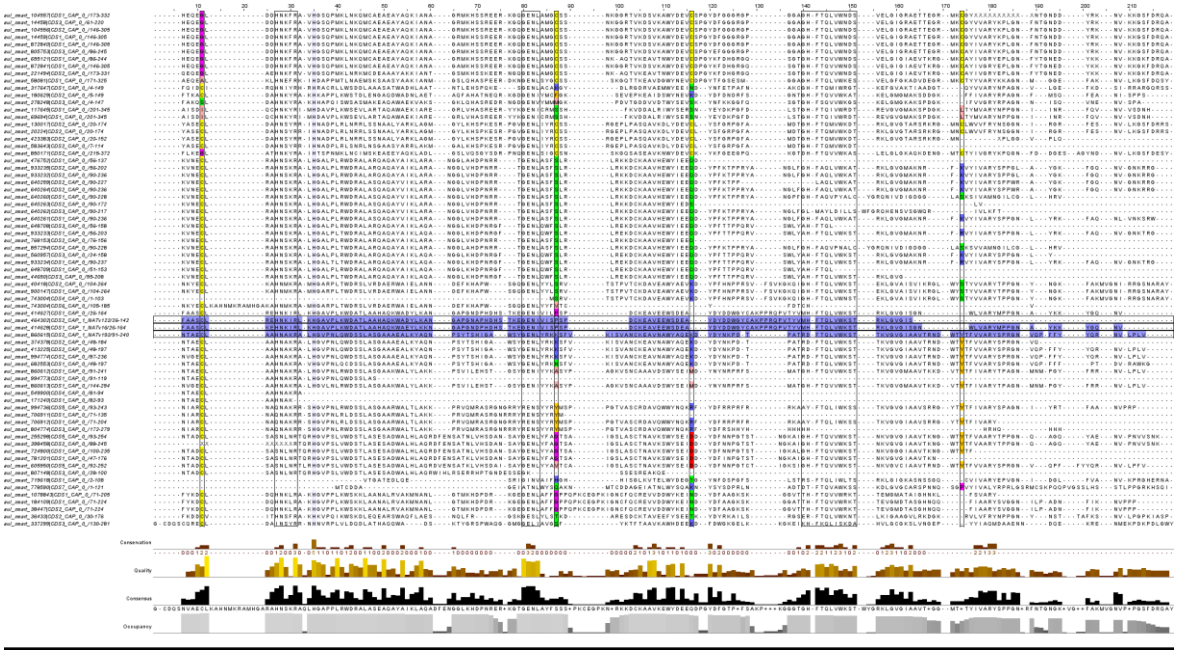

Supplementary material 2.10. Amino acid sequences of putative CAP toxins found in the proteome (blue) and transcriptome from *A. veratra*. CAP family is characterized by four possible motif signatures. The majority of sequences found in *A. veratra* present at least one of three CAP motifs: CAP1, CAP3 and CAP4 domains. CAP1 is represented by [GDER][HR][FYWH][TVS][QA][LIVM][LIVMA]Wxx[STN]; CAP3 by (HNxxR) and CAP4 motif by (G[EQ]N[ILV]). Residues between [] are variable, residues between () are permanent. Such motifs are highlighted. The signal peptide and C- terminal from sequences were removed for better visualization.

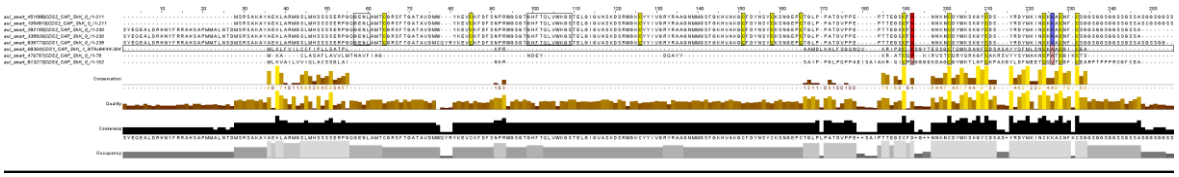

Supplementary material 2.11. Amino acid sequences of putative CAP-ShK toxins found in the transcriptome from *A. veratra*. CAP family is characterized by four possible motif signatures. Sequences presenting CAP motifs (CAP1 or CAP4) associated with ShK domain (CXDXnCXnCXnKKXnCXKXCX2C) were present only in the transcriptome. CAP1 is represented by [GDER][HR][FYWH][TVS][QA][LIVM][LIVMA]Wxx[STN] and CAP4 motif by (G[EQ]N[ILV]). Residues between [] are variable, residues between () are permanent. CAP motifs and ShK domain are highlighted. The signal peptide and C- terminal from sequences were removed for better visualization.

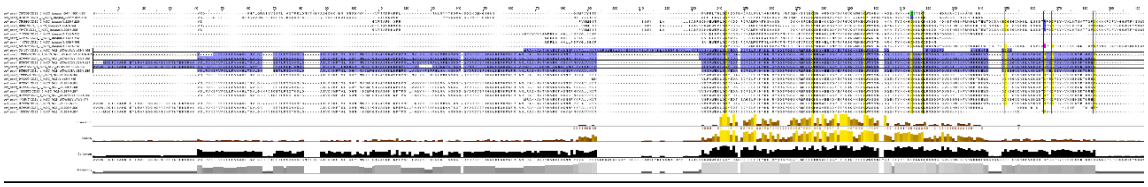

Supplementary material 2.12. Amino acid sequences of putative WSC toxins found in the proteome (blue) and transcriptome from *A. veratra*. The eight cysteine residues ($CX_{31}CX_{19}CX_{15}CX_3CX_{26}CX_{14}CX_2CX_{15}C$) characteristic of WSC domain are highlighted. Cysteine residues (C) are highlighted and X correspond to any amino acid. The signal peptide and C- terminal from sequences were removed for better visualization.

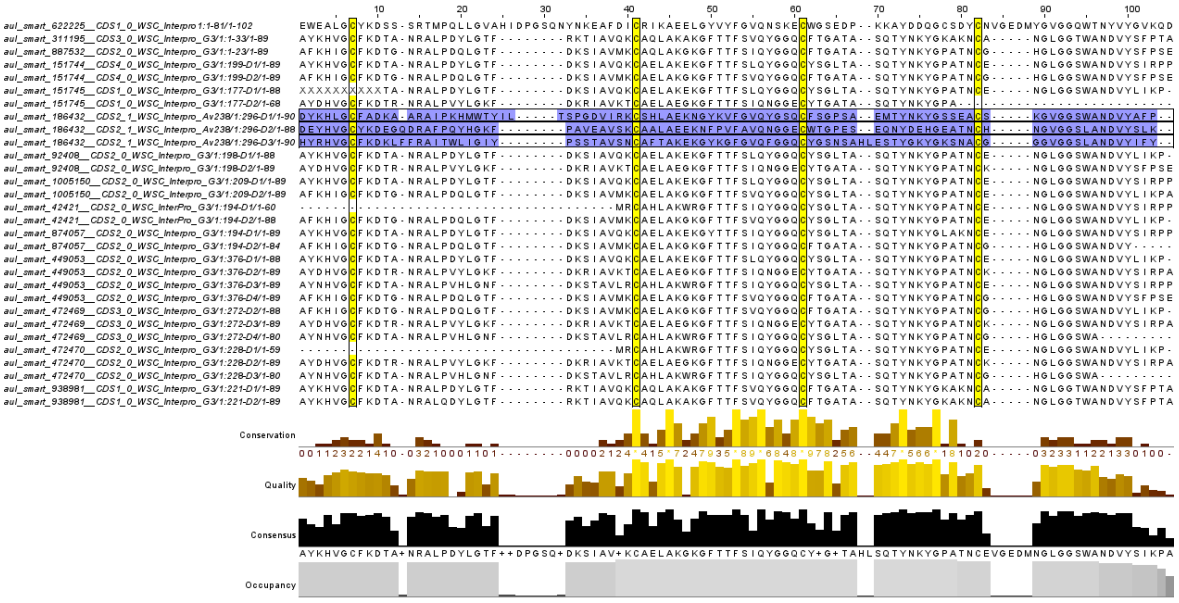

Supplementary material 2.12. Amino acid sequences of putative repeat WSC toxins found in the proteome (blue) and transcriptome from *A. veratra*. Sequences presenting the repeat of four cysteines ($CX_{25}CX_{19}CX_{18}CX_{22}$) were characterised as WSC. Cysteine residues (C) are highlighted and X correspond to any amino acid. Sequences presenting repeat were split into the number of domains found (D1 to D4). Such homologues can be identified with D1 to D4 at the end of the sequence ID. The signal peptide and C- terminal from sequences were removed for better visualization.

Supplementary material 2.13. Amino acid sequences from Scaffold 1 putative toxins found in the proteome (blue) and transcriptome from *A. veratra*. The four cysteine residues ($X_{31}CX_{21}CX_5CX_{33}CX_7$) characteristic from the domain are highlighted. C represents cysteine residues; X correspond to any amino acid. The signal peptide was removed for better visualization.

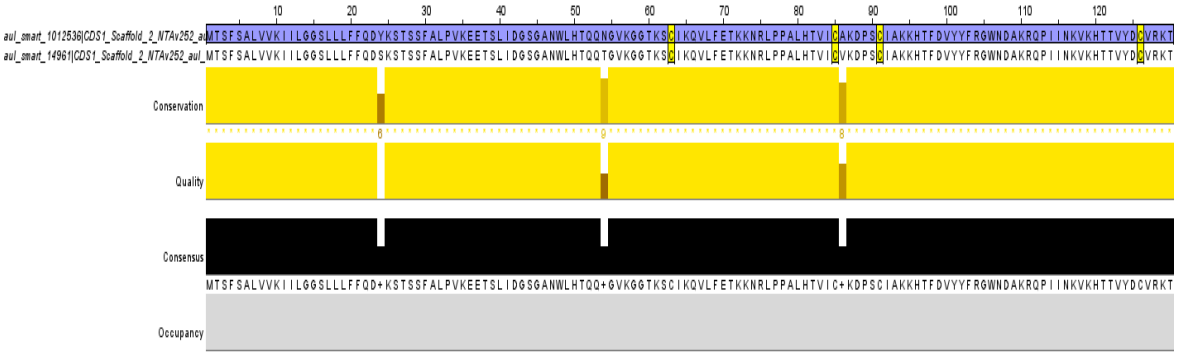

Supplementary material 2.14. Amino acid sequences from Scaffold 2 putative toxins found in the proteome (blue) and transcriptome from *A. veratra*. The four cysteine residues ($CX_{21}CX_5CX_{34}CX_4$) characteristic from the domain are highlighted. C represents cysteine residues; X correspond to any amino acid.

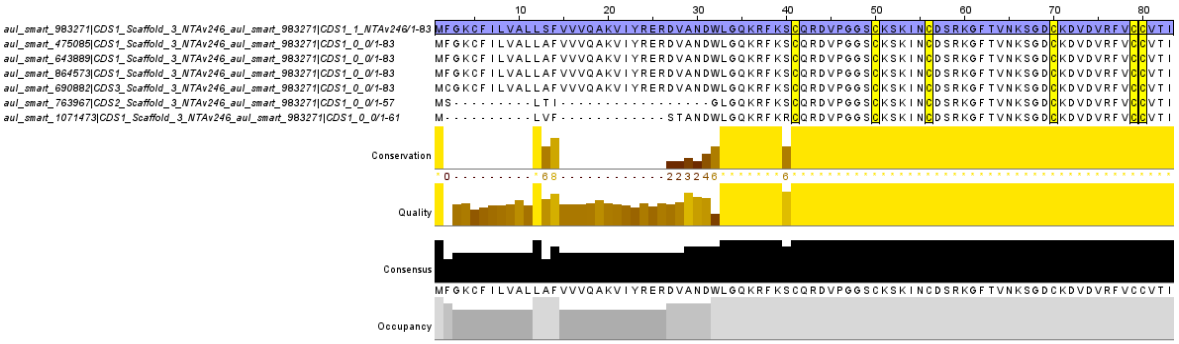

Supplementary material 2.15. Amino acid sequences from Scaffold 3 putative toxins found in the proteome (blue) and transcriptome from *A. veratra*. The six cysteine residues ($X_3CX_8CX_5CX_{13}CX_8CCX_3$) characteristic from the domain are highlighted. C represents cysteine residues; X correspond to any amino acid.

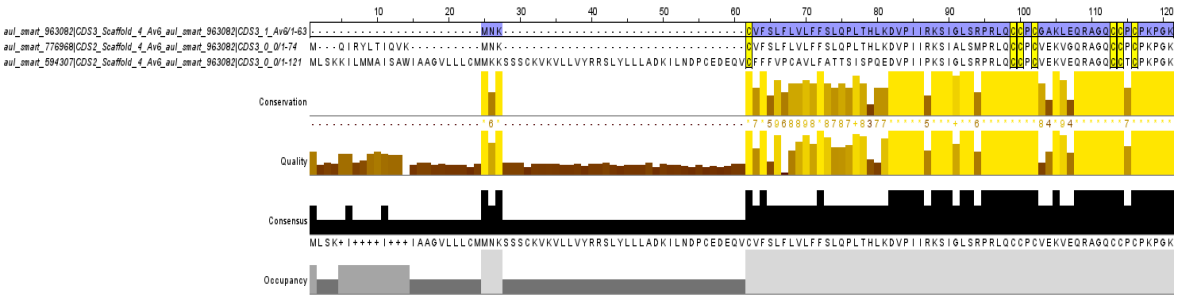

Supplementary material 2.16. Amino acid sequences from Scaffold 4 putative toxins found in the proteome (blue) and transcriptome from *A. veratra*. The six cysteine residues ($X_{10}CCXCX_{10}CCXCX_3$) characteristic from this domain are highlighted. C represents cysteine residues; X correspond to any amino acid.

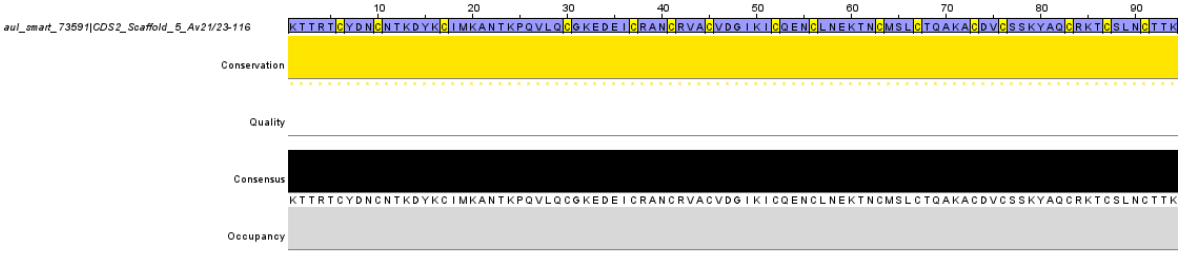

Supplementary material 2.17. Amino acid sequences from Scaffold 5 putative toxin found in the proteome (blue) and transcriptome from *A. veratra*. The sixteen cysteine residues ($X_5CX_3CX_6CX_{12}CX_6CX_3CX_3CX_6CX_3CX_6CX_3CX_5CX_2CX_6CX_3CX_3CX_3$) characteristic from this domain are highlighted. C represents cysteine residues; X correspond to any amino acid.

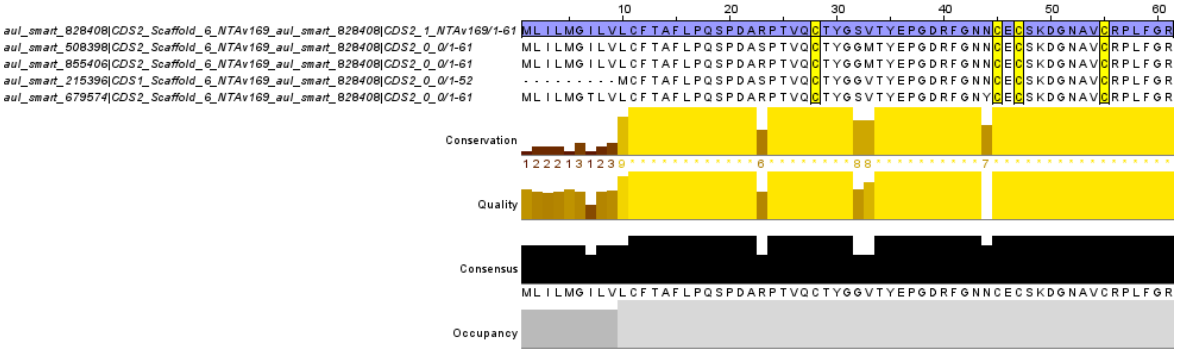

Supplementary material 2.18. Amino acid sequences from Scaffold 6 putative toxins found in the proteome (blue) and transcriptome from *A. veratra*. The four cysteine residues ($X_5CX_{16}CXCX_7CX_6$) characteristic from this domain are highlighted. C represents cysteine residues; X correspond to any amino acid.

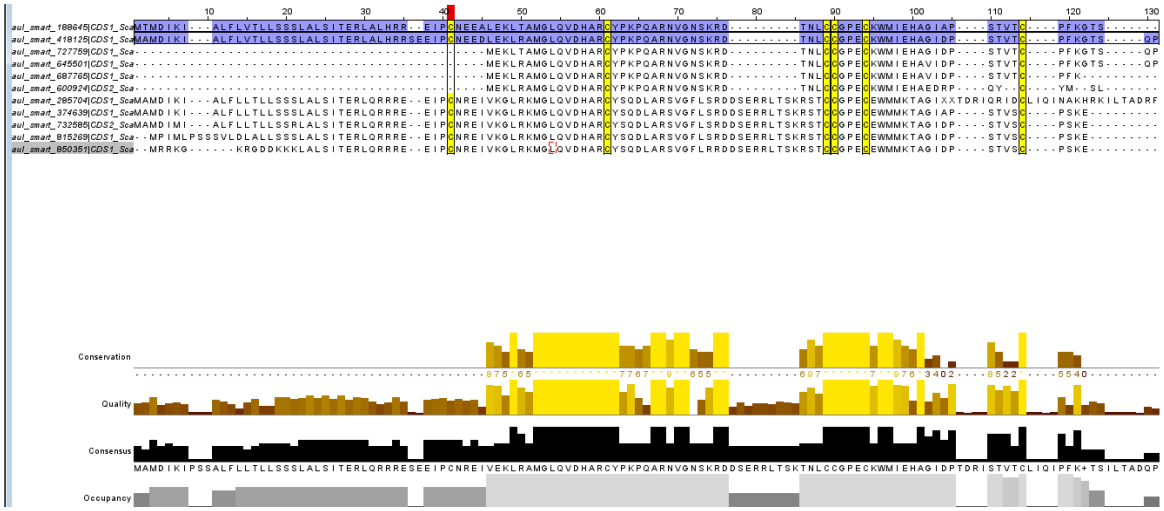

Supplementary material 2.19. Amino acid sequences from Scaffold 7 putative toxins found in the proteome (blue) and transcriptome from *A. veratra*. The six cysteine residues ($X_5CX_{19}CX_{18}CCX_3CX_{15}CX_3$) characteristic from this domain are highlighted. C represents cysteine residues; X correspond to any amino acid.

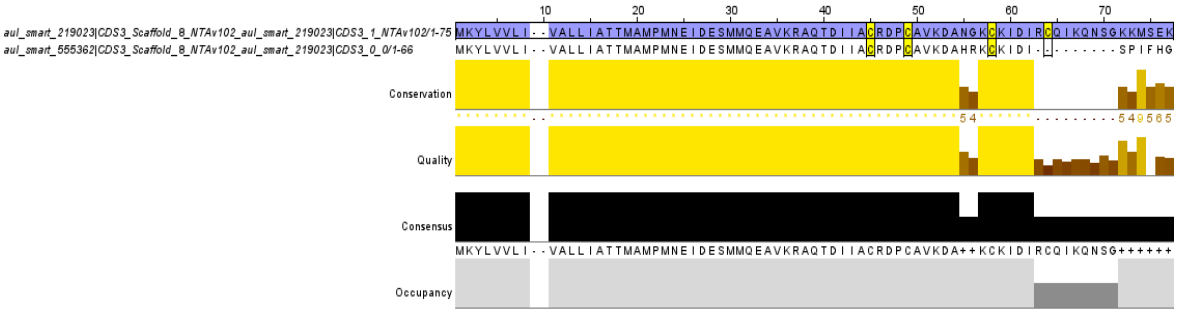

Supplementary material 2.20. Amino acid sequences from Scaffold 8 putative toxins found in the proteome (blue) and transcriptome from *A. veratra*. The six cysteine residues ($X_7CX_3CX_8CX_5CX_6$) characteristic from this domain are highlighted. C represents cysteine residues; X correspond to any amino acid.

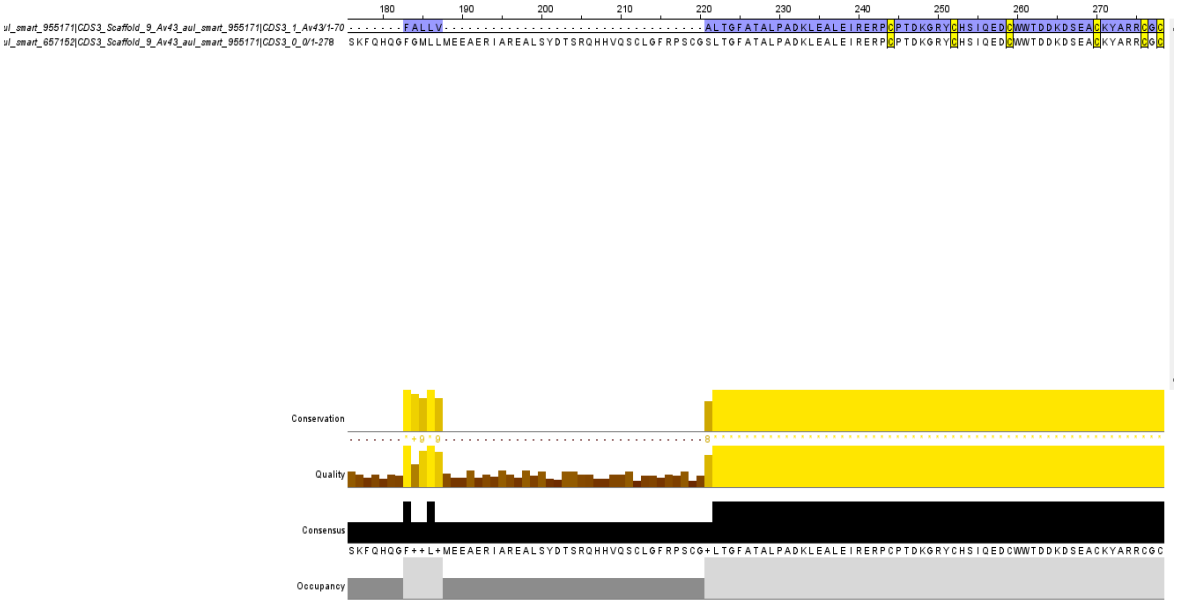

Supplementary material 2.21. Amino acid sequences from Scaffold 9 putative toxins found in the proteome (blue) and transcriptome from *A. veratra*. The six cysteine residues ($X_{15}CX_7CX_6CX_{10}CX_5CXC$) characteristic from this domain are highlighted. C represents cysteine residues; X correspond to any amino acid.

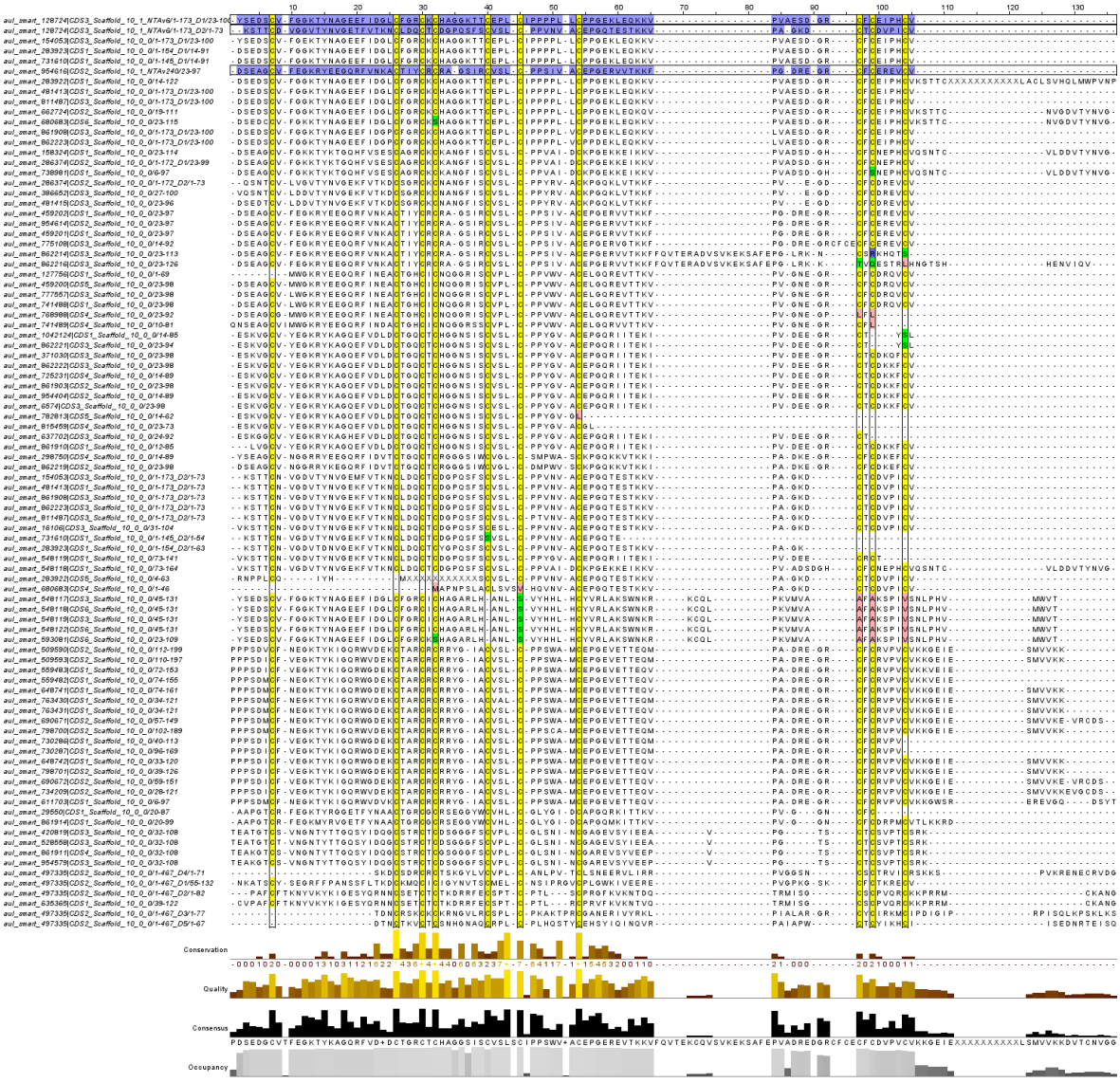

Supplementary material 2.22. Amino acid sequences from Scaffold 10 putative toxins found in the proteome (blue) and transcriptome from *A. veratra*. The ten cysteine residues ($X_3CX_{17}CX_3CXCX_7CX_3CX_7CX_{19}CXCX_4CX_5$) characteristic from this domain are highlighted. C represents cysteine residues; X correspond to any amino acid. Sequences presenting repeat domains were split into the number of domains found (D1 to D2). Such homologues can be identified with D1 and D2 at the end of the sequence ID. The signal peptide and C- terminal from sequences were removed for better visualization.

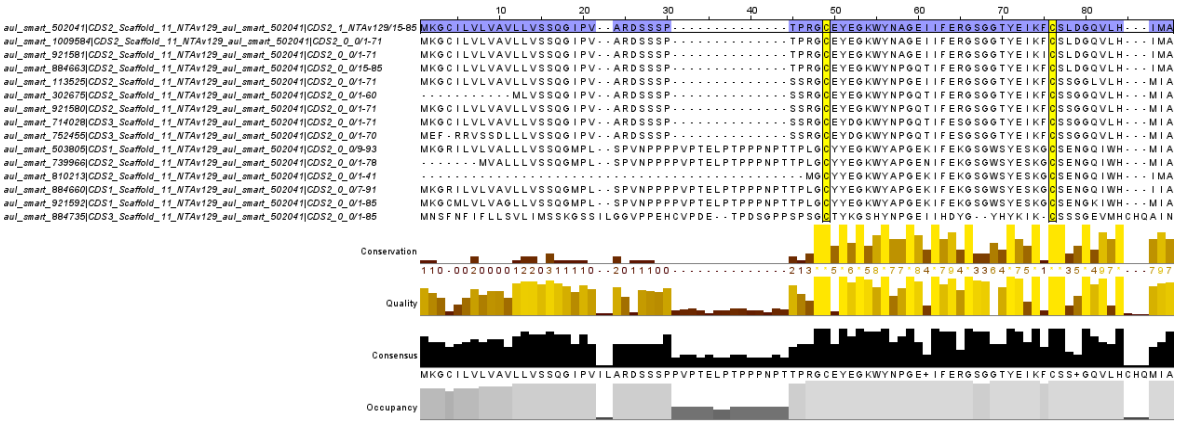

Supplementary material 2.23. Amino acid sequences from Scaffold 11 putative toxins found in the proteome (blue) and transcriptome from *A. veratra*. The two cysteine residues ($X_{16}CX_{26}CX_{10}$) characteristic from this domain are highlighted. C represents cysteine residues; X correspond to any amino acid.

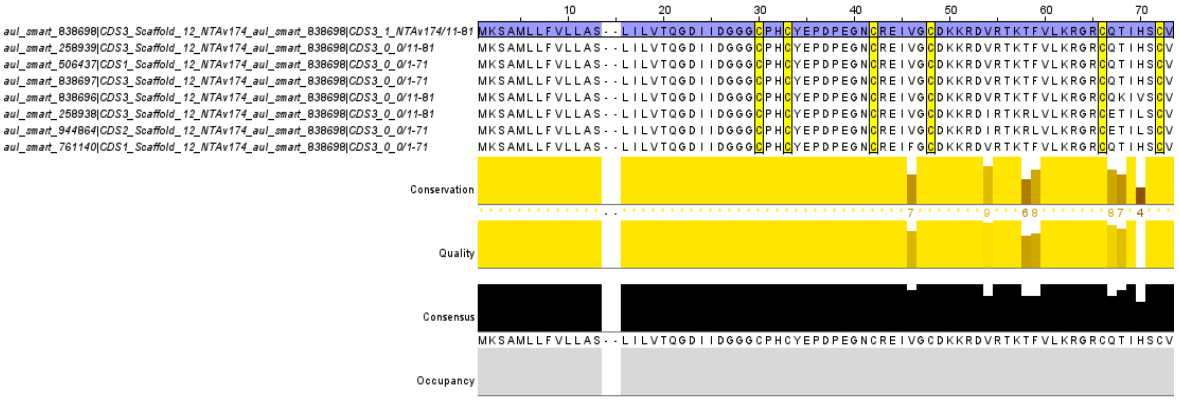

Supplementary material 2.24. Amino acid sequences from Scaffold 12 putative toxins found in the proteome (blue) and transcriptome from *A. veratra*. The six cysteine residues ($X_7CX_2CX_8CX_5CX_{17}CX_5CX$) characteristic from this domain are highlighted. C represents cysteine residues; X correspond to any amino acid.

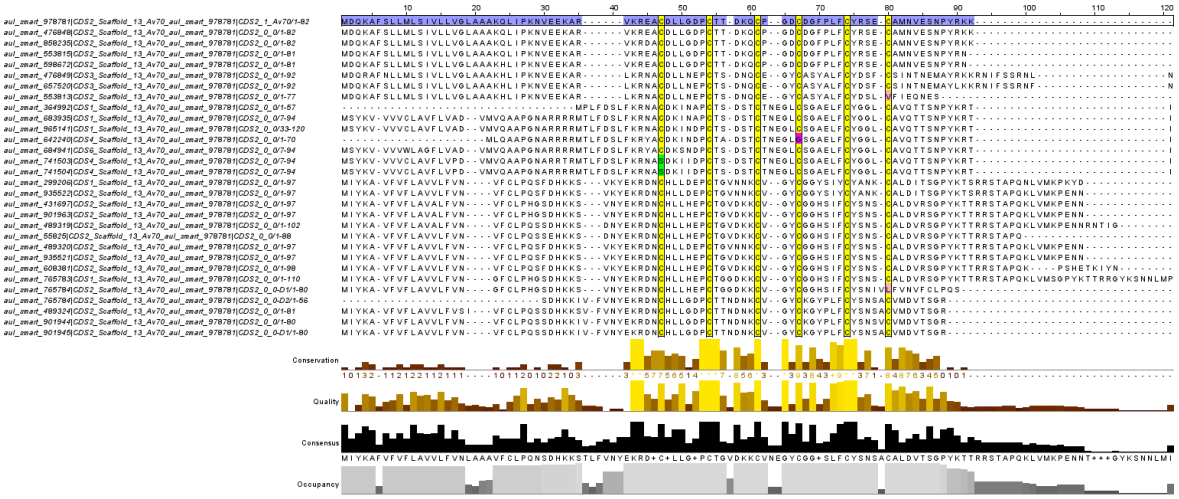

Supplementary material 2.25. Amino acid sequences from Scaffold 13 putative toxins found in the proteome (blue) and transcriptome from *A. veratra*. The six cysteine residues ($X_2CX_6CX_5CX_3CX_6CX_4CX_{12}$) characteristic from this domain are highlighted. C represents cysteine residues; X correspond to any amino acid.

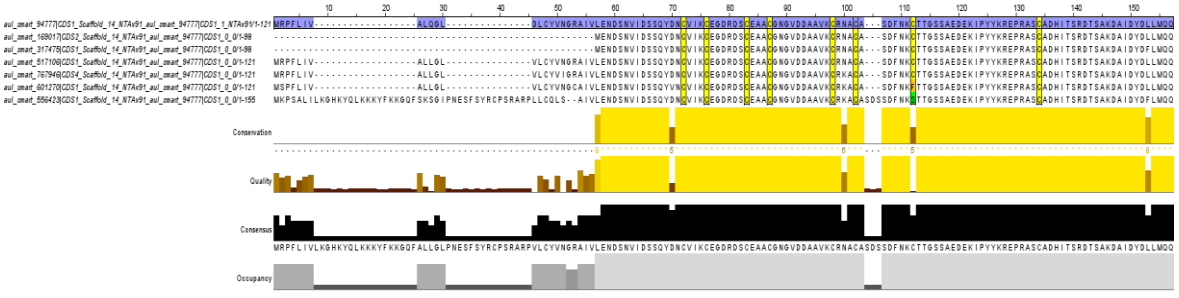

Supplementary material 2.26. Amino acid sequences from Scaffold 14 putative toxins found in the proteome (blue) and transcriptome from *A. veratra*. The eight cysteine residues ($X_{19}CX_3CX_6CX_3CX_{10}CX_3CX_6CX_{21}CX_{23}$) characteristic from this domain are highlighted. C represents cysteine residues; X correspond to any amino acid.

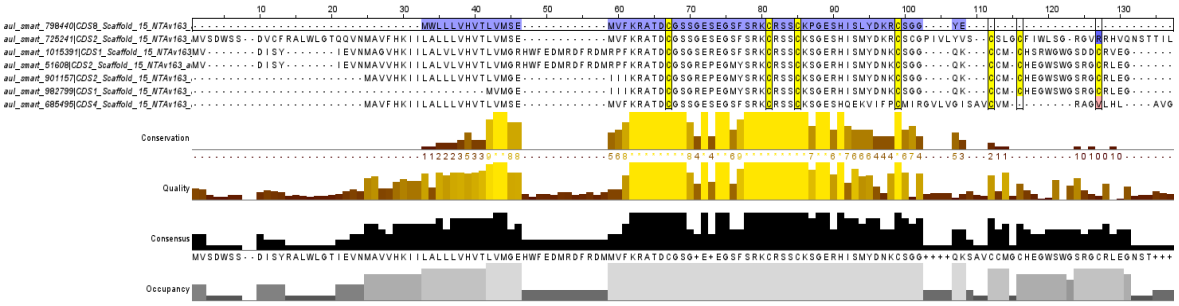

Supplementary material 2.27. Amino acid sequences from Scaffold 15 putative toxins found in the proteome (blue) and transcriptome from *A. veratra*. The four cysteine residues ($X_3CX_{13}CX_3CX_{13}CX_5$) characteristic from this domain are highlighted. C represents cysteine residues; X correspond to any amino acid.

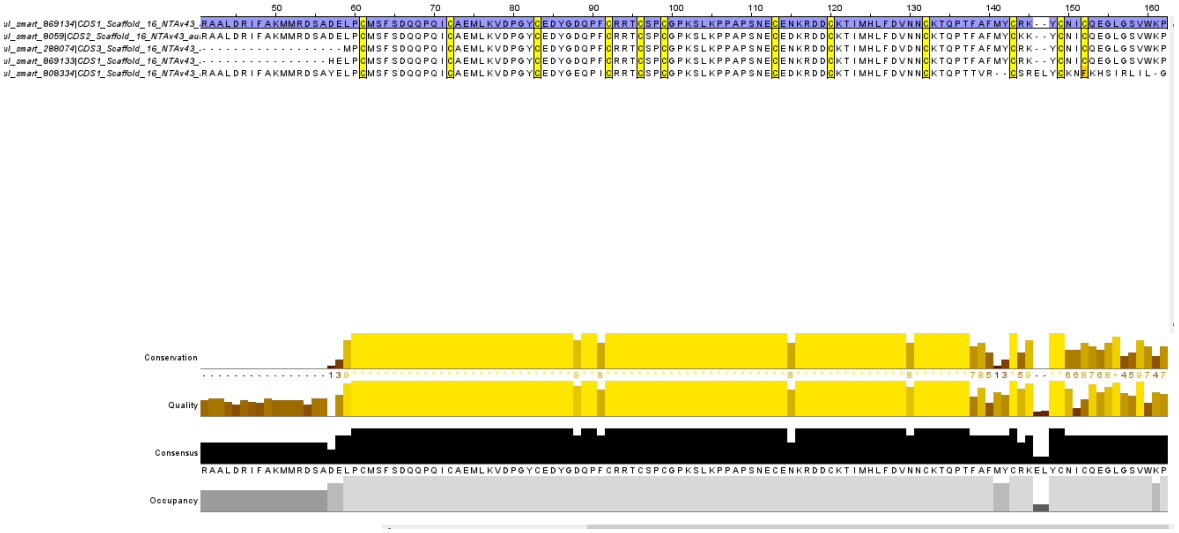

Supplementary material 2.28. Amino acid sequences from Scaffold 16 putative toxins found in the proteome (blue) and transcriptome from *A. veratra*. The twelve cysteine residues ($X_{19}CX_{10}CX_{10}CX_8CX_3CX_2CX_{13}CX_6CX_{11}CX_{10}CX_3CX_2CX_{10}$) characteristic from this domain are highlighted. C represents cysteine residues; X correspond to any amino acid.

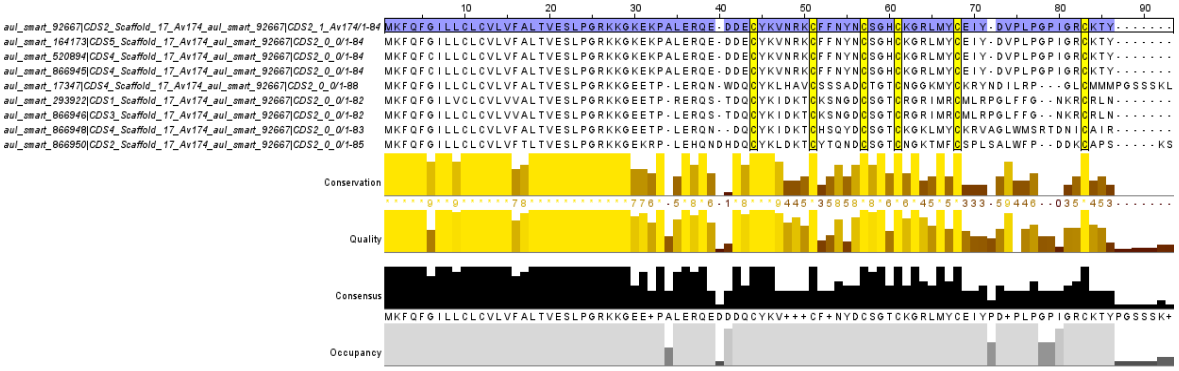

Supplementary material 2.29. Amino acid sequences from Scaffold 17 putative toxins found in the proteome (blue) and transcriptome from *A. veratra*. The six cysteine residues ($X_4CX_6CX_5CX_3CX_6CX_{13}CX_3$) characteristic from this domain are highlighted. C represents cysteine residues; X correspond to any amino acid.

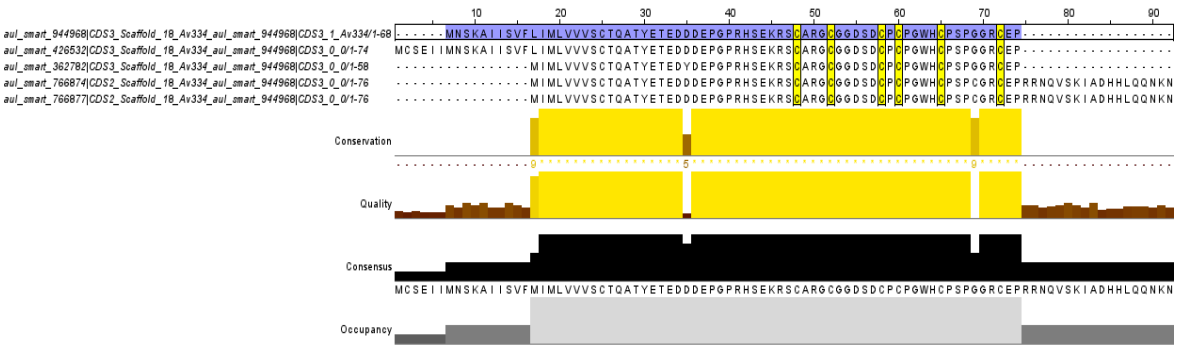

Supplementary material 2.30. Amino acid sequences from Scaffold 18 putative toxins found in the proteome (blue) and transcriptome from *A. veratra*. The six cysteine residues ($XCX_3CX_5CXCX_4CX_6CX_2$) characteristic from this domain are highlighted. C represents cysteine residues; X correspond to any amino acid.

Supplementary Material 3

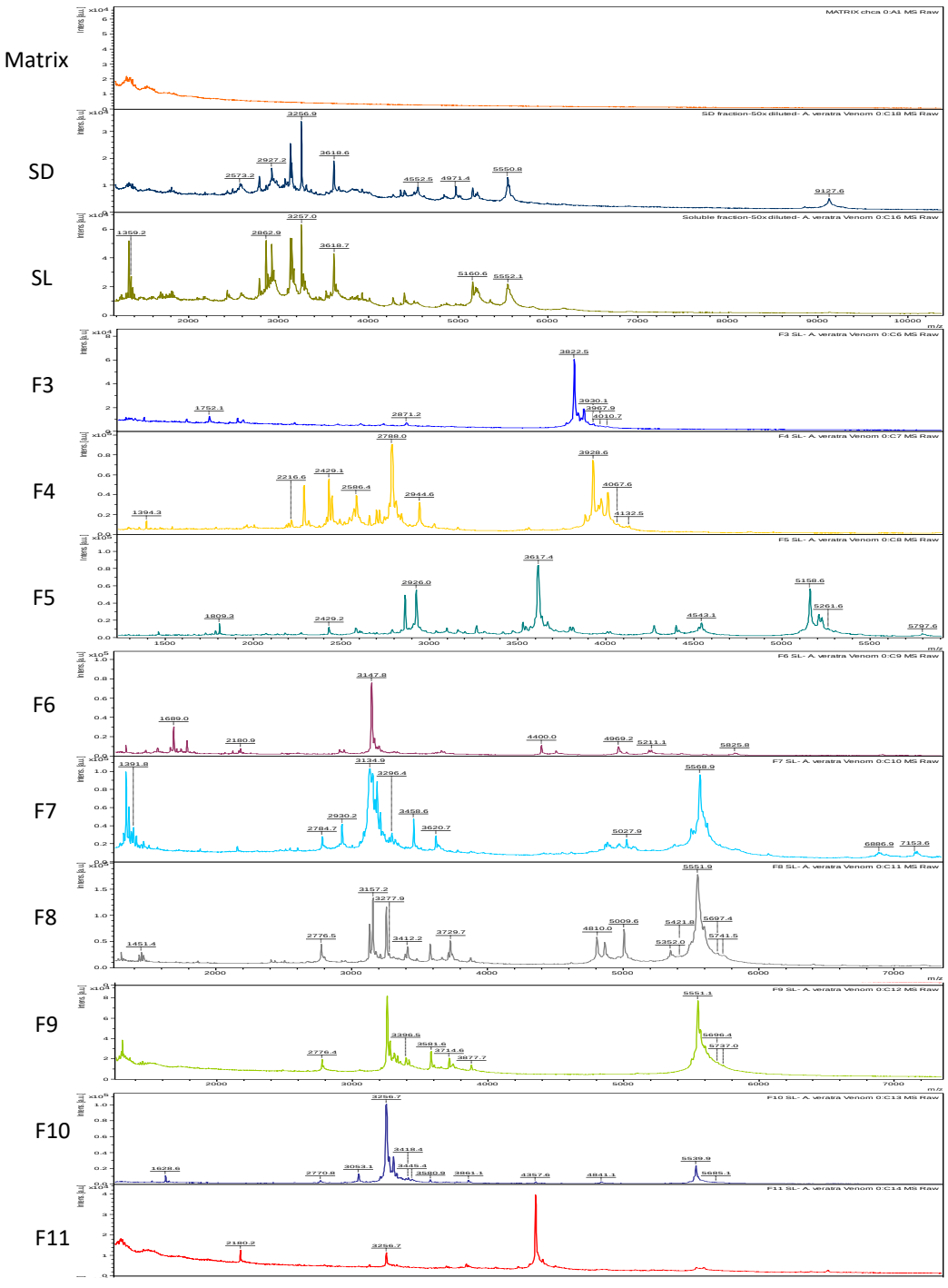

Supplementary material 3. MALDI-TOF analysis of venom's fractions from *A. veratra.* The mass spectra show m/z ranging from 1000 to 10000. The profile of the CHCA matrix is shown as the spectrum above SD. The m/z profile of precipitate fraction (SD), soluble fraction (SL) and RP-HPLC fractions from the venom (F3-F11) was acquired in linear positive mode. F1 and F2 did not present ionization.

ANEXOS

ANEXO A – ARTIGO PUBLICADO NA TOXINS – Neglected Venomous Animals and Toxins: Underrated Biotechnological Tools in Drug Discovery

Toxins 2021, 13, 851. https://doi.org/10.3390/toxins13120851

toxins

MDPI

Review

Neglected Venomous Animals and Toxins: Underrated Biotechnological Tools in Drug Development

Guilherme Rabelo Coelho [1], Daiane Laise da Silva [1], Emidio Beraldo-Neto [1], Hugo Vigerelli [2], Laudiceia Alves de Oliveira [3], Juliana Mozer Sciani [4] and Daniel Carvalho Pimenta [1,*]

1 Laboratório de Bioquímica, Instituto Butantan, São Paulo 05503-900, Brazil; guilherme.coelho@butantan.gov.br (G.R.C.); daiane.silva@esib.butantan.gov.br (D.L.d.S.); emidio.beraldo@butantan.gov.br (E.B.-N.)
2 Laboratório de Genética, Instituto Butantan, São Paulo 05503-900, Brazil; hugo.barros@esib.butantan.gov.br
3 Laboratório de Moléstias Infecciosas—Faculdade de Medicina de Botucatu, São Paulo State University (UNESP), São Paulo 01049-010, Brazil; laudiceia.oliveira@unesp.br
4 Laboratório Multidisciplinar em Pesquisa, Universidade São Francisco, Bragança Paulista 12916-900, Brazil; juliana.sciani@usf.edu.br
* Correspondence: dcpimenta@butantan.gov.br

Abstract: Among the vast repertoire of animal toxins and venoms selected by nature and evolution, mankind opted to devote its scientific attention—during the last century—to a restricted group of animals, leaving a myriad of toxic creatures aside. There are several underlying and justifiable reasons for this, which include dealing with the public health problems caused by envenoming by such animals. However, these studies became saturated and gave rise to a whole group of animals that become neglected regarding their venoms and secretions. This repertoire of unexplored toxins and venoms bears biotechnological potential, including the development of new technologies, therapeutic agents and diagnostic tools and must, therefore, be assessed. In this review, we will approach such topics through an interconnected historical and scientific perspective that will bring up the major discoveries and innovations in toxinology, achieved by researchers from the Butantan Institute and others, and describe some of the major research outcomes from the study of these neglected animals.

Keywords: toxins; venoms; skin secretion; drug discovery

Key Contribution: This review brings up the issue of the limitations in current toxinology, that is the poor appraisal of the poisonous animals, opposed to the venomous ones. It is meant to expand the readers' perspective on venoms and toxins and the possible scientific developments associated with these thematic lines of research.

check for updates

Citation: Coelho, G.R.; da Silva, D.L.; Beraldo-Neto, E.; Vigerelli, H.; de Oliveira, L.A.; Sciani, J.M.; Pimenta, D.C. Neglected Venomous Animals and Toxins: Underrated Biotechnological Tools in Drug Development. *Toxins* 2021, *13*, 851. https://doi.org/10.3390/toxins13120851

Received: 16 October 2021
Accepted: 25 November 2021
Published: 29 November 2021

Publisher's Note: MDPI stays neutral with regard to jurisdictional claims in published maps and institutional affiliations.

1. Introduction

"Around 1896, a modest physician that used to practice medicine in Botucatu became notorious due to his strange fascination with snakes and their venoms. It was Dr Vital Brazil that, from the tranquility of the countryside, was taking the initial steps on the brilliant research that would make him famous not only in Brazil but also all over the educated world". This free translation of the beginning of the first paragraph (Figure 1C) of the book "Memória Histórica do Instituto Butantan" (Figure 1A; Historic memory of Butantan Institute, in free translation) written by Dr Vital Brazil himself (Figure 1B) [1] refers to published news in 1914 reporting the inauguration of 'new facilities' in the Institute (Figure 1C).

Over one hundred years after the news reported above, some of the authors of this review have worked, conducted research, performed experiments, and published papers in this exact same building. Since then, a lot has changed in the Institute, including its slogan, but not the building (Figure 2). Our slogan is now "at the service of life", a humbler commitment to the institutional mission, and the research laboratories have been

decommissioned from this building, which is currently undergoing restoration and will be dedicated to cultural activities only.

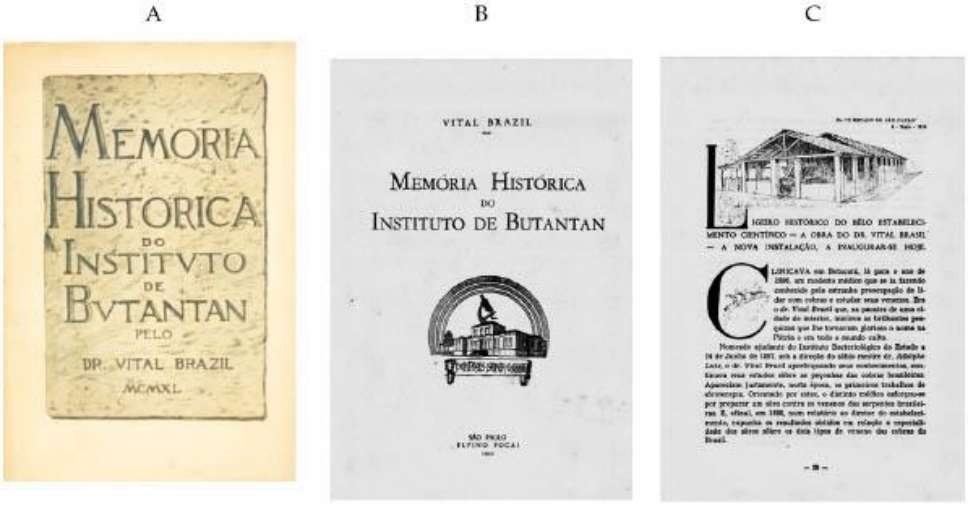

Figure 1. Selected reproductions of (**A**) the book written by Vital Brazil in 1941. This and other classic books are available at https://bibliotecadigital.butantan.gov.br/, accessed on 19 November 2021. Please note the institute logo in (**B**). It is the depiction of the main-laboratory building, underneath a microscope, bearing the motto "peritas super omnia", meaning "expert in everything" in Latin. (**C**) News advertising the inauguration of new facilities at the Institute, in 1914.

Figure 2. (**A**) A recent photograph of the main-laboratory building, in a similar framing as depicted in Figure 1. (**B**) Current Institute logotype, bearing the slogan 'A serviço da vida' (at the service of life, in free translation).

1.1. *The Origins of Negligence*

There are twenty (tropical) diseases that are officially classified as 'neglected tropical diseases' by the World Health Organization (WHO) [2]. Neglected tropical diseases persist under conditions of poverty and are concentrated almost exclusively in impoverished populations in the developing world. They are: Buruli ulcer, Chagas disease, Dengue and Chikungunya (only WHO, not CDC), Dracunculiasis, Echinococcosis, Yaws, Fascioliasis, African trypanosomiasis, Leishmaniasis, Leprosy, Lymphatic filariasis, Onchocerciasis, Rabies, Schistosomiasis, Soil-transmitted helminthiasis, Cysticercosis, Trachoma, Scabies and other ectoparasites, Snakebite envenoming, Mycetoma and deep mycoses. These diseases are common in 149 countries,

affecting more than 1.4 billion people (including more than 500 million children) and costing developing economies billions of dollars every year.

The importance of neglected tropical diseases has been underestimated since many are asymptomatic and have long incubation periods. The connection between a death and a neglected tropical disease that has been latent for a long period of time is not often realized. Additionally, neglected tropical diseases are often associated with some kind of social stigma, making their treatment more complex.

From the toxinology perspective, one can also consider that there are 'neglected' venomous and poisonous animals by employing very similar criteria to justify such negligence: Human accidents occur with individuals who are often amongst the poorest populations, living in remote, rural areas, urban slums or conflict zones; the accident causes no rapid death of the victim and/or such animals are stigmatized (cause bad luck, carry evil spells or are cursed).

Depending on the nature and origin of the venom or toxin, one can clearly perceive that there are 'preferred' subjects and matters in the field of toxinology (Table 1). Probably due to historical and/or epidemiological factors, some animals and venoms—normally the ones that elicit acute, severe lesions due to some pronounced biological activity—were selected (or elected) as 'more relevant' to the field and have been thoroughly studied throughout the years. Endemic animals, such as spiders and scorpions that have adapted to urban environments, have also 'deserved' more attention than other species. All the consulted databases indicated that there is more literature on snakes, spiders and scorpions (the triad) than the others. Interestingly, Scopus and Web of Science present the same publications ratio for triad:neglected (7.8), whereas Google and PubMed display lower ratios (5.5 and 1.8 respectively), probably due to the differences in indexed publications queried.

Table 1. Total results retrieved according to the searched terms in different academic databases.

Term	PubMed	Scopus	Web of Knowledge	Google Scholar
Snake	29,272	56,112	44,467	771,000
Scorpion	7030	10,362	8834	91,000
Spider	15,988	42,351	39,343	1,180,000
TOTAL	52,290	108,825	92,644	2,042,000
Amphibian (skin) [1]	7714	3549	3338	134,000
Sea urchin (toxin) [2]	314	183	170	19,300
Mollusk [3]	3688	902	290	19,800
Stingray	813	1717	1817	2160
Cnidarian (toxins)	2389	913	162	17,700
Insects (toxins)	12,879	6663	6037	175,000
TOTAL	27,797	13,927	11,814	367,960
Proportion	1.8×	7.8×	7.8×	5.5×

Search performed in 11 September 2021. [1] Limited to skin, in order to exclude ecological studies; [2] Limited to toxin, in order to exclude developmental/reproductive models; [3] Limited to toxins and excluding dinoflagellates.

The aim of this review is, therefore, to shed a light upon such amazing animals and their venoms and secretions, presenting a non-anthropocentric view of their venom composition and the (few, but consistent) biomedical 'cases' derived from the study of such species, and review the literature and the biotechnological developments derived from venoms and secretions from toxic animals that have not received proper attention from the scientific community over the past years and cast a light on their unique features and interesting molecules. Afterall, just like the neglected tropical diseases, it was never about the 'importance' of these animals, only their 'relevance', i.e., their economic impact, geopolitical localization, affected population, endangerment status and profit potential, in addition to formerly listed reasons.

1.2. Biodiversity

Earth's existing biodiversity is a direct consequence of Darwin's Natural Selection, i.e., the survival of the fittest, in a constant struggle to survive [3]. With an estimated 8.7 million species inhabiting our planet, the mere 1.2 million (mostly insects) that have already been identified and described have all—or are still in the process of—adapted and evolved so that, after numerous breeding cycles, poorly suited individuals are filtered out by nature.

One particularly interesting adaptation which emerged millions of years ago was the biochemical weaponry utilized for defense and/or predation by some organisms as a means of guaranteeing survival [4]. These so called 'toxins' can be found in procaryotic species, such as *Staphylococcus aureus* and *Klebsiella pneumoniae* [5,6], plants (*Cicuta maculate* (Socrates committed suicide by drinking cicuta, circa 399 B.C.) and *Nicotiana tabacum* (homage to Jean Nicot de Villemain, who introduced snuff to the French court in 1560)) and, obviously, animals.

For animals, these toxins are believed to have originated from ancestral house-keeping genes that underwent variation and neofunctionalization [4,7], resulting in molecules displaying an 'increased' biological activity, normally targeted to major biological systems that when unbalanced may result in severe risk of death, such as the hemostatic-interfering molecules. The toxins were then specifically expressed in venom-secreting cells that eventually became specialized venom glands [8]. Such specialization became an evolutionary advantage, due to unique pharmacokinetic properties that these (typically) peptides and proteins granted to such animals [9,10].

1.3. Toxins: Snakes, Spiders and Scorpions as Classical as It Can Be

Toxinology has its origins long associated with venomous animals and not poisonous ones. There might be some controversy in this separation, but it is commonly accepted that venomous animals would possess an inoculating apparatus capable of delivering toxins into the prey/aggressor. On the other hand, poisonous animals would secrete toxins in their skin or body organs and would have to be actively eaten/beaten/attacked/poked/colonized (bacteria) in order for to the toxins exert their effect.

Nevertheless, mystical, magical, medical and/or lethal uses of some animals' venoms are well known throughout history. For example: Cleopatra may have committed suicide by letting herself be bitten by a snake (*Naja haje* probably). In the Bible there are nine verses citing scorpions (Luke 10:19 and 11:12, Kings 12:11 and 12:14, Deuteronomy 8:15, Ezekiel 2:6, Revelation 9:3, 9:5 and 9:10). Greek mythology presents us the Lernaean Hydra, a serpentine water monster with many heads (depending on the myth source) with poisonous breath and blood so virulent that even its scent was deadly, as well as the Medusa, one of the three monstrous Gorgons, generally described as winged human females with living venomous snakes in place of hair.

These venomous animals are still present in modern-day fiction, such as the famous Spiderman, whose superpowers derived from mutations resulting from the bite of a radioactive spider. Even Harry Potter was forced to deal with the Basilisk, a giant snake capable of instant kill just by gazing at the victim's eyes. There are also urban legends and local habits, such as the well-known North American arachnophobia.

On the other hand, poisonous animals share a less glamorous role in human history. They have participated, for example, in human (sacrificial) rituals and attempted pharmaceutical developments throughout history. There were Maya human bloodletting rituals that employed the sting of marine stingrays as blades, due to a 'more efficient' bleeding [11]. Hunters have long sought the Central and South American Dendrobatidae 'poison arrow frogs' (self-explanatory) to use their toxic skin secretion for hunting [12]. Traditional Chinese medicine uses the 'all healing' Chan'Su (dried *Bufo bufo* skin) for mostly any illness [13]. Amazon tribes traditionally used Kambo (or Kampum) in their purification rituals [14]. This medicine is extracted from *Phyllomedusa bicolor* skin secretion and has become known as the 'frog vaccine' in urban environments. The Bible also cites such animals in the infamous passage in Exodus 8:1–4, in which the "*great LORD says: Let my*

people go, so that they may worship me. If you refuse to let them go, I will plague your whole country with frogs. The Nile will teem with frogs. They will come up into your palace and your bedroom and onto your bed, into the houses of your officials and on your people, and into your ovens and kneading troughs. The frogs will go up on you and your people and all your officials". Unfortunately, the poisonous animals are presented from a more neglected, less charming perspective, as presented above.

All this glamour associated with venomous animals has led to the establishment of what can be considered the 'greatest-hits' of (classical) toxinology: snakes, spiders, and scorpions (the triad). Undoubtedly, studying these animals' venoms has yielded a myriad of relevant scientific papers [15–19] produced by highly committed international scientific groups. The molecular dissection of the venom constituents has made it possible that effective sera could be manufactured [20–22], thus reducing mortality and morbidity associated with envenomation [23,24]. Moreover, one of the world's most administered antihypertensives (Captopril) is a direct derivative of one viper toxin [25].

Another example is a tumor-labeling molecule (tozuleristide), currently undergoing clinical phase 1 studies, that is being used in surgeries as marker and diagnostics for glioma and other tumors. This molecule is an analogue of a chlorotoxin isolated from the venom of the scorpion *Leiurus quinquestriatus* [26–28].

It is noteworthy to mention that there is young blood trying to join the party. Even though the marine mollusks of the *Conus* genus do not belong to the classic triad, they are becoming more and more famous since the discovery of ziconotide (Prialt), the strongest analgesic ever described: a calcium channel blocker, purified from the *Conus magnus* venom [29]. These animals are discussed below.

However, even for such well-studied animals there are still 'neglected' molecules present in their venoms, such as L-amino acid oxidase, crotapotin, crotamine that 'simply' for not killing or harming the animal models are put aside, turning the spotlight to the super-toxic metallopeptidases, phospholipases (A_2 and D) and ionic channel blockers.

Still, a number of other animals can (and do) cause accidents upon human encounters, displaying broad variation in terms of the clinical outcome. Marine animals are good examples: sea urchins can be solely painful [30] whereas mollusks can instantly kill [31]. Yet, for some reason, such animals have not been able to attract the attention of major research groups in toxinology, remaining in 'neglect' for the past couple of decades.

The modern reptiles are a group comprised of the Crocodila, Lepidossaura, Rhynohocephalia, Squamata, Testudines and Aves. With the exception of snakes, no other true venomous reptile (i.e., with a specialized venom inoculation apparatus) is currently known. The venomous living dinosaurs, i.e., birds pitohui, ifrita and rufous [32], and the Komodo dragon are considered to be poisonous [33,34].

However, in the end, snakes are the most classical venomous animals. Since ancient times, their behavior has been considered to be mischievous—even tempting—and their venom has been associated to magic spells and even cures. Not surprisingly, The Rod of Asclepius, i.e., the Medicine symbol (Figure 3A), is a snake serpentizing around a rod [35]. Nevertheless, the caduceus—the traditional symbol of Hermes—represented by two snakes serpentizing around a winged rod (Figure 3B) is often mistakenly used as a symbol of medicine instead of the Rod of Asclepius, especially in the United States, as a consequence of documented mistakes, misunderstandings and confusion in the late 19th and early 20th centuries. However, the two-snake caduceus design has ancient and consistent associations with trade, eloquence, negotiation, alchemy, and wisdom. Last, but not least, the current Butantan Institute logotype (created in 1983) is a clever design in which the capital 'I' and 'B' are fused and the 'B' serif becomes the snake serpentizing around the 'I', which serves as the rod (Figure 3C).

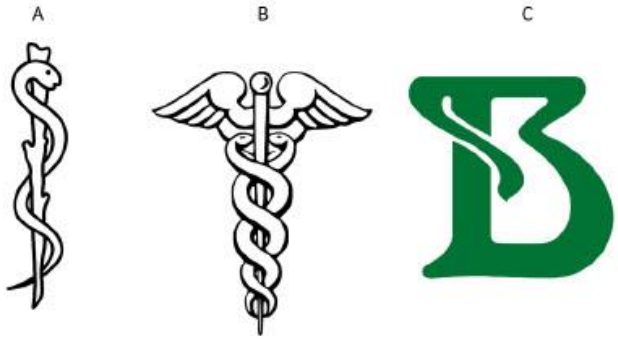

Figure 3. (**A**) Rod of Asclepius, (**B**) the caduceus and (**C**) Butantan Institute logotype.

Jumping a few centuries ahead, there is indeed current medicine based on snake venoms, such as Captopril [25,36,37], Aggrastat, Intergillin and Aggretin [30,33], proving that ancient wisdom may be old, but never outdated. Not only that, but this particular *Toxins* issue that celebrates the 120th anniversary of Butantan corroborates this. At the same time, one can easily note the iconic fascination that the snake has exerted over the local scientific community, that has—and still does—followed Vital Brazil's initial steps.

1.4. Lizards

Lizards' biting has long been discussed among the toxinology field due to the lack of an inoculating venom apparatus. *Heloderma* bites have been reported since 1882 [38,39], and the first toxic activities were described in 1900–1950. At that time, authors were aware that such lizards' toxins included neurotoxins, causing respiratory depression. Inflammation, edema and pain have also been described. However, once this animal bites 'as strong as a bulldog' according to the authors, these symptoms may not be exclusively toxin-derived [40]. Moreover, its hemolytic activity is mild, when compared to snakes, and seems to be species-specific [41].

Later, between 1950–1990, a wide range of biological activities were described, such as phospholipasic, hyaluronidasic, proteolytic [42], L-amino acid oxidase, fibrinolytic, [43] esterase, 5′-nucleotidase [44], secretagogue [45] and nerve growth factor activity [46]. Furthermore, new venom components (at the time) were isolated and identified, such as: kallikrein [47,48], Helospectins 1–2 (acting as secretagogues) [49], Gilatoxin (serine peptidase) [50], Helodermin (vasoactive peptide) [51], and Helothermine (CRISP) [52]. Hyaluronidase [53], a Phospholipase A2 [54], Helodermatin (hypotensive toxin) [55], and Exendin-3 (secretagogue) [56] were also described. Such myriad of toxins could, then, be correlated to the many established envenomation symptoms, such as hypotension and respiratory difficulties [57], smooth muscle contraction [58] and anticoagulant effect [59].

In 1992, Exendin-4 identification was a major event and *Heloderma* venom studies skyrocketed from this year onwards [60]. Several research projects have evaluated the antidiabetic potential of this molecule, which gave rise to exenatide, a new drug for the treatment of diabetes [61]. A few years later, the inhibition of platelet aggregation by a phospholipase isolated from a Helodermatid lizard was described [62]. Even though it was already known that *Heloderma* venom presents at least five anionic phospholipases, being the most abundant similar to *Apis mellifera* phospholipase [63], it was another important event.

In the following years, Helokinestatin, a toxin that acts as an antagonist of the bradykinin B2 receptor, was described [64]. Moreover, Helofensin was identified by Fry and co-workers by genetic and functional analysis [65], and classified together with a class of lethal toxins firstly described by Komori at al. in 1988 [66]. The presence of a natriuretic peptide in *Heloderma* venom was pointed out by different authors [67,68].

A work comparing the venom proteome of *Heloderma suspectum* with the venom of *H. exasperatum* and *H. horridum* presented an interesting result. Although *H. suspectum* was evolutionarily separated from the other species 30 million before, the venom composition was basically the same for the three species, presenting the same toxins with slight differences in their relative proportions [69]. Moreover, authors could also describe two new molecules: semaphorin and a bactericidal/permeability-increasing (BPI) molecule. Another study that characterized the *H. suspectum* venom proteome relates to the presence of a neuroendocrine convertase 1 homolog, and proposes that this protein is responsible for the cleavage of the proforms of exendins. In the same study, the authors also point out the high presence of phospholipase propeptides in the venom proteome [70]. Recent works allowed access to different classes of proteins, and also new biological activities from *Heloderma* venom. The venom gland transcriptome analysis from *H. horridum horridum* revealed the presence of metalloproteases, lipases, vespryns, waspryns, lectins, cystatins and serine peptidase inhibitors, but none of these proteins were actually isolated from the venom [71]. Furthermore, *Heloderma* contains neurotoxins in its venom, and these toxins are able to bind sodium and calcium channels [72]. An important work by Fry et al. [73] evaluated phylogeny between snakes and lizards and demonstrated that the venom delivery system of these animals could have evolved from the same common ancestor. This was the first study that biochemically evaluated the venom of a lizard from the Varanidae family. The crude venom from *Varanus varius* displays a hypotensive effect and an isolated PLA2 from the venom inhibits platelet aggregation, via adrenaline pathway. The LC-MS analysis indicates the presence of natriuretic peptide, PLA2, CRISP, and Kallikrein. cDNA libraries analyses indicated the presence of AVIT, cobra venom factor, cystatin, crotamine, nerve growth factor and vespryn. Later studies demonstrated that the venom of *V. komodensis* (Komodo Dragon) also induces a hypotensive action, and that the venom is composed of toxins, such as PLA2, kallikrein, natriuretic peptide, CRISP, and AVIT [74].

A cDNA libraries analysis conducted by Fry et al. [67], comparing different lizards, was able to reveal new classes of toxins presents in the Varanidae family, such as lectin, veificolin, hyaluronidase, Cholecystotoxin (binds to CCK-A), Celestoxin (hypotensive), epididymal secretory protein and Goannatyrotoxin (hypertensive/hypotensive effect).

Then, the venoms of *Lanthanotus*, *Varanus* and *Heloderma* genus were compared through proteomic approaches and enzymatic activities profiling [69]. Interestingly, the only ubiquitous protein was Kallikrein and, different from Heloderma, which presents a conservation of venom constitution and actions in different species, the Varanus genus presents a variability in venom proteins and enzymatic activities such as serine peptidases, phospholipase activity and differential potential to cleavage alpha and beta chains from fibrinogen.

Venoms from different species of the Varanus genus were evaluated for the ability to prevent blood clotting by thromboelastography, and the venoms differ regarding the activity; the most potent effects were found in arboricole species, probably due to the selective pressure, according to the authors [75]. Similar to *Heloderma*, Varanid lizards possess neurotoxins that are able to bind sodium and calcium channels [72].

1.5. Amphibian

Although a witch's recipe benefits from venomous animals, the toe of a frog and the eye of a newt would definitely spice things up. Shakespeare's Macbeth (Act 4, Scene 1) contains a recipe for a witch's brew that goes as follows:

"Fillet of a fenny snake,
In the cauldron boil and bake;
Eye of newt and toe of frog,
Wool of bat and tongue of dog,
Adder's fork and blind-worm's sting,
Lizard's leg and owlet's wing,
For a charm of powerful trouble,
Like a hell-broth boil and bubble."

Although most of the above referred ingredients can be traced back to herbs (eye of newt = mustard seed (*Sinapis alba*); toe of frog = buttercup (*Ranunculus acris* L.); wool of bat = holly leaves (*Ilex aquifolium*); tongue of dog = gypsyflower from the genus hound's tounge (*Cynoglossum officinale* L.); adder's fork = least adder's-tongue (*Ophioglossum lusitanicum* L.); blind-worm = slowworm (*Anguis fragilis*)), a really mighty witch might as well as go on literally, seeing the true herpetological powers needed for the spell.

According to Table 1, published papers on amphibian venoms are less common than the triad. The similar figure to scorpion papers is due to two characteristics belonging to the study of the amphibian skin secretion: (i) the discovery of magainin, the first antibiotic peptide by [76], which boosted the literature by making several researchers seek other antibiotic peptides in other species, and (ii) the vast Chinese literature on Chan'Su, the all healing Chinese traditional medicine. These two events have undoubtfully contributed to these numbers. However, in general, amphibian literature on accidents is scarce in comparison to venomous animals.

The amphibian defense strategy against predators/aggressors is the "passive" defense (with the exception of *Rhaebo guttatus*, which is capable of voluntarily compressing its parotoid glands and ejecting its contents [77]), and the chemical nature of their venom is mainly protein/peptide toxins and low-molecular-mass compounds (such as alkaloids, steroids and their respective derivatives).

Some of the authors of the current review have been working with amphibian skin secretion for almost twenty years. As a consequence, they have been able to produce consistent literature on the subject that encompasses the different classes of bioactive molecules commonly found on the amphibian skin secretion. A compilation of these results will be presented below, together with the related literature.

Conceição, et al. [78] have evaluated the skin secretion of the tree frog *Phyllomedusa hypochondrialis* and described that this secretion presents proteins ranging between 68 and 14 kDa, and that proteolytic and phospholipase A2 activities could be detected in vitro. Moreover, authors also report that the injection of 0.6 ug of the venom in mice induced myotoxicity, as evaluated by the increase of creatinine-kinase activity in plasma. The same dose of the skin secretion also elicited vasoconstriction (for 20 min) and leukocyte rolling, as assayed by intravital microscopy. Edema and nociception, in a dose–response manner, could also be observed. Interestingly, the observed vascular permeability alterations displayed a different mechanism, in which the lowest tested concentration caused the most intense effect, in comparison to larger concentrations. This phenomenon is mostly likely due to the presence of different molecules, in distinct relative concentrations, acting on independent biological systems.

As a consequence of the described leukocyte rolling effect, a subsequent study was performed [79] that assessed the mechanisms involved in that effect. Experiments revealed that the toxins could lead to edema formation, within 2 h, which lasted for 24 h. Moreover, authors also described that the numbers of rolling and adherent leukocytes were augmented in post-capillary venules. Cytological analysis showed that macrophages were the main cells present 2 h after the injection, whereas neutrophils were the cells present after 24 h. The cytokine profiles indicted elevated levels of chemokines MCP-1 and KC, and also IL-6 and PGE2.

Mendes et al., 2016 [80], studied the casque-headed tree frog *Corythomantis greening*, a frog bearing a cranial bone adaptation used in phragmosis. The cutaneous secretion of this animal was able to induce inflammation (edema, for 96 h after the injection) and nociception. Moreover, relevant enzymatic activities were detected in the skin secretion, such as fibrinogenolytic, hyaluronidasic and metallopeptidasic. Enzymes presenting such activities have already been described as important toxins for snake venoms [81,82] and were also described in some amphibians from different genus, for example phospholipase in *Pithecopus azureus* [83] and serine peptidases in *Duttaphrynus melanostictus* [84]. Furthermore, Fusco et al. 2020 [85] studied the epidermal secretion of *Argenteohyla siemersi* and described both phospholipasic and hemolytic activities. They also reported that that venom

is cytotoxic and capable of promoting necrosis which is independent of the proteolytic activity, a different activity pattern from *C. greeningi* (included in the same genus).

Targeting antibiotic peptides—a consequence of Zasloff's study—Conceição et al., 2006 [86], screened the skin secretion of *P. hypochondrialis* for antimicrobial peptides against Gram-positive and -negative bacteria and successfully described Phylloseptin-7 and Dermaseptin (DPh-1). These peptides were active over common pathogens, such as *Staphylococcus aureus*, *Escherichia coli*, *Pseudomonas aeruginosa* and *Micrococcus luteus*. In a complementary study, Huang and collaborators identified a new Dermaseptin from the same *P. hypochondrialis* (Dermaseptin-PH), which was active against Gram-positive/-negative bacteria and inhibited biofilm formation. This peptide was also effective against *Candida albicans*.

Other authors also reported complementary phylloseptins. For example, Wu et al., 2017 [87], isolated PNS-PC from *P. camba* the PNS-PC. This peptide displays inhibitory action against Methicillin-resistant *Staphylococcus aureus*. They also isolated PBa1–3 from *P. Burmeister*, a peptide with antibacterial and antifungal activities [88]. A recent study by Liu et al., 2020 [89], reported the antibacterial activity of PV-1, a Phylloseptin from *P. vaillantii* in vitro and in vivo. In spite of observed hemolysis (in vitro), this peptide was not toxic to hepatic and renal tissues in vivo, indicating the possible therapeutical potential of this peptide for bacterial infection.

Zhang et al., 2010 [90], isolated Phylloseptin-1 (PSN-1) from *P. sauvagei*. This peptide was active against *Staphylococcus aureus* in vitro, including bacterial biofilm formation inhibition. A few years later, Raja et al., 2013 [91], described five more Phylloseptins displaying antimicrobial activity from this species. Their work proved that the structural differences among those peptides were responsible for the different observed bactericidal potency, suggesting that the alpha-helix amphipathic conformation leads to microbial membrane disruption.

Using Zasloff's classic strategy, Conlon et al. 2007 [92] stimulated *Hylomantis lemur* skin secretion with norepinephrine and successfully purified Dermaseptin-L1 and Phylloseptin-L1, which were active against Gram-negative bacteria and *Batrachochytrium dendrobatidis*, a fungus that infect frogs.

In 2009, an unexpected antimicrobial peptide was described by Sousa et al. [93]. Leptoglycin, a peptide comprised basically by Leu and Gly (with an import Pro at the center of the sequence) was isolated from the skin secretion of *Leptodactylus pentadactylus* and was active against Gram-negative bacteria.

Bradykinin-potentiating peptides are protagonists of the most important example of drug discovery from animal venoms. Rocha e Silva's discovery of bradykinin [94] ultimately led to the discovery of the bradykinin-potentiating peptides (BBPs) from snake venoms. Such a peptide, on the other hand, led to the development of Captopril, the first drug belonging to angiotensin-converting enzyme inhibitor (ACEi) class, widely used around the world to treat arterial hypertension. In another unexpected study, Conceição et al., 2007 [78], described the first canonical BPP isolated from another source than snake venoms. Phypo-Xa, a decapeptide isolated from *P. hypochondrialis*, inhibited ACE and potentiated bradykinin both in vivo and in vitro. A few years later, those authors [95] also isolated three bradykinin-related peptides from *P. nordestina* skin secretion: two were vasodilators (Pnor3 and Pnor7) and one was a vasoconstrictor (Pnor5).

Some amphibians, particularly toads, can be considered major biological sources of low-molecular-mass compounds, such as alkaloids and steroids. Tempone et al. [96], through biomonitored assays, have isolated two bufadienolidc steroids displaying antiparasitic activity from the skin secretion of *Rhinalla jimi*. Telecinobufagin and hellebrigenin were not new molecules at that time; however, the activity against *Leishmania* sp. promastigotes and amastigotes in macrophage culture (without NO production modulation) and the anti-*Trypanossoma cruzi* trypomastigotes activity were the novelties they reported in their paper. The mechanism of action of these molecules seems to be related to the disturbance of cellular membrane and mitochondrial function. Neither steroid presented hemolytic or cytotoxic activities in the tested conditions.

That same group of authors [97] later assayed the skin secretion of *P. nordestina* on antiparasitic models. They were able to demonstrate that four antimicrobial peptides (Dermaseptins 1 and 4, and Phylloseptins 7 and 8) were able to decrease the in vitro viability of *T. cruzi*, with a high theoretical therapeutic index. The proposed mechanism of action of the peptides is cell death induction, through cellular membrane permeabilization. Phylloseptin-7 was also effective against *Leishmania* sp.

Such results (selective membrane permeation) convinced Sciani et al. [98] to investigate the possible antitumor activities of the skin secretion of some Brazilian toads. MCF-7 and MDA-MB-231 lineages (breast tumor) displayed reduced proliferation and apoptosis induction when treated with eight different amphibian skin secretions. Among them, the most promising results came from *R. guttatus*, *R. margaritifera* and *P. hypochondrialis*. Moreover, *R. guttatus* and *R. marina* displayed selective antitumor activity over HL-60 (leukemia lineage), without toxicity to human leukocytes. It is believed that the observed antiproliferative effect is due to the known presence of bufadienolides in this toad secretion.

Schemda-Hirschmann in 2014 [99] related the presence of argininyl bufadienolides in *R. schneideri* dermic secretions, which were active on different tumor lineages AGS, SK-MES-1, J82 and HL-60 (gastric adenocarcinoma, lung carcinoma, bladder carcinoma and leukemia, respectively). Later, the same group showed similar activity in the Peruvian *R. marina* venom, and the mechanism of action seems related to ROS production and cell cycle arrest, for breast cancer lineages [100]. Antitumor properties were also described for the Paraguayan *Rhinella* sp. Such skin secretion is traditionally used by locals in folk medicine to treat skin lesions and tumors [101].

The crude extract of *Physalaemus nattereri* is cytotoxic for the B16F10 melanoma cell line. Carvalho et al. [102] observed that the secretion was able to induce conformational changes in cells, exposure of phosphatidylserine on cell membrane, reduction of mitochondrial membrane potential and arrest of cell cycle in S phase, indicating that apoptosis is the probable mechanism of action that explains the antitumor activity. RP-HPLC fractionated *P. nattereri* extract points out that this biological action is due to peptides

Skin venom from the Malaysian toad *B. asper* was active against HCT 116 colorectal tumor line by apoptosis induction, via caspase 3/7 activation and mitochondrial membrane potential disruption [103]. Bufadienolides also possess the ability to inhibit Na^+/K^+ ATPase and trigger caspase-induced apoptosis, being more selective to cancer cells than normal cells [104]. The venoms of two Turkish Salamandrine amphibians were tested against cancer cell lineages. The venoms, which presented proteins in their biochemical content, were active against cervix, alveolar, colon colorectal, pancreas, prostate, astrocytoma and breast carcinoma lines. However, these secretions were also toxic to human fibroblasts (HEK 293) [105].

Marinobufagin is a molecule present on *R. marina* venom displaying activity against leukemic cells without being toxic to normal blood cells. According to Machado et al. [106], this steroid induces toxicity via apoptosis, antimitotic action and cycle cell arrest at interphase in leukemia cells, without any genotoxicity.

The bufadienolides, bufotoxins, alkaloids and arginiyl derivatives from *R. jimi* cytotoxicity effects on cancer cell lineages were studied by Filho et al. [107], whereas Spinelli et al. [108] revaluated the antitumor action of 11 different Argentine amphibians: 6 *Hylidae/Microhylidae* and 5 *Leptodactylidae*. These venoms induced apoptosis and autophagy. Interestingly, *Leptodactylidae* skin secretion induced aggregation on cancer cells.

Finally, we present bufotenine: a tryptamine alkaloid found in many species and genera across nature (animals and plants), particularly in *R. crucifer*, *R. granulosa*, *R. schneideri*, *R. icteria* and *R. jimi* [109]. This molecule was selected in biomonitored assays and has the capacity to inhibit the penetration of rabies virus in mammalian cells, through an apparent competitive mechanism [110]. Complementary studies conducted by those authors [111] showed that this molecule was active in vivo, by increasing the survival rate of intracerebrally virus-infected mice from 15 to 40%. The safety of bufotenine was then evaluated [112] and no significant effects on mice could be detected at the effective

antiviral dose. Interestingly, bufotenine acts synergically with ocellatin-F1—an antimicrobial peptide obtained from the frog *Leptodactylus labyrinthicus* skin secretion—in the rabies virus model [113]. Finally, recent in vitro assays showed that bufotenine has no antiviral action against canine coronavirus (CCoV), canine adenovirus type 2 (CAV-2) or herpesvirus type 1 (HSV-1), indicating some specificity against distinct types of viruses [114]. The mechanism of action of this alkaloid remains unclear (although the evaluation of its effects in the immune system is being assayed by these authors), but bufotenine is the perfect example of the potential of bioactive molecules isolated from a neglected venom, serving as biotechnological tool for a neglected disease drug development study.

1.6. Marine Animals

Oceans dominate planet Earth: approximately 70% of the Earth's surface is covered by water, and from that, 96.5% of this water is from the oceans [115]. More than 480,000 species of marine animals have been discovered and identified according to the World Register of Marine Species [116]. However, such a figure may be even larger: the Ward Appeltans of the Intergovernmental Oceanographic Commission of UNESCO (https://en.unesco.org/news/ocean-life-marine-age-discovery-0, accessed 19 November 2021) estimates that oceans may hold 700,000 species. These data represent what the ocean can become: a molecular library! Molecules that belong to an organism's physiology, act on hunting and prey digestion and/or chemical defense may ultimately lead to the discovery of new compounds with biotechnological or pharmaceutical uses.

Regarding bioprospection, marine animals have provided several molecules for a wide range of therapeutic applications. Some of them have already been approved by regulatory agencies and are being commercialized. The most known is ziconotide (Prialt), a ω-conotoxin peptide from *Conus magus*, applied by intrathecal route as analgesic for chronic and intense pain, whose mechanism of action is the selective blocking of neuronal N-type voltage-sensitive calcium channels [117,118]. Another known drug from marine animals is trabectedin (Yondelis), initially isolated from the marine ascidian *Ecteinascidia turbinata*, used to treat sarcomas and ovary cancer [119].

For cancer, other drugs have been developed, such as Ara-C (Cytarabine), a nucleoside isolated from a Caribbean sponge, *Cryptotheca crypta*. It is used for certain types of leukemia, including acute myeloid leukemia, acute lymphocytic leukemia and chronic myelogenous leukemia [120].

Brazilian sponges and cnidarians, such as *Zoanthus sociatus*, *Exaiptasia pallida* and *Carijoa riisei*, have yielded promising molecules active on cancer cells. Some of these authors have showed that *C. riisei* and the porifera *Tedania brasiliensis* extracts were effective in reducing the cell viability of glioblastoma, and that *C. riseii* also acts on breast and ovary cancer. Moreover, *Z. sociatus* and *E. pallida* were able to diminish leukemic cell viability [121]. Regarding the envenomation field, some of these authors have contributed for the understanding of marine animal venoms, from a biochemical and pathophysiological perspective.

1.7. Sea Urchins

Sea urchins are the most abundant animals in Brazilian shores. They are also responsible for the majority of reported marine animal accidents [122]. *Echinometra lucunter*—the rock boring urchin—can be easily found in rocky shores. Human accidents are frequent and can be associated with the animal's manipulation by bathers, or by people stepping on the animals while walking on the shore. More severe cases (in terms of the number of spines punctures) can result from people being dragged onto rocky walls by wave action. Still, the most common route that the spines penetrate the skin is through the foot or hand. This event causes local inflammatory reactions, characterized by edema, erythema and pain [123,124]. Facing this problem, the authors have wondered: is this accident solely mechanical due to the spine's penetration, or does the sea urchin have a venom that contributes to the described symptoms?

To answer that question, 'toxins' from *E. lucunter* spines were extracted, immersing the excised appendices in a physiological buffer (to avoid cell lyses by osmotic shock), followed by animal inflammation test models. Authors described that the extract induces a pro-inflammatory reaction, by increasing rolling, adhered and migrated leukocytes. Moreover, the spines extract decreased the pain threshold and induced paw edema [30]. In another study, these authors were able to isolate one molecule responsible for those effects, including its partial molecular characterization [125]. However, it was clear that there was more than one single molecule eliciting such activities; therefore, the clinical observed symptoms clearly surpass the mechanical trauma aroused by spine penetration.

This mechanism is a very successful adaptation: the venom (i.e., the 'toxins') diminishes the pain threshold—making the victim more susceptible to painful stimuli—at the same time that the spines puncture the skin. As a consequence, the mechanical accident becomes more aggressive, due to this synergism (resulting in inflammation).

E. lucunter spines do not contain typical venom glands, in the same way venomous animals do, but it is a living structure, full of granular cells, which are most likely to produce and secrete these toxins along the entire spine, particularly at in the spine tip, a region more susceptible to mechanical stress by contact (with possible predators and aggressors) [126]. Moreover, although the spine is composed mainly of calcium and/or magnesium carbonate, the myriad of cells embedded would significantly contribute to spine regeneration. It has been demonstrated that the spine secretes cathepsins B and/or X, an enzyme associated with matrix remodeling processes, contributing to the spine growth and regeneration, but also to the toxicity.

Besides spines accidents, consumption of sea urchins may elicit undesirable/toxic effects for the consumer, as they are usually eaten raw. Therefore, these authors have investigated the coelomic fluid of *E. lucunter*, searching for toxins (pro-inflammatory molecules, in particular). A bioactive peptide, termed 'echinometrin', capable of reducing rolling cells and increasing adhered and migrated ones—concomitant to edema induction—was identified. Moreover, this peptide induced mast cell degranulation, which makes us think that histamine was responsible for the observed inflammatory reaction [127]. Actually, many consumers present allergies after the consumption of raw sea urchin, and there are studies suggesting the participation of vitellogenin in such process, by increasing IgE levels [128,129]. Echinometrin is, in fact, a cryptide [130], i.e., an internal fragment of vitellogenin. Moreover, its N- and C-termini match the amino acid specificity for (the previously reported) cathepsin B/X, suggesting a local toxin generation system, in which both substrate and processing enzyme are present and ready to act.

Once the biomonitored assay reported above proved successful in the identification of one bioactive peptide, these authors decided to performed an untargeted peptidomic approach on sea urchins' peptides. The secreted peptides from *E. lucunter*, *Lytechinus variegatus* and *Arbacia lixula* were analyzed. It was possible to observe that coelomic fluids of all three species are full of peptides. On the other hand, peptides could be identified only in the spines of *L. variegatus* and *A. lixula*, whereas *E. lucunter* spines contain mainly low molecular mass compounds. Database mining suggests that some peptides may display relevant biological effects, such as antibiotic, anticancer, antiviral, phospholipase A2 inhibitor and neuroprotective properties, making sea urchin molecules a source of new therapeutic compounds [131].

1.8. Mollusks

Peptides are abundant in marine mollusks from the Gastropoda class. They are usually referred as 'conopeptides' and are responsible for prey paralysis due to their specific action on the neuromuscular ionic channels [132,133]. The genus *Conus* is a well-known source of these conopeptides. The Tox-Prot database from Uniprot/Swiss-Prot describes that 1.370 toxins are manually annotated for 117 snail species, most of them from genus *Conus* [134,135]. On the other hand, the database platform for conopeptides, ConoServer, shows that 119 *Conus* species already have at least one protein sequence/structure elucidated. Besides that,

this platform shows that conopeptides can be categorized in 12 pharmacological families or in 33 cysteine frameworks. More than 2900 mature conotoxins can be found in this database [136,137].

Conus can be classified into three main groups, according to their feeding behavior: worm-hunting, molluscivorous and fish-hunting snails [138]. One of them—*C. regius*—a species that dwells the USA, Central America, and Brazil, including the Fernando de Noronha archipelago, has been studied by these authors [139]. As feeding behavior is often related with venom composition, the authors have investigated what would be the feeding habits of these animal, since they were not known at the time. They found that *C. regius* preferentially preys on fire-worms, thus being categorized as a vermivorous species. Authors have also evaluated the homogeneity of the venom and have determined that, regardless of gender, size and season of the year, there was no significant variation on venom composition (as determined by RP-HPLC peak area and similarity). Under these conditions, they have found the major peak, isolated and characterized it, which led to the identification of rg11a, a conotoxin presenting the cysteine pattern C-C-CC-CC-C-C and ~5 kDa [140]. Later, these authors also described α-RgIB: a 2.7 kDa peptide bearing the CC-C-C pattern, which is an antagonist of neuronal acetylcholine receptor and is capable of inducing hyperactivity in mice and breathing difficulties [141].

1.9. Stingrays

Stingrays accounted for 69% of aquatic animal accidents in Brazil from 2007 to 2013. Most cases (88.4%) were reported in the north region and correspond to accidents caused by freshwater stingrays [142].

In general, symptoms of freshwater stingray accidents include skin necrosis, edema, erythema and intense pain, mainly at the lower limbs, which are the most common accident site. Several studies have focused on the mechanism of action of stingray toxins. One explanation is the release of proinflammatory interleukins that lead to the inflammatory reaction and pain, besides the direct participation of mast cell degranulation and histamine release [143,144]. The presence of inflammatory cells in the necrotic tissues was reported, most lymphoid, CD3+ and CD4+ cells, as well as the presence of eosinophils [145].

Although less frequent, marine rays also cause human accidents, but few works report them. In this sense, some of these authors have studied *Hypanus americanum*'s mucus, searching for toxins [146]. It is noteworthy to mention that a marine stingray's whole body is covered by mucus produced by epithelial cells. Some animals possess a calcified spine ('sting') on their tail, which is covered by an epithelium that secretes mucus. This secretion is rich in molecules involved in the chemical defense and skin homeostasis maintenance, including establishing a barrier against microorganisms.

These authors observed that the mucus is labile, denaturating in function of the temperature and storage time after collection. Moreover, the classical scratching method for mucus collection results in the attainment of a mucus rich in cellular debris and, consequently, intracellular content that masks the 'actual' mucus. Authors were forced to develop a new method: the whole animal was submerged—for 40 s—in a tank containing only freshwater. After the animal was removed, the water was acidified (0.1% final concentration) and the solution was filtered. This large volume was directly pumped into the C18-RP-HPLC column via system pump 'A'. After total sample loading, standard chromatography was performed [146].

Nevertheless, the chemical nature of the mucus revealed itself to be more complex than initially imagined by those authors. Several proteins, peptides and low-molecular-mass compounds could be detected. The mucus elicits inflammatory reactions, such as edema and leukocyte recruitment in mice. The performed zymograms displayed proteolytic activity. Moreover, authors describe the antimicrobial effect of molecules fractionated from the mucus. The proteomic analyses revealed proteins that are involved in the immune response, and are very similar to the proteins related to the sting, and also similar to proteins described in fishes from Teleostei class, indicating that the epidermal secretions of

stingrays could be more related to an innate immune system than with a venom delivery system [146]. This hypothesis was recently reinforced in a work that analyzed the genomic data of a venomous fish and associated the presence of aerolysin (considered as a toxin) with the immune system [147].

1.10. Cnidarians

The phylum Cnidaria comprises more than 10,000 species and is considered the most ancient venomous animal lineage, having emerged approximately 650 million years ago [148,149]. To the contrary of other venomous animals, cnidarians have the unique characteristic of lacking a centralized venom system [150]. Instead of a venom gland, these animals present little organelles distributed throughout their bodies, called cnidaes. Such structures are produced by the Golgi apparatus of specialized cells: the cnidoblasts [151]. It is divided into three main lineages: 1. Anthozoa, formed by Anthozoa class; 2. Medusozoa, comprised of Scyphozoa, Staurozoa, Cubozoa and Hydrozoa classes; 3. Endocnidozoa, comprising Myxozoa and Polypodiozoa classes. Cnidaria is a diverse phylum, rich in bioactive molecules, known to be used mainly for predation, defense and intraspecific competition [152].

Cnidaria early studies began in 1903 on *Anemonia sulcata* and *Actinia equina* tentacles extracts. Since then, several studies on sea anemones have been developed, leading to more than a century of research on these animals' venoms [150,153,154]. Sea anemones are exquisite sources of toxins and represent the greatest diversity in Anthozoa, having around 1200 species distributed in 46 families [150].

These cnidarians can cause envenomation through their nematocysts, specialized structures that inoculate venom. One particular case report of a human accident caused by anemones belonging to the *Stichodactyla* genus describes local skin irritations with blistering, edema and hemorrhage, mild symptoms when compared to the actual target of the toxin, prey, which is instantly killed by neuro- and cardiotoxins [155]. The anemone toxins molecular scaffolds are diverse: at least 17 different structural motifs are known [150].

The peptide neurotoxins found in sea anemones may act over different ion channels. ShK toxins, for example, bind to Kv type 1; some types of β-defensins can modify the action of Kv type 3 and Nav type 1, 2 and 4; while the inhibitor cystine-knot (ICK) can act over Kv type 5 and acid-sensing ion channels [150]. In this context, a study published in 2004, by some of these authors, investigated the differential selectivity between three sea anemones toxins against a wide range of Nav channels subtypes (Nav 1.1–1.6). The authors observed that for Nav1.3, the three toxins (ATX-II, AFT-II and Bc-III) were active only when at high concentrations. Additionally, it was observed that although ATX-II (from *A. sulcata*) and AFT-II (from *A. fuscoviridis*) exhibit similar sequences, a single amino difference was enough to alter the ion channels specificity. Lysine^{36} (ATX-II) seems to be fundamental for its action over Nav1.1 and Nav1.2 channels; meanwhile, AFT-II mainly exerts effects on Nav 1.4 and Nav 1.5. Moreover, the slight changes in amino acids between similar Nav channels can have a crucial role in toxins binding. For example, AFT-II had a more potent effect over Nav1.4 than Nav 1.5. These two channels are only marginally different and the presence of a Leucine at position 1611 in Nav1.4, instead of an Isoleucine at in Nav1.5 right after a neighboring Asparagine, may indicate the importance of these residues for the toxin binding [156].

In another evaluation of sea anemones venoms, Zaharenko et al. reported, for the first time, the proteomics analysis of the neurotoxic fraction of the sea anemone *Bunodosoma cangicum*. Authors processed by RP-HPLC such a fraction and identified at least 81 different molecules, distributed along 41 chromatographic peaks. Mass spectrometric analysis by MALDI-TOF and ESI-Q-TOF shows that that fraction is composed of low-molecular-mass (280–450 Da) as well as heavier molecules (4–5 kDa). Major fractions were purified and sequenced by Edman degradation, revealing nine novel peptides. Three peptides clearly presented the typical cysteine scaffold found in type 1 sodium channel toxins, and six of them presented new cysteine scaffolds belonging to two new classes of toxins. Additionally,

when tested on extracellular crab leg nerve, the new peptides called Bcg31.16 and Bcg30.24 showed that, at very low concentrations (40–50 nM), those neurotoxins were able to diminish the amplitude of CAPs (compound action potentials) and increase its duration, showing a high potency and suggesting that these toxins target sodium channels [157].

Compared to other cnidarians, the Anthozoa (anemones included) is a well-studied group, in terms of toxins investigation. ToxProt lists 256 toxins belonging to 48 species of sea anemones (manually curated; accessed October, 2021). On the other hand, only five toxins from Cubozoa; four from Hydrozoa and one from Scyphozoa classes are deposited [134]. Of particular interest, three Cubozoa toxins (caTX-A, cqTX-A, crTX-A, cfTX-1 and cfTX-2) belong respectively to four species of box jellyfishes: *Carybdea alata*, *Chiropsoides quadrigatus*, *Carybdea rastonii*; and *Chironex fleckeri* (the Australian box jellyfish, one of the most dangerous species of cnidarians) [134,158]. Regardless of the small number of curated toxins, 327 proteins from Cubozoa—computationally analyzed and available at TrEMBL—still remain to be reviewed. The literature refers to Cubozoa toxins being enzymes (phospholipases A2, metallopeptidases and serine peptidases), CRISPs, lectins, pore-forming toxins and protease inhibitors [159]. For Hydrozoa, the four proteins manually curated and described as Hydralysin toxins belong to only two different species: *Hydra viridissima* and *H. vulgaris* [134,135].

The challenge of better knowing the toxins found in Cubozoa and Hydrozoa is not limited to the proteins and peptides; little is known about the low-molecular-mass molecules from these organisms [160]. In order to increase knowledge on the biotechnological potential of Cubozoa and Hydrozoa, two studies were recently performed. The first one, conducted by Bueno et al. [161], investigated the effects of the methanolic extracts of hydromedusa *Olindias sambaquiensis* and jellyfish *Chiropsalmus quadrumanus* over the autonomic neurotransmission. In this study, researchers employed a classical model to sympathetic co-transmission: a myographic evaluation of rat vas deferens bisected in two portions (prostatic and epididymal) for purinergic or adrenergic responses. Throughout the study, both methanolic extracts were demonstrated to be of low complexity and rich in low molecular mass molecules.

Authors report that a low concentration (0.1 µg/mL) of *C. quadrumanus* extract blocked the predominantly noradrenergic contraction of the epididymal end. On the other hand, only high concentrations (1 and 10 µg/mL) of *O. sambaquiensis* extract were capable of leading to the blockade of muscle contraction. Nevertheless, both extracts did not present significant differences concerning the phasic contractions in the prostatic portion (purinergic response), when compared to the control group. Moreover, the histological analysis showed that none of the extracts promote major tissue damage in the prostatic and epididymal vas deferens ends, showing the same unaltered morphology as the control group, which indicates their effects only on the neurotransmission, not causing toxic tissue damages [161].

Another study, published by Arruda et al. [160], focused on *C. quadrumanus* tentacles methanolic extract and its biological activity over neurite growth. In this work, the extract was tested on a human SH-SY5Y neuroblastoma cell line, a neuronal cell culture model commonly used for neurodegenerative disease investigations. Authors report alterations on neurite-related structures of neurons, without affecting cell proliferation or inducing necrosis or apoptosis [160]. The specific neurite length outgrowth observed in all cells exposed to the toxins was associated with a translin-like protein (hyccin cryptein) cryptide, as well as to small molecules acting synergically to promote the neurite/branches formation, elongation and facilitating neurotransmission. Neurite formation can happen either via microtubule and motor proteins [162] or PI4P regulation—acting on plasma membrane identity and myelin development [162]. Moreover, toxins present in the methanolic extract showed no effect on the straightness of neurite's growth or cell body area, but increased branching junctions connected to cells. More than 14 low molecular mass molecules related to neuritogenesis were found through LC-MS fingerprinting and at least 4 peptides related to neuronal function [160].

1.11. Insects

Although insects are the largest group within the arthropod phylum, and most of them are well studied due to their importance, there is always room for new research. Insects are known to create the biological foundation for most of the terrestrial ecosystems by pollinating plants, dispersing seeds, controlling populations of other organisms (including decomposing dead material to recycle nutrients) and being a major food source for other taxa. On the other hand, insects also spread diseases and can compromise a significant amount of food (grains, for example).

Among the notorious insects, there is the honeybee (*Apis mellifera*). There are reports of beekeeping as old as 10,000 years. Bee domestication started in Egypt 4500 years ago, when probably human accidents must have become more frequent, as well.

Bee stinging is mischievous: one single sting may provoke allergy and the subject may die from anaphylaxis. On the other hand, one may be stung several times and, in spite of intense pain and significant swelling, no significant harm occurs. However, when a few dozen bees sting, one may become envenomed. This event is not related to allergy and is a consequence of the bee toxins acting on the victim's body, especially in the kidneys.

The difference between poison and medicine is the dose, and apitherapy is a rather popular branch of alternative medicine which includes live bee acupuncture. Such a procedure may heal some, but is not free of risks at all! Adverse reactions to bee venom therapy are frequent. Constant exposure to the venom may lead to arthropathy, for example. In sensitized individuals, allergic reactions vary from mild, local swelling to severe systemic reactions, anaphylactic shock and even death. Yet, there are claimed cosmetic uses of the bee venom. Rumor has it that the Duchess of Cambridge has used bee venom to keep her skin looking flawless and even applied the secret ingredient to ensure a glowing complexion when she wed Prince William in 2011.

In a more practical context, a few groups have explored the possibility of developing an antiapilic serum, for treating those patients that have suffered multiple bee stings and have not suffered anaphylactic shock. Among those, authors from this group have successfully developed an efficient antiapilic serum that is currently under clinical trial (phase III). Further details can be found in the works of Ferreira Jr et al., 2010 [163], and Sciani et al., 2010 [164], who set the basis for the preclinical and clinical studies summarized by Barbosa et al., 2021 [165].

2. Conclusions

Animal venoms and toxins comprise a diverse repertoire of fascinating proteins, peptides and other bioactive molecules that have evolved through natural selection, driven by adaptive pressure and the survival of the fittest. Their biological role is—mainly—predation and defense. Mankind—and its anthropocentric perspective of nature—have always tried to develop ways to use and study these venoms and toxins as pharmacological prototypes for the research and development of novel therapeutics. Such a quest has opened new venues to the identification of an unprecedented number of new molecules and/or biological effects.

According to our view, 'classic' toxinology (as we have termed the continuous study of snakes, scorpions and spiders) will lessen in the near future and the 'new' venoms and toxins will prevail, due to subject saturation. Research of unexplored—or neglected—species of animals and their venoms and secretions should become dominant, since they contain a myriad of molecules displaying relevant biological effects on human illnesses, diseases, degenerative disorders, injuries, pain, tumors and infections (viral, bacterial and fungal), either as medicines or diagnostics tools.

Therefore, we consider that the currently reviewed literature on lizards, amphibians, and marine animals is just the beginning of a new thematic approach that we hope will become dominant in the following years. Such veiled potential currently hidden in the neglected animal venoms and toxins can set the instrumental and scientific basis for the

development of new molecules with innovative potential, which could shape a "new era" in toxinology.

Author Contributions: Conceptualization, G.R.C. and E.B.-N.; writing—original draft preparation, G.R.C., D.L.d.S., E.B.-N., H.V. and L.A.d.O.; writing—review and editing, E.B.-N. and H.V.; supervision, J.M.S. and D.C.P.; funding acquisition, J.M.S. and D.C.P. All authors have read and agreed to the published version of the manuscript.

Funding: This research was funded by Conselho Nacional de Desenvolvimento Científico e Tecnológico (CNPq), grant number 301974/2019-5, Financiadora de Estudos e Projetos (FINEP), grants number 01.12.0450.00 and 01.09.0278.04, Fundação de Amparo à Pesquisa do Estado de São Paulo (FAPESP), grant number 19/19929-6. The APC was funded by Instituto Butantan.

Institutional Review Board Statement: Not applicable.

Informed Consent Statement: Not applicable.

Conflicts of Interest: The authors declare no conflict of interest.

References

1. Brazil, V. *Memória histórica do Instituto de Butantan*; Instituto Butantan: São Paulo, Brazil, 1941.
2. WHO. Investing to overcome the global impact of neglected tropical diseases. In *Third WHO Report on Neglected Tropical Diseases 2015*; World Health Organization: Geneva, Switzerland, 2015; Volume 3.
3. Darwin, C. *On the Origin of Species, 1859*; Routledge: London, UK, 2003.
4. Zhang, S.; Gao, B.; Zhu, S. Target-Driven Evolution of Scorpion Toxins. *Sci. Rep.* **2015**, *5*, 14973. [CrossRef] [PubMed]
5. Argudín, M.; Mendoza, M.C.; Rodicio, M.D.R.R. Food Poisoning and Staphylococcus aureus Enterotoxins. *Toxins* **2010**, *2*, 1751–1773. [CrossRef] [PubMed]
6. Guarino, A.; Giannella, R.; Thompson, M.R. Citrobacter freundii produces an 18-amino-acid heat-stable enterotoxin identical to the 18-amino-acid Escherichia coli heat-stable enterotoxin (ST Ia). *Infect. Immun.* **1989**, *57*, 649–652. [CrossRef]
7. Santibáñez-López, C.E.; Graham, M.R.; Sharma, P.P.; Ortiz, E.; Possani, L.D. Hadrurid Scorpion Toxins: Evolutionary Conservation and Selective Pressures. *Toxins* **2019**, *11*, 637. [CrossRef] [PubMed]
8. Hargreaves, A.D.; Swain, M.T.; Hegarty, M.J.; Logan, D.; Mulley, J.F. Restriction and Recruitment—Gene Duplication and the Origin and Evolution of Snake Venom Toxins. *Genome Biol. Evol.* **2014**, *6*, 2088–2095. [CrossRef]
9. Casewell, N.R.; Wüster, W.; Vonk, F.J.; Harrison, R.A.; Fry, B.G. Complex cocktails: The evolutionary novelty of venoms. *Trends Ecol. Evol.* **2013**, *28*, 219–229. [CrossRef]
10. Schendel, V.; Rash, L.D.; Jenner, R.A.; Undheim, E.A.B. The Diversity of Venom: The Importance of Behavior and Venom System Morphology in Understanding Its Ecology and Evolution. *Toxins* **2019**, *11*, 666. [CrossRef]
11. Haines, H.R.; Willink, P.W.; Maxwell, D. Stingray Spine Use and Maya Bloodletting Rituals: A Cautionary Tale. *Lat. Am. Antiq.* **2008**, *19*, 83–98. [CrossRef]
12. Dodd-Butera, T.; Broderick, M. Animals, Poisonous and Venomous. *Encycl. Toxicol.* **2014**, 246–251. [CrossRef]
13. Qi, J.; Tan, C.K.; Hashimi, S.M.; Zulfiker, A.H.M.; Good, D.; Wei, M.Q. Toad Glandular Secretions and Skin Extractions as Anti-Inflammatory and Anticancer Agents. *Evid. -Based Complement. Altern. Med.* **2014**, *2014*, 312684. [CrossRef]
14. Junior, V.H.; Martins, I.A. KAMBÔ: An Amazonian enigma. *J. Venom Res.* **2020**, *10*, 13. [PubMed]
15. Quintero-Hernández, V.; Jiménez-Vargas, J.; Gurrola, G.; Valdivia, H.; Possani, L. Scorpion venom components that affect ion-channels function. *Toxicon* **2013**, *76*, 328–342. [CrossRef]
16. Petricevich, V.L. Scorpion Venom and the Inflammatory Response. *Mediat. Inflamm.* **2010**, *2010*, 903295. [CrossRef]
17. Markland, F.S. Snake venoms and the hemostatic system. *Toxicon* **1998**, *36*, 1749–1800. [CrossRef]
18. Bjarnason, J.B.; Fox, J.W. Hemorrhagic metalloproteinases from snake venoms. *Pharmacol. Ther.* **1994**, *62*, 325–372. [CrossRef]
19. Gutiérrez, J.M.; Lomonte, B. Phospholipase A2 myotoxins from Bothrops snake venoms. *Toxicon* **1995**, *33*, 1405–1424. [CrossRef]
20. Kuniyoshi, A.K.; Kodama, R.T.; Moraes, L.H.F.; Duzzi, B.; Iwai, L.K.; Lima, I.F.; Carvalho, D.C.; Portaro, F.V. In vitro cleavage of bioactive peptides by peptidases from Bothrops jararaca venom and its neutralization by bothropic antivenom produced by Butantan Institute: Major contribution of serine peptidases. *Toxicon* **2017**, *137*, 114–119. [CrossRef] [PubMed]
21. Grego, K.F.; Vieira, S.E.M.; Vidueiros, J.P.; Serapicos, E.D.O.; Barbarini, C.C.; da Silveira, G.P.M.; Rodrigues, F.D.S.; Alves, L.D.C.F.; Stuginski, D.R.; Rameh-De-Albuquerque, L.C.; et al. Maintenance of venomous snakes in captivity for venom production at Butantan Institute from 1908 to the present: A scoping history. *J. Venom. Anim. Toxins Incl. Trop. Dis.* **2021**, *27*. [CrossRef] [PubMed]
22. Lucas, S.M. The history of venomous spider identification, venom extraction methods and antivenom production: A long journey at the Butantan Institute, São Paulo, Brazil. *J. Venom. Anim. Toxins Incl. Trop. Dis.* **2015**, *21*, 21. [CrossRef]
23. Heard, K.; O'Malley, G.F.; Dart, R.C. Antivenom Therapy in the Americas. *Drugs* **1999**, *58*, 5–15. [CrossRef]
24. Jorge, M.; Ribeiro, L. Dose de soro (antiveneno) no tratamento do envenenamento por serpentes peçonhentas do gênero Bothrops. *Rev. Assoc. Médica Bras.* **1997**, *43*, 74–76. [CrossRef]

25. Cushman, D.W.; Ondetti, M.A. History of the design of captopril and related inhibitors of angiotensin converting enzyme. *Hypertension* **1991**, *17*, 589–592. [CrossRef] [PubMed]
26. Patil, C.G.; Walker, D.G.; Miller, D.M.; Butte, P.; Morrison, B.; Kittle, D.S.; Hansen, S.J.; Nufer, K.L.; Byrnes-Blake, K.A.; Yamada, M.; et al. Phase 1 Safety, Pharmacokinetics, and Fluorescence Imaging Study of Tozuleristide (BLZ-100) in Adults with Newly Diagnosed or Recurrent Gliomas. *Neurosurgery* **2019**, *85*, E641–E649. [CrossRef] [PubMed]
27. Ojeda, P.G.; Wang, C.; Craik, D.J. Chlorotoxin: Structure, activity, and potential uses in cancer therapy. *Biopolymers* **2015**, *106*, 25–36. [CrossRef] [PubMed]
28. Dardevet, L.; Rani, D.; Aziz, T.A.E.; Bazin, I.; Sabatier, J.-M.; Fadl, M.; Brambilla, E.; De Waard, M. Chlorotoxin: A helpful natural scorpion peptide to diagnose glioma and fight tumor invasion. *Toxins* **2015**, *7*, 1079–1101. [CrossRef] [PubMed]
29. Wie, C.S.; Derian, A. Ziconotide. [Updated 2021 July 22]. In *StatPearls*; StatPearls Publishing: Treasure Island, FL, USA, 2021. Available online: https://www.ncbi.nlm.nih.gov/books/NBK459151/ (accessed on 19 November 2021).
30. Sciani, J.M.; Zychar, B.C.; Gonçalves, L.R.D.C.; Nogueira, T.D.O.; Giorgi, R.; Pimenta, D.C. Pro-inflammatory effects of the aqueous extract of Echinometra lucunter sea urchin spines. *Exp. Biol. Med.* **2011**, *236*, 277–280. [CrossRef]
31. Kohn, A.J. Conus envenomation of humans: In fact and fiction. *Toxins* **2019**, *11*, 10. [CrossRef]
32. Dumbacher, J.P.; Spande, T.F.; Daly, J.W. Batrachotoxin alkaloids from passerine birds: A second toxic bird genus (Ifrita kowaldi) from New Guinea. *Proc. Natl. Acad. Sci. USA* **2000**, *97*, 12970–12975. [CrossRef]
33. Diamond, J.M. Did Komodo dragons evolve to eat pygmy elephants? *Nature* **1987**, *326*, 825. [CrossRef]
34. Montgomery, J.M.; Gillespie, D.; Sastrawan, P.; Fredeking, T.; Stewart, G.L. Aerobic salivary bacteria in wild and captive komodo dragons. *J. Wildl. Dis.* **2002**, *38*, 545–551. [CrossRef] [PubMed]
35. Estevão-Costa, M.-I.; Sanz-Soler, R.; Johanningmeier, B.; Eble, J.A. Snake venom components in medicine: From the symbolic rod of Asclepius to tangible medical research and application. *Int. J. Biochem. Cell Biol.* **2018**, *104*, 94–113. [CrossRef]
36. Opie, L.H.; Kowolik, H. The discovery of captopril: From large animals to small molecules. *Cardiovasc. Res.* **1995**, *30*, 18–25. [CrossRef]
37. Ferreira, L.A.F.; Galle, A.; Raida, M.; Schrader, M.; Lebrun, I.; Habermehl, G. Isolation: Analysis and properties of three bradykinin–potentiating peptides (BPP-II, BPP-III, and BPP-V) from Bothrops neuwiedi venom. *J. Protein Chem.* **1998**, *17*, 285–289. [CrossRef]
38. Grant, M.L.; Henderson, L.J. A Case of Gila Monster Poisoning with a Summary of Some Previous Accounts. *Proc. Iowa Acad. Sci.* **1957**, *64*, 686–697.
39. Shufeldt, R.W. The bite of the Gila monster (*Heloderma suspectum*). *Am. Nat.* **1882**, *16*, 907–908.
40. Woodson, W.D. Toxicity of Heloderma venom. *Herpetologica* **1947**, *4*, 31–33.
41. Cooke, E.; Loeb, L. Hemolytic action of the venom of Heloderma suspectum. *Proc. Soc. Exp. Biol. Med.* **1908**, *5*, 104–105. [CrossRef]
42. Mebs, D. Some studies on the biochemistry of the venom gland of Heloderma horridum. *Toxicon* **1968**, *5*, 225–226. [CrossRef]
43. Stýblová, Z.; Kornalik, F. Enzymatic properties of Heloderma suspectum venom. *Toxicon Off. J. Int. Soc. Toxinolo.* **1967**, *5*, 139–140. [CrossRef]
44. Murphy, S.A.; Johnson, B.D.; Sifford, D.H. Enzymes in Heloderma horridum venom. *J. Ark. Acad. Sci.* **1976**, *30*, 61–63.
45. Raufman, J.P.; Jensen, R.T.; Sutliff, V.E.; Pisano, J.J.; Gardner, J.D. Actions of Gila monster venom on dispersed acini from guinea pig pancreas. *Am. J. Physiol. Content* **1982**, *242*, G470–G474. [CrossRef] [PubMed]
46. Banks, B.E.; Pearce, F.; Springer, C.J.; Vernon, C. On the immunology of nerve growth factor. *Neurosci. Lett.* **1985**, *61*, 127–130. [CrossRef]
47. Mebs, D. Biochemistry of Kinin-Releasing Enzymes in the Venom of the Viper Bitis Gabonica and of the Lizard Heloderma Suspectum. In *Bradykinin and Related Kinins*; Springer: Berlin/Heidelberg, Germany, 1970; pp. 107–116. [CrossRef]
48. Mebs, D. Isolierung und Eigenschaften eines Kallikreins aus dem Gift der Krustenechse *Heloderma suspectum*. *DIETRICH MEBS* **1969**, *350*, 821–826. [CrossRef]
49. Parker, D.S.; Raufman, J.P.; O'Donohue, T.L.; Bledsoe, M.; Yoshida, H.; Pisano, J.J. Amino acid sequences of helospectins, new members of the glucagon superfamily, found in Gila monster venom. *J. Biol. Chem.* **1984**, *259*, 11751–11755. [CrossRef]
50. Hendon, R.A.; Tu, A.T. Biochemical characterization of the lizard toxin gilatoxin. *Biochemistry* **1981**, *20*, 3517–3522. [CrossRef]
51. Vandermeers, A.; Vandermeers-Piret, M.-C.; Robberecht, P.; Waelbroeck, M.; Dehaye, J.-P.; Winand, J.; Christophe, J. Purification of a novel pancreatic secretory factor (PSF) and a novel peptide with VIP- and secretin-like properties (helodermin) from Gila monster venom. *FEBS Lett.* **1984**, *166*, 273–276. [CrossRef]
52. Mochca-Morales, J.; Martin, B.M.; Possani, L.D. Isolation and characterization of Helothermine, a novel toxin from Heloderma horridum horridum (Mexican beaded lizard) venom. *Toxicon* **1990**, *28*, 299–309. [CrossRef]
53. Tu, A.T.; Hendon, R.R. Characterization of lizard venom hyaluronidase and evidence for its action as a spreading factor. *Comp. Biochem. Physiol. Part B Comp. Biochem.* **1983**, *76*, 377–383. [CrossRef]
54. Sosa, B.P.; Alagon, A.C.; Martin, B.M.; Possani, L.D. Biochemical characterization of the phospholipase A2 purified from the venom of the Mexican beaded lizard (Heloderma horridum horridum Wiegmann). *Biochemistry* **1986**, *25*, 2927–2933. [CrossRef] [PubMed]
55. Alagon, A.; Possani, L.D.; Smart, J.; Schleuning, W.D. Helodermatine, a kallikrein-like, hypotensive enzyme from the venom of Heloderma horridum horridum (Mexican beaded lizard). *J. Exp. Med.* **1986**, *164*, 1835–1845. [CrossRef]

56. Eng, J.; Andrews, P.; Kleinman, W.A.; Singh, L.; Raufman, J.P. Purification and structure of exendin-3, a new pancreatic secretagogue isolated from Heloderma horridum venom. *J. Biol. Chem.* **1990**, *265*, 20259–20262. [CrossRef]
57. Patterson, R.A. Some physiological effects caused by venom from the Gila Monster, Heloderma suspectum. *Toxicon* **1967**, *5*, 5–10. [CrossRef]
58. Patterson, R.A. Smooth muscle stimulating action of venom from the Gila monster, Heloderma suspectum. *Toxicon* **1967**, *5*, 11–15. [CrossRef]
59. Patterson, R.A.; Lee, I.S. Effects of Heloderma suspectum venom on blood coagulation. *Toxicon* **1969**, *7*, 321–324. [CrossRef]
60. Eng, J.; Kleinman, W.; Singh, L.; Singh, G.; Raufman, J. Isolation and characterization of exendin-4, an exendin-3 analogue, from Heloderma suspectum venom. Further evidence for an exendin receptor on dispersed acini from guinea pig pancreas. *J. Biol. Chem.* **1992**, *267*, 7402–7405. [CrossRef]
61. Parkes, D.G.; Mace, K.F.; Trautmann, M.E. Discovery and development of exenatide: The first antidiabetic agent to leverage the multiple benefits of the incretin hormone, GLP-1. *Expert Opin. Drug Discov.* **2012**, *8*, 219–244. [CrossRef] [PubMed]
62. Huang, T.-F.; Chiang, H.-S. Effect on human platelet aggregation of phospholipase A2 purified from Heloderma horridum (beaded lizard) venom. *Biochim. Biophys. Acta (BBA) Lipids Lipid Metab.* **1994**, *1211*, 61–68. [CrossRef]
63. Vandermeers, A.; Vandermeers-Piret, M.-C.; Vigneron, L.; Rathe, J.; Stievenart, M.; Christophe, J. Differences in primary structure among five phospholipases A2 from Heloderma suspectum. *JBIC J. Biol. Inorg. Chem.* **1991**, *196*, 537–544. [CrossRef] [PubMed]
64. Kwok, H.F.; Chen, T.; O'Rourke, M.; Ivanyi, C.; Hirst, D.; Shaw, C. Helokinestatin: A new bradykinin B2 receptor antagonist decapeptide from lizard venom. *Peptides* **2008**, *29*, 65–72. [CrossRef]
65. Fry, B.G.; Winter, K.; Norman, J.A.; Roelants, K.; Nabuurs, R.J.A.; Van Osch, M.; Teeuwisse, W.M.; van der Weerd, L.; Mcnaughtan, J.E.; Kwok, H.F.; et al. Functional and Structural Diversification of the Anguimorpha Lizard Venom System. *Mol. Cell. Proteom.* **2010**, *9*, 2369–2390. [CrossRef]
66. Komori, Y.; Nikai, T.; Sugihara, H. Purification and characterization of a lethal toxin from the venom of Helodermahorridumhorridum. *Biochem. Biophys. Res. Commun.* **1988**, *154*, 613–619. [CrossRef]
67. Fry, B.G.; Roelants, K.; Winter, K.; Hodgson, W.C.; Griesman, L.; Kwok, H.F.; Scanlon, D.; Karas, J.; Shaw, C.; Wong, L.; et al. Novel Venom Proteins Produced by Differential Domain-Expression Strategies in Beaded Lizards and Gila Monsters (genus Heloderma). *Mol. Biol. Evol.* **2009**, *27*, 395–407. [CrossRef]
68. Ma, C.; Yang, M.; Zhou, M.; Wu, Y.; Wang, L.; Chen, T.; Ding, A.; Shaw, C. The natriuretic peptide/helokinestatin precursor from Mexican beaded lizard (Heloderma horridum) venom: Amino acid sequence deduced from cloned cDNA and identification of two novel encoded helokinestatins. *Peptides* **2011**, *32*, 1166–1171. [CrossRef]
69. Koludarov, I.; Jackson, T.N.W.; Sunagar, K.; Nouwens, A.; Hendrikx, I.; Fry, B.G. Fossilized Venom: The Unusually Conserved Venom Profiles of Heloderma Species (Beaded Lizards and Gila Monsters). *Toxins* **2014**, *6*, 3582–3595. [CrossRef] [PubMed]
70. Sanggaard, K.W.; Dyrlund, T.F.; Thomsen, L.R.; Nielsen, T.A.; Brøndum, L.; Wang, T.; Thøgersen, I.B.; Enghild, J.J. Characterization of the gila monster (Heloderma suspectum suspectum) venom proteome. *J. Proteom.* **2015**, *117*, 1–11. [CrossRef] [PubMed]
71. Lino-López, G.J.; Valdez-Velázquez, L.L.; Corzo, G.; Romero-Gutiérrez, M.T.; Jiménez-Vargas, J.M.; Rodríguez-Vázquez, A.; Vazquez-Vuelvas, O.F.; Gonzalez-Carrillo, G. Venom gland transcriptome from Heloderma horridum horridum by high-throughput sequencing. *Toxicon* **2020**, *180*, 62–78. [CrossRef]
72. Dobson, J.; Harris, R.; Zdenek, C.; Huynh, T.; Hodgson, W.; Bosmans, F.; Fourmy, R.; Violette, A.; Fry, B. The Dragon's Paralysing Spell: Evidence of Sodium and Calcium Ion Channel Binding Neurotoxins in Helodermatid and Varanid Lizard Venoms. *Toxins* **2021**, *13*, 549. [CrossRef] [PubMed]
73. Fry, B.G.; Vidal, N.; Norman, J.A.; Vonk, F.J.; Scheib, H.; Ramjan, S.F.R.; Kuruppu, S.; Fung, K.; Hedges, S.B.; Richardson, M.K.; et al. Early evolution of the venom system in lizards and snakes. *Nature* **2005**, *439*, 584–588. [CrossRef]
74. Fry, B.G.; Wroe, S.; Teeuwisse, W.; van Osch, M.J.P.; Moreno, K.; Ingle, J.; McHenry, C.; Ferrara, T.; Clausen, P.; Scheib, H.; et al. A central role for venom in predation by Varanus komodoensis (Komodo Dragon) and the extinct giant Varanus (Megalania) priscus. *Proc. Natl. Acad. Sci. USA* **2009**, *106*, 8969–8974. [CrossRef]
75. Dobson, J.S.; Zdenek, C.N.; Hay, C.; Violette, A.; Fourmy, R.; Cochran, C.; Fry, B.G. Varanid Lizard Venoms Disrupt the Clotting Ability of Human Fibrinogen through Destructive Cleavage. *Toxins* **2019**, *11*, 255. [CrossRef] [PubMed]
76. Zasloff, M. Magainins, a class of antimicrobial peptides from Xenopus skin: Isolation, characterization of two active forms, and partial cDNA sequence of a precursor. *Proc. Natl. Acad. Sci. USA* **1987**, *84*, 5449–5453. [CrossRef]
77. Mailho-Fontana, P.L.; Antoniazzi, M.M.; Toledo, L.F.; Verdade, V.K.; Sciani, J.M.; Barbaro, K.C.; Pimenta, D.C.; Rodrigues, M.T.; Jared, C. Passive and active defense in toads: The parotoid macroglands in Rhinella marina and Rhaebo guttatus. *J. Exp. Zool. Part A Ecol. Genet. Physiol.* **2014**, *321*, 65–77. [CrossRef] [PubMed]
78. Conceição, K.; Konno, K.; de Melo, R.L.; Antoniazzi, M.M.; Jared, C.; Sciani, J.M.; Conceição, I.M.; Prezoto, B.C.; de Camargo, A.C.M.; Pimenta, D.C. Isolation and characterization of a novel bradykinin potentiating peptide (BPP) from the skin secretion of Phyllomedusa hypochondrialis. *Peptides* **2007**, *28*, 515–523. [CrossRef] [PubMed]
79. Conceição, K.; Bruni, F.M.; Pareja-Santos, A.; Antoniazzi, M.M.; Jared, C.; Lopes-Ferreira, M.; Lima, C.; Pimenta, D.C. Unusual profile of leukocyte recruitment in mice induced by a skin secretion of the tree frog Phyllomedusa hypochondrialis. *Toxicon* **2007**, *49*, 625–633. [CrossRef] [PubMed]

80. Mendes, V.A.; Barbaro, K.C.; Sciani, J.M.; Vassão, R.C.; Pimenta, D.C.; Jared, C.; Antoniazzi, M.M. The cutaneous secretion of the casque-headed tree frog Corythomantis greeningi: Biochemical characterization and some biological effects. *Toxicon* **2016**, *122*, 133–141. [CrossRef] [PubMed]
81. Assakura, M.T.; Silva, C.A.; Mentele, R.; Camargo, A.C.; Serrano, S.M. Molecular cloning and expression of structural domains of bothropasin, a P-III metalloproteinase from the venom of Bothrops jararaca. *Toxicon* **2002**, *41*, 217–227. [CrossRef]
82. Leme, A.F.P.; Prezoto, B.C.; Yamashiro, E.T.; Bertholim, L.; Tashima, A.K.; Klitzke, C.F.; Camargo, A.C.M.; Serrano, S.M.T. BothropsproteaseA, a unique highly glycosylated serine proteinase, is a potent, specific fibrinogenolytic agent. *J. Thromb. Haemost.* **2008**, *6*, 1363–1372. [CrossRef]
83. Souza, B.B.P.; Fh, J.L.C.; Murad, A.M.; Prates, M.V.; Coura, M.M.A.; Brand, G.D.; Barbosa, E.A.; Bloch, C., Jr. Identification and characterization of phospholipases A2 from the skin secretion of Pithecopus azureus anuran. *Toxicon* **2019**, *167*, 10–19. [CrossRef]
84. Mariano, D.; Messias, M.D.G.; Neto, J.P.P.; Spencer, P.; Pimenta, D.C. Biochemical Analyses of Proteins from Duttaphrynus melanostictus (Bufo melanostictus) Skin Secretion: Soluble Protein Retrieval from a Viscous Matrix by Ion-Exchange Batch Sample Preparation. *Protein J.* **2018**, *37*, 380–389. [CrossRef]
85. Fusco, L.S.; Cajade, R.; Piñeiro, J.M.; Torres, A.M.; Da Silva, I.R.F.; Hyslop, S.; Leiva, L.C.; Pimenta, D.C.; Bustillo, S. Biochemical characterization and cytotoxic effect of the skin secretion from the red-spotted Argentina frog Argenteohyla siemersi (Anura: Hylidae). *J. Venom. Anim. Toxins Incl. Trop. Dis.* **2020**, *26*, e20190078. [CrossRef]
86. Conceição, K.; Konno, K.; Richardson, M.; Antoniazzi, M.M.; Jared, C.; Daffre, S.; Camargo, A.C.M.; Pimenta, D.C. Isolation and biochemical characterization of peptides presenting antimicrobial activity from the skin of Phyllomedusa hypochondrialis. *Peptides* **2006**, *27*, 3092–3099. [CrossRef]
87. Wu, X.; Pan, J.; Wu, Y.; Xi, X.; Ma, C.; Wang, L.; Zhou, M.; Chen, T. PSN-PC: A Novel Antimicrobial and Anti-Biofilm Peptide from the Skin Secretion of Phyllomedusa-camba with Cytotoxicity on Human Lung Cancer Cell. *Molecules* **2017**, *22*, 1896. [CrossRef] [PubMed]
88. Wu, Y.; Wang, L.; Zhou, M.; Chen, T.; Shaw, C. Phylloseptin-PBa1,-PBa2,-PBa3: Three novel antimicrobial peptides from the skin secretion of Burmeister's leaf frog (Phyllomedusa burmeisteri). *Biochem. Biophys. Res. Commun.* **2019**, *509*, 664–673. [CrossRef] [PubMed]
89. Liu, Y.; Shi, D.; Wang, J.; Chen, X.; Zhou, M.; Xi, X.; Cheng, J.; Ma, C.; Chen, T.; Shaw, C.; et al. A Novel Amphibian Antimicrobial Peptide, Phylloseptin-PV1, Exhibits Effective Anti-staphylococcal Activity without Inducing Either Hepatic or Renal Toxicity in Mice. *Front. Microbiol.* **2020**, *11*, 565158. [CrossRef]
90. Zhang, R.; Zhou, M.; Wang, L.; McGrath, S.; Chen, T.; Chen, X.; Shaw, C. Phylloseptin-1 (PSN-1) from Phyllomedusa sauvagei skin secretion: A novel broad-spectrum antimicrobial peptide with antibiofilm activity. *Mol. Immunol.* **2010**, *47*, 2030–2037. [CrossRef] [PubMed]
91. Raja, Z.; Andre, S.; Piesse, C.; Sereno, D.; Nicolas, P.; Foulon, T.; Oury, B.; Ladram, A. Structure, antimicrobial activities and mode of interaction with membranes of bovel phylloseptins from the painted-belly leaf frog, Phyllomedusa sauvagii. *PLoS ONE* **2013**, *8*, e70782. [CrossRef]
92. Conlon, J.M.; Woodhams, D.C.; Raza, H.; Coquet, L.; Leprince, J.; Jouenne, T.; Vaudry, H.; Rollins-Smith, L.A. Peptides with differential cytolytic activity from skin secretions of the lemur leaf frog Hylomantis lemur (Hylidae: Phyllomedusinae). *Toxicon* **2007**, *50*, 498–506. [CrossRef] [PubMed]
93. Sousa, J.C.; Berto, R.F.; Gois, E.A.; Fontenele-Cardi, N.C.; Honório-Júnior, J.E.; Konno, K.; Richardson, M.; Rocha, M.F.; Camargo, A.A.; Pimenta, D.C.; et al. Leptoglycin: A new Glycine/Leucine-rich antimicrobial peptide isolated from the skin secretion of the South American frog Leptodactylus pentadactylus (Leptodactylidae). *Toxicon* **2009**, *54*, 23–32. [CrossRef]
94. Silva, M.R.E.; Beraldo, W.T.; Rosenfeld, G. Bradykinin, a hypotensive and smooth muscle stimulating factor released from plasma globulin by snake venoms and by trypsin. *Am. J. Physiol. Content* **1949**, *156*, 261–273. [CrossRef] [PubMed]
95. Conceição, K.; Bruni, F.; Sciani, J.; Konno, K.; Melo, R.; Antoniazzi, M.; Jared, C.; Lopes-Ferreira, M.; Pimenta, D. Identification of bradykinin: Related peptides from Phyllomedusa nordestina skin secretion using electrospray ionization tandem mass spectrometry after a single-step liquid chromatography. *J. Venom. Anim. Toxins Incl. Trop. Dis.* **2009**, *15*, 633–652. [CrossRef]
96. Tempone, A.G.; Pimenta, D.C.; Lebrun, I.; Sartorelli, P.; Taniwaki, N.N.; de Andrade, H.F., Jr.; Antoniazzi, M.M.; Jared, C. Antileishmanial and antitrypanosomal activity of bufadienolides isolated from the toad Rhinella jimi parotoid macrogland secretion. *Toxicon* **2008**, *52*, 13–21. [CrossRef] [PubMed]
97. Pinto, E.G.; Pimenta, D.; Antoniazzi, M.M.; Jared, C.; Tempone, A. Antimicrobial peptides isolated from Phyllomedusa nordestina (Amphibia) alter the permeability of plasma membrane of Leishmania and Trypanosoma cruzi. *Exp. Parasitol.* **2013**, *135*, 655–660. [CrossRef] [PubMed]
98. Sciani, J.M.; De-Sá-Júnior, P.L.; Ferreira, A.K.; Pereira, A.; Antoniazzi, M.M.; Jared, C.; Pimenta, D.C. Cytotoxic and antiproliferative effects of crude amphibian skin secretions on breast tumor cells. *Biomed. Prev. Nutr.* **2013**, *3*, 10–18. [CrossRef]
99. Schmeda-Hirschmann, G.; Quispe, C.; Theoduloz, C.; de Sousa, P.T., Jr.; Parizotto, C. Antiproliferative activity and new argininyl bufadienolide esters from the "cururú" toad Rhinella (Bufo) schneideri. *J. Ethnopharmacol.* **2014**, *155*, 1076–1085. [CrossRef] [PubMed]
100. Schmeda-Hirschmann, G.; Quispe, C.; Arana, G.V.; Theoduloz, C.; Urra, F.A.; Cárdenas, C. Antiproliferative activity and chemical composition of the venom from the Amazonian toad Rhinella marina (Anura: Bufonidae). *Toxicon* **2016**, *121*, 119–129. [CrossRef]

101. Schmeda-Hirschmann, G.; Gomez, C.V.; de Arias, A.R.; Burgos-Edwards, A.; Alfonso, J.; Rolon, M.; Brusquetti, F.; Netto, F.; Urra, F.A.; Cárdenas, C. The Paraguayan Rhinella toad venom: Implications in the traditional medicine and proliferation of breast cancer cells. *J. Ethnopharmacol.* **2017**, *199*, 106–118. [CrossRef]
102. Carvalho, A.C. Avaliação dos Efeitos Citotóxicos e Antiproliferativos da Secreção Cutânea e de Peptídeos do Anuro Physalaemus Nattereri (Steindachner, 1863). 2015. Available online: https://repositorio.unb.br/handle/10482/18589 (accessed on 19 November 2021).
103. Dahham, S.; Asif, M.; Tabana, Y.; Sandai, D.; Majid, A.; Harn, G. Antiproliferative and apoptotic activity of Crude Skin Secretion from Malaysian Toad (Bufo asper) on in vitro colorectal cancer cells. *J. Appl. Pharm. Sci.* **2017**, *7*, 1–6. [CrossRef]
104. de Sousa, L.Q.; Machado, K.; Oliveira, S.F.D.C.; Araújo, L.D.S.; Monção-Filho, E.D.S.; Cavalcante, A.; Junior, G.M.V.; Ferreira, P.M.P. Bufadienolides from amphibians: A promising source of anticancer prototypes for radical innovation, apoptosis triggering and Na+/K+-ATPase inhibition. *Toxicon* **2017**, *127*, 63–76. [CrossRef]
105. Karış, M.; Şener, D.; Yalçın, H.T.; Nalbantsoy, A.; Göçmen, B. Major biological activities and protein profiles of skin secretions of Lissotriton vulgaris and Triturus ivanbureschi. *Turk. J. Biochem.* **2018**, *43*, 605–612. [CrossRef]
106. Machado, K.; de Sousa, L.Q.; Lima, D.J.B.; Soares, B.M.; Cavalcanti, B.C.; Maranhão, S.S.A.; de Noronha, J.D.C.; de Jesus Rodrigues, D.; Militão, G.C.G.; Chaves, M.H.; et al. Marinobufagin, a molecule from poisonous frogs, causes biochemical, morphological and cell cycle changes in human neoplasms and vegetal cells. *Toxicol. Lett.* **2018**, *285*, 121–131. [CrossRef]
107. Filho, E.S.M.; Pio, Y.P.F.; Chaves, M.H.; Ferreira, P.M.P.; Fonseca, M.G.; Pessoa, C.; Lima, D.J.B.; Araújo, B.Q.; Vieira, G.M., Jr. Chemical Constituents and Cytotoxic Activity of Rhinella jimi (Anura: Bufonidae). *J. Braz. Chem. Soc.* **2021**. [CrossRef]
108. Spinelli, R.; Guevara, L.A.B.; López, J.A.; Camargo, C.M.; De Restrepo, H.G.; Siano, A.S. Cytotoxic and antiproliferative activities of amphibian (anuran) skin extracts on human acute monocytic leukemia cells. *Toxicon* **2020**, *177*, 25–34. [CrossRef]
109. Sciani, J.M.; Angeli, C.B.; Antoniazzi, M.M.; Jared, C.; Pimenta, D.C. Differences and Similarities among Parotoid Macrogland Secretions in South American Toads: A Preliminary Biochemical Delineation. *Sci. World J.* **2013**, *2013*, 937407. [CrossRef] [PubMed]
110. Vigerelli, H.; Sciani, J.M.; Jared, C.; Antoniazzi, M.M.; Caporale, G.M.M.; Silva, A.D.C.R.D.; Pimenta, D.C. Bufotenine is able to block rabies virus infection in BHK-21 cells. *J. Venom. Anim. Toxins Incl. Trop. Dis.* **2014**, *20*, 45. [CrossRef]
111. Vigerelli, H.; Sciani, J.; Pereira, P.M.C.; Lavezo, A.A.; Silva, A.C.R.; Collaço, R.; Rocha, T.; Bueno, T.C.; Pimenta, D.C. Bufotenine, a tryptophan-derived alkaloid, suppresses the symptoms and increases the survival rate of rabies-infected mice: The development of a pharmacological approach for rabies treatment. *J. Venom. Anim. Toxins Incl. Trop. Dis.* **2020**, *26*, e20190050. [CrossRef]
112. Vigerelli, H.; Sciani, J.M.; Eula, M.A.C.; Sato, L.A.; Antoniazzi, M.M.; Jared, C.; Pimenta, D.C. Biological Effects and Biodistribution of Bufotenine on Mice. *BioMed Res. Int.* **2018**, *2018*, 1032638. [CrossRef]
113. Neto, R.D.S.C.; Vigerelli, H.; Jared, C.; Antoniazzi, M.M.; Chaves, L.B.; Silva, A.D.C.R.D.; De Melo, R.L.; Sciani, J.M.; Pimenta, D.C. Synergic effects between ocellatin-F1 and bufotenine on the inhibition of BHK-21 cellular infection by the rabies virus. *J. Venom. Anim. Toxins Incl. Trop. Dis.* **2015**, *21*, 50. [CrossRef] [PubMed]
114. Barboza, C.M.; Pimenta, D.C.; Vigerelli, H.; Silva, A.D.C.R.D.; Garcia, J.G.; Zamudio, R.M.; Castilho, J.G.; Montanha, J.A.; Roehe, P.M.; Batista, H.B.D.C.R. In vitro effects of bufotenine against RNA and DNA viruses. *Braz. J. Microbiol.* **2021**, *52*, 2475–2482. [CrossRef] [PubMed]
115. Santoro, F.; Selvaggia, S.; Scowcroft, G.; Fauville, G.; Tuddenham, P. *Ocean Literacy for All: A Toolkit*; UNESCO Publishing: Paris, France, 2017; Volume 80.
116. WoRMS Editorial Board. World Register of Marine Species. 2021. Available online: https://www.marinespecies.org (accessed on 19 November 2021).
117. McIntosh, M.; Cruz, L.; Hunkapiller, M.; Gray, W.; Olivera, B. Isolation and structure of a peptide toxin from the marine snail Conus magus. *Arch. Biochem. Biophys.* **1982**, *218*, 329–334. [CrossRef]
118. Miljanich, G.P. Ziconotide: Neuronal Calcium Channel Blocker for Treating Severe Chronic Pain. *Curr. Med. Chem.* **2004**, *11*, 3029–3040. [CrossRef] [PubMed]
119. Larsen, A.K.; Galmarini, C.M.; D'Incalci, M. Unique features of trabectedin mechanism of action. *Cancer Chemother. Pharmacol.* **2015**, *77*, 663–671. [CrossRef] [PubMed]
120. Schwartsmann, G.; da Rocha, A.B.; Berlinck, R.G.; Jimeno, J. Marine organisms as a source of new anticancer agents. *Lancet Oncol.* **2001**, *2*, 221–225. [CrossRef]
121. Longato, G.B.; De Barros, H.V.; de Lima, C.; Picolo, G.; Zambelli, V.O.; Morandini, A.; Marques, A.C.; Sciani, J.M. Screening of Brazilian marine animals extracts on tumor cell line panel. *Toxicon* **2019**, *168*, S31. [CrossRef]
122. Haddad, V., Jr.; Lupi, O.; Lonza, J.P.; Tyring, S.K. Tropical dermatology: Marine and aquatic dermatology. *J. Am. Acad. Dermatol.* **2009**, *61*, 733–750. [CrossRef]
123. Cracchiolo, A.; Goldberg, L. Local and Systemic Reactions to Puncture Injuries by the Sea Urchin Spine and the Date Palm Thorn. *Arthritis Rheum.* **1977**, *20*, 1206–1212. [CrossRef] [PubMed]
124. Rossetto, A.L.; Mora, J.D.; Haddad Junior, V. Sea urchin granuloma. *Rev. Do Inst. Med. Trop. São Paulo* **2006**, *48*, 303–306. [CrossRef]
125. Sciani, J.M.; Zychar, B.; Gonçalves, L.R.; Giorgi, R.; Nogueira, T.; Pimenta, D.C. Preliminary molecular characterization of a proinflammatory and nociceptive molecule from the Echinometra lucunter spines extracts. *J. Venom. Anim. Toxins Incl. Trop. Dis.* **2017**, *23*, 43. [CrossRef]

126. Sciani, J.M.; Antoniazzi, M.M.; Neves, A.D.; Pimenta, D.C. Cathepsin B/X is secreted by Echinometra lucunter sea urchin spines, a structure rich in granular cells and toxins. *J. Venom. Anim. Toxins Incl. Trop. Dis.* **2013**, *19*, 1–8. [CrossRef]
127. Sciani, J.M.; Sampaio, M.C.; Zychar, B.C.; Gonçalves, L.R.D.C.; Giorgi, R.; Nogueira, T.D.O.; De Melo, R.L.; Teixeira, C.D.F.P.; Pimenta, D.C. Echinometrin: A novel mast cell degranulating peptide from the coelomic liquid of Echinometra lucunter sea urchin. *Peptides* **2014**, *53*, 13–21. [CrossRef]
128. Yamasaki, A.; Higaki, H.; Nakashima, K.; Yamamoto, O.; Hein, K.; Takahashi, H.; Chinuki, Y.; Morita, E. Identification of a Major Yolk Protein as an Allergen in Sea Urchin Roe. *Acta Derm. Venereol.* **2010**, *90*, 235–238. [CrossRef]
129. Rodriguez, V.; Bartolomé, B.; Armisen, M.; Vidal, C. Food allergy to Paracentrotus lividus (sea urchin roe). *Ann. Allergy Asthma Immunol.* **2007**, *98*, 393–396. [CrossRef]
130. Pimenta, D.C.; Lebrun, I. Cryptides: Buried secrets in proteins. *Peptides* **2007**, *28*, 2403–2410. [CrossRef]
131. Sciani, J.M.; Emerenciano, A.K.; Silva, J.R.; Pimenta, D.C. Initial peptidomic profiling of Brazilian sea urchins: Arbacia lixula, Lytechinus variegatus and Echinometra lucunter. *J. Venom. Anim. Toxins Incl. Trop. Dis.* **2016**, *22*. [CrossRef] [PubMed]
132. Olivera, B.M.; Cruz, L.J. Conotoxins, in retrospect. *Toxicon* **2001**, *39*, 7–14. [CrossRef]
133. Kaas, Q.; Westermann, J.-C.; Craik, D.J. Conopeptide characterization and classifications: An analysis using ConoServer. *Toxicon* **2010**, *55*, 1491–1509. [CrossRef]
134. Jungo, F.; Bairoch, A. Tox-Prot, the toxin protein annotation program of the Swiss-Prot protein knowledgebase. *Toxicon* **2005**, *45*, 293–301. [CrossRef]
135. The UniProt Consortium, UniProt: The universal protein knowledgebase in 2021. *Nucleic Acids Res.* **2021**, *49*, D480–D489. [CrossRef] [PubMed]
136. Kaas, Q.; Westermann, J.-C.; Halai, R.; Wang, C.; Craik, D. ConoServer, a database for conopeptide sequences and structures. *Bioinformatics* **2008**, *24*, 445–446. [CrossRef] [PubMed]
137. Kaas, Q.; Yu, R.; Jin, A.-H.; Dutertre, S.; Craik, D.J. ConoServer: Updated content, knowledge, and discovery tools in the conopeptide database. *Nucleic Acids Res.* **2011**, *40*, D325–D330. [CrossRef]
138. Terlau, H.; Olivera, B.M. ConusVenoms: A Rich Source of Novel Ion Channel-Targeted Peptides. *Physiol. Rev.* **2004**, *84*, 41–68. [CrossRef]
139. Eston, V.R.; Migotto, A.E.; Oliveira Filho, E.C.; Rodrigues, S.D.; Freitas, J.C. Vertical distribution of benthic marine organisms on rocky coasts of the Fernando de Noronha Archipelago (Brazil). *Bol. Do Inst. Oceanográfico* **1986**, *34*, 37–53. [CrossRef]
140. Braga, M.C.V.; Konno, K.; Portaro, F.C.; de Freitas, J.C.; Yamane, T.; Olivera, B.M.; Pimenta, D.C. Mass spectrometric and high performance liquid chromatography profiling of the venom of the Brazilian vermivorous mollusk Conus regius: Feeding behavior and identification of one novel conotoxin. *Toxicon* **2005**, *45*, 113–122. [CrossRef]
141. Braga, M.C.V.; Nery, A.A.; Ulrich, H.; Konno, K.; Sciani, J.M.; Pimenta, D.C. α-RgIB: A Novel Antagonist Peptide of Neuronal Acetylcholine Receptor Isolated from Conus regius. *Venom. Int. J. Pept.* **2013**, *2013*, 543028. [CrossRef] [PubMed]
142. Reckziegel, G.C.; Dourado, F.S.; Garrone, D.; Haddad, V. Injuries caused by aquatic animals in Brazil: An analysis of the data present in the information system for notifiable diseases. *Rev. Soc. Bras. Med. Trop.* **2015**, *48*, 460–467. [CrossRef] [PubMed]
143. Magalhães, M.R.; da Silva, N.J., Jr.; Ulhoa, C.J. A hyaluronidase from Potamotrygon motoro (freshwater stingrays) venom: Isolation and characterization. *Toxicon* **2008**, *51*, 1060–1067. [CrossRef]
144. Kimura, L.; Neto, J.P.P.; Távora, B.C.; Faquim-Mauro, E.; Pereira, N.A.; Antoniazzi, M.M.; Jared, S.G.; Teixeira, C.F.; Santoro, M.L.; Barbaro, K.C. Mast cells and histamine play an important role in edema and leukocyte recruitment induced by Potamotrygon motoro stingray venom in mice. *Toxicon* **2015**, *103*, 65–73. [CrossRef]
145. Germain, M.; Smith, K.; Skelton, H. The cutaneous cellular infiltrate to stingray envenomization contains increased TIA+ cells. *Br. J. Dermatol.* **2000**, *143*, 1074–1077. [CrossRef]
146. Coelho, G.R.; Neto, P.P.; Barbosa, F.C.; Dos Santos, R.S.; Brigatte, P.; Spencer, P.J.; Sampaio, S.C.; D'Amélio, F.; Pimenta, D.C.; Sciani, J.M. Biochemical and biological characterization of the Hypanus americanus mucus: A perspective on stingray immunity and toxins. *Fish Shellfish. Immunol.* **2019**, *93*, 832–840. [CrossRef]
147. Lima, C.; Disner, G.R.; Falcão, M.A.P.; Seni-Silva, A.C.; Maleski, A.L.A.; Souza, M.M.; Tonello, M.C.R.; Lopes-Ferreira, M. The Natterin Proteins Diversity: A Review on Phylogeny, Structure, and Immune Function. *Toxins* **2021**, *13*, 538. [CrossRef]
148. Jouiaei, M.; Yanagihara, A.A.; Madio, B.; Nevalainen, T.J.; Alewood, P.F.; Fry, B.G. Ancient Venom Systems: A Review on Cnidaria Toxins. *Toxins* **2015**, *7*, 2251–2271. [CrossRef]
149. Van Iten, H.; Leme, J.M.; Pacheco, M.L.A.F.; Simões, M.G.; Fairchild, T.R.; Rodrigues, F.; Galante, D.; Boggiani, P.C.; Marques, A.C. Origin and Early Diversification of Phylum Cnidaria: Key Macrofossils from the Ediacaran System of North and South America. In *The Cnidaria, Past, Present and Future*; Springer: Berlin/Heidelberg, Germany, 2016; pp. 31–40. [CrossRef]
150. Madio, B.; King, G.F.; Undheim, E.A.B. Sea Anemone Toxins: A Structural Overview. *Mar. Drugs* **2019**, *17*, 325. [CrossRef]
151. Beckmann, A.; Özbek, S. The Nematocyst: A molecular map of the Cnidarian stinging organelle. *Int. J. Dev. Biol.* **2012**, *56*, 577–582. [CrossRef]
152. Ashwood, L.M.; Norton, R.S.; Undheim, E.A.B.; Hurwood, D.A.; Prentis, P.J. Characterising Functional Venom Profiles of Anthozoans and Medusozoans within Their Ecological Context. *Mar. Drugs* **2020**, *18*, 202. [CrossRef]
153. Richet, C. De l'action de la congestine (virus des Actinies) sur les lapins et de ses effects anaphylactiques. *CR Soc. Biol. Paris* **1905**, *58*, 109–112.
154. Richet, C. De la thalassine toxine cristalliseé et pruritogène. *CR Soc. Biol. Paris* **1903**, *55*, 707–710.

155. Tsai, H.-S.; Niu, K.-Y. Acute Skin Manifestation of Sea Anemone Envenomation. *J. Emerg. Med.* **2021**, *60*, 536–537. [CrossRef]
156. Oliveira, J.S.; Redaelli, E.; Zaharenko, A.J.; Cassulini, R.R.; Konno, K.; Pimenta, D.C.; Freitas, J.C.; Clare, J.J.; Wanke, E. Binding specificity of sea anemone toxins to Nav 1.1-1.6 sodium channels: Unexpected contributions from differences in the IV/S3-S4 outer loop. *J. Biol. Chem.* **2004**, *279*, 33323–33335. [CrossRef]
157. Zaharenko, A.J.; Ferreira, W.A., Jr.; Oliveira, J.S.; Richardson, M.; Pimenta, D.C.; Konno, K.; Portaro, F.C.V.; de Freitas, J.C. Proteomics of the neurotoxic fraction from the sea anemone Bunodosoma cangicum venom: Novel peptides belonging to new classes of toxins. *Comp. Biochem. Physiol. Part D Genom. Proteom.* **2008**, *3*, 219–225. [CrossRef]
158. Yanagihara, A.A.; Shohet, R.V. Cubozoan Venom-Induced Cardiovascular Collapse Is Caused by Hyperkalemia and Prevented by Zinc Gluconate in Mice. *PLoS ONE* **2012**, *7*, e51368. [CrossRef]
159. Jaimes-Becerra, A.; Chung, R.; Morandini, A.C.; Weston, A.J.; Padilla, G.; Gacesa, R.; Ward, M.; Long, P.; Marques, A.C. Comparative proteomics reveals recruitment patterns of some protein families in the venoms of Cnidaria. *Toxicon* **2017**, *137*, 19–26. [CrossRef]
160. Arruda, G.L.M.; Vigerelli, H.; Bufalo, M.C.; Longato, G.B.; Veloso, R.V.; Zambelli, V.O.; Picolo, G.; Cury, Y.; Morandini, A.C.; Marques, A.C. Box jellyfish (Cnidaria, Cubozoa) extract increases neuron's connection: A possible neuroprotector effect. *BioMed Res. Int.* **2021**, *2021*, 8855248. [CrossRef] [PubMed]
161. Bueno, T.C.; Collaço, R.D.C.; Cardoso, B.A.; Bredariol, R.F.; Escobar, M.L.; Cajado, I.B.; Gracia, M.; Antunes, E.; Zambelli, V.O.; Picolo, G.; et al. Neurotoxicity of Olindias sambaquiensis and Chiropsalmus quadrumanus extracts in sympathetic nervous system. *Toxicon* **2021**, *199*, 127–138. [CrossRef]
162. Stein, J.M.; Bergman, W.; Fang, Y.; Davison, L.; Brensinger, C.; Robinson, M.B.; Hecht, N.B.; Abel, T. Behavioral and Neurochemical Alterations in Mice Lacking the RNA-Binding Protein Translin. *J. Neurosci.* **2006**, *26*, 2184–2196. [CrossRef]
163. Junior, R.S.F.; Sciani, J.M.; Marques-Porto, R.; Junior, A.L.; Orsi, R.D.O.; Barraviera, B.; Pimenta, D.C. Africanized honey bee (Apis mellifera) venom profiling: Seasonal variation of melittin and phospholipase A2 levels. *Toxicon* **2010**, *56*, 355–362. [CrossRef] [PubMed]
164. Sciani, J.M.; Marques-Porto, R.; Lourenço, A.; Orsi, R.D.O.; Junior, R.S.F.; Barraviera, B.; Pimenta, D.C. Identification of a novel melittin isoform from Africanized Apis mellifera venom. *Peptides* **2010**, *31*, 1473–1479. [CrossRef] [PubMed]
165. Barbosa, A.N.; Ferreira, R.S., Jr.; de Carvalho, F.C.T.; Schuelter-Trevisol, F.; Mendes, M.B.; Mendonça, B.C.; Batista, J.N.; Trevisol, D.J.; Boyer, L.; Chippaux, J.-P. Single-arm, multicenter phase I/II clinical trial for the treatment of envenomings by massive africanized honey bee stings using the unique apilic antivenom. *Front. Immunol.* **2021**, *12*, 860. [CrossRef]